Determining the functional consequences of circadian regulation of intestinal IgA plasma cell responses

A thesis submitted to The University of Manchester for the degree of Doctor of Philosophy in the Faculty of Biology, Medicine and Health

2021

Hugo A Penny

School of Biological Sciences

The Lydia Becker Institute of Immunology and Inflammation

TABLE OF CONTENTS

TABLE OF CONTENTS……2

LIST OF FIGURES……6

LIST OF TABLES……9

ABBREVIATIONS……10

ABSTRACT……12

DECLARATION……13

COPYRIGHT STATEMENT……14

EXPERIMENTAL CONTRIBUTIONS……15

ACKNOWLEDGEMENTS……16

1.0 GENERAL INTRODUCTION……17

1.1. The intestinal barrier……18

1.2. Orchestration of tolerance and GI homeostasis by the intestinal immune system……19

1.3. The generation and maintenance of intestinal IgA responses……24

1.3.1 The origins of intestinal IgA responses……24

1.3.2 IgA class switch recombination……25

1.3.3 Somatic hypermutation and affinity maturation within the GALT…… 27

1.3.4 The maintenance of plasma cell responses……28

1.3.5 IgA structure and subtypes……29

1.4 IgA responses towards intestinal bacteria……30

1.5 Circadian rhythmicity within the body……33

1.5.1 Overview……33

1.5.2 The organisation and regulation of biological clocks within the body……33

1.5.3 Molecular aspects of the biological clock……34

1.5.4 Circadian regulation of the immune system……36

1.5.5 Circadian regulation of the gut microbiota……38

1.6. Hypothesis of the research……40

2.0 MATERIALS AND METHODS……41

2.1. Animals……42

2.1.2 Mouse strains……42

2.1.2 Genotyping of IgMi and $Mb1^{cre}$ x $Arntl1^{flox}$ mice……42

2.2. Administration of diets……43

2.2.1 Reverse feeding……43

2.2.2 High fat diet and high/ low protein diet experiments……43

2.3. *In vivo* 2-NBDG and bodipy experiments……44

2.4. Preparation of single cell suspensions……44

2.4.1 Intestinal lamina propria……44

2.4.2 Peyer's patches and mesenteric lymph nodes……45

2.5. Flow cytometry……45

2.5.1 Surface staining……45

2.5.2 Sample acquisition……45

2.6 *In vitro* 2-NBDG uptake assay……46

2.7 In vitro assessment of lipid accumulation within cells……46

2.8 Kynurenine uptake assay……47

2.9 Fluorescence activated cell sorting……47

2.10 Antibody secretion assays……47

2.11 Extracellular flux analysis……48

2.12 RNA quantification……48

2.12.1 RNA purification……48

2.12.2 Reverse transcription PCR……..49

2.12.3 Realtime PCR……49

2.13 RNA sequencing……50

2.13.1 Sample preparation……50

2.13.2 Data analysis……50

2.14 Evaluation of intestinal IgA……50

2.14.1 Processing of small intestinal washes……50

2.14.2 Processing of faeces……51

2.14.3 IgA bacterial coating assay……51

2.14.4 IgA ELISA……51

2.14.5 BCA protein assay……52

2.15 16S rRNA sequencing……52

2.15.1 Sample preparation……52

2.15.2 Data analysis……53

2.16 Shotgun metagenomics sequencing……53

2.17 Metabolomic analysis……53

2.18 Data handling and statistical analysis……53

3.0 CHARACTERISING INTESTINAL IGA RESPONSES OVER THE CIRCADIAN DAY……..55

3.1 Introduction……56

3.2 Results……57

3.2.1 The concentration of sIgA within the intestines is rhythmic over a 24-hour period……57

3.2.2 Oscillatory intestinal IgA is not the result of time of day differences in PC differentiation……60

3.2.3 PC IgA production and secretion varies over the course of the day ……66

3.4 Discussion……80

4.0 DEFINING THE MECHANISMS THAT ENTRAIN INTESTINAL IGA RHYTHMICITY OVER THE CIRCADIAN DAY……84

4.1 Introduction……85

4.2 Results……86

4.2.1 IgA+ PCs have a cell-intrinsic biological clock……86

4.2.2 Generation of a mouse model of biological clock disruption in IgA+ PCs……89

4.2.3 Bmal1 is not required for rhythmicity of intestinal sIgA responses……91

4.2.4 Feeding cues drives rhythmicity in sIgA and augments the expression of IgA+ PC-intrinsic biological clock genes……95

4.2.5 IgA+ PCs have a higher metabolic activity than IgA+ B cells and IgD+ B cells……101

4.2.6 No difference in the uptake of nutrients or metabolic capacity of IgA+ PCs over the course of the day……107

4.2.7 Modulation of metabolic substrate availability alters the magnitude of IgA secretion……110

4.3 Discussion……117

5.0 DETERMENING THE CONSEQUENCES OF RHYTHMIC INTESTINAL IGA SECRETION ON HOST-MICROBIAL INTERACTIONS……120

5.1 Introduction……121

5.2 Results……122

5.2.1 Characterisation of a mouse model devoid of secretory antibodies……122

5.2.2 The global composition of intestinal commensal bacteria is similar in IgMi and littermate control mice……124

5.2.3 Altered diurnal rhythmicity in the composition and function of intestinal commensal bacteria in IgMi mice……128

5.3 Discussion……142

6.0 FINAL DISCUSSION……146

7.0 REFERENCES……157

WORD COUNT 37.444

LIST OF FIGURES

Figure 1. The basic structure of a single antibody molecule……25

Figure 2. The secretory (s)IgA complex……29

Figure 3. Schematic of the biological clock……35

Figure 3.1. Faecal sIgA varies over the course of the circadian day……58

Figure 3.2. Small intestinal sIgA varies over the course of the circadian day……59

Figure 3.3. No consistent time of day variation in IgA induction within Peyer's patches……..61

Figure 3.4. No consistent differences in the frequency or cell counts of small intestinal IgA+ PCs over the circadian day……63

Figure 3.5. No change in the frequency or counts of large intestinal IgA+ PCs over the circadian day……64

Figure 3.6. IgA+ PCs are the major IgA-secreting B cell subset in the intestines……65

Figure 3.7. Time of day difference in PC secretion of IgA……67

Figure 3.8. The transcriptional profile of IgA+ PCs is appropriately different to that of IgD+ B cells…..68

Figure 3.9. The transcriptional profile of IgA PCs oscillates over the circadian day……..69

Figure 3.10. Differentially expressed genes in IgA+ PCs at light/ dark and rest/ wake periods consistently map to IgA production……70

Figure 3.11. Genes mapping to the BAFF/ APRIL signalling pathway display rhythmicity over the circadian day in IgA+ PCs……..72

Figure 3.12. Genes mapping to the mTOR1 signalling pathway display rhythmicity in IgA+ PCs over the circadian day……74

Figure 3.13. Genes mapping to the cholesterol transport and biosynthesis pathway display rhythmicity in IgA+ PCs over the circadian day……76

Figure 3.14. Key genes involved in nutrient sensing, metabolism and immunoglobulin production oscillate in IgA+ PC over the circadian day……..78

Figure 3.15. Biological clock genes within IgA+ PCs oscillate over the circadian day……79

Figure 4.1. Diurnal oscillations of expression of core biological clock genes in the liver and small intestines……..86

Figure 4.2. Core biological clock genes oscillate in IgA+ PCs, but are variably rhythmic in IgD+ B cells, over the circadian day……..88

Figure 4.3. Characterisation of a mouse model of B-cell specific *Arntl* (Bmal1) deletion……90

Figure 4.4. Sustained oscillations in faecal sIgA in the absence of PC Bmal1……91

Figure 4.5. Altered temporal expression of genes associated with the cell-intrinsic clock, PC function and metabolism in in *Mb1-Cre*$^{+/-}$ x *Arntl*$^{flox/flox}$ mice……..93

Figure 4.6. The pIgR does not drive oscillations in intestinal sIgA……94

Figure 4.7. Sustained oscillations in faecal sIgA in the absence of SCN Bmal1……95

Figure 4.8. Inverting the feeding schedule reverses the rhythmic profile of sIgA……96

Figure 4.9. No differences in small intestinal IgA+ PCs, or T and B cell subsets within the Peyer's patches, during feeding or fasting……98

Figure 4.10. Inverting the feeding schedule alters the expression of core-clock genes in IgA+ PCs and peripheral tissues……..100

Figure 4.11. IgA+ PCs uptake more glucose but have similar glycolysis rates to B cells……102

Figure 4.12. IgA+ PCs uptake large amounts of amino acids via the LAT1 transporter……104

Figure 4.13. IgA+ PCs contain more lipids than B cell precursors……106

Figure 4.14. No time of day differences in the capacity of IgA+ PCs to take up nutrients, metabolise glucose via glycolysis, or in the lipid content of cells……..108

Figure 4.15. No difference in the capacity of small intestinal IgA+ PCs to take up nutrients during feeding or fasting……110

Figure 4.16. Modulation of metabolic substrate availability alters the magnitude of IgA secretion *in vitro*……111

Figure 4.17. Metabolic parameters of mice on a high fat diet……112

Figure 4.18. A high fat diet is associated with elevated intestinal sIgA and loss of diurnal oscillations in intestinal sIgA……113

Figure 4.19. A high fat diet is associated with a reduced frequency and number of IgA+ PCs in the small and large intestines……..114

Figure 4.20. Altered sIgA rhythmicity in mice fed a high protein diet……116

Figure 5.1. Characterisation of the IgMi mouse……123

Figure 5.2. No difference in the amount of faecal bacteria bound by IgA over the course of the day…125

Figure 5.3. Similarities in alpha and beta diversity of faecal and colonic bacteria in IgMi and WT littermate control mice……..126

Figure 5.4. The composition of commensal bacteria is similar in the colon and faeces of IgMi and WT littermate control mice……..127

Figure 5.5. Altered diurnal oscillations of intestinal commensal bacteria in IgMi mice……..129

Figure 5.6. Alterations in compositional diurnal oscillations of intestinal bacteria in IgMi mice……..131

Figure 5.7. Representative plots of retained oscillations of intestinal bacteria in IgMi mice……..132

Figure 5.8. Relative abundance of Helicobacter, Akkermansia and Lactobacillus over the experimental timepoints in WT and IgMi mice……..133

Figure 5.9. Similarities in the composition of intestinal bacteria in IgMi and WT mice over the experimental timepoints……..134

Figure 5.10. Loss of functional diurnal oscillations of intestinal bacteria in IgMi mice……136

Figure 5.11. Loss of rhythmicity of microbial glycolysis and gluconeogenesis in IgMi mice……132

Figure 5.12. Loss of rhythmicity of microbial metabolic enzyme activity in IgMi mice……139

Figure 5.13. Gain of rhythmicity of pathways relating to extrachromosomal circular DNA and flagellum assembly in IgMi mice……139

Figure 5.14. Dysregulation of circadian metabolites in the absence of mucosal antibody……141

Figure 5.15. Loss of oscillatory serum glucose in the absence of IgA……141

Figure 6.1 Summary figure……..148

LIST OF TABLES

Table 1. Antibodies and fluorochromes used for flow cytometry analysis……46

Table 2. Primers/ probes used for RT-PCR analysis……50

ABBREVIATIONS

AID	Activation-induced cytidine deaminase
APC	Antigen presenting cell
APRIL	A proliferation inducing ligand
BAFF	B cell activating factor
BCH	2-amino-2-Norbornanecarboxylic Acid
BCR	B cell receptor
Blimp1	B-lymphocyte-induced maturation protein 1
Bmal1	Brain and Muscle Arnt-like 1
CCR	Chemokine receptor
CDC	Conventional dendritic cell
CD	Cluster of differentiation
CLOCK	Circadian Locomotor Output Cycles protein Kaput
CSR	Class-switch recombination
CTLA-4	Cytotoxic T-lymphocyte-associated protein 4
CXCR	Chemokine receptor
DC	Dendritic cell
DEG	Differentially expressed gene
2DG	2-Deoxy-D-glucose
ECAR	Extracellular acidification rate
FACS	Fluorescence-activated cell sorting
FDR	False discover rate
FKPM	Fragments Per Kilobase of transcript per Million mapped reads
FoxP3	Forkhead box P3
GALT	Gut-associated lymphoid tissue
GC	Germinal centre
GF	Germ free
GI	Gastrointestinal
GM-CSF	Granulocyte-macrophage colony-stimulating factor
GO	Gene ontology
HFD	High fat diet
Hk2	Hexokinase 2
IEC	Intestinal epithelial cell
Ig	Immunoglobulin
IL	Interleukin
ILC	Innate lymphoid cell
ILF	Isolated lymphoid follicle
IRF-4	Interferon Regulatory Factor 4
LAT1	L-type / large neutral amino acid transporter 1
LP	Lamina propria
MFI	Mean fluorescence intensity
MHCII	Major histocompatibility complex II
mLN	Mesenteric lymph node
mTOR	Mechanistic target of rapamycin

2NBDG	2-(N-(7-Nitrobenz-2-oxa-1,3-diazol-4-yl)Amino)-2-Deoxyglucose
PC	Plasma cell
PP	Peyer's patch
pIgR	Polymeric immunoglobulin receptor
RA	Retinoic acid
RORα	Retinoic acid receptor-related orphan receptor
SCFA	Short-chain fatty acids
SFB	Segmented filamentous bacteria
S1PR1	Sphingosine-1-Phosphate Receptor 1
SREBP-2	Sterol regulatory element binding protein 2
TACI	Transmembrane activator and CAML interactor
TCR	T-cell receptor
TD	T-dependent
TfH	T-follicular helper cell
TfR	T-follicular regulatory cell
TGFβ	Transforming growth factor-β
Th	T helper
TI	T-independent
Treg	T regulatory
Xbp1	X-box binding protein

ABSTRACT

The intestinal immune system provides protection from potential pathogens and promotes beneficial interactions with the commensal microbiota. In turn, the commensal microbiota confers protection to the host from invading pathogens and plays a major role in producing diet-derived nutrients which are essential for host development and survival. Dysregulated immune responses towards commensal microbes manifest in a wide variety of inflammatory and metabolic disorders. Thus, immune regulation of the intestinal microbiota is closely linked with mammalian health and metabolism. However, the pathways governing this relationship are incompletely understood.

Intestinal plasma cells produce several grams of immunoglobulin (Ig)A each day, which promotes mutualism with the commensal microbiota and intestinal homeostasis. The constitutive production of large quantities of IgA suggests that significant metabolic resources may be utilised to maintain mucosal antibody responses. To minimise metabolic cost, several biological processes are imprinted with rhythmicity over the 24-hour (circadian) day. Peak responses align with the time of greatest exposure to environmental challenge and/ or nutrient resources, to maximise the response around the time of greatest need.

Whether intestinal IgA responses are imprinted with circadian rhythmicity in the steady state is not known. We hypothesised that IgA-mediated regulation of the microbiota is subject to temporal entrainment by circadian cues. We further postulated that dysregulation of rhythmicity in mucosal antibody secretion could have important consequences for host metabolism.

Here, I found that intestinal plasma cell-intrinsic IgA secretion exhibits circadian rhythmicity, which was subject to entrainment by dietary-derived metabolic cues and a cell-intrinsic circadian clock. Moreover, I found that compositional and functional oscillations in the intestinal commensal microbiota, and microbial metabolites, are altered in the absence of mucosal antibodies, suggesting that IgA may in part entrain circadian rhythmicity of the microbiota and nutrient availability. Together, these data suggest a previously unappreciated circadian dialogue exists between dietary cues, IgA and the commensal microbiota. This has clinical implications for furthering our understanding of the progression of human metabolic diseases, which are recognised to associate with circadian misalignment.

DECLARATION

No portion of the work referred to in the thesis has been submitted in support of an application for another degree or qualification of this or any other university or other institute of learning.

Hugo Penny

04/06/2021

COPYRIGHT STATEMENT

EXPERIMENTAL CONTRIBUTIONS

Experiments were designed, performed and analysed by myself with significant input from my supervisor, Dr Matthew Hepworth. Dr Julie Gibbs and Professor Richard Grencis provided additional layers of support and knowledge in helping me design and analyse results. Members of the Hepworth group, including Dr Felipe Melo-Gonzalez, Dr Maria Krauss, Dr Rita Domingues and Suzie Hodge helped with sample collection and acquisition/ processing. Members of the Veiga-Fernandes group (Professor Henrique Veiga-Fernandes; Champalimaud Research, Champalimaud Centre for the Unknown, Portugal), helped collect faecal samples from the Camk2a-cre mouse model. The RNA-sequencing sample acquisition and analysis was performed by Novogene (UK) Company Limited, Cambridge, UK. The 16S rRNA sequencing data was generated by the University of Manchester Genomic Technologies Core Facility. Dr. Rachel Scholey of the Bioinformatics and Genomic Technologies Core Facilities for provided support with the analysis of the 16S data. The shotgun metagenomics data was generated and analysed by CosmosID, Rockville, USA. The metabolomic data was generated by the Swann group (Professor Jonathan Swann, University of Southampton, UK).

ACKNOWLEDGEMENTS

My three-year Clinical PhD Fellowship would not have been possible without the continued support and patience of my family and all members of the Hepworth lab. Special mention to Dr Matthew Hepworth who has been a guiding light through the planning, implementation, execution and data assimilation stages of my PhD. Dr Felipe Melo-Gonzalez, Dr Maria Krauss and Dr Rita Domingues have also contributed significant time and energy in training me on the range of assays used herein, as well as driving forward aspects of this research. Special mention also to Professor Richard Grencis, who gave me the opportunity to do this research in the first instance.

1.0 GENERAL INTRODUCTION

1.1 The intestinal barrier

Barrier sites comprise a complex network of cells which include the skin, lungs and gastrointestinal (GI) tract. Collectively, these sites have fundamental roles in UV protection, gas exchange and nutrient absorption and act as a first line of defence against external pathogens [1]. However, these barrier sites – particularly the intestinal tract – also foster mutualistic interactions with commensal microbes which are important for host development and survival [2]. Disruption in the integrity or homeostatic function of these tissues can lead to a wide range of chronic inflammatory diseases both locally within barrier tissues, such as psoriasis [3], asthma [4] and inflammatory bowel disease (IBD) [5], as well as malignancy [6], and diseases at peripheral sites, including the joints [7], brain [8], pancreas [9], liver [10] and heart [11]. Thus, the maintenance of homeostasis at barrier sites is essential for mammalian health.

The GI tract comprises one of the largest mucosal barrier sites in the body and is primarily responsible for dietary nutrient and water absorption [12]. The length of the intestines is colonised from birth by a microbial community consisting mainly of bacteria, but can also include fungi, viruses and archea [13, 14]. The proximal small intestine has a relatively low density of microorganisms, while densities increase down the length of the GI tract and peak at around 10^{14} in the large intestines [15, 16]. The commensal microbes within the intestines fulfil a critical role in the metabolism of dietary components, and in providing signalling cues that promote the development and maturation of immune cells both within the intestines and systemically throughout the body [17-20]. Thus, for the host to maintain health, a highly regulated response must prevent inflammation and promote mutualism towards beneficial commensal microbes, and also provide effective protective immunity against pathogens [21].

Host surveillance and tolerance of the microbiota is largely mediated by the intestinal immune system [22]. The intestinal epithelial cell (IEC) layer, as well as the organised mucus layers and secreted antimicrobial peptides, also fulfil important roles in both host protection and fostering the colonisation of beneficial microbes – the mucus layer physically segregates bacteria from the epithelium to minimise contact and antimicrobial peptides act to prevent microbial residence within the mucus and control the balance of the species present within the niche [23, 24]. In this manner, the epithelial barrier, mucus layer and intestinal immune system act in concert to maintain GI homeostasis [25].

Importantly, failure to maintain mutualistic and tolerogenic immune responses towards gut commensal microbes can adversely impact mammalian health [26]. Indeed, human and murine studies have shown that loss of immunoregulatory mechanisms within the GI tract are linked with the development of IBD [27] and colorectal cancer [28], as well as peripheral and systemic disease, including rheumatoid arthritis [29], neurodegenerative disease [30], chronic liver disease [31, 32] and metabolic disorders such as obesity, diabetes and atherosclerosis [11, 33, 34]. Moreover, while dietary components themselves do not cause disease, failure to maintain regulatory immune responses towards dietary antigens can lead to the development of food allergy and coeliac disease [35, 36]. These conditions are common and debilitating and have been shown to have significant impact on the quality of life, morbidity and mortality of sufferers [37-42]. Thus, it is important to understand the mechanisms that promote and maintain immune tolerogenic responses towards beneficial gut microorganisms, and dietary antigens, to enable better identification, treatment and in some cases prevention, of a wide range of human diseases.

1.2 Orchestration of tolerance and GI homeostasis by the intestinal immune system

Under steady state conditions, the intestinal immune system generates a multitude of immune responses tasked with inducing a state of tolerance and mutualism, while regulating and suppressing inflammatory responses towards commensal microbes and dietary antigens [22]. Collectively, these responses maintain tissue health and homeostasis within the GI tract. Cells of the immune system which are primarily responsible for generating these responses include dendritic cells (DCs), group 3 innate lymphoid cells (ILC3s), CD4+ T cell subsets (especially regulatory T cells [Tregs] and T helper 17 [Th17] cells) and B lymphocytes.

Dendritic cells: Dendritic cells (DCs) comprise two major subsets – conventional (c)DCs and plasmacytoid DCs [43]. CDCs are the major antigen presenting cell (APC) within the intestines [44]. They are present within gut-associated organised lymphoid tissue (GALT) such as the Peyer's patches (PPs) and mesenteric lymph nodes (mLN), as well as the intestinal lamina propria (LP) of the small and large intestines [45]. CDCs continuously acquire antigens from the gut lumen via several different mechanisms, including goblet cell-associated antigen passages [46], via specialised microfold cells (M) cells which are present within the epithelium overlying PPs [47], or indirectly from non-migratory macrophages (expressing CX_3CR_1), which sample intestinal antigens by extending trans-epithelial processes into the lumen [48].

Soluble materials that have crossed the epithelium by paracellular or transcellular routes may also be sampled by DCs residing within the LP [49].

Antigen-loaded DCs typically migrate to areas within organised lymphoid tissue that are rich in naïve lymphocytes, such as the T cell zone within the mLN, which is densely populated with naïve CD4+ T cells [50]. At these sites, antigen presented on Major Histocompatibility Complex (MHC) class II on APCs can bind to the T-cell receptor (TCR) expressed on the surface of naïve CD4+ T cells, which, in conjunction with co-stimulatory signals, leads to T cell activation and polarisation towards a specific subset [44]. During activation, DCs imprint the ability of lymphocytes to home to the intestines by inducing the expression of gut homing receptors, such as the pan-gut homing receptor α4β7, and the small intestine-specific receptor CCR9 [51-53].

CD4+ T cells: Naïve CD4+ T cells can differentiate towards several different subtypes upon antigen-specific interactions with DCs or other APCs. The major cell subsets include Th1, Th2, Tregs, T follicular helper (TfH) cells and Th17 cells [54]. The function and phenotype of each subtype is determined by a different transcription factor – induced by APC-derived cues – meaning differentiated T cells acquire the capacity to respond to different infections or inflammatory stimuli, and are functionally distinct from one another [54].

Th1 cells express the major intracellular transcription factor Tbet and primarily produce pro-inflammatory cytokines (such as interferon-γ, tumour necrosis factor-α and lymphotoxins, among others) which are responsible for the control of intracellular pathogens such as viruses and bacteria [55]. In contrast, Th2 cells express GATA3 and produce cytokines including IL-4, IL5 and IL-13 which contribute to tissue regeneration and repair, as well as defence against extracellular pathogens such as helminths [56].

Tregs, on the other hand, express the transcription factor FoxP3 and have a critical role in maintaining GI tolerance and homeostasis by modulating innate and adaptive immune responses [57]. This is illustrated in individuals with immune dysregulation polyendocrinopathy enteropathy X-linked (IPEX) syndrome, which is caused by loss of function mutations in the FoxP3 gene, who develop a broad clinical phenotype including a severe enteropathy, often with fatal consequences [58]. The regulatory Treg response is largely mediated via the local production of cytokines such as IL-10 [59], TGF-β [60] and IL-35

[62], as well as cytotoxic T-lymphocyte-associated protein 4 (CTLA-4) [61] expression, which have a suppressive effect on inflammatory effector T cell differentiation, cytokine responses and proliferation [63]. Treg-derived cytokines such as transforming growth factor-β (TGF-β) can also modulate the generation of antibody (humoral) responses towards the commensal microbiota [64]. As will be discussed further, immunoglobulin (Ig)A responses towards gut microbes play an increasingly appreciated role in fostering the colonisation of an appropriately diverse microbial community within the intestines [65-67] and are also an important component of host protective immunity against foreign pathogens in the GI tract [68].

Furthermore, a subset of Tregs, called T follicular regulatory cells (TfR), indirectly regulates gut humoral responses by modulating another subset of CD4+ T cells – TfH cells – within organised lymphoid tissue [69]. TfH cells themselves are present within the PP and mLN at sites close to clusters of naïve B cells called B cell follicles [70]. From here, TfH cells can form cognate TCR-MHCII interactions with activated B cells and provide survival and co-stimulatory signals which 'help' B cells to differentiate into antibody secreting plasma cells (PCs) [71].

Naïve CD4+ T cells can differentiate into TfH cells in the presence of DC-derived signals during antigen presentation [72, 73], but can also be derived from Th17 cells [74]. Th17 cells themselves express retinoic acid receptor-related orphan receptor (ROR)γt and differentiate in response to APC-derived cues [75], as well as those derived from commensal microbes such as segmented filamentous bacterium (SFB) [19, 76]. Th17 cells fulfil key roles in promoting barrier function via the secretion of cytokines such as IL-17 and IL-22 [77, 78]. For instance, IL-17 indirectly acts to modulate gut microbes via the regulation of AMPs and the polymeric immunoglobulin receptor (pIgR) [79, 80], which is the major transport mechanism that delivers IgA into the intestinal lumen [81]. Notably, however, both protective and pathogenic roles for IL-17 have been demonstrated both in experimental models of colitis and in patients with IBD [82-84]. Th17 cells also produce IL-22 which acts to reinforce the epithelial barrier in part through the maintenance of crypt stem cells which give rise to IECs [85-87], as well as via promoting differentiation of mucous producing goblet cells and inducing antimicrobial peptide production [88]. Furthermore, IL-22 induces the regulation of the epithelial enzyme fucosyltransferase 2, which promotes the addition of fucose residues to epithelial glycans

which can be utilised by beneficial gut commensals as an energy source to enhance their colonisation resistance within the intestinal niche [89].

ILC3s: The major source of IL-22 within the intestines are ILC3s. ILCs are family of tissue-resident effector lymphocytes that respond rapidly to host, microbial or environmental stimuli to promote immunity, wound healing or tissue homeostasis [90]. ILCs comprise several distinct subsets that are subdivided into distinct groups based on transcription factor expression and cytokine production that mirror the effector profiles of Th cells [91]. In this manner, major ILC subsets include T-bet+ IFN-γ producing group 1 ILCs, GATA-3+ IL-5 and IL-13 producing group 2 ILCs and RORγt+ IL-17 and IL-22 producing ILC3s, which mirror Th1, Th2 and Th17 cells respectively [91, 92].

Aside from their ability to produce IL-17 and IL-22, ILC3s also promote mutualistic and tolerogenic responses in the gut via direct or indirect interactions with the adaptive immune system [93]. In this manner, ILC3s have been shown to promote negative selection of commensal-reactive effector T cells in the gut, through establishing MHCII:TCR interactions which lead to activation of apoptotic programming in commensal-specific effector T cells [88]. In addition, ILC3s integrate signals from macrophages to produce granulocyte-macrophage colony-stimulating factor (GM-CSF) which supports the differentiation of Treg cells by DCs [94]. As well as modulating T cell responses, ILC3s can also regulate the generation of IgA antibody responses [95-97]. In this manner, interactions between ILC3s and TfH cells at the interfollicular border of the mLN modulates the production of IgA antibodies towards gut commensals [98]. Moreover, interactions between ILC3s and stromal cells are critical for the formation of lymphoid aggregates called cryptopatches, which develop shortly after birth at the bottom of the crypts within the intestinal LP [17, 97]. Cryptopatches can give rise to more organised lymphoid structures called isolated lymphoid follicles (ILFs) in response to signals derived from the commensal microbiota [96], which serve as activation sites for B cells and the generation of IgA antibody responses towards commensal microbes [95-97].

B cells: B cells are a population of lymphocytes which mediate the production of antibodies [99]. Antibodies can either be surface expressed and act as the B cell antigen receptor (BCR), or be secreted in soluble form and bind foreign antigens during homeostasis [99].

Within in the intestines, antigen-naïve mature B cells typically reside within the GALT such as the PPs, mLNs and ILFs [100]. They express IgM antibodies on their cell surface which act as the BCR [101, 102], although IgD antibodies can also be surface expressed [102-105]. Antigen binding the BCR leads to B cell activation and maturation towards short-lived antibody-secreting plasmablasts and, in turn, fully differentiated antibody-secreting PCs [101]. During the early stages of B cell activation, class switch recombination (CSR) occurs, whereby B cells switch the subclass (isotype) of antibody they produce from IgM to IgD, IgG, IgE or IgA [103]. The Ig isotype selected depends on the nature of the antigen, as well as the presence of cytokines produced within the local microenvironment, and determines the effector profile of the antibody [106].

Within the GI tract, IgA is the most abundant antibody isotype produced, with around 80-90% of the PCs within the intestinal LP producing IgA antibodies in the steady state [107]. IgM- and IgG-secreting PCs can be found within the intestines at steady state, albeit at lower frequencies than IgA-secreting PCs, whereas IgD and IgE secreting PCs are scarcely found within the intestines in health [108]. The number of IgA+ PCs in the intestines actually outnumbers the total number of PCs present in health in the rest of the body combined [107], which results in the production of around 3 to 5 grams of intestinal IgA per day [109]. Together with recent evidence which demonstrates that PCs have elevated metabolic requirements and activity [110, 111], suggests that the body commits significant metabolic (energetic) resources towards the abundant production of intestinal IgA during homeostasis [100].

Intestinal IgA has an established role in re-enforcing the epithelial barrier against invading pathogenic microbes via mechanisms which enhance pathogen clearance from the gut [112-114]. However, a significant proportion of the intestinal commensal microbiota are bound by IgA in the steady state [66, 115-117] and it is increasingly appreciated that IgA targeting commensal microbes helps foster mutualism and their appropriate colonisation of the gut both in early life and throughout adulthood [118-121]. It is widely regarded that the microbiota itself is a critical determinant for intestinal and systemic health and metabolism [65, 122-125], suggesting that intestinal IgA responses towards commensal microbes may have broad consequences for host health.

In summary, within the GI tract, immune cells execute distinct and complementary functions that together suppress inflammation and tissue damage towards gut-luminal antigens,

maintain the integrity of the intestinal epithelial barrier and promote the appropriate colonisation of a beneficial microbial community. Collectively, this promotes mutualism and tolerance towards commensal microbes and GI homeostasis [25]. IgA-mediated regulation of the commensal microbiota is a topic of great recent interest. However, much remains unclear about how IgA regulates the composition and function of the gut microbiota in homeostasis. The increasingly appreciated role that the gut microbiota has on health, alongside the mounting evidence that IgA directly interacts with and regulates the gut microbiota, underscores the requirement to better understand intestinal IgA responses towards intestinal commensals. Doing so, may provide further insights into how microbial mutualism impacts host health and metabolism.

1.3 The generation and maintenance of intestinal IgA responses

1.3.1 The origins of intestinal IgA responses

There are two principal classes of B cells in mice and humans – B1 and B2 B cells [108]. B2 B cells develop from common lymphoid progenitors of haematopoietic stem cells within the bone marrow in response to signals released from stromal cells [126]. Conventionally, B2 B cells differentiate into PCs with help from TfH cells in organised lymphoid structures, such as the PPs and mLNs in the intestines [127, 128]. Interactions between CD40 and CD40 ligand on the surface of TfH and B cells, as well as TfH-derived IL-21, encourages CSR and the formation of a germinal centre (GC) within the B cell follicle of the lymph node [129, 130]. Within the GC, B cells undergo multiple rounds of proliferation, Ig gene mutation and positive and negative selection based on their affinity towards the presented antigen [131-134], termed somatic hypermutation, which results in a B cell pool that produces antibodies with high affinity towards specific antigens, such as soluble proteins [135]. T-cell dependent (TD) B cell activation in this manner typically leads to the generation of PCs that secrete high affinity antibodies towards specific protein antigens, as well as the generation of memory B cells [66, 136].

By contrast, B1 B cells reside within the peritoneal cavity [137] and develop from precursors that originate either within the bone marrow – B1b B cells – or are a self-renewing population that originate in the foetal liver – B1a B cells [138, 139]. B1 B cells typically differentiate into PCs in the absence of T cell help, so-called T-cell independent (TI) B cell activation [140]. In

this instance, local production of B cell survival and antibody generating factors such as TGF-β, lymphotoxin, B cell activating factor (BAFF) and a proliferation inducing ligand (APRIL), by connective tissue stromal cells, IECs, ILC3s and/ or DCs, drives B cell differentiation into PCs [97, 141-143]. TI B cell activation typically occurs in the absence of GCs and produces PCs that secrete polyreactive antibodies with low affinity for non-protein antigens, such lipopolysaccharides present within the cell wall of microbes [144, 145].

The specific contributions of each subset of B cells to the intestinal IgA+ PC pool is unclear [146]. However, recent work has demonstrated that IgA responses towards the commensal microbiota typically originate from bone marrow derived B1b and B2 B cells, in both a TI and TD manner [66].

1.3.2 IgA class switch recombination

The basic structure of a single antibody molecule consists of two Ig light (IgL) and two Ig heavy (IgH) chains linked by disulphide bonds (Figure 1) [147]. Each chain contains a *variable* (V) region and a *constant* (C) domain [148]. The antigen-binding fragment region (Fab) of the antibody molecule comprises the terminal end of the IgL and IgH chains [149]. The fragment crystallizable (Fc) region is composed solely of the C domains of the IgH chain and confers the isotype and effector function of the antibody.

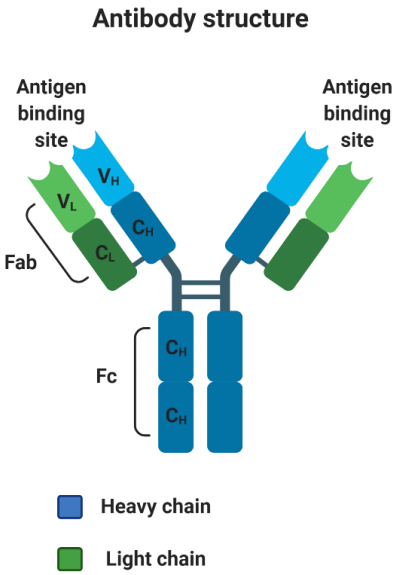

Figure 1. The basic structure of a single antibody molecule (adapted from [149]). Each antibody molecule consists of two light (IgL) and two heavy (IgH) chains linked by disulphide bonds. Each chain contains a *variable* (V) region and a *constant* (C) domain; the IgL chain contains only a single V and C domain, whereas the IgH chain contains a single V region and three or four C domains. The antigen-binding fragment region (Fab) of the antibody molecule is composed of the terminal end of the IgL and IgH chains. The fragment crystallizable (Fc) region which confers the effector function of the antibody molecule is composed solely of C domains. Image generated with BioRender.

During CSR, the genes encoding the C domain of the IgH chain are switched from Cμ and Cδ, which encode IgM and IgD, to Cγ, Cε, or Cα, which encode IgG, IgE or IgA, respectively [150]. Central to all CSR is the expression of activation-induced cytidine deaminase (AID) by the activated B cell, as mice with deletion of the AID gene (*Aicda*) [151], or individuals who have loss of function mutations in *Aicda* [152] (Hyper-IgM Syndrome Type 2), have defective CSR and are only able to produce IgM antibodies.

Induction of AID expression typically requires activation of B cells by antigen binding the BCR and cell proliferation [153], as well as IL-4, IL-21 and CD40 signalling [130, 154-156], the latter two of which are provided by TfH cells [157]. In the absence of T-cell interactions, local production of BAFF and APRIL by DCs or ILC3s can induce AID expression within B cells, by binding to their respective B cell surface receptors, which include the BAFF receptor, B cell maturation antigen (BCMA) or transmembrane activator and calcium-modulating cyclophilin-ligand interactor (TACI) [158-161]. The AID enzyme introduces DNA breaks into specific regions of the IgH locus called switch regions [68, 151, 162, 163]. Repair of these breaks leads to rearranging of the IgH C domains from Cμ and Cδ, to Cγ, Cε, or Cα [164].

The class of antibody isotype that results from CSR is determined by the integration of multiple inputs by the B cell including the type of antigen and local production of growth factors and cytokines [71]. Within the GALT, the presence of cytokines such as TGFβ [165-167], IL-10 [168] and IL-21 [169], have been implicated in directing CSR towards IgA [71]. Of particular importance is TGFβ, as mice deficient for the TGFβ receptor on B cells have almost complete loss of all IgA responses [165]. TGFβ is produced locally by antigen-loaded DCs and/ or Tregs within the intestines [64, 143]. DCs are also a local source of vitamin A-derived retinoic acid (RA) which can enhance TGFβ-induced Cα transcription [168, 170].

ILC3s modulate the presence of DCs within the GALT via expression of membrane bound lymphotoxins [143] and can also regulate inducible nitric oxide synthase (iNOS) expression by DCs, which can promote TI IgA production possibly via regulation of TGF-β receptor expression on B cells [142, 159]. TfH cells and/ or ex-Th17 cells, which can adopt a TfH cell phenotype within the PPs [74], can also induce IgA responses via the production of IL-21 [169] and TGFβ, the latter of which has been shown to have a co-operative effect alongside CD40L on generating TD IgA responses [166, 167]. Moreover, the local production of BAFF and APRIL by ILC3s, T cells, DCs, as well as other cells, such as IECs, also enhances CSR towards IgA [141,

158-161, 171]. Therefore, under steady state conditions, immune and non-immune cells within the intestines produce cytokines and growth factors which direct CSR within the activated B cell towards the IgA isotype.

1.3.3 Somatic hypermutation and affinity maturation within the GALT

Following activation and the initiation of CSR, B cells differentiating in a TD manner typically expand to form the GC around specialised antigen-loaded stromal cells called follicular DCs (fDCs) [172]. This process is dependent on CD40L:CD40 interactions between TfH and B cells respectively, as blocking this interaction disrupts the formation of GCs in PPs [173, 174]. The GC is organised into distinct components called the 'light' and 'dark' zones [172]. B cells within the dark zone undergo rapid proliferation during which random mutations are introduced into the IgH and IgL chains [175]. Following this, B cells with random clonal variants transition to the light zone [175, 176] where fDCs and TfH cells provide positive selection signals including BAFF and TGFβ to B cells with BCRs demonstrating high affinity for the antigen [177]. These cells then shuttle back towards the dark zone where they undergo further expansion and SHM, before transitioning back towards the light zone to repeat the process [178]. It is thought that several rounds of SHM and affinity-based selection and maturation occur before B cells exit the GC to develop into memory B cells or proliferative plasmablasts [178]. A subset of FoxP3+ Tregs present within the lymphoid tissue called TfR cells [179] evolve as the GC is developed and regulate the magnitude of the output of the GC response, in part by supressing IL-4 and IL-21 production by TfH cells [180]. Modifying the rearranged Ig sequences in this manner enables B cells expressing antibodies with high affinity variants for the antigen to be selected and undergo expansion and maturation into either plasmablasts and subsequently PCs that secrete high affinity antibodies for specific antigen, or into memory B cells that retain specificity for the antigen over the long-term [172].

B cell responses towards foreign pathogens and model protein antigens demonstrate typical TD B cell differentiation with SHM and affinity maturation within the GALT as part of the initial immune response [181]. However, the mechanisms governing IgA responses towards commensal microbes under homeostatic conditions are less well defined. On the one hand, GCs are continuously present in the PPs – the primary site for IgA production against commensal microbes in the steady state [174] – and commensal-reactive IgA antibodies are often highly mutated [182], suggesting that IgA responses towards the microbiota are derived

from TD B cell differentiation [66, 136, 183]. However, SHM in GC PP B cells has been demonstrated in mice that are deficient of their BCR [184], suggesting that PP B cells can enter the GC reaction in the absence of cognate antigen recognition, and thus without T cell help [145]. In line with this, PP GCs were able to form independently of T cells [185] and IgA targeting commensal microbes is almost entirely preserved in the absence of T cells [66]. Therefore, to account for these findings, it has been suggested that commensal-reactive IgA likely represents both polyreactive/ non-antigen specific responses [66, 183], and specific IgA responses that may result from a progressive process of repeated rounds of affinity B cell selection in constitutively active GCs over time [186].

1.3.4 The maintenance of plasma cell responses

B cells that have undergone differentiation via TD/ TI programmes exit the lymph node as plasmablasts in a S1PR1-dependent manner [187]. Plasmablasts migrate in lymphatic vessels via the thoracic duct into the circulation where they circulate towards different tissue niches depending on the presence of chemokines imprinted within the cell during their differentiation [168, 169, 188]. The presence of CCR9 directs the cells towards the small intestinal LP, while the presence of CCR10 directs them towards the colonic LP [53, 189]. The specific point at which dividing plasmablasts become post-mitotic terminally differentiated PCs is unclear, but coincides with downregulation of canonical B cell transcription factors such as Pax-5 [190] and upregulation of the major PC transcription factor B lymphocyte-induced maturation protein-1 (Blimp-1) [191]. Along with Interferon Regulatory Factor 4 (IRF-4) and X-box binding protein 1 (Xbp1), Blimp-1 regulates pathways that enable appropriate PC secretory function and metabolism [191-199].

The bone marrow and spleen are typically considered as the primary tissue niches that support long-term PC responses [200]. Within these tissues, PCs have access to pro-survival signals such as APRIL and BAFF which support their survival [201], along with locally derived cytokines including IL-4, IL-5, IL-6, and signalling via PC surface expressed CD44, CD93, CD138 and CD28 [202-206]. In addition, recent work has shown that the ability of bone marrow and splenic PCs to uptake key nutrients such as glucose and amino acids is an important determinant of their secretory capacity and survival [110, 111].

Studies using radioactive isotopes [207], flow cytometry to detect antigen-specific PCs [208], or auxotrophic bacterial mutants [209] have identified the presence of long-lived PCs within the intestines of mice. In line with this, carbon dating studies have identified that PCs can persist for more than two decades in the human small intestines [210]. These findings indicate that the intestines can also support long-term PC responses. Interestingly, the small intestines are the major site of dietary nutrient exposure and absorption within the body. While dietary factors such as microbial-derived short-chain fatty acids (SCFAs) [211], vitamin B1 [212] and lipids [122] have been shown to modulate IgA+ B cell and PC responses within the gut, the regulation of intestinal IgA+ PC function by nutrient cues is not fully understood.

1.3.5 IgA structure and subtypes

Unlike other antibody isotypes, IgA exists in multiple forms within different anatomical compartments throughout the body [108]. Mucosal secretory (s)IgA is typically produced in dimeric form, whereas circulating IgA is composed mainly of monomers [108]. Dimeric IgA is assembled prior to secretion by PCs by linking monomeric Igs via a polypeptide synthesised by PCs, called the joining (J) chain (Figure 2) [213, 214]. Following secretion, the J chain of dimeric IgA interacts with the pIgR at the basolateral surface of the intestinal epithelium [215]. Dimeric IgA is subsequently transcytosed across the epithelium and released into the intestinal lumen along with the cleaved pIgR ectodomain, which forms the secretory component that enwraps the IgA molecules and completes the secretory sIgA complex [216]. The secretory component confers mucophilic properties to the antibody complex and may also enable interactions with the microbiota [217].

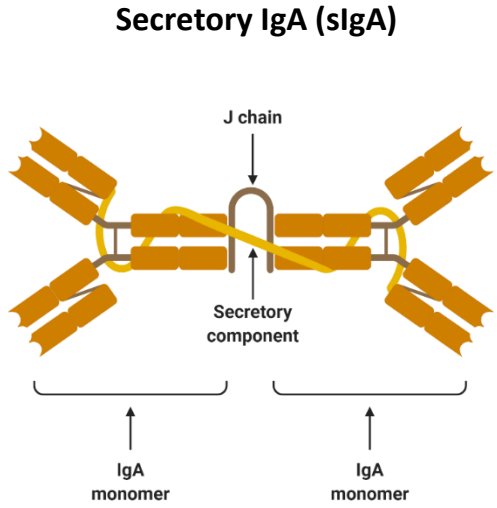

Figure 2. The secretory (s)IgA complex (adapted from [108]). IgA monomers are attached by a joining (J) chain. The ectodomain of the polymeric immunoglobulin receptor ensheaths the dimeric IgA complex following successful transport across intestinal epithelial cells, to form sIgA. Image generated with BioRender.

A major fundamental difference in the IgA system of mice and humans is that there are two subclasses of human IgA, IgA1 and IgA2, while only one subtype in mice [147]. These human subtypes differ in the structure of their hinge region and in the number of glycosylation sites [218], which confer different functional properties to these subtypes. Structural differences in the hinge region of IgA2 make is less susceptible to degradation by proteases [219] and the glycosylation of profile of IgA2 renders it more pro-inflammatory than IgA1 [220]. Systemic IgA is enriched for IgA1 (around 90% of the IgA monomers), whereas mucosal IgA is composed of both subtypes [108]. However, dominance of IgA1 has been demonstrated in the small intestines and IgA2 in the colon [221], which may be the result of preferential induction of IgA1 responses by dietary protein antigens and IgA2 by conserved microbial products such as LPS [108, 222]. In this respect, regional differences in mucosal IgA responses may be imprinted by their local environment.

1.4 IgA responses towards intestinal bacteria

Intestinal sIgA has an established role in protective humoral immunity against enteric pathogens [223, 224]. This has been studied closely in the context of bacterial infections with *Shigella flexneri, Vibrio cholerae*, *Salmonella typhimurium* and *Enterococcus faecium* [112-114, 225, 226]. These studies have demonstrated that sIgA binding can reduce bacterial motility, or can entrap, or agglutinate, bacteria which facilitates their clearance from the gut [112-114, 225-227]. More recent work in the setting of *non-Typhoidal Salmonellosis* has demonstrated that vaccine-induced sIgA can crosslink dividing bacteria at the point of separation which leads to 'enchained growth' and the generation of clonally-related sIgA-bound bacterial clumps, which facilitates transit from the intestines [114]. Furthermore, sIgA has been shown to neutralise pathogen associated molecular patterns such as LPS during its transport across epithelial cells, leading to a reduction in the development of acute local inflammation [228]. Moreover, sIgA can protect against enteric viral pathogens such as rotavirus and reovirus, by blocking replication and assembly of virus particles during pIgR-mediated transcytosis across the epithelial barrier [229-232]. Thus, sIgA can promote the exclusion, and/ or reduce the pathogenicity, of microbes to promote protective immunity [114].

Aside from binding pathogenic microbes, sIgA also binds intestinal commensal microbes in the steady state [66, 115-117], which is increasingly understood to shape the composition of

the intestinal microbial community [67, 233]. The mechanisms through which sIgA exerts this effect are partially understood. IgA has been shown to promote adherence of certain commensal strains, such as *Bifidobacterium lactis*, *Lactobacillus rhamnosus* [234] and *Bacteroides fragilis* [67], to the surface of cultured epithelial cells by binding capsular polysaccharides on the bacterial cell wall [67]. By binding to these sites, IgA was further shown to enhance colonisation resistance of *Bacteroides fragilis* against competing strains *in vivo* [67]. In addition, non-Fab-dependent interactions between a heavily glycosylated monoclonal IgA and *Bacteroides thetaiotaomicron* was shown to promote its survival within the intestinal niche and cross-fostered the expansion of other beneficial microbes within the colon [65, 235]. By contrast, IgA has been shown to bind conserved epitopes on commensal bacterial flagellins [123, 183, 236], which reduces bacterial motility *in vitro* [236] and thus may accelerate the intestinal clearance of certain commensal microbes *in vivo* [125]. Moreover, sIgA may regulate the composition of the intestinal microbial community by enchained growth of rapidly dividing commensals [114, 237].

Recent work has begun to elucidate the importance of IgA-mediated regulation of the gut microbiota. Preterm infants who do not receive passive transfer of sIgA in maternal milk are at increased risk of necrotizing enterocolitis due to reduced diversity within the developing intestinal microbial community [118]. These findings convey an important role for sIgA in promoting the establishment of an appropriately diverse microbial community during the period of early development. Early life gut microbial dysbiosis has been associated with an increased risk for obesity [238, 239], asthma [240], allergies [240] and inflammatory diseases, such as IBD [241], in later life, suggesting that IgA-mediated regulation of the early microbial colonisation period may be a critical determinant of general health.

Individuals with IBD mount robust IgA responses towards disease driving gut microbes, that have transferable colitogenic potential in GF mice [117]. Similarly, severely malnourished children have reduced IgA binding of beneficial gut commensals [120] and exaggerated IgA responses towards enteropathogenic microbes including the family *Enterobacteriaceae*, that promote the development of diet-dependent enteropathy upon transmission into GF mice [242]. Therefore, aberrant microbiota-reactive IgA responses may contribute to the development of inflammation within the gut. However, it is not clear whether these findings are due to dysbiosis, epithelial barrier disruption and/ or aberrant immune responses in these

individuals [120]. Interestingly, malnutrition itself may drive adaptive changes in the microbiota which may alter the binding ability of sIgA. In this manner, recent data has demonstrated that undernutrition leads to metabolic adaptations of beneficial microbes such as *Lactobacillus*, resulting in impaired sIgA binding and reduced mucosal colonisation [120]. Thus, dietary factors may influence IgA-mediated modulation of the intestinal microbiota [120].

The intestinal microbiota itself generates nutrient metabolites from the diet which exerts an important role in host metabolism. Indeed, faecal microbial transfer from lean or obese twins into GF mice leads to recapitulation of the donor phenotype in the recipient animal [243]. Studies since have shown that obesity and related metabolic disorders such as T2DM are associated with intestinal dysbiosis [244-248]. Interestingly, mice with enhanced anti-flagellar IgA responses that develop following immunisation, have altered microbiota compositions and are protected against diet-induced obesity [123], suggesting that IgA-mediated regulation of the microbiota may modulate metabolic outcomes for the host. In support of this, IgA deficient mice have more impaired glucose homeostasis following high fat diet (HFD) feeding than wild-type control mice [122]. Moreover, mice which lack mucosal antibodies have altered dietary lipid absorption across intestinal epithelium [124] and increased circulating levels of non-esterified fatty acids [125], suggesting that mucosal antibody responses may regulate the local and systemic availability of nutrient metabolites within the host [125].

In summary, several lines of evidence demonstrate that IgA responses targeting commensal microbes modulates the composition of the intestinal microbial community in the steady state. This is increasingly recognised to be important for mammalian health and metabolism and may, in part, explain why the host dedicates a significant metabolic cost to the continuous abundant production of intestinal IgA. Many energetically demanding and constitutive homeostatic processes are regulated by evolutionary mechanisms to regulate biological function over the course of a day in line with its requirement. One way this is achieved in mammals is via circadian (~24 hour) rhythmicity, which may help limit bioenergetic cost by co-ordinating cell responses around temporal changes in environmental cues, or by partitioning their maximal response around the time of greatest need [249]. Below we discuss the emerging evidence for circadian regulation of immunity and provide a rationale that formed the basis of my thesis.

1.5 Circadian rhythmicity within the body

1.5.1 Overview

Multiple physiological processes including sleep/ wake cycles, cardiovascular reflexes, feeding and digestion, energy metabolism and immune cell function, are imprinted with rhythmicity over the 24-hour (circadian) day [250, 251]. This enables the host to anticipate, or adapt to, changing environmental cues, such as light/ dark cycles generated by the earth rotating around its axis, or temporal fluctuations in temperature, food availability or pathogen exposure [249]. In doing so, circadian rhythmicity is thought to provide an evolutionary advantage that favours survival for the host [252], for example through limiting bioenergetic expenditure, or via the temporal partitioning of beneficial responses from detrimental ones [251], although the precise reasons why such a vast number of biological processes oscillate over the circadian day are not fully understood [253].

A major mechanism responsible for regulating these circadian rhythms are biological clocks [254]. These molecular timing systems comprise intracellular mechanisms that generate self-sustained circadian oscillations in a set of specific proteins, called clock proteins [255]. Oscillations in clock proteins, in turn, regulate rhythmic gene expression within cells, which leads to near 24-hour oscillations in a range of biological processes [256]. Biological clock genes are present within nearly all mammalian cells [257]. However, it is increasingly apparent that not all clock systems within cells oscillate [258, 259]. That said, clock gene disruption, or impaired circadian rhythmicity (for example due to shift work, jet-lag, or dietary changes), can lead to adverse metabolic consequences including altered glucose homeostasis [260], diabetes [261] and obesity [262, 263], cardiovascular disease [263], as well as the exacerbation of chronic inflammatory diseases such as IBD [264], and even various types of cancer [265, 266], which underscores the importance that the biological clock system and circadian rhythmicity has on general mammalian health.

1.5.2 The organisation and regulation of biological clocks within the body

Biological clocks oscillate in a cell autonomous manner and can persist in constant conditions and/ or the absence of external stimuli [251, 267]. Therefore, in order to synchronise responses across all levels, biological clocks are entrained by a range of systemic and environmental cues, often referred to as Zeitgebers [268]. Light is the principle Zeitgeber in

mammals [269]. Light signals are detected by retinal ganglionic cells which entrain the master clock, which is located in the supra-chiasmatic nucleus (SCN) of the hypothalamus [270, 271]. In turn, the master clock sends out signals which synchronise oscillations in peripheral clocks within cells throughout the body [268, 270, 271]. The mechanisms through which the master clock mediates its control over peripheral oscillators are not fully understood, but the key pathways involve neuronal signalling, body temperature and the modulation of systemic hormone levels such as glucocorticoids and melatonin [257, 272]. The result is near 24-hour co-ordinated oscillations in cellular functions across different organs, tissues and cells [251, 271, 273].

Feeding, is the other major Zeitgeber in mammals [269]. Feeding behaviour demonstrates clear diurnal rhythmicity in most mammals, with the majority of food consumption occurring during wakefulness [269]. In this manner, nocturnal mice housed under 12hour light:dark lighting schedules with access to food *ad libitum*, consume around 75% of their food during the dark period [274]. Notably, restricting access to food during the light (resting) phase leads to phase inversion (reversal) of peripheral clock oscillators, such as those within the intestines and liver [275-277], but does not alter the phase of oscillation of the master clock [276, 277], demonstrating that feeding cues can uncouple biological clocks within peripheral tissues from signals emitted from the master clock [275-277]. Importantly, feeding-related cues involve numerous complex pathways including behavioural, metabolic and endocrine pathways [255], that may provide additional layers of control of circadian rhythmicity within the body [272], but this is not well understood. Moreover, it is apparent that rhythmic food intake itself can drive rhythmic gene expression in peripheral tissues such as the liver independent of the liver clock [274], highlighting the complex dialogue between light signals, food intake, biological clocks and circadian rhythmicity within the body.

1.5.3 Molecular aspects of the biological clock

The molecular mechanism of the biological clock is considered to be the same throughout the body [251]. At the cellular level, transcriptional-translational feedback loops of molecular clock protein expression drive oscillations in the transcription of clock-controlled genes [251] (Figure 3). At the centre of this, are the core molecular clock proteins *Circadian Locomotor Output Cycles protein Kaput* (CLOCK) and *Brain and Muscle Arnt-like 1* (Bmal1) [278, 279]. CLOCK and Bmal1 (encoded by *Arntl* gene) form a dimer and bind to the binding site E-box,

which leads to the transcription of a broad range of clock-controlled genes [278, 279]. The binding of the CLOCK:Bmal1 complex to the E-box region also leads to the transcription of genes that, once translated, provide negative feedback on the CLOCK:Bmal1 complex, such as Period 1 and 2 (Per1 and Per2) [280], and Cryptochrome 1 and 2 (Cry1 and Cry2) [281], as well as nuclear receptors Rev-erb alpha (Rev-erbα; encoded by *Nr1d1* gene) [282] and RORα, which repress and activate Bmal1, respectively [283]. Over the course of the day, conformational changes in Bmal1, as well as degradation of the period and cryptochrome proteins, leads to loss of inhibition of the CLOCK:Bmal1 complex, which results in the generation of an oscillation in gene transcription [256, 284].

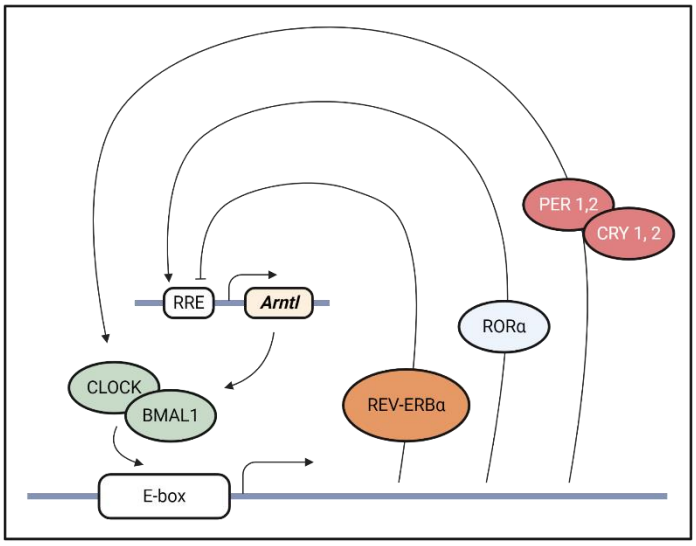

Figure 3. Schematic of the biological clock.

Schematic overview of the core molecular clock (adapted from [269). Core molecular clock proteins *Circadian Locomotor Output Cycles protein Kaput* (CLOCK) and *Brain and Muscle Arnt-like 1* (Bmal1) form dimer and bind to the binding site E-box, which leads to the transcription of a broad range of clock-controlled genes that once translated, either provide negative feedback on the CLOCK: BMAL1 complex such as *Period 1* and *2* (Per1 and Per2) and *Cryptochrome 1* and *2* (Cry1 and Cry2), or modulate Bmal1 gene (*Arntl*) expression such as Rev-erbα and RORα. The result is near 24-hour co-ordinated oscillations in cellular functions within different tissues or organs. Image generated with BioRender.

1.5.4 Circadian regulation of the immune system

It is well established that inflammatory diseases follow a circadian rhythm, as a result of temporal variation of immune cell responses over the course of the day. In this manner, asthma symptoms are worse at night, which times with increased inflammation in the lungs [285] and individuals with rheumatoid arthritis suffer with more joint stiffness and pain in the early morning, which times with early morning rises in pro-inflammatory cytokines in these patients [286]. In addition, susceptibility to bacterial or viral infection is highest at the beginning of the resting period (in mice), which times with greater pathogen colonisation and replication, as well as increased inflammation, within the host [287].

The oscillatory immune mechanisms underlying these effects have more recently been investigated. Over the last decade, studies have demonstrated the presence of a cell-intrinsic biological clock system across several immune cell subsets including, but not limited to, natural killer (NK) cells [288, 289], macrophages [290, 291], DCs [275, 291], ILC3s [292, 293], CD4+ T cells [259, 294], and B cells [291]. These biological clocks are necessary for the appropriate development of lymphocytes such as ILC3s and Th17 cells [295-299] and several lines of evidence also demonstrate a role for these clocks in regulating rhythmic cytokine secretion [253, 275, 290, 292, 293, 300, 301] and rhythmic trafficking of immune cells around the body [273, 302-305]. It is considered that oscillatory immune function may align these processes around anticipated temporal changes in environmental challenges such as peak dietary antigen and potential pathogen exposure [272]. Optimising the immune response when it is most needed may consequently help limit the utilisation of metabolic resources associated with these responses, and thus benefit host survival [269].

To this end, NK cell activity – which help mediates the elimination of microbe-infected or tumour cells via the production of effector cytokines such as IFN-γ or cytolytic factors such as perforin and granzyme B [306] – peaks during wakefulness [307-309], which times with the anticipated greatest risk of exposure to environmental challenges. Loss of rhythmic IFN-γ production and the secretion of perforin and granzyme B by splenic NK cells is apparent in *Per1*-deficient mice [288, 310], indicating the importance of the biological clock in driving these rhythms. Similarly, splenic macrophages stimulated with LPS at different times of the day produce different levels of pro-inflammatory cytokines such as IL-6, tumour necrosis factor-α (TNF-α) and IL-12(p40) [253, 290], an effect which is lost in macrophages with a

deletion of the gene encoding Bmal1 (*Arntl*), or Rev-erbα (*Nr1d1*) [253], indicting the importance of the cell-intrinsic clock in this process. More recent studies have also demonstrated that IL-22 production by ILC3s demonstrates rhythmicity over the 24-hour day [292, 301]. In these studies, genetic disruption of the ILC3 cell-intrinsic clock, via deletion of *Arntl* or *Nr1d1,* leads to altered IL-22 secretion [293, 301, 311]. Furthermore, *Nr1d1* deletion leads to increased IL-17 in ILC3s, which is also evident in Th17 cells [272, 299, 311]. Thus, immune cell clocks drive oscillations in both inflammatory and tolerogenic cytokine secretion.

Early studies also identified that mice subjected to circadian disruption through altering the lighting schedule to induce chronic jet lag, displayed dysregulated cytokine secretion and cell-intrinsic clock disruption [312], suggesting that rhythmic cytokine secretion was entrained by environmental factors via the cell-intrinsic clock. More recent data has demonstrated that the ILC3 cell-intrinsic clock is entrained by SCN-derived cues [293], providing a mechanism through which environmental cues may entrain rhythmic immune cell cytokine secretion. However, others have shown that that feeding cues can also drive rhythmic IL-22 production from ILC3s via the neuronal-derived signalling mediator vasoactive intestinal peptide (VIP), in a pathway that does not involve the cell-intrinsic clock [292, 300]. Therefore, rhythmic immune cell cytokine secretion may be entrained by environmental cues which may converge on, or act independently of, the circadian clock system.

Biological clocks also fulfil an important role in co-ordinating lymphocyte trafficking around the body. Indeed, the migration of lymphocytes into and out of the circulation and/ or peripheral lymph nodes, such as the mLN, axillary, brachial and inguinal lymph nodes, demonstrates rhythmicity over the 24-hour day [273, 302, 303, 305], which is dependent on biological clock-regulated expression of receptor-ligand pairs on lymphocytes and endothelial cells lining lymph and blood vessels [273, 302]. Adrenergic tone and hormonal signals may provide further layers of regulation of rhythmic cell trafficking around the body [303, 305].

Oscillatory lymphocyte trafficking around the body may have functional consequences on the generation of rhythmic adaptive immune responses. In this manner, peak lymphocyte accumulation appears to time with DC ingress into lymph modes, which suggests that antigen-presentation and consequent adaptive immune cell-priming may be subject to diurnal regulation [273]. In support of this, mice immunized to induce experimental T cell-mediated autoimmune encephalomyelitis at a time when cell counts are high in the lymph nodes (mid-

light phase) develop more significant disease than mice immunized at a time when lymph node cell counts are low (mid-dark phase) [273]. Furthermore, mice infected with *Listeria monocytogenes* develop a greater pathogen-specific T cell response when exposed at a time that correlates with greater numbers of lymphocytes in the lymph nodes [303]. Additionally, mice infected with the helminth *Trichuris muris* at different times of the day, generate different parasite-specific T cell and humoral responses, which results in different levels of effective parasite expulsion and consequently disease burden between the groups [275]. Moreover, others have shown that injection of a model dietary TD antigen (NP-ovalbumin) at a time when lymphocyte counts are highest in peripheral lymph nodes (in this instance the early-dark phase), leads to increased circulating antigen-specific antibodies, compared with mice administered with antigen at a time when lymphocyte numbers were at their lowest (the early light phase) [303, 305]. Thus, circadian entrainment of lymphocyte migration into and out of lymph nodes may have clinical implications in disease development, pathogen susceptibility and humoral immunity.

In summary, several lines of evidence demonstrate that innate and adaptive immune responses – including cytokine secretion and cell trafficking around the body – are subject to diurnal regulation, which may have functional consequences on host immune responses. However, much remains to understood about the scope of circadian rhythmicity across different immune cell subsets and in tissue specific compartments. Indeed, whether humoral responses in tissue compartments such as the GI tract demonstrate rhythmicity is unclear. This is intriguing, as the GI tract is a major site of temporal changes in environmental cues associated with feeding. Moreover, recent evidence also suggests that the commensal microbiota itself demonstrates circadian rhythmicity.

1.5.5 Circadian regulation of the gut microbiota

Several recent studies have demonstrated that the intestinal microbiota displays robust oscillations in its composition, location and function over the circadian day [313-319]. In this manner, around a fifth of the entire composition of the microbiota oscillates each day, leading to specific time of day compositional configurations of microbes within the intestines [313, 316]. The location of mucosal dwelling commensals within the colonic niche also oscillates, with bacteria demonstrating increased adherence to the colonic epithelium when mice are awake and feeding [314]. Furthermore, bacterial function is rhythmic, with pathways relating

to energy metabolism and cell growth increased when mice are awake (dark phase) and those relating to detoxification, chemotaxis and nutrient sensing increased when mice are asleep (light phase) [314, 320].

These rhythms are predominantly entrained by both host circadian clock and feeding cues [313] and have important consequences for maintaining host physiology [321]. Rhythmic bacterial adherence to the epithelium regulates the appropriate oscillatory gene expression in intestinal tissue [314], which includes nutrient uptake into small intestinal epithelial cells [322]. Furthermore, oscillatory commensal microbes were recently shown to entrain rhythmic MHCII expression on small intestinal IECs, which is important in regulating the tolerogenic intra-epithelial T cell responses and barrier function [323]. Moreover, oscillatory bacterial function leads to the rhythmic production of bacterial metabolites, such as SCFAs, lipids, amino acids and carbohydrates [314, 317, 324, 325]. These are present both locally within the GI tact and are disseminated systemically through the circulation, suggesting that bacterial rhythmicity has a systemic effect on host metabolism [314, 317, 320, 324, 325].

Indeed, circadian disruption leads to dysbiosis [313, 314, 326, 327] and is associated with an increased risk of metabolic diseases such as obesity and T2DM [313, 328-330]. Furthermore, obesity and T2DM are associated with loss of oscillations of microbial abundance in humans [331] and loss of functional rhythmicity of microbial pathways that process metabolic intermediates such as fatty acids in mice [318], suggesting a causative link. Moreover, faecal microbial transfer from jet-lagged humans or mice can confer an obesity phenotype into non-jet-lagged GF mice [313], providing mechanistic evidence that aberrant gut microbial oscillations may drive adverse systemic metabolic outcomes for the host. Thus, intestinal microbial rhythmicity is entrained by host-derived and environmental cues and in-turn has important consequences on host health and metabolism. Intriguingly, sIgA promotes host:microbial mutualism in homeostasis, but there is a lack of understanding of how IgA:microbial interactions manifest over the circadian day.

1.6 Hypothesis of the research

IgA-mediated regulation of the gut microbiota is important for host health and metabolism. Continuous abundant IgA production within the intestines would impart a significant metabolic cost on the host. Increasing evidence suggests that immune cells are imprinted with circadian rhythmicity, which may be co-ordinated around optimal environmental conditions, or optimised around the time of greatest need, and consequently limit bioenergetic expenditure. It is unclear whether IgA responses within the gut are imprinted with circadian rhythmicity.

We hypothesise that intestinal IgA responses are subject to temporal entrainment by environmental and/ or circadian cues.. We further postulated that rhythmicity in mucosal antibody secretion could have important consequences for IgA-mediated regulation of the microbiota in homeostasis and host metabolism.

In order to explore this hypothesis, this project aims to:

1. Characterise intestinal IgA responses over the course of the circadian day. To do this, we aim to explore whether the amount of IgA produced by the intestines varies over the course of the day and determine whether this is the result of time-of-day differences in PC frequencies, or in the amount of IgA produced by PCs, over the course of the day.
2. Determine the mechanisms that entrain intestinal IgA rhythmicity over the circadian day. To do this, we aim to explore whether environmental factors such as the circadian clock and/ or feeding cues entrain oscillations in intestinal IgA.
3. Determine the consequences of rhythmic intestinal IgA secretion on host-microbial interactions. To do this, we aim to characterise whether oscillatory IgA regulates compositional and functional oscillations in the commensal microbiota in the steady state.

2.0 MATERIALS AND METHODS

2.1 Animals

2.1.1 Mouse strains

C57BL/6 mice were purchased from Envigo laboratories. IgMi mice were obtained from Ari Waisman (University of Mainz, Germany) and *Mb1^{Cre} x Arntl^{flox}* mice were obtained from Kai-Michael Toellner (University of Birmingham). Both strains were bred in-house, within the Biological Services Unit (BSU), University of Manchester. Other transgenic strains used during this fellowship included *Villin^{cre} x Arntl^{flox}* and *Camk2a^{Cre} x Arntl^{flox}* mice. Mice from these strains were kindly provided by Dr Julie Gibbs (University of Manchester) and Professor Henrique Veiga-Fernandes (Champalimaud Research, Portugal), respectfully.

All mice were maintained under specific pathogen-free conditions within the BSU. Mice were maintained under a strict 12-hour light/ dark lighting schedule and had access to food and water *ad libitum*, unless otherwise indicated. For circadian experiments, mice were maintained in ventilated cabinets that were set to individual 12-hour light/ dark lighting schedules. In this instance, mice were left to acclimatise to the lighting schedule for at least 2 weeks before experiments were undertaken. Experiments were performed in either female, or mixed male and female cohorts, aged between 8-14 weeks of age as indicated. Where indicated, mice were euthanised in complete darkness. All animal experiments were conducted in accordance with the Animal (Scientific Procedures) Act 1986 and all protocols were approved by the University of Manchester Animal Welfare and Ethical Review Board.

2.1.2 Genotyping of IgMi and *Mb1^{Cre} x Arntl^{flox}* mice

Routine genotyping of *Mb1^{Cre} x Arntl^{flox}* mice was outsourced to Transnetyx® (Cordova, USA). Genotyping of IgMi mice was performed inhouse by polymerase chain reaction (PCR). DNA was extracted from ear punches by incubating each ear punch with 6.25µl of tissue preparation solution (Sigma Aldrich) and 25 µl of extraction solution (Sigma Aldrich) for ten minutes at room temperature, followed by 5 minutes at 95°C. Subsequently, 25µl of neutralisation buffer (Sigma Aldrich) was added to each sample.

DNA was amplified by adding 2µL of DNA extract, to 10µL GoTaq (Sigma Aldrich), 7µL nuclease free water and 0.5µL of forward primer ((Life Technologies) CCTTCCTCCTACCCTACAAGCC) and 0.5µL of reverse primer ((Life Technologies) GAGACGAGGGGGAAGACATTTG). For the PCR

cycles, samples were first heated to 94°C for 5 minutes, followed by 35 cycles of the following temperatures: 94°C for 30 seconds, 55°C for 30 seconds and 72°C for 30 seconds. Following 35 cycles, samples were heated to 72°C for 10 minutes and then cooled to 4°C. The polymerase chain reaction (PCR) products were run on a 1.5% agarose gel (in 1x Tris/Borate/EDTA [TBE] buffer containing SYBR® Safe DNA stain (Invitrogen, USA) at 120 voltages for 1 hour). The PCR product bands were identified on a benchtop UV transluminator (Fisher Scientific).

2.2 Administration of diets

2.2.1 Reverse feeding

To reverse the feeding schedule, groups of age and sex-matched mice (6-8 week old) were first housed in ventilated cabinets with opposing 12-hour light:dark lighting schedules for two weeks with access to normal mouse chow (NC) and water *ad libitum*. Subsequently, food access was restricted over a two-week period, by physically removing food hoppers from the cages each day at a time that corresponded with 3 hours into the light (ZT3), or dark (ZT15) phase. Food hoppers were then replaced 6 hours later, meaning that mice had access to food only during the mid-light (ZT3-ZT9) or mid-dark (ZT15-ZT21) phase. To ensure no cross-contamination from food dropping through the hopper, mice were transferred to a new cage at the end of each feeding period.

2.2.2 High fat diet and high/ low protein diet experiments

For HFD-feeding experiments, age and sex-matched mice (6-8 weeks old) were fed either NC or a HFD (D12492, Research Diets, Inc, USA) *ad libitum* for 6 weeks. Mice were weighed before the dietary treatment phase (baseline) and weekly, thereafter. Resting (morning) glucose was measured in *ad libitum* feeding conditions at baseline, week 2 and week 6 of the dietary treatment phase by tail pricking mice at ZT1 and using a blood glucose meter (AccuCheck®, Roche, Switzerland). Fasting serum glucose was measured in mice after an 8 hour fast (ZT3-ZT11) at baseline, week 2 and week 6 of the dietary treatment phase by tail pricking mice at ZT11 and using a blood glucose meter (AccuCheck®, Roche, Switzerland).

For high/ low protein diet experiments, age and sex-matched mice (6-8 weeks old) were fed either a high or low protein diet (Envigo, USA) for 3 weeks. Mice were weighed before the dietary treatment phase (baseline) and weekly, thereafter.

2.3. *In vivo* 2-NBDG and bodipy experiments

Animals were injected with either 100µg 2-NBDG (ThermoFisher, USA) reconstituted in sterile PBS (Sigma, UK), or 50µg bodipy (ThermoFisher, USA) reconstituted in sterile dimethyl sulfoxide (DMSO) (Sigma, UK), via the intraperitoneal (IP) route and euthanized 20, or 60 minutes later, respectively. Single cell suspensions of small intestinal LP cells were then prepared, stained with fluorophore-labelled antibodies and analysed by flow cytometry (as described below).

2.4 Preparation of single cell suspensions

2.4.1 Intestinal lamina propria

For LP single cell suspensions, the small intestine and colon were removed at necropsy, cut longitudinally and washed thoroughly in 1x PBS (Sigma, UK) to remove faecal and luminal contents. To remove IECs, the tissues were suspended in stripping buffer (3% bovine serum albumin, 1 mM EDTA, 1 mM DTT in 1x PBS (Sigma-Aldrich, St Louis, MO)) and placed on a water shaker at 37^{o}C for 10 minutes. Subsequently, the stripping buffer was renewed and placed back on the water shaker for a further 20 minutes. The remaining tissue was suspended in digestion buffer (20 µg/ml DNase [Sigma-Aldrich, St Louis, MO] and 1mg/mL collagenase D [small intestines; Roche, Switzerland], or 1 mg/mL collagenase/dispase [large intestines; Roche, Switzerland], in RPMI-1640 containing 2% FCS, 500 IU/ml penicillin, 500 µg/ml streptomycin and 2mM L-glutamine [all from Sigma-Aldrich, St Louis, MO]) on a water shaker at 37^{o}C for 45 minutes. The media was then poured through 70µm nylon filters (Falcon, USA) into fresh falcon tubes. Following this, single cell suspensions were centrifuged at 1500rpm for 5 minutes, re-suspended in fresh complete media (RPMI-1640 containing 2% FCS, 500 IU/ml penicillin, 500 µg/ml streptomycin and 2mM L-glutamine [all from Sigma-Aldrich, St Louis, MO]) and transferred to 96 well plates (Thermo Fisher Scientific, USA) for flow cytometry antibody staining. Cell counts were performed using a Casy TT counter (Roche Innovatis, Germany).

2.4.2 Peyer's patches and mesenteric lymph nodes

Four to six PPs were excised from small intestines at necropsy and placed in media containing 0.16mg/ml liberase (Roche, Switzerland) and 40 µg/ml DNAse (Sigma-Aldrich, St Louis, MO) and placed on ice. Subsequently, PPs incubated within the media were placed on a water shaker at 37^{o}C for 30 minutes. Cells were then mashed through 70µm nylon filters (Falcon, USA) into complete media.

For mLN cell suspensions, mLNs isolated at necropsy were mashed through 70µm nylon filters (Falcon, USA) into complete media. Following isolation of PP and mLN single cell suspensions, cells were centrifuged at 1500rpm for 5 minutes, re-suspended in fresh complete media and transferred to 96 well plates (Thermo Fisher Scientific, USA) for flow cytometry antibody staining.

2.5 Flow cytometry

2.5.1 Surface staining

For surface staining, single cell suspensions were incubated at 4◦C in the dark for 30 minutes with fluorophore-labelled antibodies (Table 1) diluted in FACS buffer (4% bovine serum albumin in 1x PBS (both Sigma-Aldrich, St Louis, MO). Subsequently, cells were washed with FACS buffer, centrifuged at 1500rpm for 5 minutes, resuspended in fresh FACS buffer and either maintained at 4°C or analysed immediately. For circadian experiments including 4 timepoints, cells were fixed in 2% paraformaldehyde (PFA) for 10 minutes at room temperature following extracellular staining. Cells were then washed twice with PBS and resuspended in 200µl FACS buffer until sample acquisition.

2.5.2 Sample acquisition

Flow cytometric analysis was performed using a Fortessa flow cytometer (BD Bioscience, Oxford, UK) and analysed with FlowJo software (Tree Star). Where mean fluorescence intensity (MFI) was calculated, fluorescence minus one (FMO) samples were included in the analysis as controls.

Marker	Clone	Source
Aqua Dead Cell Stain	-	Life Technologies
CD45	30-F11	BioLegend
CD3	145-2C11	eBioscience
MHCII	M5/114.15.2	eBioscience
B220	RA3-6B2	eBioscience
IgD	11-26c.2a	BioLegend
IgA	mA-6E1	eBioscience
CD138	281–2	BioLegend
GL7	GL7	BioLegend
Fas	15A7	eBioscience
CXCR5	L138D7	BioLegend
CD4	GK1.5	BD Biosciences
PD-1	RMP1-30	BioLegend
CD98	RL388	BioLegend

Table 1. Antibodies and fluorochromes used for flow cytometry analysis

2.6 *In vitro* 2-NBDG uptake assay

For assessment of 2-NBDG uptake *in vitro*, $1x10^6$ small intestinal cells were cultured in glucose-free DMEM medium (Seahorse, USA) supplemented with 2mM L-glutamine and 100µM 2-NBDG (Thermo Fischer, USA) for 10 minutes at 37◦C. Surface antibody staining of samples was then performed and acquisition of samples on the flow cytometer was undertaken within 2 hours.

2.7 *In vitro* assessment of lipid accumulation within cells

For assessment of lipid accumulation within cells *in vitro*, $1x10^6$ small intestinal cells were cultured in glucose-free DMEM medium (Seahorse, USA) supplemented with 2mM L-glutamine and LipidTOX (Thermo Fischer, USA) for 30 minutes at 37◦C. Cells were then washed, surface antibody staining of samples was then performed and acquisition of samples on the flow cytometer was undertaken within 2 hours.

2.8 Kynurenine uptake assay

Assessment of kynurenine uptake *in vitro* was performed as previously described [332]. Briefly, after surface antibody staining, $2x10^6$ cells were resuspend in 200µl warmed Hanks Balanced Salt Solution (HBSS; Sigma, UK) in FACS tubes. 100µl of HBSS, or BCH (40mM, in HBSS), or leucine (20mM, in HBSS) was added to appropriate samples. 100µl kynurenine (800µM, in HBSS) was then added to all samples, apart from the no kynurenine controls (which had 100µl HBSS added to them). Kynurenine uptake was stopped after 4 minutes by adding 125µl 4% PFA for 30min at room temperature in the dark. After fixation, cells were washed twice in HBSS and then resuspend in HBSS prior to acquisition on the flow cytometer.

2.9 Fluorescence activated cell sorting

For cell sorting experiments, single cell suspensions were prepared for flow cytometry as described and acquired on a FACSAria Fusion cell sorter (BD Bioscience, Oxford, UK). Cells were sorted to a purity of >90% directly into lysis buffer (Qiagen, Germany; for RNA extraction) or sterile complete media (for cell culture/ extracellular flux analysis).

2.10 Antibody secretion assays

For antibody secretion assays, IgA+ PCs (+/- IgA+ B cells, +/- IgD+ B cells where indicated), were FACS-sorted from pooled small intestinal LP single cell suspensions, or PPs, into complete media. Cells were plated in 96-well round-bottom plates at a density of 10^4 cells/ well and left for 16 hours in a humidified incubator at 37°C (5% O2, 5% CO2). After the incubation period, plates were spun at 1500rpm for 5 minutes and supernatants removed and stored at -80◦C. IgA antibody concentrations in the supernatants were measured by ELISA (as described below).

To determine the effects of metabolic substrate availability on IgA secretion, IgA+ PCs were incubated in either leucine free media (US Biological, USA) or glucose free media (Gibco, UK), with IL-6 (10ng/ml) (Peptrotech, USA) and BAFF (200ng/ml) (Biolegend, UK), supplemented with either low, or physiological, concentrations of leucine (0mM & 0.15mM, respectively), or glucose (1mM & 9mM, respectively) (both Sigma, UK). Physiological ranges for leucine and glucose concentrations were calculated as previously described [111]. To determine the effects of inhibiting nutrient uptake or metabolic signalling on IgA secretion, IgA+ PCs were cultured in complete media with IL-6 (10ng/ml) and BAFF (200ng/ml) with/ without the addition of metabolic

inhibitors including pp242 (500nM), BCH (10mM), 2-Deoxy-D-glucose (2DG) (1mM) (all Sigma, UK). Cells were incubated for 16 hours at 37◦C, following which culture supernatants were removed and IgA concentrations determined by ELISA. Cell viability was determined under different culturing conditions, by either staining cells with Trypan Blue (Sigma, UK) and counting live cells using a haemocytometer, or cells were re-stained with viability dye for 15 minutes and analysed on the flow cytometer.

2.11 Extracellular flux analysis

For the glycolytic stress test, a XF96e extracellular flux analyser (Seahorse Bioscience/Agilent, USA) was used to measure extracellular acidification rate (ECAR) in real-time. IgA+ PCs and IgD+ B cells were isolated from the small intestines as described previously and washed in Seahorse medium (Seahorse/Agilent, USA). $1.5x10^5$ cells were adhered to each well of the Seahorse plate (Seahorse/Agilent, USA) using CellTak (Corning, USA). Cells were rested in Seahorse medium (glucose-free DMEM) at 37°C without CO2 for at least 30 minutes prior to the run. For the test, Seahorse medium was supplemented with 2mM of L-glutamine (Sigma, UK) and pH was adjusted to 7.35±0.05 (at 37°C). Glucose (10mM final concentration) (Fischer Scientific, USA), oligomycin (1µM final concentration (Sigma, UK) and 2-DG (100mM final concentration; Sigma), were added to individual ports to complete this assay.

2.12 RNA quantification

2.12.1 RNA purification

For whole tissue, tissue segments taken at necropsy were placed in eppendorfs and snap frozen, pending storage at -80◦C. RNA was purified from whole tissue using the RNeasy RNA purification mini kit (Qiagen, Netherlands) following the manufacturer's instructions. Briefly, tissue was transferred to a lysing matrix tube (MP Biomedicals, USA) and 600µl of RLT buffer was added. The tissue was homogenised for 30seconds at 4.0m/s on a tissue homogeniser (Fastprep 24, MP Biomedicals). Following this, an equal volume of 70% ethanol was added. The lysate was then transferred to a spin column and centrifuged at 8000xg for 30seconds, after which the flow through was discarded. 700µl of RW1 buffer was then added to the spin column and following a further centrifugation, the flow through was discarded. 500µl of buffer RPE was then added and the flow through was discarded after a further centrifugation. This step was then repeated. Finally, the spin column was placed in a new tube and the RNA was eluted in 50µl of nuclease-free water. Purified RNA was kept at -80◦C for further downstream applications.

For sorted cells, isolated IgA+ PCs and IgD+ B cells were stored at -20◦C in lysis buffer prior to RNA extraction. RNA was purified from cells using the RNeasy RNA purification micro kit (Qiagen, Netherlands) following the manufacturer's instructions. Briefly, the cells were thawed, and an equal volume of 70% ethanol was added. The lysate was transferred to a spin column and centrifuged at 8000xg for 30seconds, after which the flow through was discarded. 700µl of RW1 buffer was then added to the spin column and following a further centrifugation, the flow through was discarded. 500µl of buffer RPE was then added and the flow through was discarded after a further centrifugation. 80% ethanol was then added to the spin column and following a further centrifugation, the flow through was discarded. Finally, the spin column was placed in a new tube and the RNA was eluted in 14µl of nuclease-free water. Purified RNA was kept at -80◦C for further downstream applications.

2.12.2 Reverse transcription PCR

For sorted cells, all eluted RNA was reverse transcribed to cDNA, using a commercial RNA to cDNA kit (Applied biosystems, Thermo Fisher Scientific). Each reaction consisted of RNA (14µl), 10x RT buffer (2 µl), 25x dNTP mix (0.8 µl), 10x RT Random Primers (2 µl), Multiscribe RT (1 µl), nuclease-free water (0.2 µl). For RNA extracted from whole tissue, 2µg RNA was converted to cDNA using the RNA to cDNA kit (Applied biosystems, Thermo Fisher Scientific). Each reaction consisted of RNA plus nuclease free water (2mM), 10x RT buffer (2 µl), 25x dNTP mix (0.8 µl), 10x RT Random Primers (2 µl), Multiscribe RT (1 µl), nuclease-free water (up to a final volume of 20µl). PCR was undertaken using a benchtop thermocycler (Applied Biosystems, USA). For the PCR cycles, samples were first heated to 25◦C for 5 min, followed by 1hour at 42◦C and finally 95◦C for 5 minutes. The PCR products were either used immediately or stored at -20◦C for future use.

2.12.3 Realtime PCR

Realtime (RT-)PCR was performed in 96, or 384, well plates (Thermo Fisher Scientific, USA) on a StepOne plus machine (Thermo Fisher Scientific, USA), using Taqman probes and primers (listed in Table 2) and Takyon MasterMix (Eurogentec, Belgium). Each reaction consisted of 1µl cDNA, 3.4µl nuclease-free water, 5µl master mix and 0.2µl of each primer/ probe. Samples without cDNA were included as controls and where possible, samples were run in duplicate. For the RT-PCR cycles, samples were heated to 95°C for 2 minutes, followed by 40 cycles of the following temperatures: 95°C for 1 minute and 60°C for 10 minutes. Following this, the baseline and threshold were reviewed and adjusted manually where necessary.

Gene	Forward	Reverse	Probe
Gapdh	CAA TGT GTC CGT CGT CGA TCT	GTC CTC AGT GTA GCC CAA GAT G	CGT GCC GCC TGG AGA AAC CTG CC (FAM, TAMRA)
Arntl	CCA AGA AAG TAT GGA CAC AGA CAA A	GCA TTC TTG ATC CTT CCT TGG T	TGA CCC TCA TGG AAG GTT AGA ATA TGC AGA A
Per2	GCC TTC AGA CTC ATG ATG ACA GA	TTT GTG TGC GTC AGC TTT GG	ACT GCT CAC TAC TGC AGC CGC TCG T
Nr1d1	Applied Biosystems	Mm00520708_m1	(FAM, NFQB)

Table 2. Primers/ probes used for RT-PCR analysis

2.13 RNA sequencing

2.13.1 Sample preparation

IgA+ PCs and IgD+ B cells were sorted from the small intestines and RNA was extracted from cells as described previously. The concentration of RNA was assessed using the Qubit™ RNA HS Assay Kit (Thermo Fisher Scientific, USA) according to the manufacturer's instructions. Subsequently, RNA samples were frozen and shipped on ice packs to NovogeneUK (Cambridge, UK) for sequencing.

2.13.2 Data analysis

Raw FASTQ files underwent quality control and normalisation inhouse by NovogeneUK. Normalised reads (Fragments per kilobase of transcript per million mapped reads, FPKM) were used to generate comparison plots, whilst fold change was calculated and used for volcano plots and z-scores were calculated and plotted on heatmaps. Kyoto Encyclopedia of Genes and Genomes (KEGG) enrichment of differentially expressed genes (DEGs) between paired timepoints was performed by NovogeneUK (Cambridge, UK). Ingenuity Pathway Analysis (IPA) of DEGs across all timepoints was performed using QIAGEN IPA (link: www.qiagen.com/ingenuity).

2.14 Evaluation of intestinal IgA

2.14.1 Processing of small intestinal washes

At necropsy, the small intestines were excised and laid out longitudinally; the terminal ileum was identified as the distal 8cm and was separated from the rest of the tissue. The terminal ileum was then flushed with 5mls of ice-cold sterile PBS (Sigma, UK) using a mouse gavage needle. The flow through was collected directly into a 50ml falcon (Fisher Scientific, USA) and placed on ice. The

luminal contents were then vortexed at maximum speed for 1 minute, followed by centrifugation at 150g for 10 minutes to remove large debris. The supernatants were passed through 70µm nylon filters (Falcon, USA) then spun at 8000g for 5minutes. The bacterial pellet was saved and stored at -80^{o}C for future use. The supernatant was retrieved and spun at a further 10000g to remove remaining debris. The supernatant was then recovered and stored at -80^{o}C for further analysis.

2.14.2 Processing of faeces

Fresh faecal pellets were collected and placed into pre-weighed 1.5mL Eppendorf tubes (Starlab). Tubes were then re-weighed and faecal pellets were resuspended in sterile PBS (at 10µl/mg) (Sigma, UK). Contents were then homogenised for 30seconds at 4.0m/s on a tissue homogeniser (Fastprep 24, MP Biomedicals). Samples were then centrifuged for 10 minutes at 150g to remove large debris. The supernatant was filtered through 70µm nylon filters (Falcon, USA) then spun at 8000g for 5minutes. The bacterial pellet was saved and stored at -80^{o}C for future use. The supernatant was retrieved and spun at a further 10000g to remove remaining debris. The supernatant was then recovered and stored at -80^{o}C for further analysis.

2.14.3 IgA bacterial coating assay

The bacterial pellet was thawed and washed with sterile FACS buffer. Following centrifugation at 8000g for 5 minutes, the pellet was resuspended in SYTO-60 (1:600; Thermo Fisher Scientific, USA) and anti-mouse IgA (1:200) diluted in FACS buffer; samples were incubated for 30 minutes at 4°C in the dark. Samples were then washed with FACS buffer, centrifuged at 8000g for 5 minutes and then resuspended in fresh FACS buffer and either maintained at 4°C or analysed by flow cytometry immediately. For sample acquisition, the flow cytometer threshold was changed to side scatter.

2.14.4 IgA ELISA

The total concentration of sIgA within faecal supernatants was determined by ELISA using a commercial kit (Bethyl laboratories, USA) according to the manufacturer's instructions. Briefly, purified coat anti-mouse IgA antibody was diluted (1:100) in 0.05M carbonate-bicarbonate coating buffer (pH 9.6) and coated on 96 well ELISA plates (Thermo Fisher Scientific, USA). After 60 minutes, plates were washed three times in 1xPBS-0.05% tween 20 (Acros Organics). Subsequently, wells were blocked with 1% bovine serum albumin (BSA) (Sigma-Aldrich, St Louis, MO). After 60 minutes, plates were washed three times in PBS-0.05% tween 20 and then 50µl of standards (including blanks; prepared according to manufacturer's protocol) and stool supernatants (1:100-1:200 dilutions) were added in duplicate to plates. Plates were incubated for

1 hour following which plates were washed three times in PBS-0.05% tween 20 and then 50µl of horseradish peroxidase detection antibody (0.1 mg/ml diluted to 1:15000 in 1% BSA) was added to wells. Plates were incubated for 60 minutes at room temperature after which they were washed five times in PBS-tween 20 and 100ul of TMB substrate solution (BD Bioscience, Oxford, UK) was added. Plates were incubated in the dark for 15 minutes after which 50µl of 0.18M H_2SO_4 was added to stop the reaction. Plates were read on a plate spectrophotometer (Versamax, Molecular Devices) at an optical density of 450nm.

2.14.5 BCA protein assay

To determine the total protein concentration of stool supernatants, the Pierce BCA Protein Assay Kit (ThermoFisher Scientific) was used according to the manufacturer's instructions. Briefly, each standard and sample replicate were pipetted onto a 96-well plate; the working solution was added at a sample:working solution ratio of 1:20. The plates were then covered and incubated at 37◦C for 30 minutes, after which the plates were cooled and absorbance was determined on a spectrophotometer (Versamax, Molecular Devices) at an optical density of 562nm.

2.15 16S rRNA sequencing

2.15.1 Sample preparation

Bacterial DNA from faecal bacteria was isolated using the PowerSoil DNA Isolation Kit (Qiagen, Netherlands) according to the manufacturer's instructions. Pre-amplification of the V3V4 region of 16S rRNA was performed by PCR in triplicate using 2xKAPA HiFi Hot Start ReadyMix (Roche) using primer pairs containing adaptor sequences for down-steam use on Illumina platforms, as follows:

16S Amplicon PCR Forward Primer =

5' TCGTCGGCAGCGTCAGATGTGTATAAGAGACAGCCTACGGGNGGCWGCAG

16S Amplicon PCR Reverse Primer =

5' GTCTCGTGGGCTCGGAGATGTGTATAAGAGACAGGACTACHVGGGTATCTAATCC

For the PCR cycles, samples were first heated to 95°C for 3 minutes, followed by 25 cycles of the following temperatures: 95°C for 30 seconds, 55°C for 30 seconds and 72°C for 30 seconds. Following 25 cycles, samples were heated to 72°C for 5 minutes and then cooled to 4°C. Following this, AMPure XP beads (Fisher Scientific) were used to purify the 16S V3V4 amplicon away from

free primers and primer dimer species. Illumina sequencing adapters were then attached using the Nextera XT Index Kit (Illumina Inc, USA), according to the manufacturer's instructions. For the PCR stage, samples were first heated to 95°C for 3 minutes, followed by 8 cycles of the following temperatures: 95°C for 30 seconds, 55°C for 30 seconds and 72°C for 30 seconds. Following 8 cycles, samples were heated to 72°C for 5 minutes and then cooled to 4°C. Following this, the samples underwent a further cleaning stage using AMPure XP beads. The concentration of DNA (ng/µl) was then assessed using the Qubit DNA HS Assay Kit (Thermo Fisher Scientific, USA) according to the manufacturer's protocol. The size of the DNA amplicons was determined by using an Agilent 4200 TapeStation system (Aglient, USA) as per the manufacturer's protocol. Using these data, the DNA concentration, in nM, was then determined using the following formula:

(Concentration in ng/µl)/ (660g/mol × library size) × 10^6 = concentration in nM

Each library was finally diluted to 4nM using 10 mM Tris pH 8.5 (Sigma, UK). For pooling libraries with unique indices, 5µl of diluted DNA from each sample was then transferred into a single 1.5ml Eppendorf. 16S sequencing was performed by using the Illumina MiSeq platform (Illumina, USA).

2.15.2 Data analysis

Initial processing, quality assessment and normalisation of the sequencing data was performed by the Department of Bioinformatics, University of Manchester, Manchester, UK. Normalised abundance values were subsequently either potted against individual ZT times, or used to calculate z-scores which were plotted on heatmaps.

2.16 Shotgun metagenomics sequencing

Whole faecal pellets were sent for bacterial DNA extraction and shotgun metagenomics sequencing at CosmosID (Rockville, USA). Data generation, quality control and normalisation was conducted by CosmosID using an in-house pipeline. Normalised reads were subsequently compared across each time-point and group.

2.17 Metabolomic analysis

Whole faecal samples were sent for metabolomic analysis by Jon Swann, University of Southampton. The metabolic profiles of fecal samples were measured using ^{1}H nuclear magnetic resonance spectroscopy as previously described [333].

2.18 Data handling and statistical analysis

All graphs were created, and statistical analysis performed, using GraphPad Prism 7.02 (GraphPad, USA), unless otherwise specified. Data represents mean ± standard error of the mean (SEM), unless otherwise indicated. The Unpaired T-Test, or ANOVA with appropriate post hoc testing, was employed to evaluate differences between groups of parametric data. To evaluate statistically significant variance in the data across different timepoints, we used Kruskal-Wallis test or analysis of variance (ANOVA) tests, for non-parametric and parametric data, respectively. The JTK_CYCLE algorithm was used to determine statistically significant circadian rhythmicity (defined as having a period ranging between 20 to 28 hours) [334]. *P* values were plotted on individuals graphs as represented by asterixis (*); *p* values were adjusted using the Bonferroni correction when multiple comparisons were made. When large datasets were analysed (for example RNA sequencing, 16S sequencing and metagenomics data) we used a false discovery rate (FDR) threshold (as indicated in the text) to identify significance within the data, which was determined using the Benjamini-Hochberg Procedure, as previously reported [313, 334].

3.0 CHARACTERISING INTESTINAL IGA RESPONSES OVER THE CIRCADIAN DAY

3.1 Introduction

Under homeostatic conditions, intestinal IgA acts to both protect against foreign pathogens and modulate the composition of the commensal microbial community [66, 183]. IgA responses targeting commensal microbes are linked with mammalian health and metabolism, as dysregulated intestinal antibody responses can lead to adverse health outcomes including an increased susceptibility to infections, the development of chronic intestinal inflammation and impaired metabolic homeostasis [122, 124].

PCs have enhanced metabolic activity [110, 111] and IgA-mediated regulation of the microbiota by continuous, abundant production of intestinal IgA could impose a significant metabolic cost to the host. It is increasingly appreciated that numerous immune cell processes are imprinted with circadian rhythmicity, which may help limit bioenergetic cost, by co-ordinating cell responses around temporal changes in environmental cues, or partitioning their maximal response around the time of greatest need [249, 253, 272, 273, 292, 300, 302, 335]. However, whether intestinal IgA secretion and/ or PC function are imprinted with circadian rhythmicity is unclear.

Several lines of evidence suggest a link between the circadian system and B cell/ antibody responses. Indeed, splenic B cells have a cell-intrinsic clock system [291] and mice with disrupted clock function, via global deletion of circadian clock proteins *Cry1* and *Cry2*, have altered circulating levels of IgG antibodies [336]. In addition, B cells migrate into and out of peripheral lymph nodes at specific times of the day [273, 302], which effects the magnitude of the humoral response towards administered antigens [305], suggesting that antibody responses may fluctuate over the course of the day in homeostasis. In accordance with this, the concentration of faecal sIgA in mice and rats varies over the course of the day [337-340], suggesting temporal changes in IgA production may occur within the GI tract.

Together, these findings provoke the hypothesis that intestinal IgA responses are imprinted with circadian rhythmicity in homeostasis. In this chapter, we interrogated this hypothesis, by characterising intestinal IgA responses over the circadian day.

3.2 Results

3.2.1 The concentration of sIgA within the intestines is rhythmic over a 24-hour period

To begin to evaluate our hypothesis, we sought to determine whether the amount of sIgA produced within the intestines varies over the course of the day. To do this, age and sex-matched mice were housed under strict 12 hour light:dark cycles. Mice were left undisturbed for 1 week, after which fresh faecal pellets were collected from each mouse at 5 timepoints, 6 hours apart over a single 24-hour period. Following normalisation (by pellet weight) and processing, the concentration of sIgA in the faecal pellets was measured by ELISA. Comparing the variance of means across the different timepoints revealed a significant difference in the amount of sIgA present in the faeces over the 24-hour period (Figure 3.1A-C).

We next employed the commonly used analysis tool JTK_CYCLE (hereafter referred to as JTK), to evaluate rhythmic elements in the data and determine whether the data exhibited a significant oscillation over a circadian timeframe, which was defined as having a period ranging between 20 to 28 hours [334]. In doing so, we consistently detected significant oscillations in faecal sIgA over the circadian day (Figure 3.1A-C).

We reasoned that the volume, composition, and total protein content of faecal pellets within the intestines may also vary over a 24-hour period, in line with active and resting periods as well as feeding [186]. To evaluate whether intrinsic differences within in the quality of faeces could account for the observed time of day changes, we further normalised the concentrations of sIgA to the total protein concentration in each sample, determined by BCA assay. Analysis revealed both significant variance and circadian oscillations were still present (Figure 3.1D-F), suggesting that the temporal changes that we detected were a result of differences in the amount of sIgA present within the intestines across different timepoints.

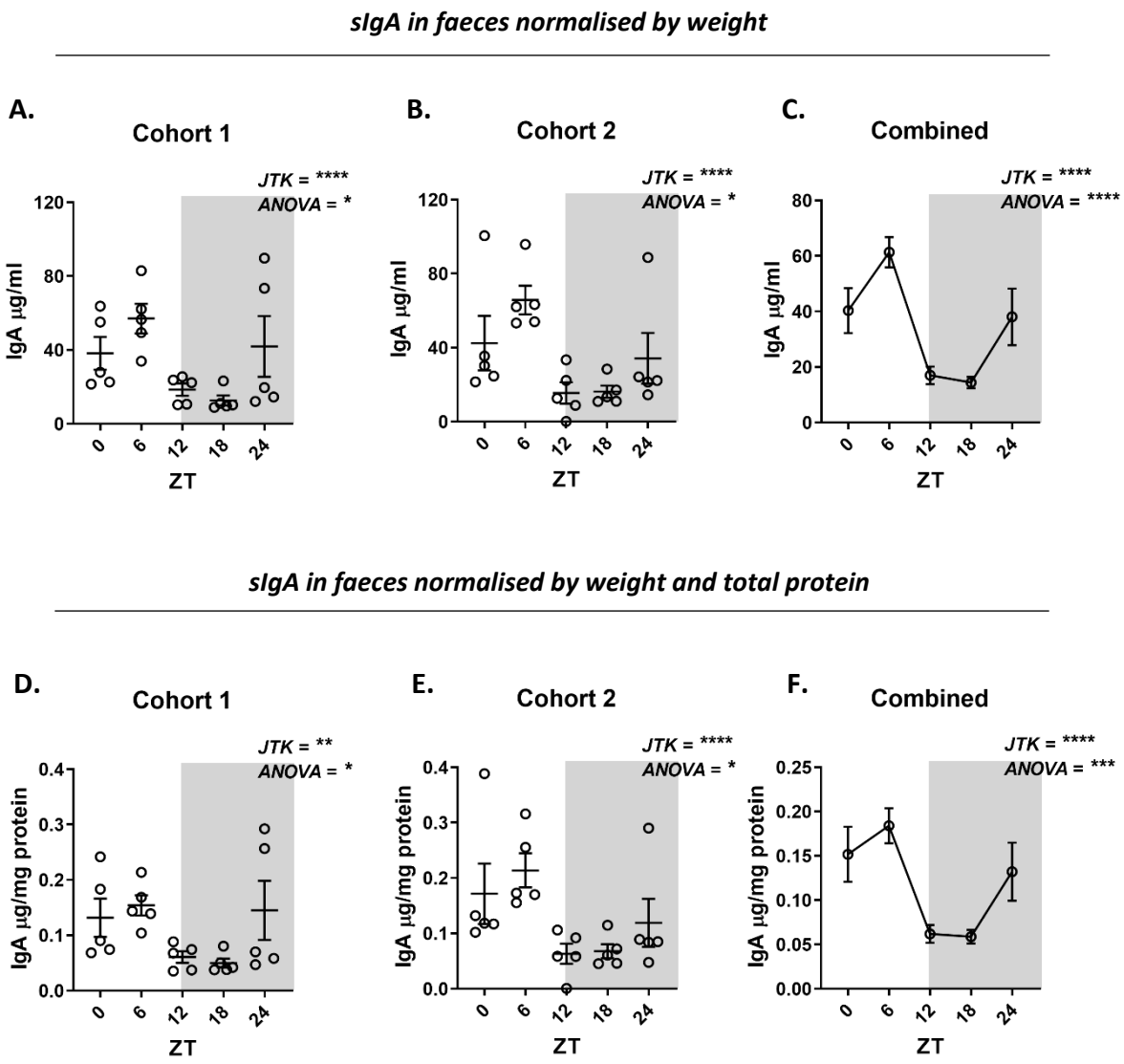

Figure 3.1. Faecal sIgA varies over the course of the circadian day

Example data from 2 independent cohorts of mice (n=5/ group; C57BL/6 female mice aged 8-10 weeks) prospectively sampled for faeces over the circadian day, from which the concentration of sIgA was determined. Mice were housed under strict 12-hour light:dark conditions and fed *ad libitum*. Faecal samples were sampled at 5 timepoints, six hours apart over a 24-hour period, illustrated by Zeitgeber times (ZT; time after light onset) 0 to 24 on graph x-axis. (A&B) Concentration of faecal secretory (s)IgA normalised by weight over the circadian day in two independent cohorts of n=5 mice determined by ELISA. (C) Mean faecal sIgA concentration over the circadian day, with data pooled from cohort 1 and 2. (D&E) Concentration of faecal sIgA normalised by weight and total faecal protein over the circadian day in each cohort. (F) Mean normalised faecal sIgA concentration over the circadian day, with data pooled from cohort 1 and 2. Variance in the data across the experimental timepoints assessed by Analysis of Variance (ANOVA). Rhythmicity assessed by JTK analysis. *= $p<0.05$; **= $p<0.01$; ***= $p<0.001$; ****= $p<0.0001$. Data representative of 8 independent experiments. Horizontal bars represent mean±SEM. Shaded area on graphs represents the dark phase.

Most of the IgA+ PCs in the GI tract reside within the small intestinal LP [66]. Therefore, we next sought to determine whether the circadian oscillations in sIgA were also evident in the luminal contents of the small intestines. To achieve this, we isolated and flushed the terminal ileum of mice housed in opposing 12 hour light:dark cycles at 2 times, 6 hours apart, with an equal volume of sterile PBS (Figure 3.2A). Following processing, the concentration of sIgA in the terminal ileal washes was measured by ELISA. Analysis revealed that the concentrations of terminal ileal sIgA exhibited rhythmicity over the experimental timepoints in a similar manner to that found in the faeces (Figure 3.2B). Together, these data suggest that the concentration of intestinal sIgA oscillates over the circadian day.

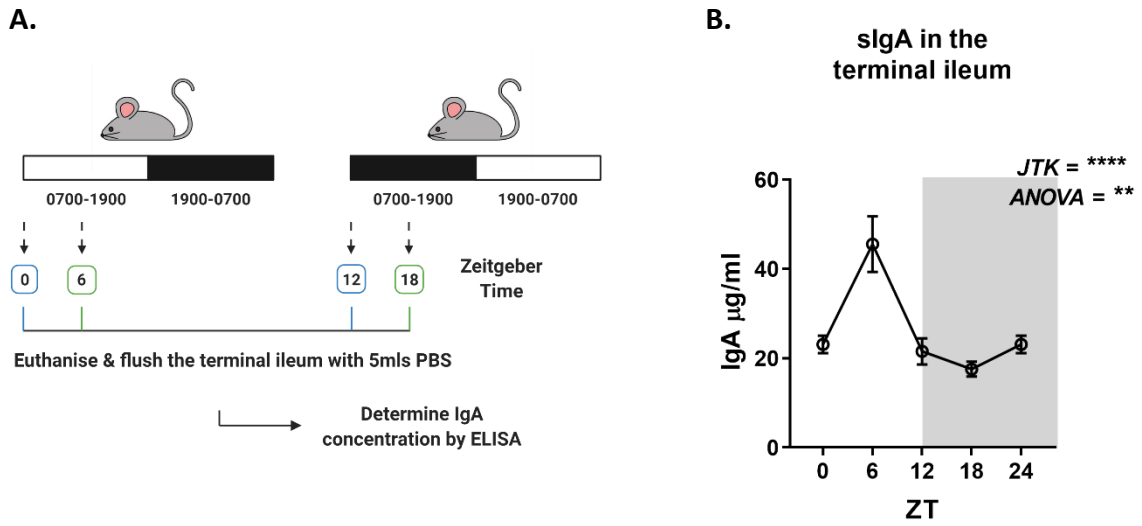

Figure 3.2. Small intestinal sIgA varies over the course of the circadian day

(A) Schematic of the experiment. Mice were housed in cabinets with opposing 12-hour light:dark schedules and fed *ad libitum*. One group of mice from each cabinet was euthanised in the morning (7am; representing ZT 0 and 12 – blue boxes) and one from each cabinet in the afternoon (1pm; representing ZT6 and 18 – green boxes). The terminal ileum was isolated and flushed with 5mls PBS. Image created with BioRender. (B) Concentration of sIgA in the terminal ileal washes at each timepoint determined by ELISA. ZT0 is double plotted as ZT24 to facilitate viewing the data. Variance in the data across the experimental timepoints assessed by ANOVA. Rhythmicity assessed by JTK analysis. **= $p<0.01$; ****= $p<0.0001$. Data representative of one experiment; n=5 mice/ timepoint; C57BL/6 female mice aged 8-10 weeks. Horizontal bars represent mean±SEM. Shaded area on graphs represents the dark phase.

3.2.2 Oscillatory intestinal IgA is not the result of time of day differences in PC differentiation

We postulated that time of day differences in IgA CSR and/ or IgA+ PC differentiation could lead to the observed oscillations in intestinal sIgA. To evaluate this, we used the same experimental approach (Figure 3.2A) to sample mice at 6-hourly intervals over the period of a single day. At necropsy, the PPs, small and large intestines were removed and processed. We then used a flow cytometry-based approach to determine the frequency and number of relevant lymphocyte subsets within each tissue.

Analysis of the PPs demonstrated consistent time of day differences in the frequency of CD4+ T cells that expressed CXCR5 and PD-1 (TfH cells) (Figure 3.3A). However, when normalised to the total CD45+ pool, the overall frequency of TfH cells in the tissue was not significantly rhythmic (Figure 3.3B). To determine the significance of any potential time of day difference in TfH on B cell differentiation, we next identified GC B cells from naive B cells on the basis of GL7 and Fas expression, which further enabled us to evaluate the proportion of IgA class-switched B cells undergoing affinity maturation (GC IgA B cells; Figure 3.3C). Analysis revealed no significant variation or rhythmicity in the frequency of IgA+ B cells undergoing affinity maturation over the experimental timepoints (Figure 3.3D).

A.

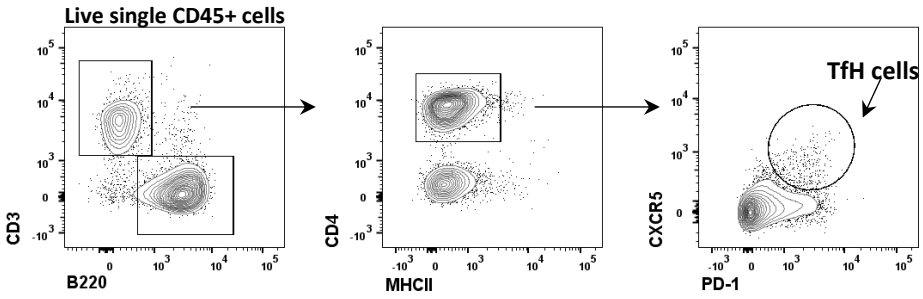
Live single CD45+ cells
CD3
B220
CD4
MHCII
CXCR5
PD-1
TfH cells

B.

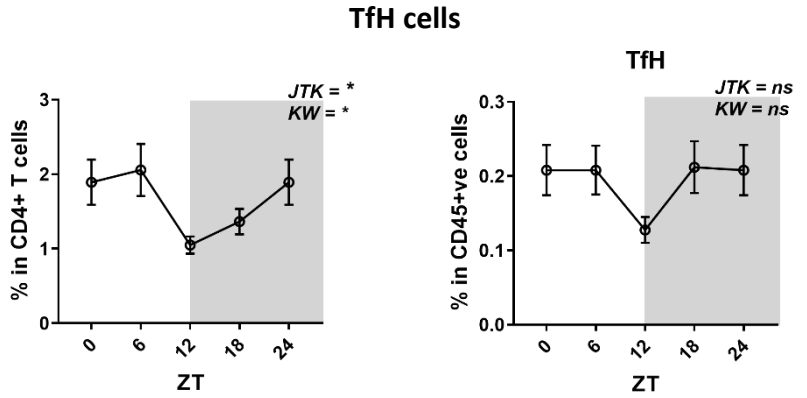
TfH cells
JTK = *
KW = *
% in CD4+ T cells
ZT
TfH
JTK = ns
KW = ns
% in CD45+ve cells
ZT

C.

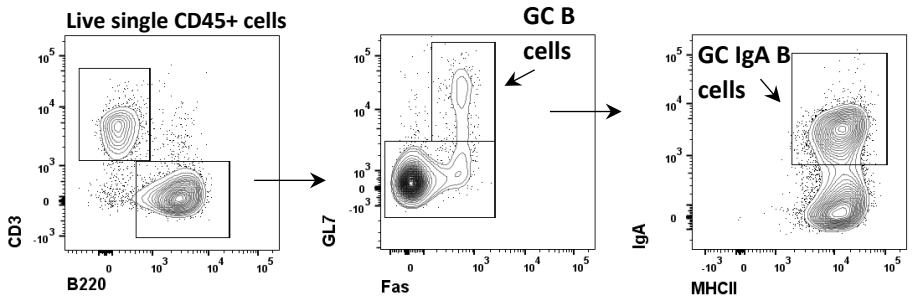
Live single CD45+ cells
CD3
B220
GC B cells
GL7
Fas
GC IgA B cells
IgA
MHCII

D.

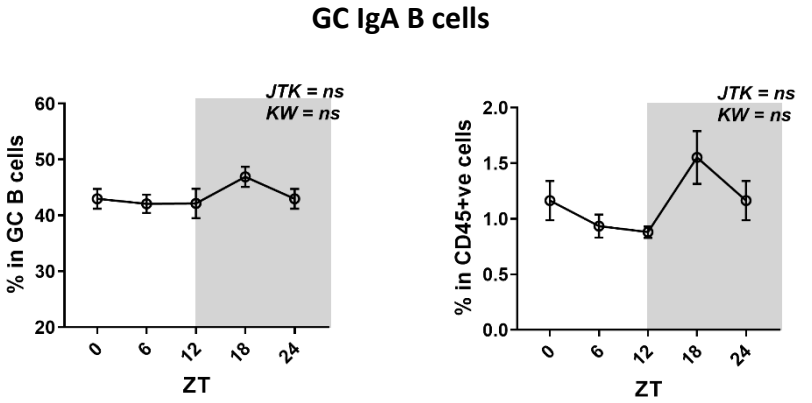
GC IgA B cells
JTK = ns
KW = ns
% in GC B cells
ZT
JTK = ns
KW = ns
% in CD45+ve cells
ZT

Figure 3.3. No consistent time of day variation in IgA induction within Peyer's patches

At necropsy, the Peyer's patches (PP) were removed from each mouse and processed for flow cytometry. (A) Gating strategy for T-follicular helper (TfH) cells in the PP. (B) Frequency of TfH cells, in the PP as a % of their parent population (left) and as a % of total CD45+ cells (right). (C) Gating strategy for germinal centre (GC) IgA+ B cells and non-GC IgA+ B cells. (D) Frequency of GC IgA+ B cells in the PP as a % of their parent population (left) and as a % of total CD45+ cells (right). ZT0 is double plotted as ZT24 to facilitate viewing the data. Variance in the data across the experimental timepoints assessed by Krushkal Wallis (KW) test. Rhythmicity assessed by JTK analysis. *p=<0.05; ****p= <0.0001. Bars indicate mean±SEM. Shaded areas on graphs represent the dark phase. Data representative of two independent experiments (n=5 mice/ timepoint; C57BL/6 female mice aged 8-12 weeks).

Following, CSR and maturation in the PP, B cells differentiate into PCs which reside within the intestinal LP [71]. Therefore, we then analysed the frequency and number of IgA+ PCs within the intestinal LP. Over several experimental repeats, we did not detect any consistent, significant variation or rhythmicity in the frequency or number of IgA+ PCs over the experimental timepoints (Figure 3.4A&B). IgA+ PCs were distinguished based on their expression of surface-bound IgA, the transmembrane proteoglycan syndecin-1 (CD138) and downregulated expression of B220 [333]. This gating strategy worked appropriately in the small intestines, but we found the flow cytometry staining to be variable in the large intestines, despite using the same fluorescently tagged anti-CD138 antibodies (data not shown). Therefore, we used an alternative, previously optimised [98], gating strategy to identify IgA+ PCs in the large intestines (Figure 3.5A). Again, analysis revealed no consistent time-of-day differences in the frequency or number of IgA+ PCs in the large intestines (Figure 3.5B). Together, this suggested that the frequency of IgA+ PCs within the intestines is stable over a 24-hour period.

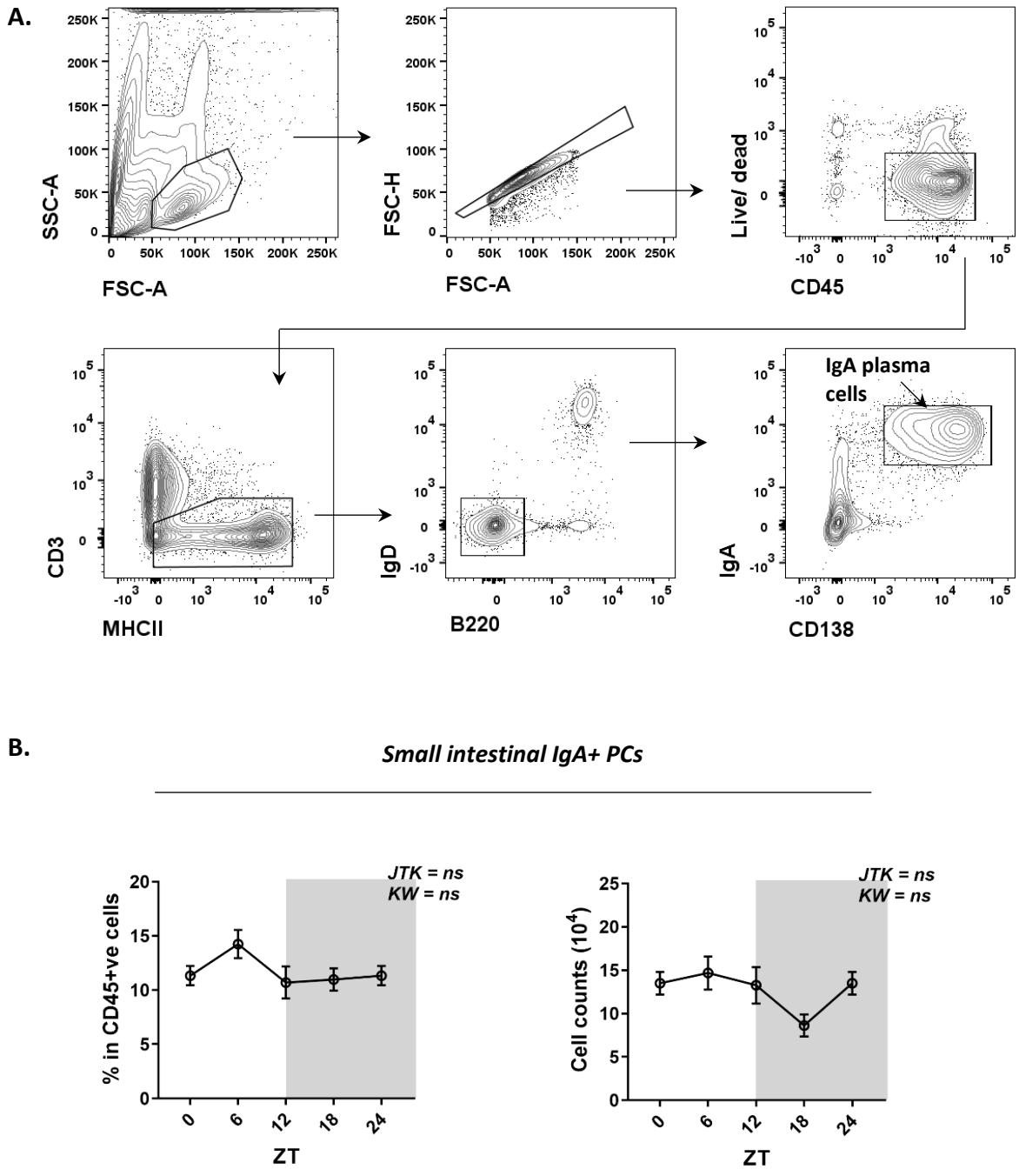

Figure 3.4. No consistent differences in the frequency or cell counts of small intestinal IgA+ PCs over the circadian day

(A) Flow cytometry gating strategy for small intestinal CD138+ IgA+ PCs. (B) Frequency (left) and counts (right) of small intestinal IgA+ PCs assessed by flow cytometry. ZT0 is double plotted as ZT24 to facilitate viewing the data. Variance in the data across the experimental timepoints assessed by Krushkal Wallis (KW) test. Rhythmicity assessed by JTK analysis. (n=5 mice/ timepoint; C57BL/6 female mice aged 8-12 weeks). Bars indicate mean±SEM. Data representative of two independent experiments. Shaded areas on graphs represent the dark phase.

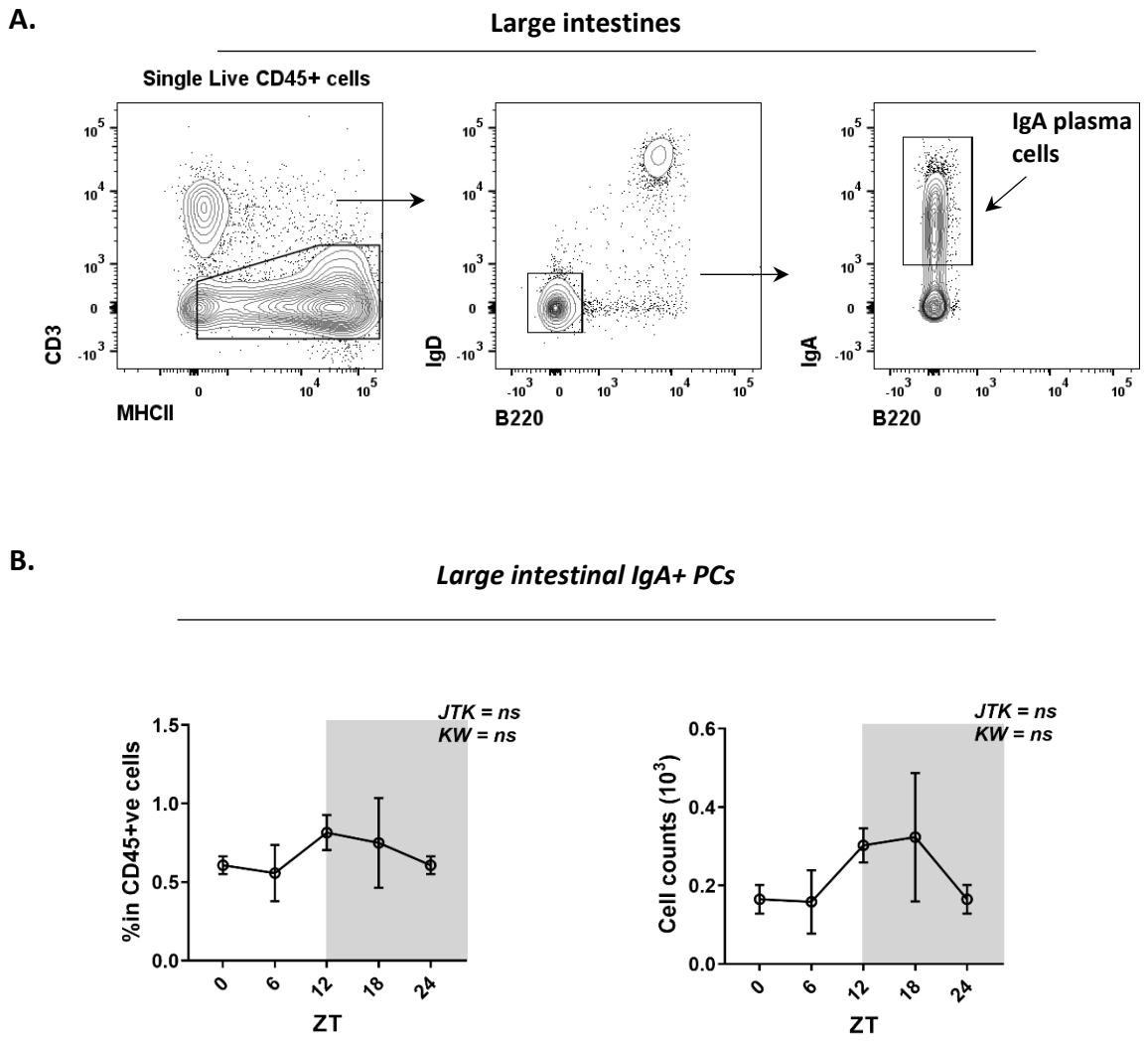

Figure 3.5. No change in the frequency or counts of large intestinal IgA+ PCs over the circadian day

(A) Flow cytometry gating strategy for large intestinal B220- IgA+ PCs. (B) Frequency (left) and counts (right) of large intestinal IgA+ PCs assessed by flow cytometry. ZT0 is replotted as ZT24 to facilitate viewing the data. Variance in the data across the experimental timepoints assessed by Krushkal Wallis (KW) test. Rhythmicity assessed by JTK analysis. (n=5 mice/ timepoint; C57BL/6 female mice aged 8-12 weeks). Bars indicate mean±SEM. Shaded areas on graphs represent the dark phase. Data representative of two independent experiments.

To ensure that non-significant fluctuations in the frequency of B cell subsets in the PPs were not biologically significant in contributing to oscillations in faecal sIgA, we then sought to determine the relative amount of IgA secreted by both IgA+ PCs cells and IgA+ B cells. To do this, we FACS-sorted IgA+ B cells from the PPs (Figure 3.6A) and IgA+ PCs from the small intestines, along with a population of naïve IgD+ B cells as a control (post-sort purity >95%; Figure 3.6B). Cells were then cultured in complete media and left for 16 hours, after which the concentration of IgA in the supernatants was determined by ELISA. This demonstrated that IgA+ B cells have limited secretory capacity in contrast to terminally differentiated IgA+ PCs, which were the major IgA-secreting cell subset within the small intestinal tissues (Figure 3.6C).

Collectively, these results demonstrate that intestinal sIgA rhythms are not accounted for by changes in the absolute frequencies or numbers of IgA+ cells within the intestines over the circadian day and provoke the hypothesis that IgA secretion may instead be regulated at the level of cell-intrinsic secretory activity.

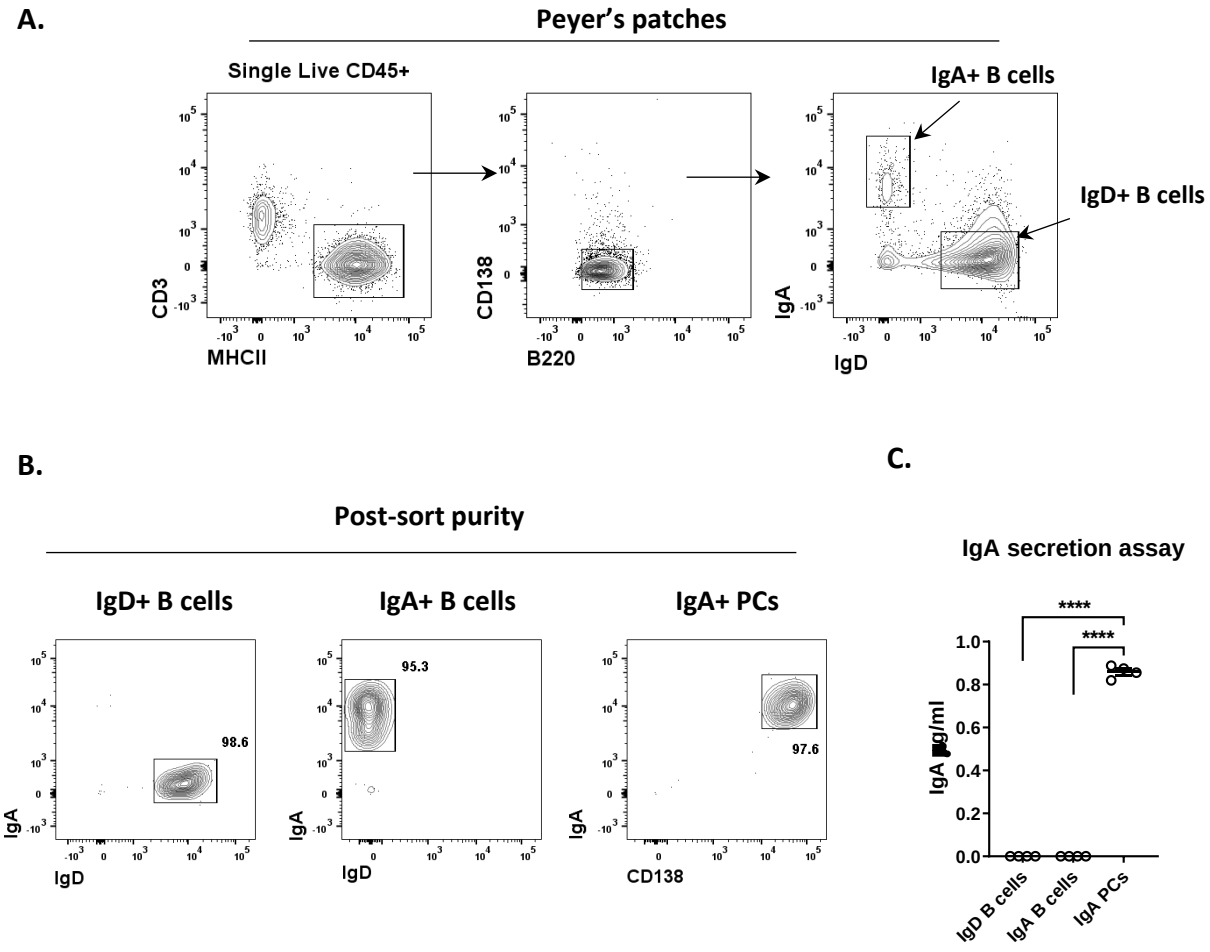

Figure 3.6. IgA+ PCs are the major IgA-secreting B cell subset in the intestines

IgD+ B cells, IgA+ B cells and IgA+ PCs were FACS-sorted from the Peyer's patches and small intestinal lamina propria, respectively. Cells were plated at 10k cells/ well in complete media and cultured for 16 hours at 37◦C. (A) Gating strategy for IgD+ and IgA+ B in Peyer's patches. IgA+ CD138+ PCs were pre-gated as CD45+ CD3- MHCII+ B220- IgD-. (B) Post-sorting purity plots of IgD+ B cells, IgA+ B cells and IgA+ PCs (left to right). Number represents frequency of all events. (D) Concentration of IgA in the supernatants of sorted cells post-culture determined by ELISA. ANOVA with post-hoc Tukey test used to determine differences between groups; ****= $p<0.0001$. Data representative of two independent experiments; n=4 mice/ experiment; C57BL/6 male and female mice aged 6-12 weeks).

3.2.3 PC IgA production and secretion varies over the course of the day

To determine whether PCs themselves secrete varying amounts of IgA at different times of the day, we FACS-sorted IgA+ PCs from the small intestinal LP of mice housed in opposing 12-hour light:dark cabinets, at a time that corresponded with the beginning, or end, of the light phase (Figure 3.7A). An equal number of cells were then plated and cultured for 16 hours in complete media, and the concentration of IgA determined in the supernatants by ELISA. This demonstrated a strong trend towards increased IgA secretion by PCs isolated at ZT0 compared to ZT12 (Figure 3.7B).

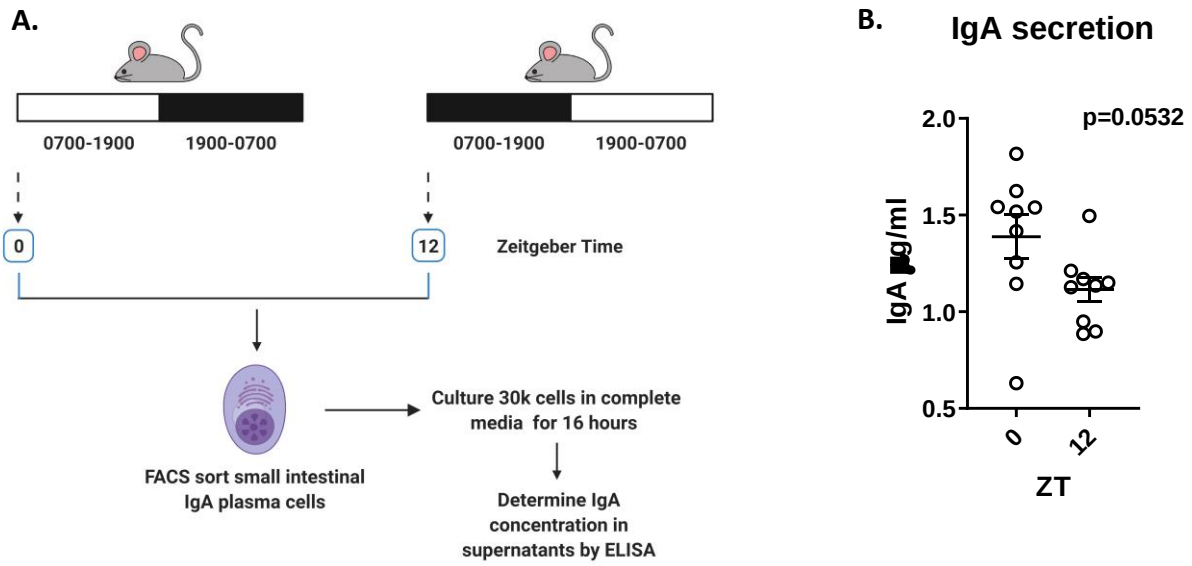

Figure 3.7. Time of day difference in PC secretion of IgA

(A) Schematic of the experiment. Mice were housed in cabinets with opposing 12-hour light:dark schedules. One group of mice from each cabinet were euthanised at the same time (representing ZT0 and ZT12 – blue boxes). IgA+ PCs were FACS sorted from the small intestines and cultured for 16 hours in complete media. Image created using BioRender. (B) Concentration of IgA in the supernatants of cultured IgA+ PCs as determined by ELISA. Data pooled from two independent experiments (n=4-5 mice/ timepoint; C57BL/6 female mice aged 10-12 weeks); bars indicate mean±SEM. Unpaired T test performed to determine differences between the groups (p value included on graph).

We then reasoned that time of day differences in IgA secretory capacity may therefore be determined by oscillations in PC-intrinsic function and general activity. To evaluate this, we performed bulk RNA sequencing on FACS-sorted small intestinal IgA+ PCs at multiple timepoints over a 24-hour period. As a quality control measure, to ensure that our RNA sequencing data was truly representative of IgA+ PCs, we simultaneously FACS-sorted and performed RNA sequencing on a population of IgD+ B cells at a single timepoint.

For the analysis, we first determined differences between the IgA+ PC and IgD+ B cell sequencing data. IgA+ PCs and IgD+ B cells displayed distinct transcriptomes with 14397 transcripts being significantly altered (2275 upregulated in IgA+ PCs and 12122 downregulated, compared with IgD+ B cells) (Figure 3.8A). Differentially expressed genes (DEGs) highly upregulated within IgA+ PC group included *Jchain, Igha* and *Igkc* genes, which

are specific to the IgA+ PC subsets expected, while there was a relative lack of expression of B cell genes including the transcription factor gene *Pax5*. This confirmed that the transcriptome of our FACS-sorted IgA+ PCs was truly representative of this cell population.

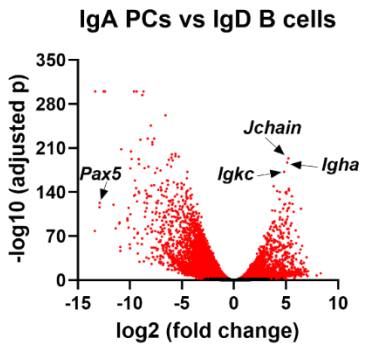

Figure 3.8. The transcriptional profile of IgA+ PCs is appropriately different to that of IgD+ B cells

(A) Volcano plot illustrating differentially expressed genes (DEGs) in IgA+ PCs compared with IgD+ B cells. 14397 transcripts were significantly different (coloured red); 2275 upregulated and 12122 downregulated (p adj. <0.05). Normalised reads (Fragments per kilobase of transcript per million mapped reads; FPKM) from biological replicates were averaged for DEG comparison (n=3 mice for IgD+ B cell and n=20 mice for IgA+ PC group; C57BL/6 female mice aged 10 weeks). Data representative of one experiment.

We next evaluated whether PC gene expression oscillated over the experimental timepoints. To do this, we performed JTK analysis on the entire IgA+ PC RNA sequencing dataset. We considered values with an adjusted p<0.01 and a FDR <0.01 as significantly oscillatory. This analysis identified robust oscillations in 2713 genes (Figure 3.9A). Unbiased analysis of the top 20 genes identified as having the greatest amplitude of oscillation, included those encoding IgH and IgL chain components, including the constant alpha region of IgA, *Igha*, and those regulating protein translation and processing including *Xbp1*, *Hsp90ab1*, *Hsp90b1*, *Eef1a1*, *Eef2*, *Rps24*, *Sec11c* (Figure 3.9B). Among the 2713 oscillating genes, *Igha* was identified as having the greatest amplitude of oscillation (Figure 3.9C).

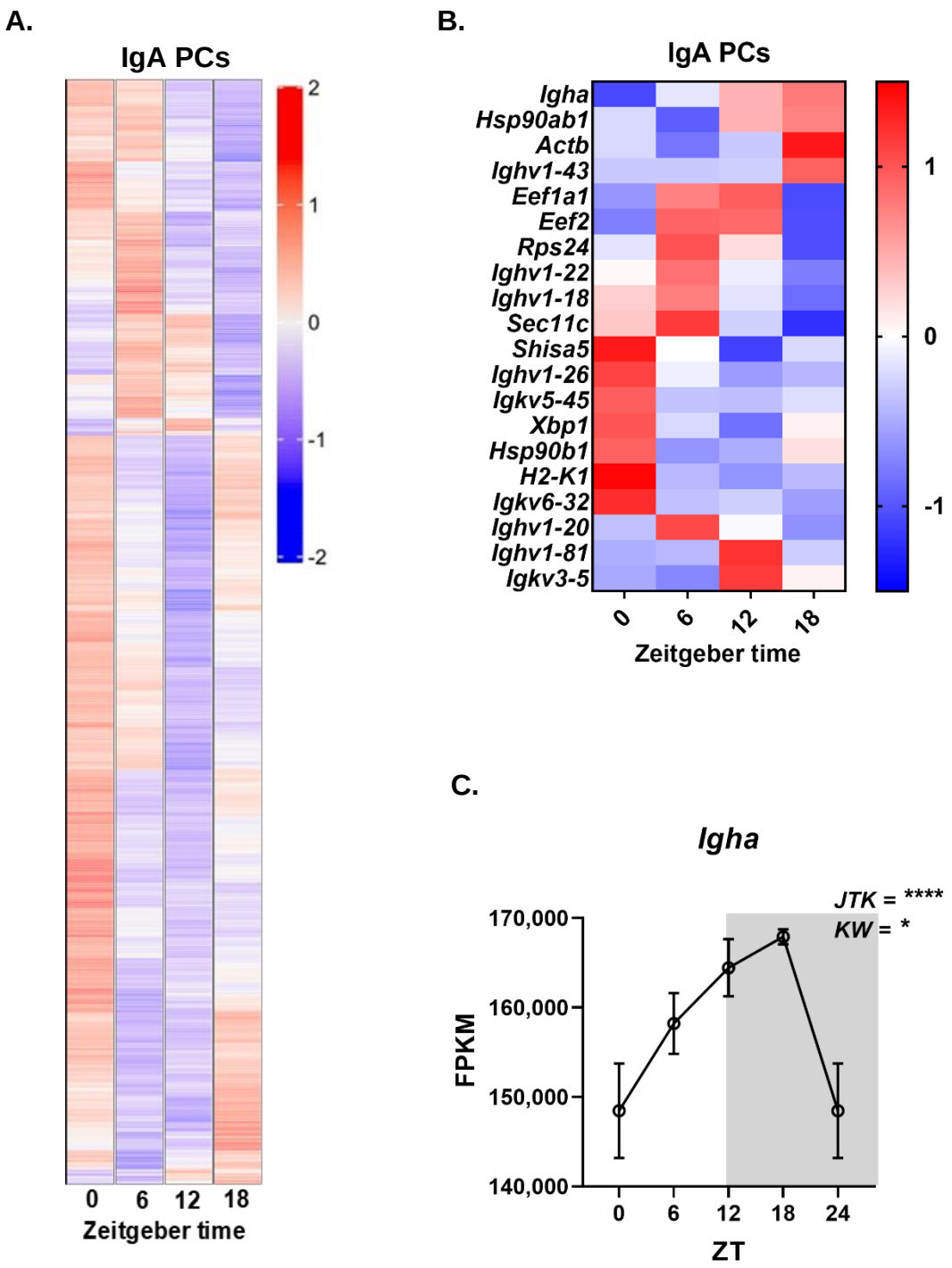

Figure 3.9. The transcriptional profile of IgA+ PCs oscillates over the circadian day

(A) Heatmap of 2713 genes identified as significantly oscillatory by JTK analysis (adj. p<0.01; false discovery rate <0.01). Normalised reads in FPKM are expressed as mean z-scores (red, high; blue, low). (B) Heatmap of the top twenty genes demonstrating the greatest oscillatory amplitude by JTK analysis, clustered according to phase of oscillation. Normalised reads in FPKM are expressed as mean z scores (red, high; blue, low). (C) Normalised reads in FPKM of *Igha* over the experimental timepoints. ZT0 is double plotted as ZT24 to facilitate viewing the data. Variance in the data assessed by Kruskal Wallis (KW) test. *= p<0.05; ****= p<0.0001. Data representative of one experiment (n=5 mice/ timepoint; C57BL/6 female mice aged 10 weeks). Horizontal bars represent mean±SEM. Shaded area on graphs represents the dark phase.

To infer the biological processes within IgA+ PCs that were differentially expressed during light/ dark cycles, and rest/ wake periods, we next performed functional enrichment analysis of DEGs at ZT0 (light)/ ZT12 (dark), and ZT6 (rest)/ ZT18 (wake), by using Kyoto Encyclopedia of Genes and Genomes (KEGG) pathways analysis (Figure 3.10A-D). Excluding the disease-associated pathways, this analysis identified that genes mapping to IgA production were consistently within the top five significantly differentially expressed pathways across the analysed timepoints (Figure 3.10A-D).

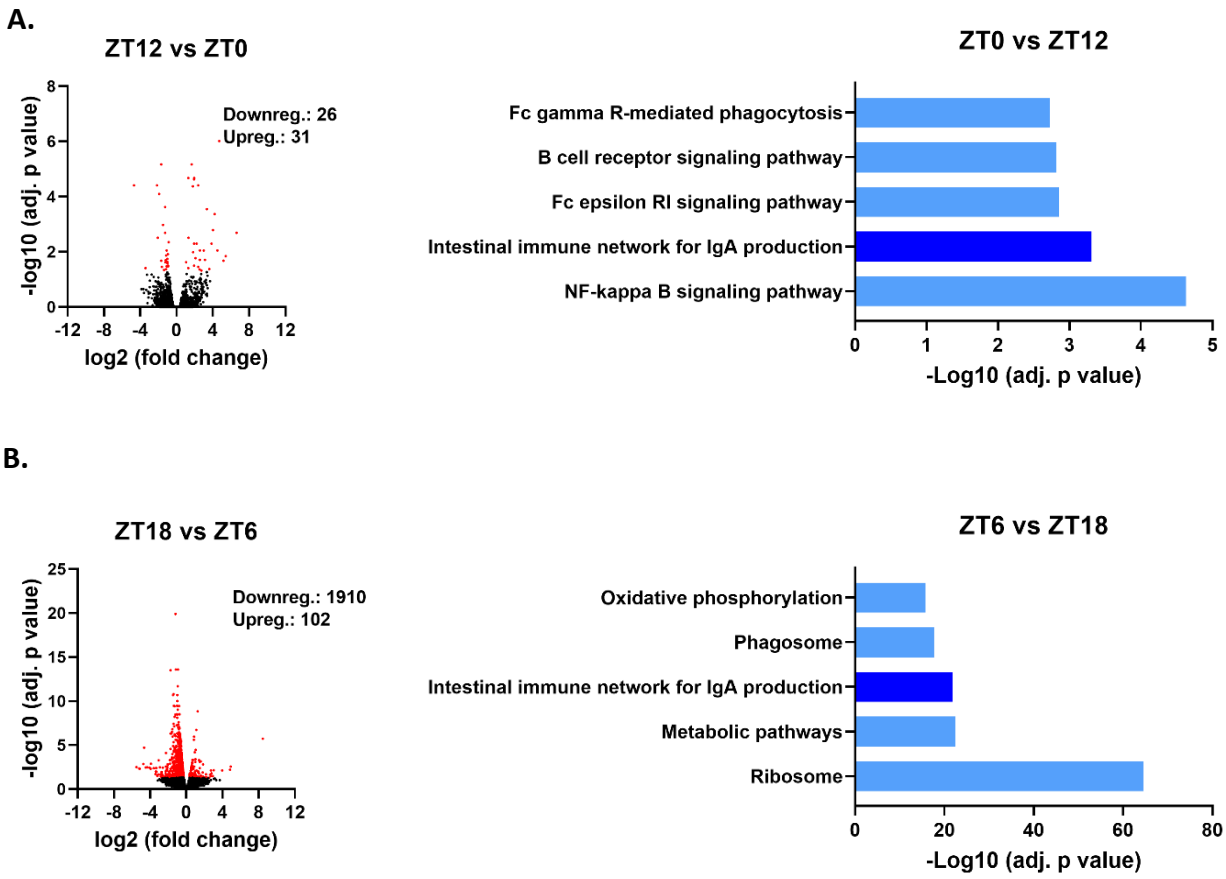

Figure 3.10. Differentially expressed genes in IgA+ PCs at light/ dark and rest/ wake periods consistently map to IgA production

Volcano plots of differentially expressed genes (DEGs) (left) and functional enrichment analysis of DEGs by KEGG analysis (right) in IgA+ PCs at (A) ZT12 vs ZT0 and (B) ZT18 vs ZT6. The top five most significant KEGG pathways are shown (disease-associated pathways are omitted). Data representative of one experiment (n=5 mice/ timepoint; C57BL/6 female mice aged 10 weeks). Downreg. = downregulated; upreg. = upregulated. Columns in dark blue represent pathways which are consistently different across both datasets.

To explore further the functional relevance of rhythmic gene expression in IgA+ PCs, we then performed Ingenuity Pathway Analysis (IPA) on all genes that were identified as significantly oscillatory by JTK analysis, at all timepoints. This identified that genes enriched in pathways relating to B cell survival, metabolism, proliferation and protein translation, as well as cholesterol biosynthesis pathways, had significant enrichment of oscillating genes. Key examples of these pathways are plotted in Figures 3.11-3.13.

Of note, genes encoding proteins relating to the BAFF/ APRIL signalling pathway, such as the cell surface receptors BCMA (encoded by *Tnfrsf17*) and TACI (*Tnfrsf13b*), genes encoding intracellular signalling proteins (such as the tumour necrosis factor receptor-associated factor [TRAF] proteins), as well those encoding transcription factors such as nuclear factor-κB1 (NF-κB1), NF-κB2 and ETS Like-1 (Elk1) – which regulate T cell-independent antibody production and the maintenance of PCs, respectively [341] – were significantly rhythmic within IgA+ PCs over the course of the day (Figure 3.11A-F).

BAFF/ APRIL Signalling Pathway

A.

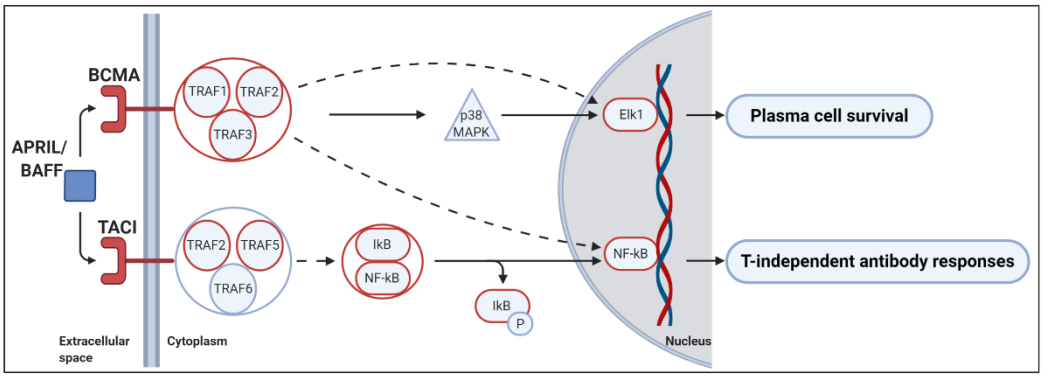

Boxed in red = JTK significant

B.

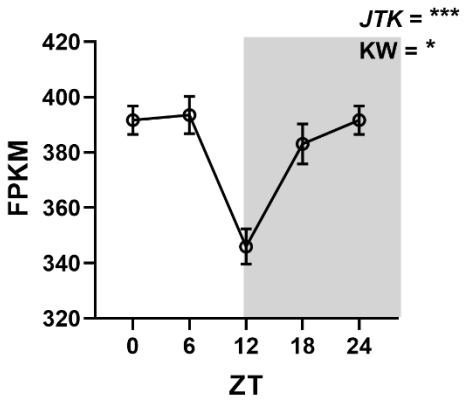

C.

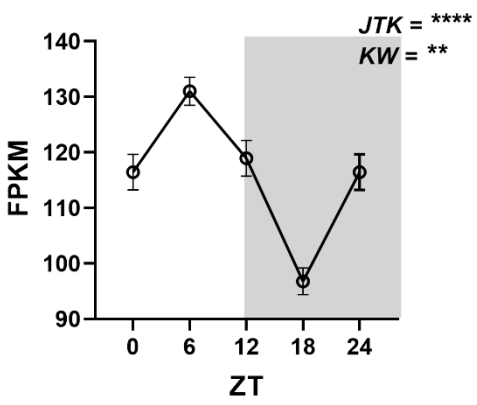

D.

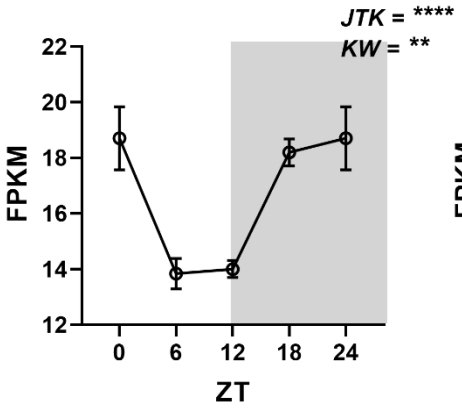

E.

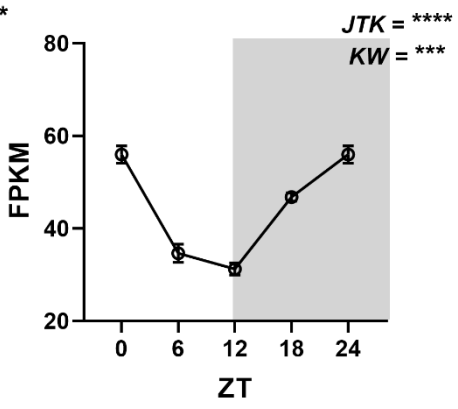

F.

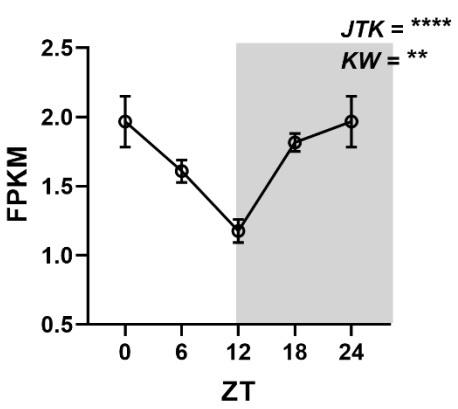

Figure 3.11. Genes mapping to the BAFF/ APRIL signalling pathway display rhythmicity over the circadian day in IgA+ PCs

(A) Schematic overview of the BAFF/ APRIL signalling pathway in PCs (adapted from [341]). Both BAFF and APRIL can engage the two PC surface receptors, B cell maturation antigen (BCMA, encoded by the *Tnfrsf17* gene) and transmembrane activator and calcium-modulating cyclophilin ligand interactor (TACI, *Tnfrsf13b*) [341]. In PCs, BAFF/ APRIL engagement with TACI/ BCMA leads to the activation of the tumour necrosis factor receptor-associated factor (TRAF) family of intracellular signalling proteins and subsequent activation of transcription factors nuclear factor-κBs (NF-κB1 and NF-κB2) and ETS transcription factor ELK1 (Elk1) [341]. In PCs, the TACI pathway regulates T cell-independent antibody production, whereas BCMA modulates the maintenance of PCs within their tissue niche [341]. Genes encoding receptors/ signalling proteins outlined in red were found to oscillate significantly by JTK analysis (adjusted p <0.01; FDR <0.01). Image created in BioRender.

(B-F) Selected plots of genes encoding proteins highted in (A), including (B) *Tnfrsf17* (encoding BCMA), (C) *Tnfrsf13b* (TACI), (D) *NF-κB1* (NF-κB1) (E) *NF-κB2* (NF-κB2) and (F) *Elk1* (Elk1). Mean FPKM values are plotted over each timepoint. ZT0 is double plotted as ZT24 to facilitate viewing the data. Variance in the data across the experimental timepoints assessed by Krushkal Wallis (KW) test. Rhythmicity assessed by JTK analysis. *= p<0.05; **= p<0.01; ***= p<0.001; ****= p<0.0001. Data representative of one experiment (n=5 mice/ timepoint; C57BL/6 female mice aged 10 weeks). Horizontal bars represent mean±SEM. Shaded area on graphs represents the dark phase.

Furthermore, circadian oscillations were detected in the expression of key genes involved in the mTOR signalling pathway (Figure 3.12A). Specifically, we found enrichment of genes relating to mTOR1 signalling (Figure 3.12B), such as *Ribosomal Protein S6 Kinase B1* (*Rps6kb1*), *Ribosomal protein S6* (*Rps6*), *Eukaryotic Translation Initiation Factor 4E-Binding Protein 1* (*Eif4ebp1*) and *Eukaryotic translation initiation factor 4B* (*Eif4b*) (Figures 3.12C-F). These genes encode proteins which regulate intracellular protein synthesis in response to environmental cues such as nutrient availability and cellular energy status [342].

A.

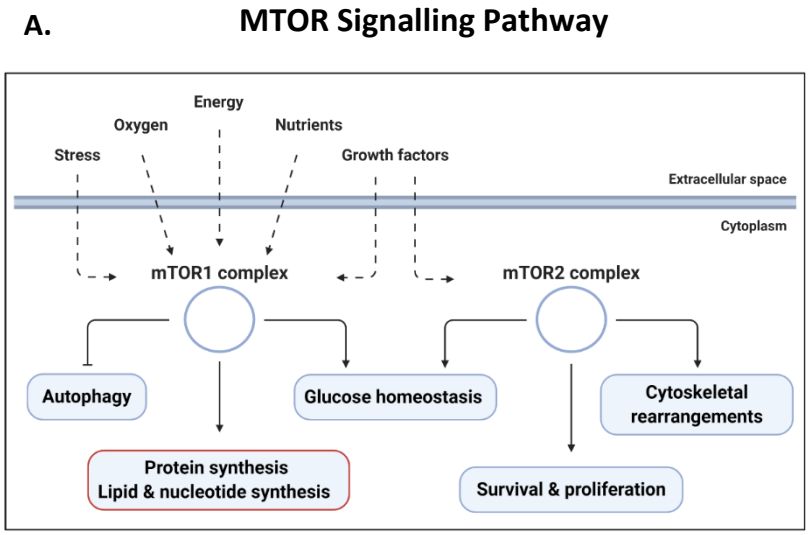

Boxed in red = JTK significant

B.

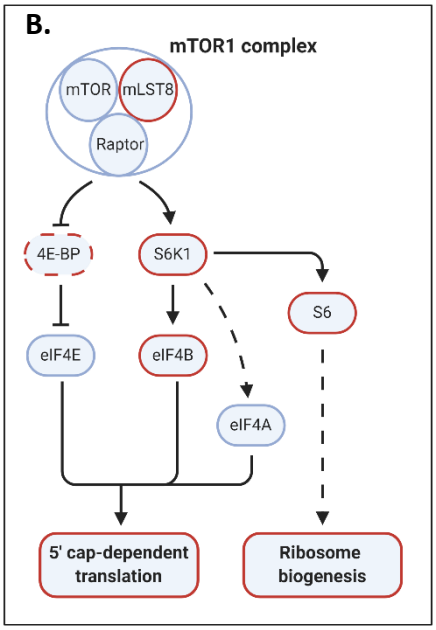

C.

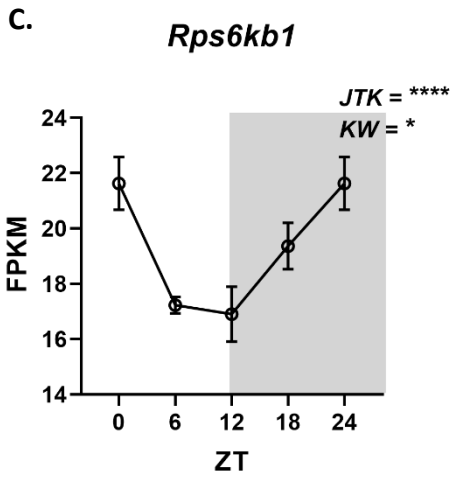

D.

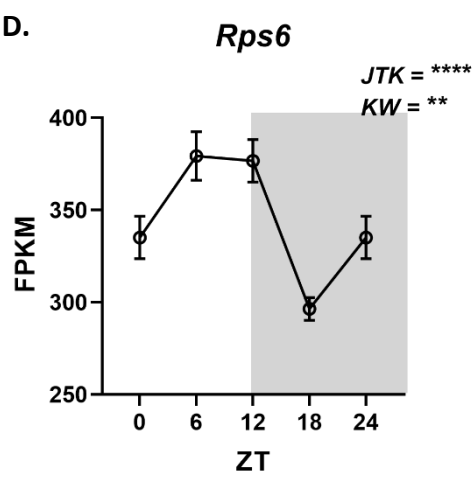

E.

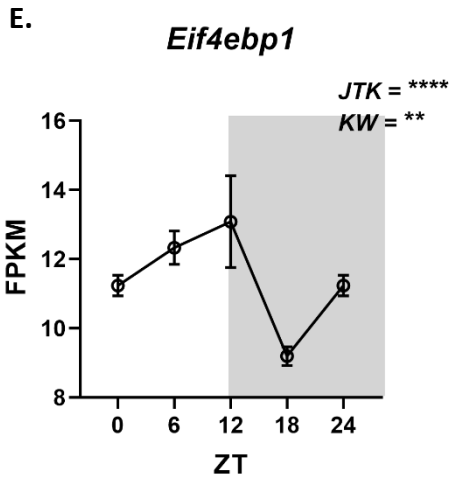

F.

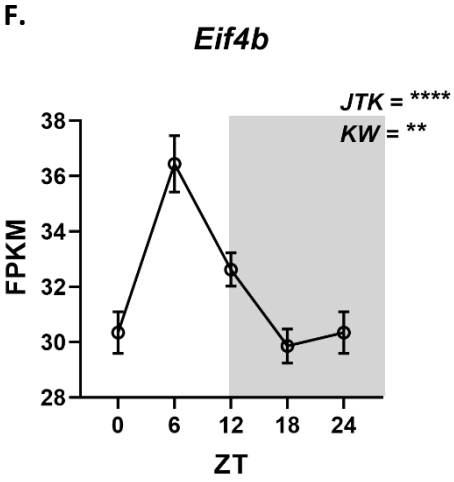

Figure 3.12. Genes mapping to the mTOR1 signalling pathway display rhythmicity in IgA+ PCs over the circadian day

(A) Schematic overview of the mTOR signalling pathway (adapted from [342]). The mTOR signalling pathway comprises two complexes (mTOR1 and mTOR2) which integrate nutritional and environmental cues and subsequently regulate the metabolism, growth, proliferation and survival of the cell [342]. (B) Schematic of the major components of the mTOR1/ protein synthesis signalling pathway (adapted from [342]. MTORC1 promotes protein synthesis by phosphorylating the eukaryotic initiation factor 4E (eIF4E)-binding protein 1 (4E-BP1) and the p70 ribosomal S6 kinase 1 (S6K1) [342]. The phosphorylation of 4E-BP1 prevents its binding to eIF4E, enabling eIF4E to enhance 5'cap-dependent translation [342]. The stimulation of S6K1 activity by mTORC1 leads to increases 5'cap-dependent translation and the translation of ribosomal proteins, such as ribosomal protein S6 (Rps6) [342]. The net result is increase in protein translation within the cell. Genes encoding proteins/ processes in A&B outlined in red were found to oscillate significantly by JTK analysis (adjusted p <0.01 and false discovery rate <0.01). Image created using BioRender.

(C-F) Selected plots of genes encoding proteins highted in (B). Mean FPKM values are plotted over each timepoint. ZT0 is double plotted as ZT24 to facilitate viewing the data. Variance in the data across the experimental timepoints assessed by Krushkal Wallis (KW) test. Rhythmicity assessed by JTK analysis. *= p<0.05; **= p<0.01; ***= p<0.001; ****= p<0.0001. Data representative of one experiment (n=5 mice/ timepoint; C57BL/6 female mice aged 10 weeks). Horizontal bars represent mean±SEM. Shaded area on graphs represents the dark phase.

Moreover, analysis identified that genes enriched in pathways relating to cholesterol biosynthesis demonstrated significant circadian oscillations within IgA+ PCs (Figure 3.13A). This included genes encoding enzymes involved in the mevalonate pathway, which is an essential metabolic pathway that converts Acetyl-CoA to isoprenoids, such as cholesterol, which play important roles in multiple cellular processes including cell growth, organelle assembly and the post-translational modification of proteins (Figure 3.13B). We also identified that major regulators of cholesterol synthesis and cellular uptake (such as *Srebf2* – which encodes sterol regulatory element binding transcription factor 2 [SREBP-2]] and *Ldlr* – encoding the lipoprotein receptor [LDLR]), as well as cholesterol efflux (such as *Nr1h2* – which encodes liver X receptor beta [LXRβ] and *Abca1* – encoding ATP-binding cassette subfamily A member 1 [ABCA1]) were significantly rhythmic over the circadian day in IgA+ PCs (Figure 3.13A; Figure3.13C-F).

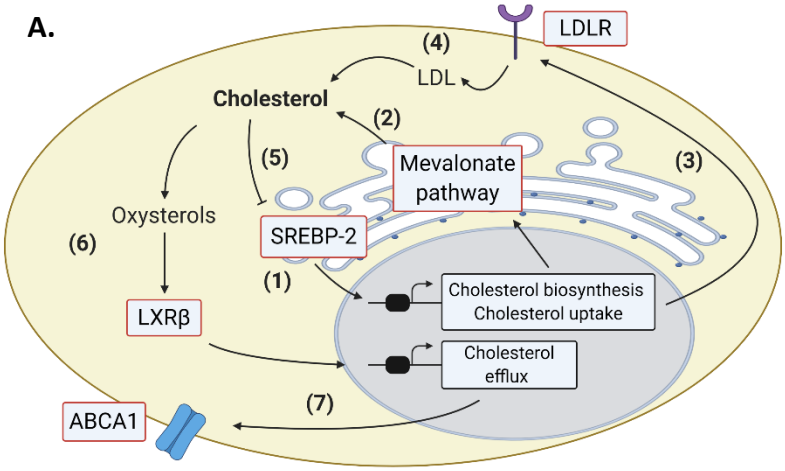

Boxed in red = JTK significant

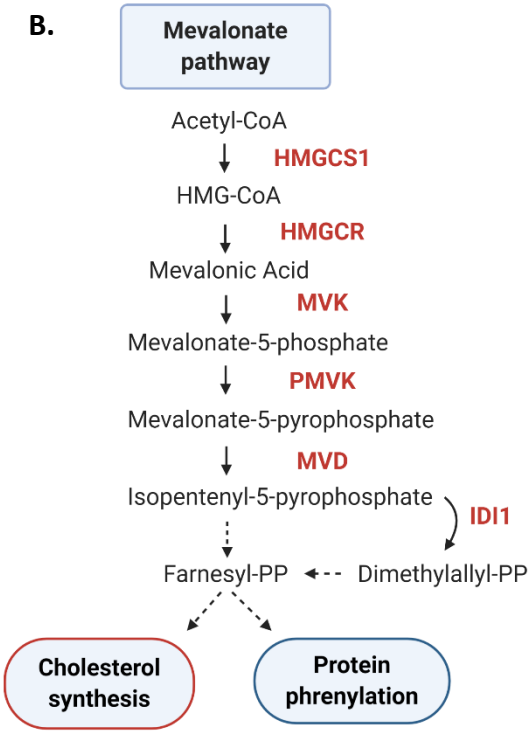

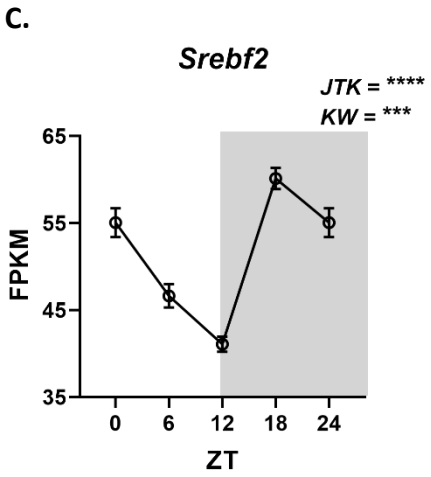

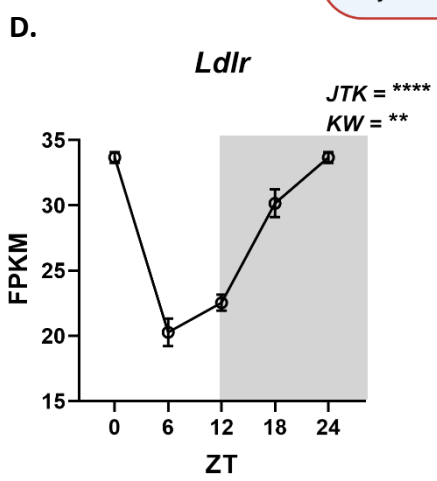

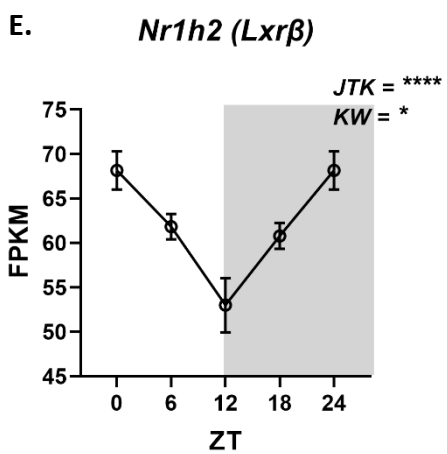

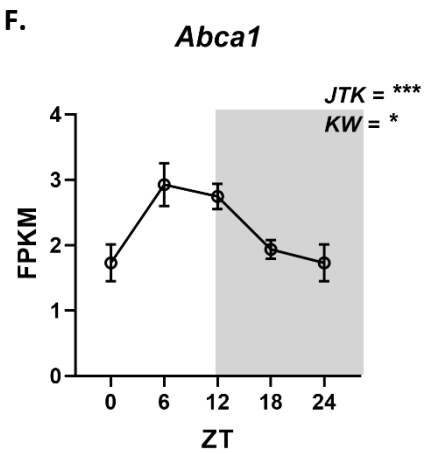

Figure 3.13. Genes mapping to the cholesterol transport and biosynthesis pathway display rhythmicity in IgA+ PCs over the circadian day

(A) Schematic overview of cholesterol homeostasis in cells (Adapted from [343]. (1) In the setting of lipid deprivation, or in the presence of ER stress, low pH and/ or inflammatory cytokines, ER-membrane bound sterol regulatory element binding protein 2 (SREBP-2) undergoes activation and processing in the glogi and subsequently translocation to the nucleus, where it modulates transcription of genes required for endogenous cholesterol synthesis via the Mevalonate pathway (2), and exogenous cholesterol uptake via upregulation of the low-density lipoprotein (LDL) receptor (LDLR) (3+4) [344]. Cholesterol can negatively regulate its own levels through the inhibition of processing of SREBP-2 (5), or through its conversion to oxysterols that activate liver X receptors, such as liver X receptor beta (LXRβ), which lowers cellular cholesterol levels, in part by upregulating expression of the cholesterol efflux pump, ABCA1 (7) [343, 344]. Genes encoding receptors/ signalling proteins outlined in red were found to oscillate significantly by JTK analysis (adjusted $p<0.01$; false discovery rate <0.01). Image created using BioRender.

(B) Schematic overview of the Mevalonate pathway (adapted from [345]. Metabolites of the pathway are shown in black and enzymes of the pathway are shown in red. Genes encoding all enzymes in red were identified as significantly oscillatory by JTK analysis (adjusted $p<0.01$; FDR <0.01).

(C-F) Selected plots of genes encoding (C) SREBP-2, (D) LDLR, (E) LXRβ, (F) ABCA1 receptor proteins, over the course of the day. Mean FPKM values are plotted over each timepoint. ZT0 is double plotted as ZT24 to facilitate viewing the data. Variance in the data across the experimental timepoints assessed by Krushkal Wallis (KW) test. Rhythmicity assessed by JTK analysis. *= $p<0.05$; **= $p<0.01$; ***= $p<0.001$; ****= $p<0.0001$. Data representative of one experiment (n=5 mice/ timepoint; C57BL/6 female mice aged 10 weeks). Horizontal bars represent mean±SEM. Shaded area on graphs represents the dark phase.

In addition, other select genes identified as significantly oscillatory included *Slc7a5*, *Hk2* and *Prdm1*, which encode the Large Amino Acid Transporter 1 (LAT1), Hexokinase 2 and Blimp1, which are important genes involved in nutrient sensing, PC metabolism and Ig production, respectively (Figure 3.14A-C).

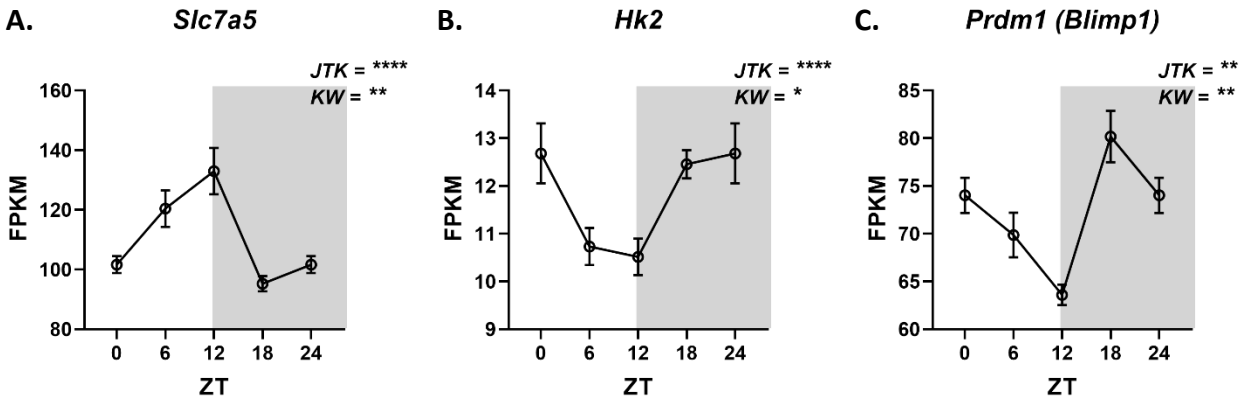

Figure 3.14. Key genes involved in nutrient sensing, metabolism and immunoglobulin production oscillate in IgA+ PC over the circadian day

(A-C) Selected plots of significantly oscillating genes involved in (A) nutrient sensing: *Slc7a5* (encoding LAT1), (B) metabolism: *Hk2*, and (C) immunoglobulin production: *Prdm1* (encoding Blimp1). Mean FPKM values are plotted over each timepoint. ZT0 is double plotted as ZT24 to facilitate viewing the data. Variance in the data across the experimental timepoints assessed by Krushkal Wallis (KW) test. Rhythmicity assessed by JTK analysis (A and C have an adjusted $p<0.01$ and FDR <0.01; B has an adjusted $p<0.01$ and FDR of 0.014). *= $p<0.05$; **= $p<0.01$; ***= $p<0.001$; ****= $p<0.0001$. Data representative of one experiment (n=5 mice/ timepoint; C57BL/6 female mice aged 10 weeks). Horizontal bars represent mean±SEM. Shaded area on graphs represents the dark phase.

Interestingly, JTK analysis also identified that the expression of genes encoding core biological clock components, including *Arntl* (encoding Bmal1), *Per2* (Per2) and *Nr1d1* (Rev-erbα), displayed significant rhythmicity, suggesting that IgA+ PCs may have a cell-intrinsic biological clock (Figure 3.15A-C).

In summary, this data provides evidence that PC secretion of IgA varies over the course of the day and that the cell-intrinsic transcriptome relating to metabolism and IgA synthesis demonstrates circadian rhythmicity over a 24-hour period. Taken together, this suggests that diurnal regulation of PC IgA production drives the observed rhythms in intestinal sIgA.

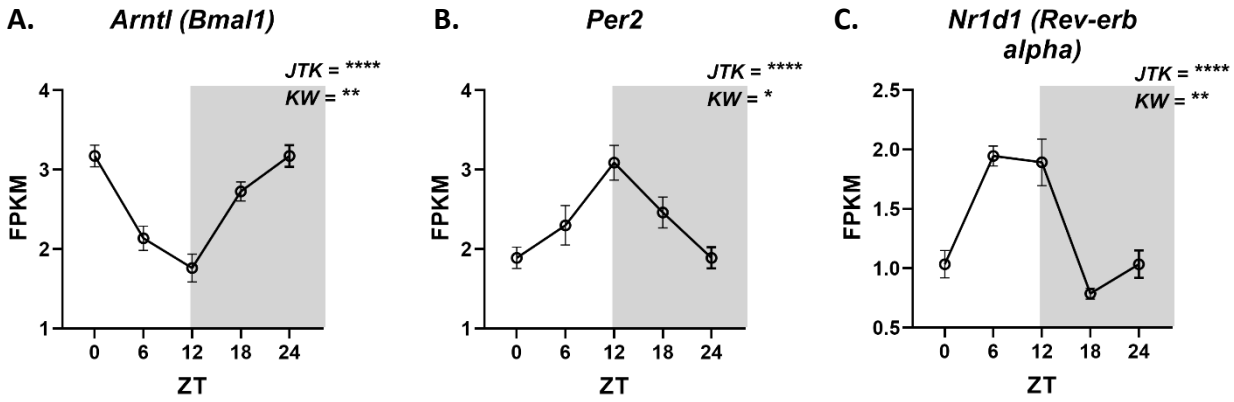

Figure 3.15. Biological clock genes within IgA+ PCs oscillate over the circadian day

(A-C) Selected plots of significantly oscillating core molecular clock genes (JTK analysis adjusted p<0.01; FDR <0.01). Mean FPKM values are plotted over each timepoint. ZT0 is double plotted as ZT24 to facilitate viewing the data. Variance in the data across the experimental timepoints assessed by Krushkal Wallis (KW) test. Rhythmicity assessed by JTK analysis. *= p<0.05; **= p<0.01; ***= p<0.001; ****= p<0.0001. Data representative of one experiment (n=5 mice/ timepoint; C57BL/6 female mice aged 10 weeks). Horizontal bars represent mean±SEM. Shaded area on graphs represents the dark phase.

3.4 Discussion

In this chapter, we have identified circadian oscillations in the concentration of faecal sIgA. We have also shown that PCs secrete different amounts of IgA antibodies at different times of the day and that components of the PC transcriptome relating to IgA production display robust oscillations over a 24-hour period. In accordance with this, we found that cell-intrinsic gene pathways relating to nutrient sensing, metabolism and biological clock genes exhibited rhythmicity within IgA+ PCs. Together, this data demonstrates that intestinal IgA is imprinted with circadian rhythmicity and that oscillatory IgA may be the result of cell-intrinsic regulation of IgA+ PC function – potentially by both circadian clock and environmental nutrient cues.

In agreement with previous studies [337-340], we found time of day changes in the concentration of murine faecal sIgA, with peak concentrations occurring in the early to mid-light (resting) phase. We also demonstrated that sIgA within small intestinal washes demonstrated a similar rhythmic profile to sIgA within the faeces. These findings provoke the question of the relevance of the timing of peak sIgA values. It could be hypothesised that enhanced sIgA responses are present during the light phase to anticipate a period of host vulnerability to foreign pathogens during resting. By contrast, elevated sIgA responses identified in the faeces and intestinal washes around the early to mid-light phase may actually be the result of enhanced intrinsic PC function during the active phase, owing to the time-lag between initiation of PC Ig synthesis, secretion and detection of sIgA in intestinal content, which could be up to several hours [346-348]. In either instance, the functional consequence of oscillatory IgA is intriguing and given the known role of gut IgA responses, may have relevance for host protective immunity, or the modulation of the intestinal commensal microbiota.

Our data suggests that rhythmic intestinal sIgA is in part the result of cell-intrinsic regulation of IgA+ PC function. In support of this, and in line with previous observations, we found no time of day differences in the generation of class-switched B cells within the PPs [303]. Furthermore, we found no consistent differences in the frequency of IgA+ PCs within the intestines over the period of the circadian day. This is not surprising, as terminally differentiated PCs are typically considered as tissue resident cells and to exert their effect over a period of days to weeks (and even years) [209, 349], which argues against dynamic changes in the total number of PCs within a 24hour period.

Another major finding was that around 14% of the PC transcriptome demonstrated robust circadian oscillations. While this only accounts for a minority of the whole gene network, previous work has identified that only around 8% of the macrophage transcriptome demonstrates rhythmicity [290], but this accounts for oscillations in the major functional capacity of macrophages, such as cytokine production [253], phagocytosis [335] and antibacterial activity [350].

Of particular interest from our RNA sequencing data in IgA+ PCs, was that genes encoding upstream and downstream effectors of the mTOR pathway were found to be oscillatory. The mTOR pathway integrates intracellular and extracellular environmental cues such as nutrient availability, to regulate key cell-intrinsic process including protein, lipid and nucleic acid synthesis, as well as cell metabolism, proliferation and survival [342]. Within B cells, signalling via mTOR promotes the differentiation of PCs from naïve B cell subsets [351-354]. In fully differentiated bone marrow PCs, mTOR1 signalling is important for the generation of antibody responses. Indeed, inhibition of mTORC1 signalling leads to reversible inhibition of antibody production [352]. By contrast, PCs that have hyperactive mTOR signalling, by deletion of the negative regulator TSC1, have enhanced antibody secretion [353], together highlighting the importance of mTOR signalling on PC antibody production. Previous work has identified that mTOR activity is rhythmic and oscillatory mTOR activity leads to rhythmic protein synthesis in non-immune cells such as fibroblasts [355-357]. Thus, our data suggest the possibility that oscillatory mTOR may drive rhythmic IgA production within PCs. Moreover, leucine is an amino acid that stimulates mTOR upon entry into the cell via a heterodimeric amino acid transporter comprising LAT1 and the glycoprotein CD98 [342]. In PCs, surface CD98 expression and mTOR activity is regulated by Blimp1 [196]. Intriguingly, we identified that the genes encoding LAT1 (*Scl7a5*) and Blimp1 (*Prmd1*) were rhythmic in IgA+ PCs. This suggests that a dialogue may exist between nutrient cues and rhythmic IgA, via mTOR signalling, in intestinal PCs.

Extending this further, we also found that genes promoting fatty acid and cholesterol metabolism demonstrated robust circadian oscillations in IgA+ PCs. Recent data suggests that cholesterol metabolism plays an important role in modulating immunoregulatory responses in B cells [358] and in regulating B cell differentiation towards IgA+ PCs in the PPs [359]. Moreover, the ability of PCs to accommodate high Ig synthesis is dependent on massive ER

expansion during differentiation [196, 197], which itself is in part reliant upon *de novo* synthesis of fatty acids such as cholesterol [360]. However, there is a lack of data evaluating cholesterol metabolism in fully differentiated PCs and/ or in the setting of Ig production [200]. Intriguingly, individuals with genetic defects in cholesterol metabolism, such as mevalonate kinase deficiency – caused by mutations in the *Mvk* gene, leading to reductions in kinase activity – demonstrate increased serum levels of antibodies, including increased circulating IgA titres [361], suggesting a mechanistic link between fatty acid synthesis/ cholesterol metabolism and antibody production. Furthermore, prior work has demonstrated that SREBP1 is a highly circadian transcription factor whose activity regulates genes involved in fatty acid biosynthesis [362] and is strongly regulated by nutrient availability [363]. Therefore, our findings also suggest an interplay between nutrient cues, fatty acid and cholesterol metabolism and IgA rhythmicity in PCs.

Analysis of the RNA sequencing data also identified circadian oscillations in the expression of genes encoding BCMA and TACI, as well as those relating to their downstream signalling mediators. BCMA and TACI are able to bind locally produced APRIL and BAFF [364], which primarily mediates PC survival within the tissue niche via activation of NFκB and Elk-1 which, in turn, regulate anti-apoptotic and cell survival pathways within the cell [196, 197, 201, 365, 366]. In addition, *Sdc1* (encoding CD138), which is upregulated during PC differentiation [367], promotes the longevity of mature PCs via augmenting pro-survival cell-intrinsic signalling pathways [206], and was also identified as rhythmic. The significance of oscillations in the expression of genes belonging to cell survival and anti-apoptotic pathways within PCs is unclear. Intriguingly, BCMA, TACI and CD138 are overexpressed in multiple myeloma cells and interactions with their cognate ligands are critical for myeloma cell growth and survival [368-370]. Epidemiological studies have identified that circadian misalignment (for example through jet lag, shift work or sleep deprivation) is a risk factor for tumourigenesis [371]. While the underlying mechanisms are not well understood, recent data has identified that circadian dysregulation leads to altered cell survival and proliferation [372]. Thus, it could be speculated that loss of rhythmicity of signalling pathways that regulate PC survival, may be implicated in part, in the multistep neoplastic process in multiple myeloma.

The RNA sequencing data also demonstrated the presence of oscillating core biological clock genes within IgA+ PCs. Core biological clock proteins have been characterised in splenic B cells

previously [291] and some evidence suggests that oscillatory *Nr1d1* is required for co-ordinating the rhythmic trafficking of B cells around the body [273, 302]. While B-cell specific Bmal1 is not required for the differentiation PCs [259], the role of the biological clock in PCs and/or in the generation of antibody responses remains poorly defined. Mice deficient of the biological clock genes *Cry1* and *Cry2* have elevated titres of serum IgG antibodies towards TI antigens and bone marrow B cells isolated from *Cry1/Cry2*-deficient mice showed a significant upregulation of recombinant Ig heavy and light chain genes, including *Igha*, suggesting a link between the biological clock and antibody production [336]. Furthermore, across different cells, biological clock outputs generate rhythmicity in cell-intrinsic processes relating to nutrient sensing, metabolism and protein synthesis [355, 373-376]. This includes the mTOR pathway [375] and unfolded protein response, which involves genes such as *Xbp1* [376], which were identified as oscillatory in our RNA sequencing data, and which are critical for IgA production within PCs [196, 352]. Therefore, rhythmic IgA PC production may be regulated by a PC-intrinsic biological clock.

Collectively, these findings demonstrate circadian rhythmicity of intestinal PC IgA production, which may be entrained by circadian clock and/ or environmental nutrient cues. The mechanisms driving rhythmic IgA PC production are explored in the following chapter.

4.0 DEFINING THE MECHANISMS THAT ENTRAIN INTESTINAL IGA RHYTHMICITY OVER THE CIRCADIAN DAY

4.1 Introduction

Our findings indicate that PC-intrinsic IgA production exhibits rhythmicity over the circadian day. However, the factors entraining rhythmicity in intestinal PC IgA production are unclear. Circadian rhythms of immune cell responses involved in maintaining health in the gut and host-commensal interactions may be imprinted by a range of cell-intrinsic and cell-extrinsic cues. In this manner, surgical ablation of, or genetic deletion of *Arntl* in, the master clock has been shown to result in loss of oscillations in ILC3 responses, suggesting that immune cell rhythmicity within the gut can be entrained by environmental light cues via centrally-mediated SCN-driven signals [292, 293]. Alternatively, feeding cues can also provide synchronising signals for immune cell clocks within the gut, as time-specific feeding has been shown to alter daily circadian rhythms in clock-related genes within ILC3s [293] and the magnitude of the immune cell response [377]. However, feeding may also entrain rhythmic gut immune cell function without involving the cell-intrinsic clock, via pathways involving the enteric nervous system and neuropeptide secretion [292, 300, 378], suggesting that environmental and systemic cues may converge on, or act independently of, cell-intrinsic biological clocks to entrain rhythmicity in gut immune cell processes.

We have demonstrated the presence of rhythmic clock genes within IgA+ PCs and oscillations in nutrient sensing pathways such as mTOR, but whether the PC-intrinsic clock and/ or nutrient cues mediates rhythmic IgA production or oscillations in PC IgA transcription has not yet been determined. Intriguingly, diurnal oscillations in salivary IgA are evident in mice [379], humans [380, 381] and elephants [382]. In mice, salivary IgA rhythms are impaired following surgical ablation of the SCN, or in *CLOCK*-deficient mice, suggesting that environmental cues may entrain rhythms in mucosal IgA via the (central) circadian clock system [379]. However, PCs, like other immune cells, located within different tissue niches may be regulated via distinct pathways defined by the local environment [12, 383].

Together, these observations provoke the question of which cell-intrinsic and/ or cell-extrinsic cues entrain rhythmicity in intestinal PC IgA production. In this chapter, we address this by defining the mechanisms that entrain rhythmic PC IgA production over the circadian day.

4.2 Results

4.2.1 IgA+ PCs have a cell-intrinsic biological clock

Our RNA-seq data suggested IgA+ PCs may be subject to cell-intrinsic regulation by circadian clock genes. It is well regarded that the liver and intestinal tissue have a prominent circadian clock system [384, 385]. Therefore, to validate that we could detect expected circadian rhythmicity in whole tissue, we evaluated clock gene expression in liver and terminal ileal samples from mice taken at necropsy over four, six-hourly intervals over the period of a single day. RT-PCR analysis revealed that the oscillatory profile of biological clock gene expression within whole tissue was consistent with what is known within the literature (Figure 4.1 A&B) [384, 385].

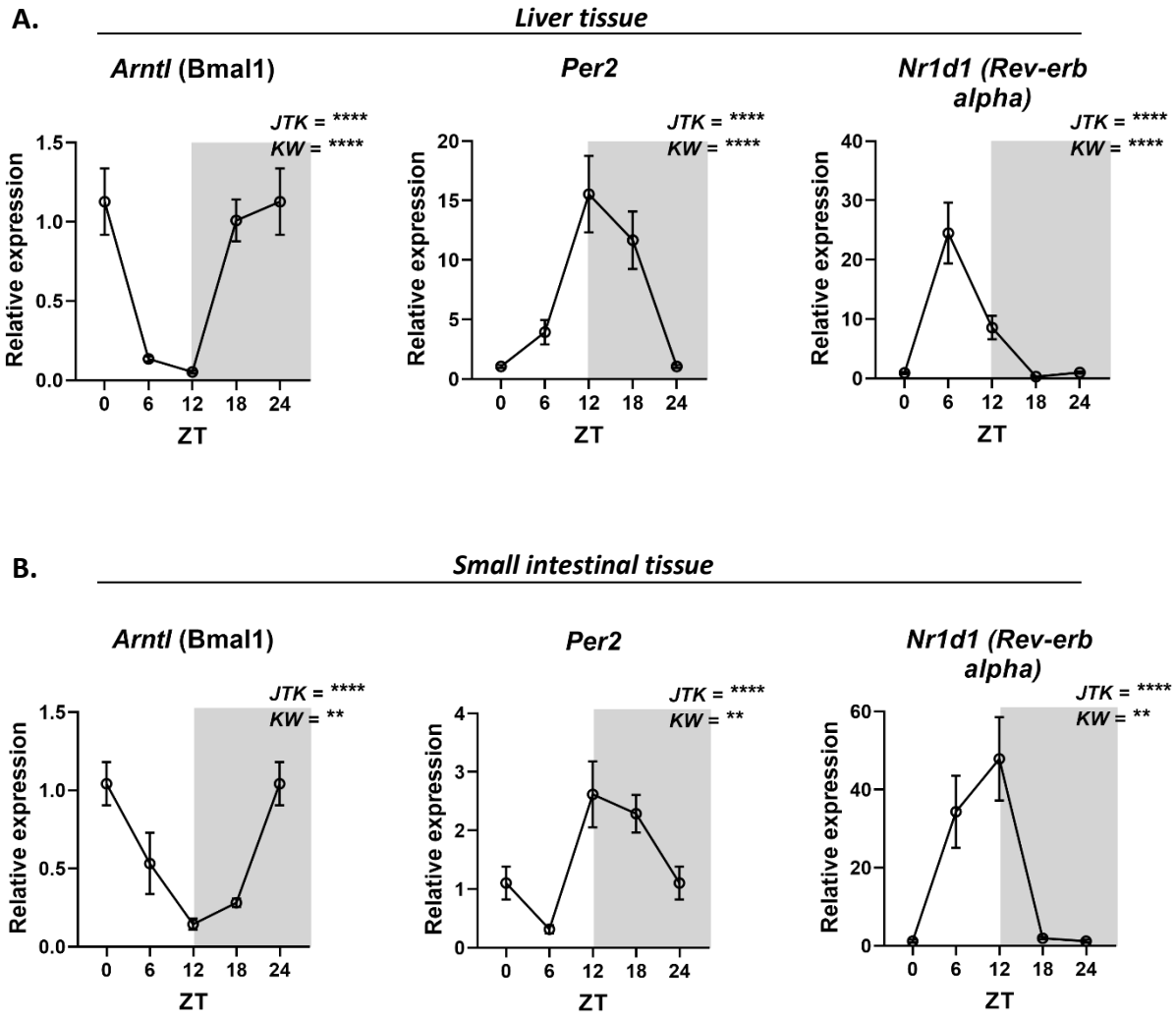

Figure 4.1. Diurnal oscillations of expression of core biological clock genes in the liver and small intestines

(A) Expression of *Arntl* (Bmal1), *Per2* and *Nr1d1* (Rev-erb alpha) (left to right) analysed by RT-PCR relative to the housekeeping gene *Gapdh* in liver tissue over the course of the day. (B) Expression of *Arntl* (Bmal1), *Per2* and *Nr1d1* (Rev-erb alpha) (left to right) analysed by RT-PCR relative to the housekeeping gene *Gapdh* in liver tissue over the course of the day. Delta CT values obtained were normalised to ZT0 to calculate relative gene expression. ZT0 is double plotted as ZT24 to facilitate viewing the data. Variance in the data across the experimental timepoints assessed by Krushkal Wallis (KW) test. Rhythmicity assessed by JTK analysis. Data represents mean+/-SEM. Data representative of two independent experiments (n=4-5 mice per ZT time point; C57BL/6 female mice aged 8-12 weeks). *= $p<0.05$; ***= $p<0.001$; ****= $p<0.0001$. Shaded area on graphs represents dark phase.

We then FACS-sorted IgA+ PCs from the small intestinal LP of mice over the same four timepoints. For comparison, we simultaneously sorted naive IgD+ B cells from the same small intestinal single cell suspensions, over the same experimental timepoints. RT-PCR analysis demonstrated diurnal oscillations in expression of core clock genes within IgA+ PCs including *Arntl1, Per2 and Nr1d1* in a similar manner to that observed in our RNA sequencing data (Figure 4.2A). Gene expression over the experimental timepoints was also consistent with oscillatory phase detected in the liver and TI samples, although the amplitude of oscillations tended to be higher in whole tissue preparations. Interestingly, there was no evidence of significant time of day variation in *Arntl1* nor *Per2* expression in IgD+ B cells. Surprisingly however, IgD+ B cell *Nr1d1* expression displayed diurnal oscillations which aligned with those found in IgA+ PCs (Figure 4.2B). Together, these findings are in support of a rhythmic biological clock system within IgA+ PCs, but not within IgD+ B cells.

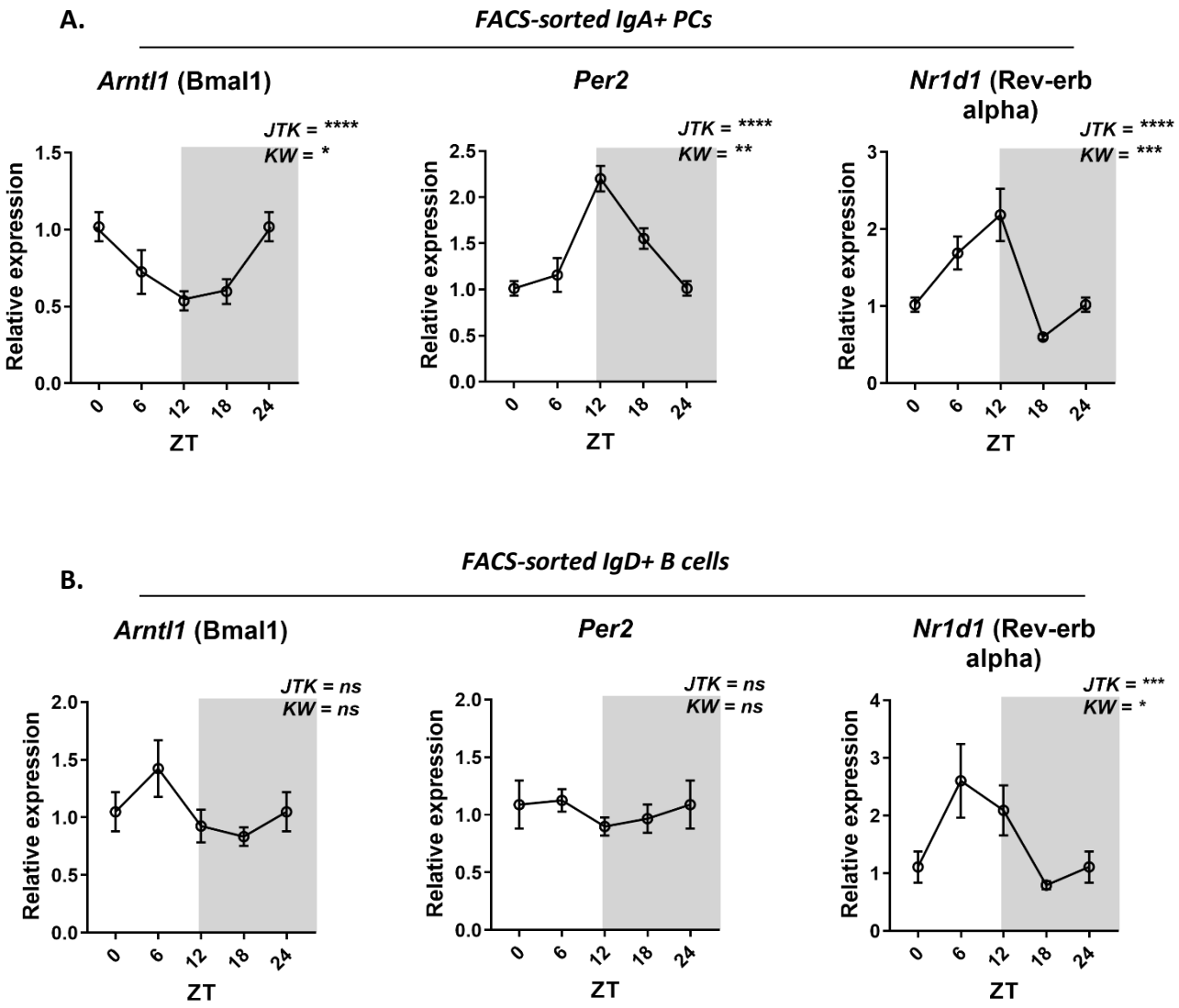

Figure 4.2. Core biological clock genes oscillate in IgA+ PCs, but are variably rhythmic in IgD+ B cells, over the circadian day

(A) Expression of *Arntl* (Bmal1), *Per2* (Per2) and *Nr1d1* (Rev-erb alpha) (left to right) in FACS-sorted IgA+ PCs from the small intestines. (B) Expression of *Arntl* (Bmal1), *Per2* (Per2) and *Nr1d1* (Rev-erb alpha) (left to right) in FACS-sorted IgD+ B cells from the small intestines. Gene expression levels analysed by RT-PCR relative to the housekeeping gene GAPDH. Delta CT values obtained were normalised to ZT0 to calculate relative gene expression. ZT0 is double plotted as ZT24 to facilitate viewing the data. Variance in the data across the experimental timepoints assessed by Krushkal Wallis (KW) test. Rhythmicity assessed by JTK analysis. *= p<0.05; **= p<0.01; ***= p<0.001; ****= p<0.0001. Data representative of three independent experiments (n=3-5 mice/ timepoint; C57BL/6 female mice aged 8-12 weeks). Horizontal bars represent mean±SEM. Shaded area on graphs represents the dark phase.

4.2.2 Generation of a mouse model of biological clock disruption in IgA+ PCs

To assess the role of the PC-intrinsic clock on biological function, we generated mice with deletion of Bmal1 in the B cell lineage *(Arntl)* (*Mb1*$^{Cre+/-}$ *x Arntl*$^{flox/flox}$) (Figure 4.3A). This construct has previously been shown to effectively disrupt the circadian clock system within B cells [259]. Deletion of *Arntl* was confirmed by RT-PCR analysis of FACS-sorted small intestinal IgA+ PCs. As expected, IgA+ PCs from *Mb1*$^{Cre+/-}$ *x Arntl*$^{flox/flox}$ mice had markedly reduced *Arntl* and *Nr1d1* gene expression, at a single timepoint (ZT0), compared with littermate control mice (*Mb1*$^{Cre-/-}$ *x Arntl*$^{flox/flox}$) (Figure 4.3B). In accordance with previous work [258], *Mb1*$^{Cre+/-}$ *x Arntl*$^{flox/flox}$ mice had similar expression of Per2 as littermate controls at a single timepoint. We further demonstrated that the frequency and number of small intestinal IgA+ PCs was similar between *Mb1*$^{Cre+/-}$ *x Arntl*$^{flox/flox}$ and control mice (Figure 4.3C), which mirrors previous findings that B cell and PC differentiation is not affected by B-cell specific deletion of Bmal1 [259]. Together, this data validates this model of biological clock disruption in IgA+ PCs and confirms that B cell-intrinsic clock disruption does not affect PC differentiation in the intestines.

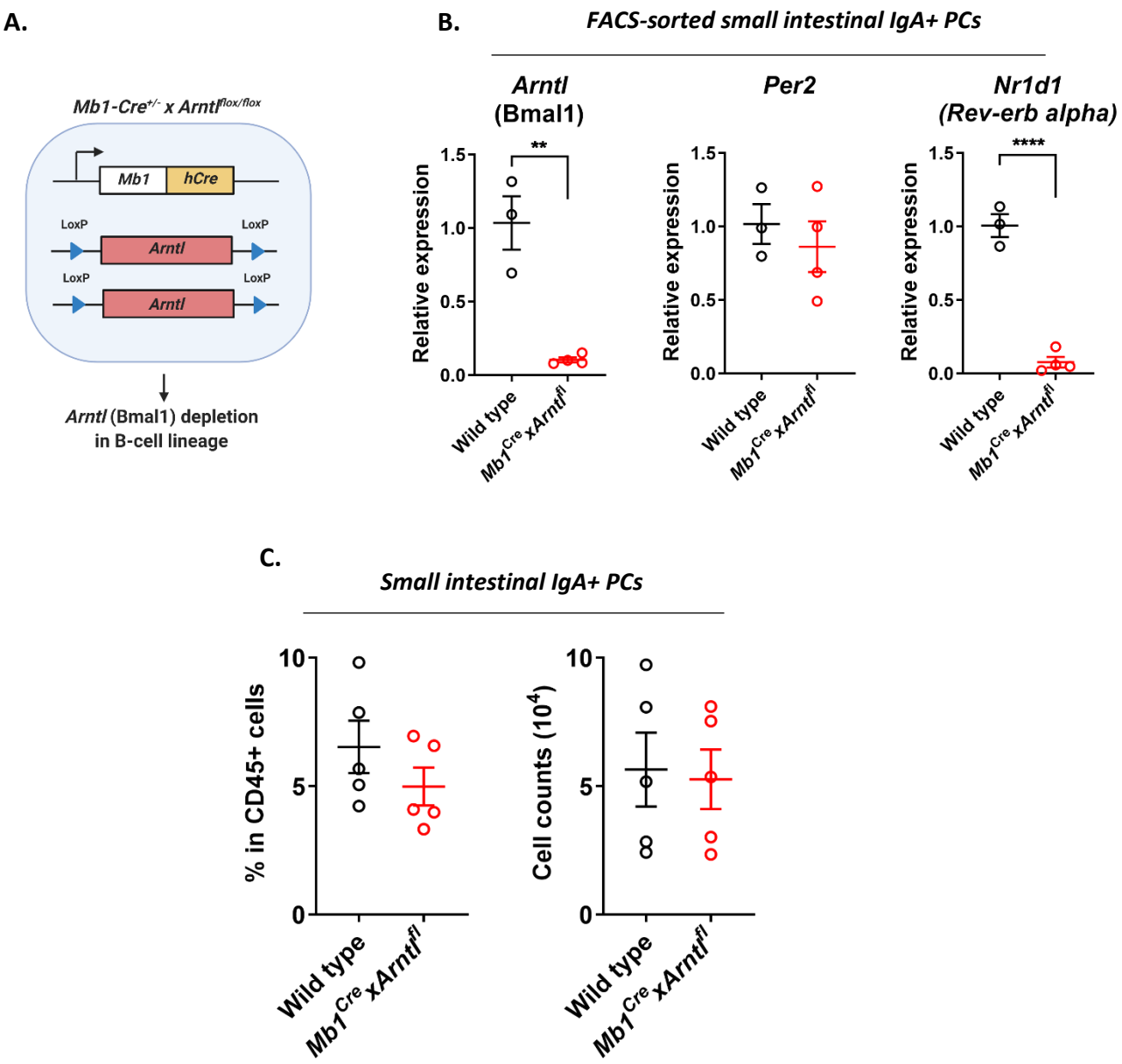

Figure 4.3. Characterisation of a mouse model of B-cell specific *Arntl* (Bmal1) deletion

(A) Schematic of the *Mb1*$^{Cre+/-}$ x *Arntl*$^{flox/flox}$ mouse. *Mb1*$^{Cre+/-}$ x *Arntl*$^{flox/flox}$ mice had a humanised cre recombinase (hCre) integrated into one of the Mb1 loci (*Mb1*) and LoxP sites flanking both *Arntl* (Bmal1) gene loci. Wild type littermate control mice were bred as *Mb1*$^{Cre-/-}$ x *Arntl*$^{flox/flox}$. (B) Expression of *Arntl*, *Per2* and *Nr1d1* (left to right) analysed by RT-PCR relative to the housekeeping gene *Gapdh* in IgA+ PCs FACS-sorted from the small intestinal lamina propria of wild type and *Mb1*$^{Cre+/-}$ x *Arntl*$^{flox/flox}$ (*Mb1*^{Cre} x *Arntl*^{fl}) mice. Delta CT values obtained were normalised to mean control values to calculate relative gene expression. (C) Frequency (left) and cell counts (right) of IgA+ PCs in small intestinal single cell suspensions from wild type and *Mb1*$^{Cre+/-}$ x *Arntl*$^{flox/flox}$ (*Mb1*^{Cre} x *Arntl*^{fl}) mice. IgA+ CD138+ PCs were pre-gated as Live CD45+ CD3- MHCII+ B220- IgD-. Data from one experiment plotted (n=3-5 mice/ group; male and female mice aged 8-12 weeks); bars indicate mean ± SEM. **= p<0.01; ****= p<0.0001.

4.2.3 Bmal1 is not required for rhythmicity of intestinal sIgA responses

We next sought to determine whether the PC-intrinsic clock entrained rhythmicity in sIgA. To do this, we collected fresh faecal pellets from *Mb1*$^{Cre+/-}$ x *Arntl*$^{flox/flox}$ mice and littermate controls at four, six-hourly intervals over the course of a single day. Analysis surprisingly revealed that deletion of Bmal1 in PCs did not alter the diurnal rhythmicity of faecal sIgA (Figure 4.4).

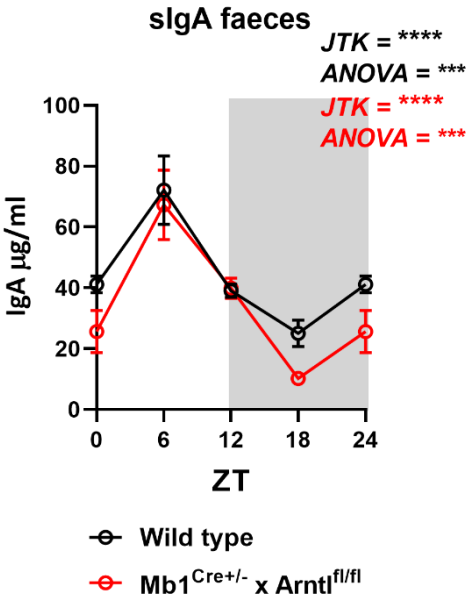

Figure 4.4. Sustained oscillations in faecal sIgA in the absence of PC-Bmal1

The concentration of faecal secretory (s)IgA normalised by weight was determined by ELISA in *Mb1*$^{Cre+/-}$ x *Arntl*$^{flox/flox}$ and wild type littermates (*Mb1*$^{Cre-/-}$ x *Arntl1*$^{flox/flox}$). Mice were housed under strict 12-hour light:dark conditions and had access to food *ad libitum*. Fresh faecal pellets were sampled at 4 timepoints, six hours apart over the period of one day; sampling times illustrated by Zeitgeber times (ZT). ZT0 is double plotted as ZT24 to facilitate viewing the data. Variance in the data across the experimental timepoints assessed by ANOVA test. Rhythmicity assessed by JTK analysis. ***= p<0.001; ****= p<0.0001. Data representative of two independent experiments (n=4-5 mice/ group; male and female mice aged 8-12 weeks). Horizontal bars represent mean±SEM. Shaded area represents dark phase.

Despite these findings, to determine whether Bmal1 regulated the IgA+ PC transcriptome, we performed bulk RNA-sequencing on FACS-sorted small intestinal IgA+ PCs from *Mb1*$^{Cre+/-}$ *x Arntl*$^{flox/flox}$ and littermate control mice at two timepoints (ZT0 and ZT12). Analysis revealed that in total, 1893 genes were differentially expressed across the timepoints in both *Mb1*$^{Cre+/-}$ *x Arntl*$^{flox/flox}$ and littermate control mice (Figure 4.5A). Further analysis revealed time of day-dependent signatures in control animals that were lost (Figure 4.5A cluster I and IV), suppressed (Figure 4.5A cluster II and V), or retained (Figure 4.5A cluster III) in the absence of a functional PC-intrinsic clock. In addition, we also identified a time of day-dependent signature that was expressed only in *Mb1*$^{Cre+/-}$ *x Arntl*$^{flox/flox}$ mice (Figure 4.5A cluster VI).

As expected, analysis of clock gene expression in the *Mb1*$^{Cre+/-}$ *x Arntl*$^{flox/flox}$ mice confirmed disrupted time of day profiles of core clock genes (Figure 4.5B). The data also confirmed time of day variation in the expression of major genes associated with PC function that we had previously identified as rhythmic (Chapter 3.4), including *Igha*, *Xbp1* and *Sdc1* (Figure 4.5C). Interestingly, these genes did not demonstrate time of day variation in IgA+ PCs from clock-disrupted *Mb1*$^{Cre+/-}$ *x Arntl*$^{flox/flox}$ mice (Figure 4.5C). In addition, genes encoding mTOR protein subunits 1 and 2, (*Raptor* and *Rictor*, respectively), as well as *Hk2* which mediates the initial step in glycolysis, displayed time of day variation in littermate control mice, but not in *Mb1*$^{Cre+/-}$ *x Arntl*$^{flox/flox}$ mice (Figure 4.5D). By contrast, a group of other genes involved in metabolism and nutrient transport, including *Mvk*, *Srebf2* and *Ldlr – genes of the cholesterol metabolism pathway*, as well as *Slc7a5 – a key amino acid transporter*, that we had previously determined as rhythmic (Chapter 3.4), showed a similar temporal expression profile in both *Mb1*$^{Cre+/-}$ *x Arntl*$^{flox/flox}$ and littermate control mice (Figure 4.5E).

Therefore, collectively, this data suggests that while Bmal1 modulates the temporal expression of key genes involved in PC function, Ig synthesis, and some aspects of metabolism, others involved in nutrient transport, cholesterol metabolism and biosynthesis appear to retain rhythmicity in the absence of Bmal1.

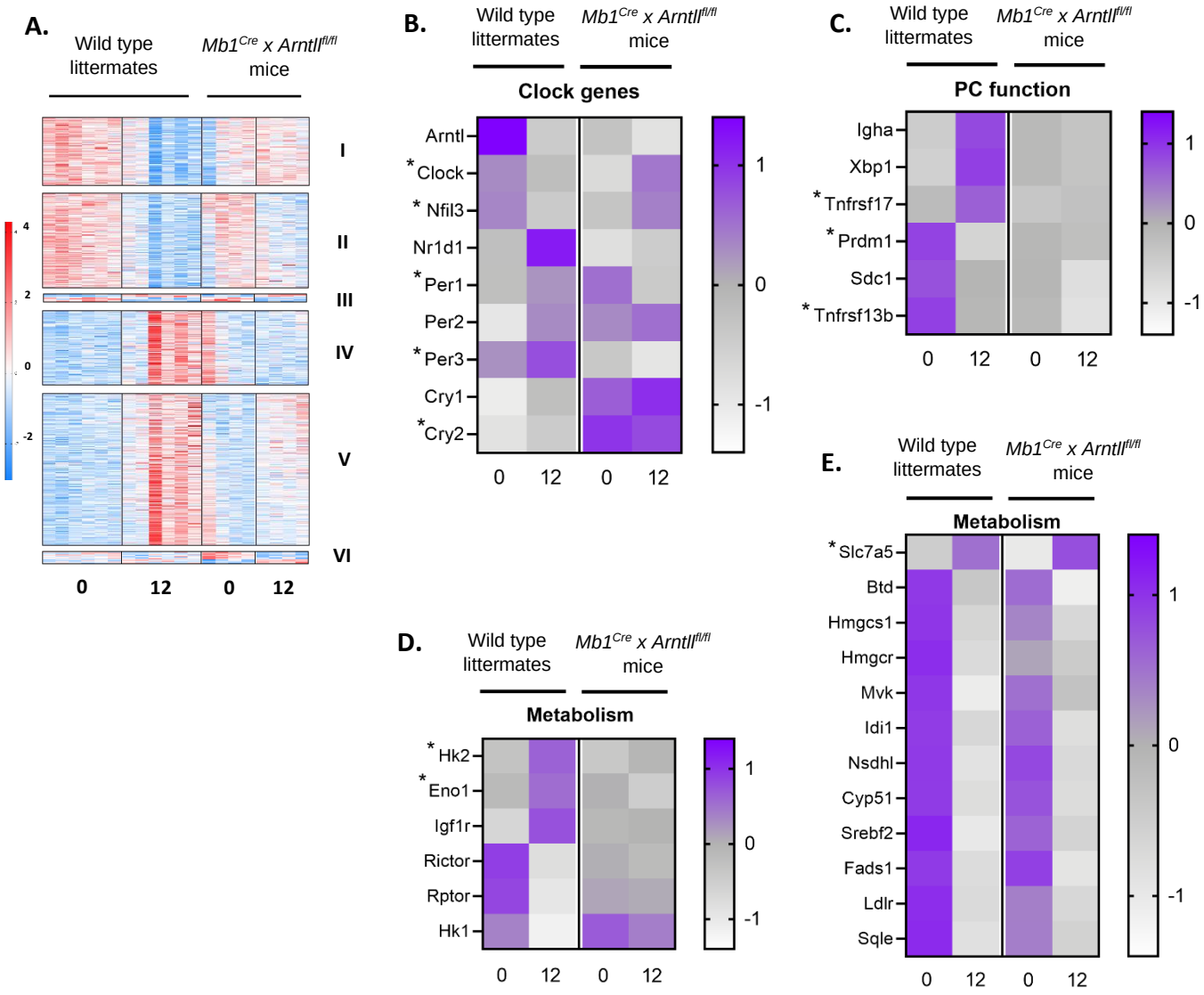

Figure 4.5. Altered temporal expression of genes associated with the cell-intrinsic clock, PC function and metabolism in ***Mb1-Cre*$^{+/-}$ x *Arntl*$^{flox/flox}$ mice**

(A) Heatmap of 1893 genes identified as differentially expressed (adjusted p <0.01) across ZT0 and ZT12 timepoints in either wild type littermates and/ or in *Mb1*$^{Cre+/-}$ x *Arntl*$^{flox/flox}$ mice, clustered according to whether they were (I and II) differentially expressed across timepoints in wild type mice only with peak expression at ZT0; (III) differentially expressed across timepoints in both wild type littermate and in *Mb1*$^{Cre+/-}$ x *Arntl*$^{flox/flox}$ mice; (IV and V) differentially expressed across timepoints in wild type only with peak expression at ZT12; (VI) differentially expressed across timepoints in in *Mb1*$^{Cre+/-}$ x *Arntl*$^{flox/flox}$ only. Normalised reads in FPKM are expressed as mean z-scores (red, high; blue, low) for each repeat. (B) Heatmap of selected molecular clock genes at ZT0 and ZT12 in each group. (C) Heatmap of selected PC function genes at ZT0 and ZT12 in each group. (D) Heatmap of selected metabolic genes that were different in wild type mice, but not in in *Mb1*$^{Cre+/-}$ x *Arntl*$^{flox/flox}$ mice. (E) Heatmap of selected metabolic genes that had conserved differences across timepoints in wild type and in *Mb1*$^{Cre+/-}$ x *Arntl*$^{flox/flox}$ mice. Data representative of one experiment (n=5 mice/ timepoint; male and female mice aged 8-12 weeks). Normalised reads in FPKM are expressed as mean z-scores for (A) each repeat, or, (B-E) the average is displayed for each group. *= gene expression not significantly different between ZT0 and ZT12 in the wild type littermate group.

IECs are the major site of IgA transport [216]. Dimeric IgA secreted by PCs binds to the pIgR at the basolateral surface of the intestinal epithelium and is transported to the apical surface, where it is released into the intestinal lumen along with the receptor ectodomain to form sIgA [216]. Therefore, having observed that oscillatory IgA may be the result of cell-intrinsic regulation of IgA+ PC function and that the transcriptome within PCs is disrupted in the absence of a functional clock, we next sought to determine that rhythmic IgA was not controlled at level of transcytosis over IECs. To do this, we used a mouse model with an epithelial-cell specific deletion of Bmal1 *(Arntl)* (*Villin*$^{cre+/-}$ *x Arntl*$^{flox/flox}$). This construct has previously been shown to effectively disrupt the circadian clock system within IECs (data not shown). Fresh faecal pellets were sampled from *Villin*$^{cre+/-}$ *x Arntl*$^{flox/flox}$ mice and littermate controls as previously described (Chapter 3). Analysis revealed that deletion of Bmal1 in IECs did not alter the diurnal rhythmicity of faecal sIgA (Figure 4.6A). To confirm these findings, we analysed by RT-PCR *pIgR* gene expression in small intestinal tissue taken at serial timepoints over the course of the day. Analysis revealed no difference in intestinal *pIgR* expression over the course of the day (Figure 4.6B).

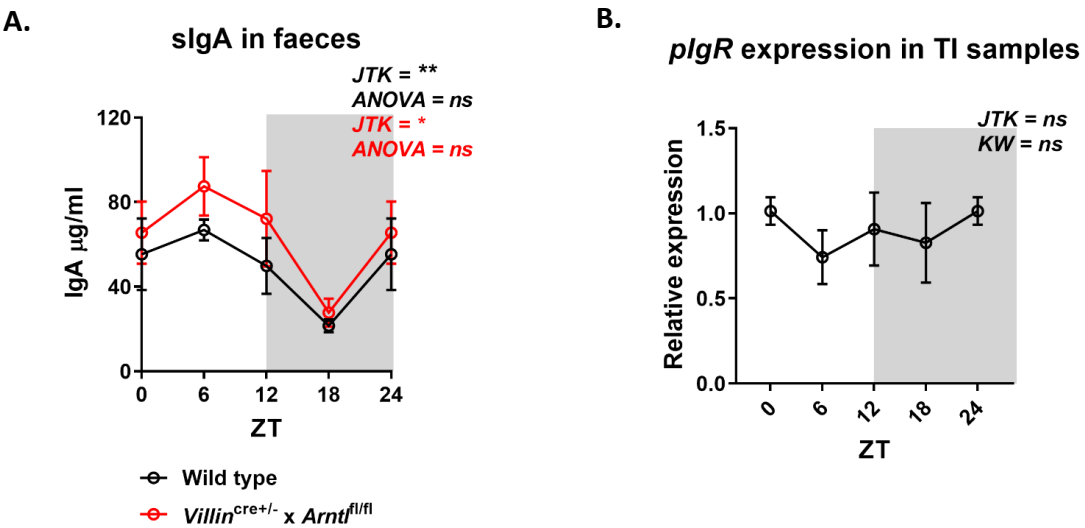

Figure 4.6. The pIgR does not drive oscillations in intestinal sIgA

(A) The concentration of faecal secretory (s)IgA normalised by weight was determined by ELISA in *Villin*$^{Cre+/-}$ x *Arntl*$^{flox/flox}$ and wild type littermates (*Villin*$^{Cre-/-}$ x *Arntl1*$^{flox/flox}$). Fresh faecal pellets were sampled at 4 timepoints, six hours apart over the period of one day; sampling times illustrated by Zeitgeber times (ZT). (B) Polymeric immunoglobulin receptor (pIgR) gene expression was analysed by RT-PCR relative to the housekeeping gene GAPDH in terminal ileal samples collected at necropsy. ZT0 is replotted as ZT24 to facilitate viewing the data. Variance in the data assessed by ANOVA or Kruskal-Wallis (KW) test. Rhythmicity assessed by JTK analysis. Bars indicate mean±SEM. *= $p<0.05$; **= $p<0.01$. Shaded areas on graphs represent the dark phase. Data representative of two independent experiments (n=5mice/ ZT; male and female mice; aged 8-12 weeks).

We next hypothesised that extrinsic entrainment as mediated by the SCN could be responsible for maintaining rhythmicity in IgA secretion. Therefore, to determine the influence of the master clock within the SCN on intestinal IgA rhythmicity, we sampled faecal pellets from mice with genetic ablation of Bmal1 (*Arntl*) in the SCN, (*Camk2a*$^{Cre+/-}$ *x Arntl*$^{flox/flox}$) [293]. To exclude confounding SCN-independent rhythms, mice were housed in complete darkness for at least 4 weeks prior to faecal pellet collection [293]. Analysis demonstrated that impairment in the master clock did not ablate rhythmic intestinal IgA production (Figure 4.7). Collectively, this data suggests that the circadian clock system is dispensable for oscillatory secretion of IgA under normal feeding and lighting conditions. However, a dialogue may exist between nutrient sensing, metabolic and survival pathways and the cell-intrinsic clock, which act together to regulate PC responses over the course of the circadian day.

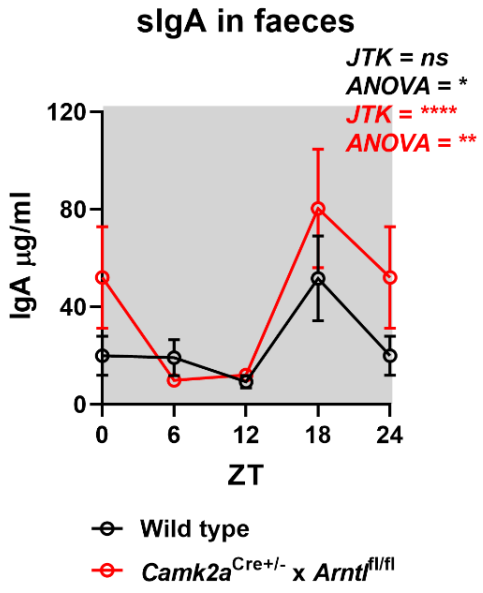

Figure 4.7. Sustained oscillations in faecal sIgA in the absence of SCN Bmal1

The concentration of faecal secretory (s)IgA normalised by weight was determined by ELISA in *Camk2a*$^{Cre+/-}$ x *Arntl*$^{flox/flox}$ and wild type littermates (*Camk2a*$^{Cre-/-}$ x *Arntl1*$^{flox/flox}$). Mice were maintained in constant darkness for 4 weeks prior to the collection of faecal pellets. Faecal pellet collected as previously described. ZT0 is double plotted as ZT24 to facilitate viewing the data. Variance in the data assessed by ANOVA. Rhythmicity assessed by JTK analysis. *= $p<0.05$; **= $p<0.01$. Data representative of one independent experiments (n=5mice/ timepoint; male and female mice aged 10-12 weeks). Horizontal bars represent mean±SEM. Shaded area represents dark phase.

4.2.4 Feeding cues drive rhythmicity in sIgA and augment the expression of IgA+ PC-intrinsic biological clock genes

Prior work has demonstrated that feeding cues can entrain rhythmic biological processes in peripheral tissues and immune cells, independent of-, or in concert with-, cell-autonomous clocks [274, 292, 300]. To determine whether food availability entrains rhythmicity in intestinal sIgA production, we restricted mice access to food, to a six-hour window during the

mid-dark phase (dark-fed) or mid-light phase (light-fed) for a 2-week period. Following this, we collected fresh faecal pellets from both groups of mice at four, six-hourly intervals over a single day (Figure 4.8A). In doing so, we found that feeding mice exclusively during the light-phase resulted in a phase inversion in the rhythmicity of sIgA, in comparison with mice fed exclusively during the dark-phase (Figure 4.8B). As previously demonstrated (Chapter 3), we did not identify any rhythmic variation in the frequency of small intestinal IgA+ PCs over the experimental timepoints from either group (Figure 4.8C).

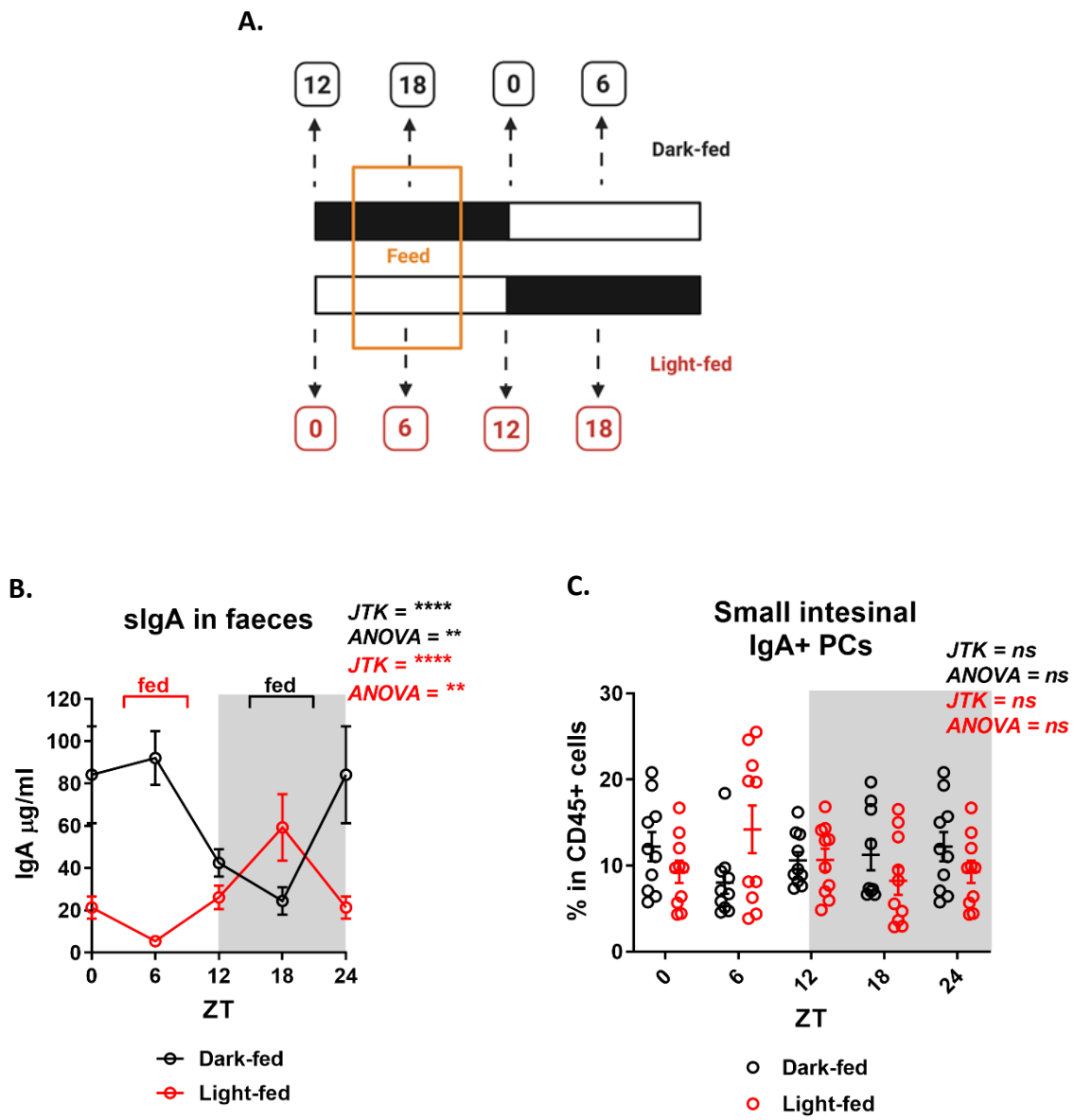

Figure 4.8. Inverting the feeding schedule reverses the rhythmic profile of sIgA

(A) Schematic of the feeding regime. Mice were housed under strict 12-hour light:dark conditions and had access to food for a 6-hour window during the mid-dark phase (dark-fed) or mid-light phase (light-fed). Mice had access to water *ad libitum*. Faecal samples were collected at 4 timepoints, six hours apart over the period of one day; sampling times illustrated by dashed arrows and boxes. (B) Concentration of faecal secretory (s)IgA normalised by weight over the experiment determined by ELISA. (C) Frequency of small intestinal IgA+ PCs in dark-fed and light-fed mice assessed by flow cytometry. IgA+ B220- PCs were pre-gated as CD45+ MHCII+ IgD- B220-. (B&C) Pooled data from two independent experiments (n=4-5 mice per ZT time point; C57BL/6 female mice aged 8-10 weeks). ZT0 is double plotted as ZT24 to facilitate viewing the data. Variance in the data across the experimental timepoints assessed by ANOVA. Rhythmicity assessed by JTK analysis. **= $p<0.01$; ****= $p<0.0001$. Horizontal bars represent mean±SEM. Shaded area represents dark phase.

Previous work has suggested that prolonged fasting (>36 hours) reduces lymphocyte numbers in the PPs and attenuates IgA responses within the intestines [386]. To confirm that short-term fasting (6 hours) did not alter small intestinal IgA responses, we adjusted the experimental design to enable a direct comparison of lymphocyte numbers from mice in a relative fed and fasted state (Figure 4.9A). In doing so, we found no differences in the frequency or number of small intestinal IgA+ PCs, TfH or IgA+ B cell subsets within the PPs, in mice housed under either condition (Figure 4.9B&C), suggesting that variation in IgA could not be explained by previously reported effects of fasting on PP response [386].

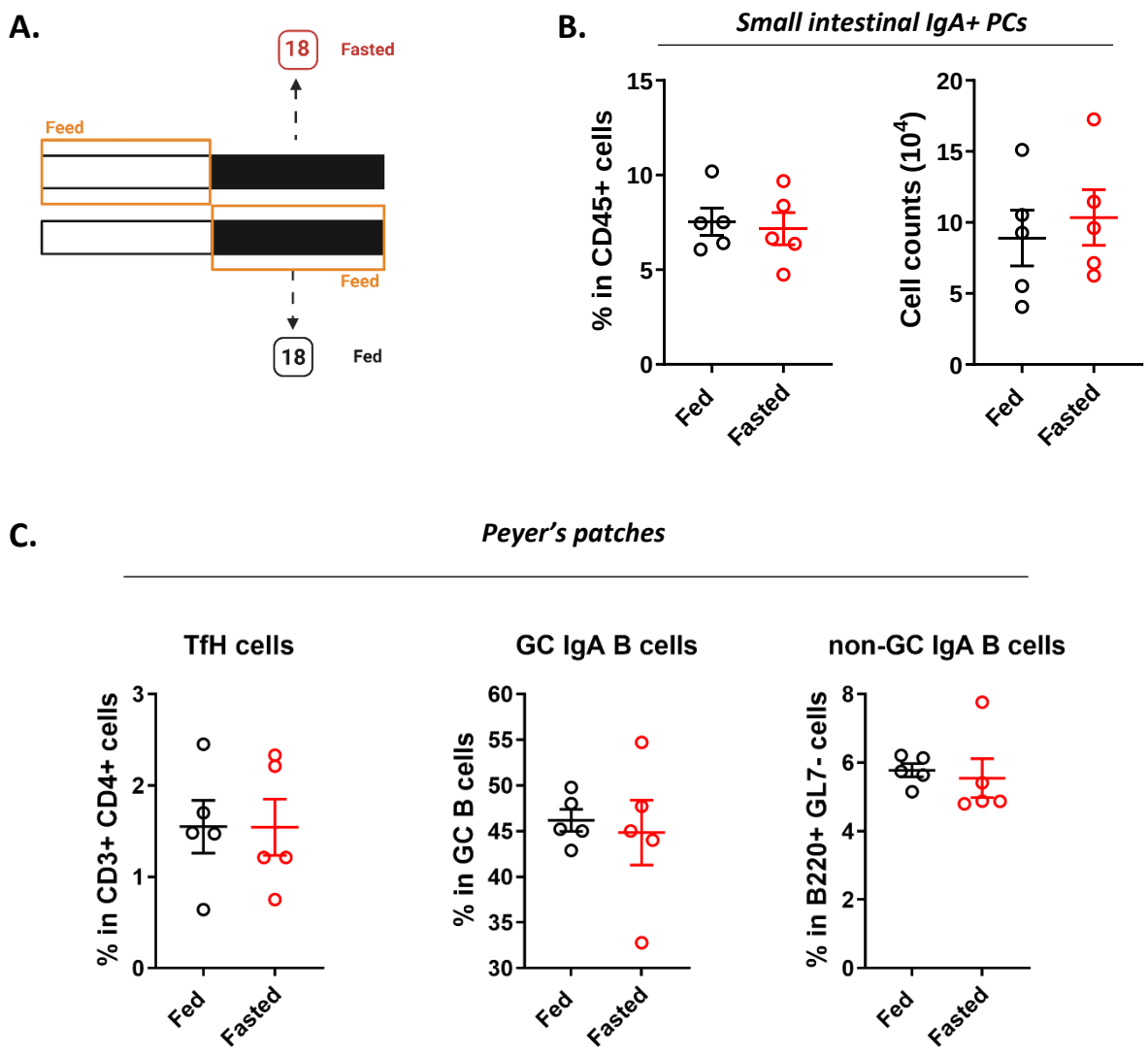

Figure 4.9. No differences in small intestinal IgA+ PCs, or T and B cell subsets within the Peyer's patches, during feeding or fasting.

(A) Schematic of the feeding regime. Mice were housed under the same strict 12-hour light:dark conditions and had access to food for a 12-hour window during the mid-dark phase or mid-light phase. Mice had access to water *ad libitum*. Mice from each group were euthanised at ZT18 which represented a relative fasting-, or fed-, state for light-, and dark-, fed mice respectively (ZT times represented by the boxed numbers). (B) Frequency (left) and cell counts (right) of small intestinal lamina propria IgA+ PCs assessed by flow cytometry. IgA+ CD138+ PCs were pre-gated as CD45+ MHCII+ IgD- B220-. (C) Frequency of TfH cells, germinal centre (GC) IgA+ B cells and non-GC IgA+ B cells in the Peyer's patches of fed and fasted mice assessed by flow cytometry. PD-1, CXCR5 double +ve TfH cells were pre-gated as live, single, CD45+CD3+B220-CD4+MHCII- cells. GC IgA+ B cells were pre-gated as live, single. CD45+CD3-B220+GL7+Fas+ cells; non-GC IgA+ B cells were pre-gated as live, single, CD45+CD3-B220+GL7-Fas- cells. Data representative of two experiments (n=5 mice/ timepoint; C57BL/6 female mice aged 8-10 weeks); bars indicate mean±SEM. Unpaired T-test applied to all illustrated datasets.

Peripheral circadian clock oscillators can be entrained by feeding cues [276]. Therefore, we next determined whether, by manipulating the feeding schedule, we could alter the expression of biological clock genes in IgA+ PCs. To do this, we placed mice on the same restricted feeding regime (Figure 4.8) and FACS-sorted small intestinal IgA+ PCs and IgD+ B cells at ZT0 and ZT12 timepoints from dark-fed and light-fed mice and acquired liver tissue at necropsy. Clock gene expression was determined in whole tissue and sorted cells by RT-PCR analysis. Time of day differences were seen in clock genes from liver tissue in dark fed mice and reversing the feeding led to reversal of *Arntl* and *Per2* gene expression (Figure 4.10A), as has been demonstrated previously [275]. There was a statistically significant difference in *Nr1d1* expression in whole tissue from dark-fed mice, with loss of this difference in light-fed animals (Figure 4.10A). In IgA+ PCs, time of day differences were seen in clock genes in dark fed mice (Figure 4.10B). By contrast, reversing feeding led to reversal of *Arntl*, and loss of difference in *Nr1d1*, but surprisingly no difference in *Per2* expression levels (Figure 4.10B). As previously, *Arntl* and *Per2* gene expression in IgD+ B cells from dark fed animals did not follow the expected pattern across the experimental timepoints, whilst differences in *Nr1d1* expression in dark fed animals were lost in light-fed animals (Figure 4.10C). This data suggests that feeding cues modulate Bmal1 (*Arntl*) expression, but misaligned feeding (i.e. feeding during the resting phase) may disrupt the expression of PC-intrinsic clock genes.

Collectively, this data indicates that feeding cues entrain rhythmicity in intestinal IgA and modulates the temporal expression of the PC-intrinsic circadian clock, thus suggesting that nutritional and metabolic cues act in concert with clock-mediated signals to regulate PC-transcription.

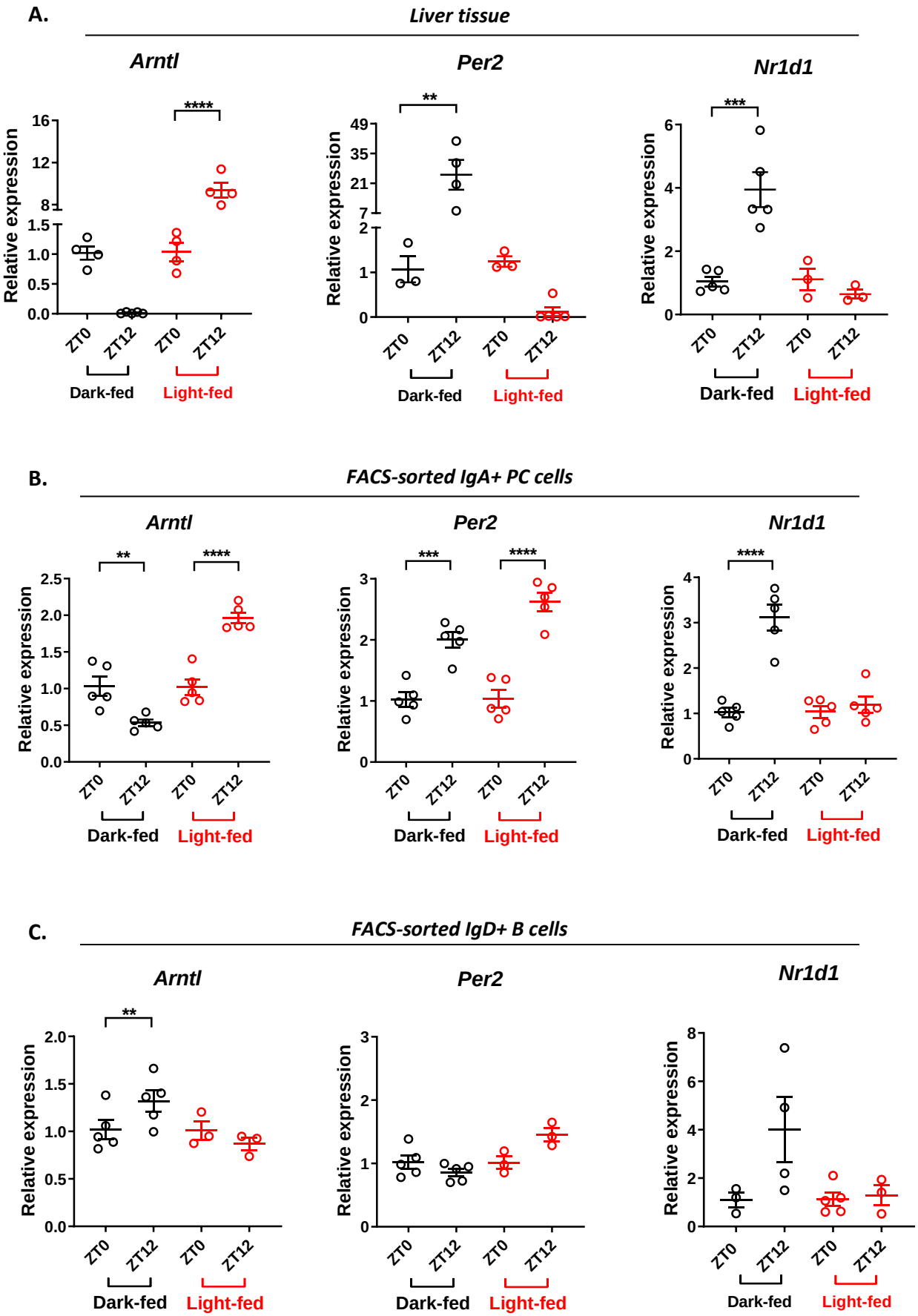
A.
Liver tissue
Arntl
Per2
Nr1d1
Relative expression
ZT0
ZT12
Dark-fed
Light-fed
B.
FACS-sorted IgA+ PC cells
C.
FACS-sorted IgD+ B cells

Figure 4.10. Inverting the feeding schedule alters the expression of core-clock genes in IgA+ PCs and peripheral tissues

Mice had access to food for a 6-hour window during the mid-dark phase (dark-fed) or mid-light phase (light-fed). (A) Expression of *Arntl*, *Per2* and *Nr1d1* (left to right) analysed by RT-PCR relative to the housekeeping gene *Gapdh* in (A) liver tissue and (B) IgA+ PCs and (C) IgD+ B cells FACS-sorted from small intestinal lamina propria. To calculate relative gene expression, delta CT values obtained were normalised to dark-fed (dark-fed group) or light-fed (light-fed group) ZT0. Statistical analysis was conducted by ANOVA and post-hoc Tukey's Test. Bars indicate mean+/-SEM; (A) data represents two experiments; (B&C) data representative of one experiment (n=3-5 mice per ZT time point; C57BL/6 female mice aged 8-10 weeks). **= p<0.01; ***= p<0.001; ****= p<0.0001.

4.2.5 IgA+ PCs have a higher metabolic activity than IgA+ B cells and IgD+ B cells

Having established that feeding cues entrain rhythmicity in sIgA and that the expression of genes regulating nutrient sensing and metabolism oscillate in IgA+ PCs (Chapter 3.4), we next sought to characterise the cellular uptake and processing of major metabolic substrates (glucose, amino acids and lipids) that are required to fuel immune cell activity and cell intrinsic metabolism [200]. For comparison, we evaluated differences between small intestinal IgA+ PCs, class-switched IgA+ B cells and naïve IgD+ B cells. Initial analysis revealed marked cell size differences between IgA+ PCs, IgA+ B cells and IgD+ B cells – a crude indicator of cellular proliferation or metabolic capacity (Figure 4.11A). As a proxy measure of glucose uptake, we analysed fluorescently labelled glucose analogue 2-NBDG uptake into cells *in vivo*. To ensure that potential differences in mean fluorescent intensity of 2-NBDG was not the consequence of differences in cell size between groups, we normalised 2-NBDG fluorescence to cell size. In doing so, the data showed that IgA+ PCs displayed significantly higher 2-NBDG uptake than both B cells subsets, and IgA+ B cells had greater uptake of 2-NBDG than IgD+ cells (Figure 4.11B). We next sought to evaluate the capacity of IgA+ PCs and B cell subsets to metabolise glucose via glycolysis. To do this, we subjected FACS-sorted small intestinal IgA+ PCs and IgD+ B cells to the Agilent Seahorse Extracellular Flux Analyser Glycolysis Stress Test. Using this test, we demonstrated that IgA+ PCs have a higher metabolic activity but similar overall glycolytic capacity to IgD+ B cells (Figure 4.11C). The basal ECAR reflects non-glycolytic acidification, whereas the glycolytic capacity rate reflects the production of lactate from pyruvate in the presence of glucose – resulting in changes in pH. Therefore, together, this demonstrates that *ex vivo* IgA+ PCs have a higher metabolic rate than naive IgD+ B cells; however, this difference is unlikely to be driven solely by glycolysis.

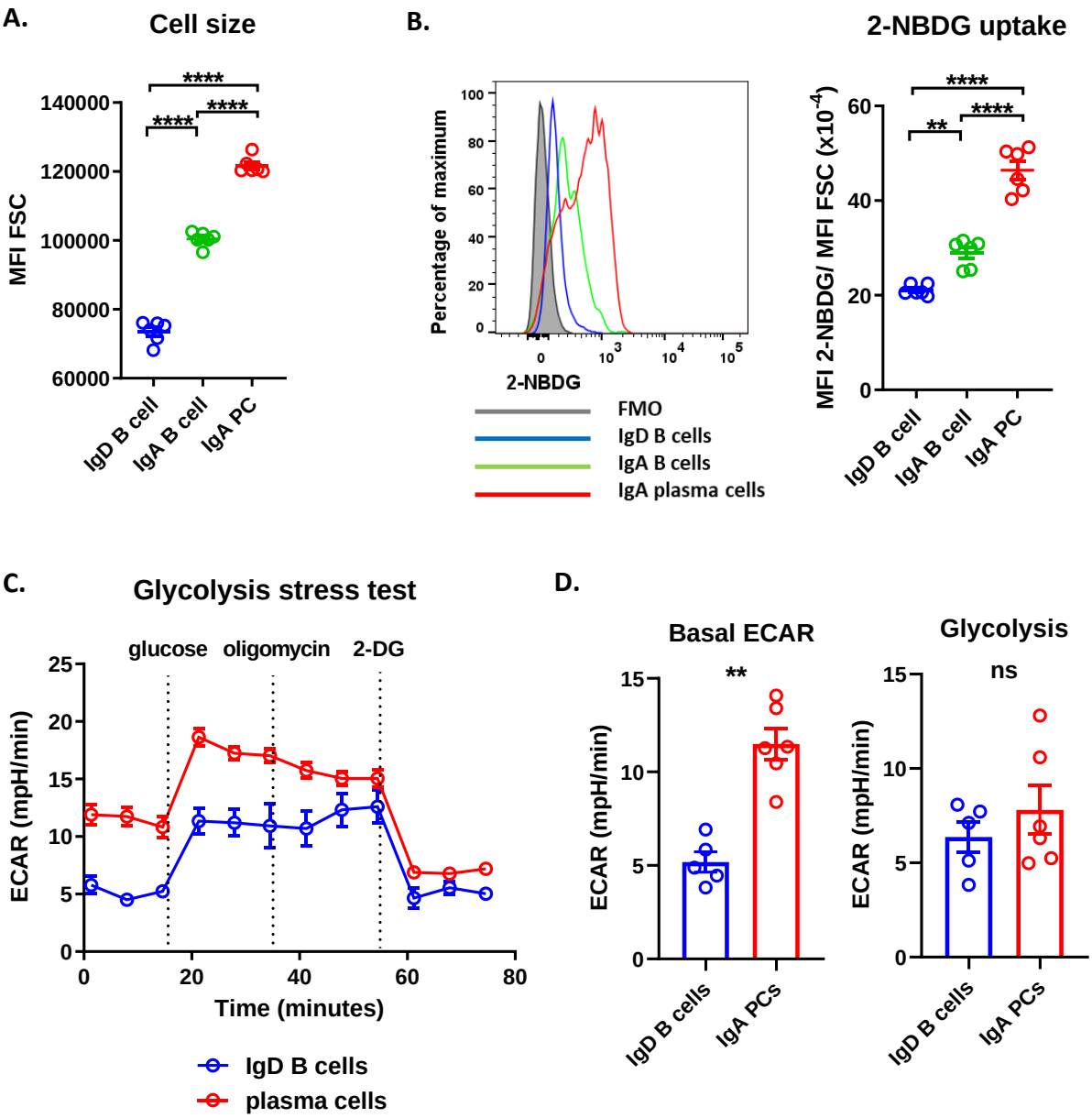

Figure 4.11. IgA+ PCs uptake more glucose but have similar glycolysis rates to B cells.

(A) Analysis of cell size; enumerated forward scatter (FSC) mean fluorescence intensity (MFI) for each group. (B) Analysis of *in vivo* uptake of the glucose analogue 2-NBDG. (Left) Example histogram plot of MFI. FMO gated on IgA+ PCs. IgD+ B cells were pre-gated as CD45+B220+CD3-IgA-CD138-; IgA+ B cells were pre-gated as CD45+B220+CD3-IgD-CD138-; IgA+ CD138+ PCs were pre-gated as CD45+MHCII+CD3-B220-IgD-; (right) enumerated 2-NBDG MFI normalised to cell size determined by FSC MFI. Statistical analysis was conducted by ANOVA and post-hoc Tukey's Test. Data representative of three independent experiments (n=6 mice per experiment). (C) Seahorse Glycolysis Stress Test in FACS-sorted small intestinal IgA+ PCs and IgD+ B cells. Cells were plated at 150,000 cells/well; n=4-6 replicates per experiment. Plot indicates representative trace of mean extracellular acidification rate (ECAR). The ECAR value was not normalised. (D) (Left) Mean basal ECAR values; (right) glycolysis levels; glycolysis data was calculated by subtracting the last basal ECAR measurement from the maximum measurement after glucose injection. Mean±SEM plotted. Data representative of two independent experiments (C57BL/6 female mice aged 8-10 weeks).

Our RNA sequencing data showed diurnal rhythms in *Slc7a5* gene expression (encoding LAT1) in IgA+ PCs. LAT1 together with CD98 forms a transmembrane protein complex – system L transporter – that acts as the major transporter for large neutral amino acids such as leucine, which upon entry into the cell, licenses mTOR and enables protein translation [200, 332]. To evaluate amino acid uptake by IgA+ PCs, we initially evaluated the surface expression of CD98 in cells by flow cytometry. We observed that IgA+ PCs displayed greater surface expression of CD98 than both IgA+ B cells and IgD+ B cells (Figure 4.12A). We next confirmed high amino acid uptake in these cells by incubating small intestinal single cell suspensions with the auto-fluorescent tryptophan metabolite, kynurenine – shown to accurately reflect amino acid uptake by large neutral amino acid transporters [332]. After normalising to cell size, we found higher kynurenine uptake in IgA+ PCs compared with naïve IgD+ and IgA+ class-switched B cells (Figure 4.12B).

The transport of kynurenine into the cell has been shown to be competitively blocked using excess concentrations of leucine, to a comparable level as seen with inhibition of the system L transporter using the inhibitor BCH [332]. Therefore, we next validated the specificity of kynurenine uptake in IgA+ PCs in the presence of excess leucine or BCH. The data showed that uptake of kynurenine into IgA+ PCs was inhibited by both excess leucine and BCH (Figure 4.12C), which demonstrates that kynurenine transport in IgA+ PCs is likely mediated by the System L transporter. Together, these data demonstrate that IgA+ PCs have a greater capacity to uptake amino acids via the System L transporter family compared with IgA+ or IgD+ B cells.

A.

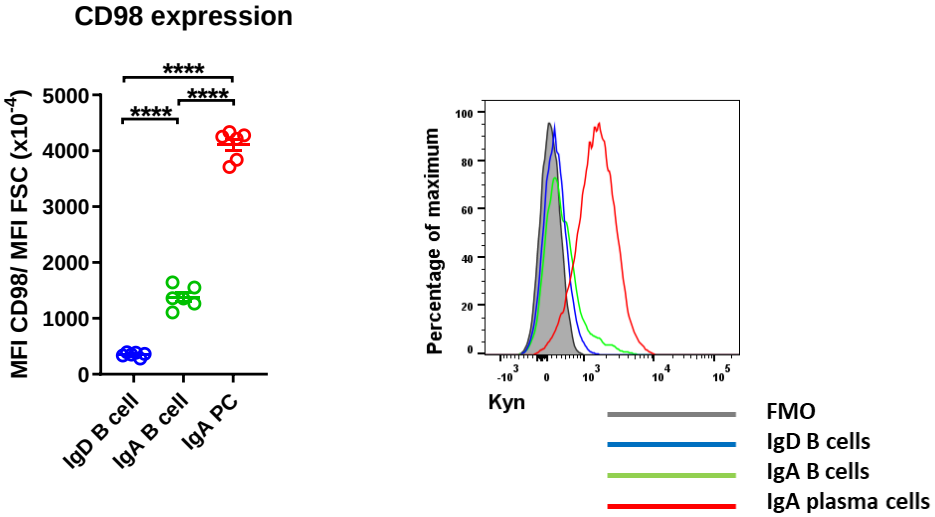
CD98 expression
MFI CD98/ MFI FSC (x10-4)
5000
4000
3000
2000
1000
0
****
****
****
IgD B cell
IgA B cell
IgA PC
Percentage of maximum
Kyn
FMO
IgD B cells
IgA B cells
IgA plasma cells

B.

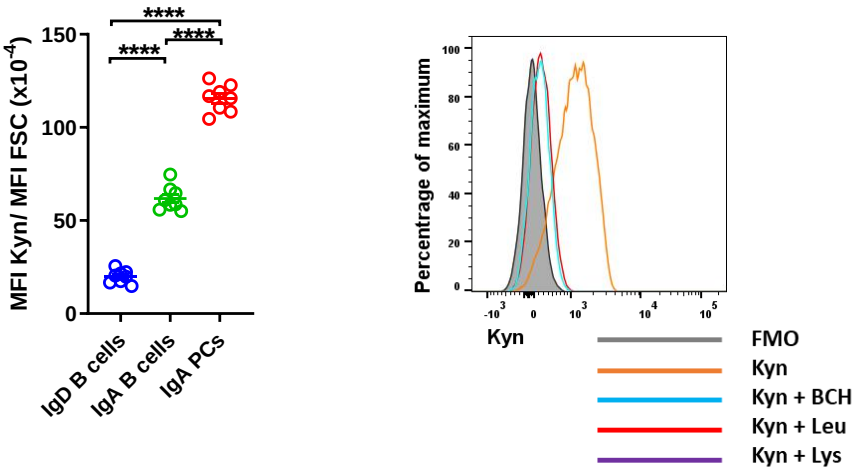
Kyneurinine uptake
MFI Kyn/ MFI FSC (x10-4)
150
100
50
0
****
****
****
IgD B cells
IgA B cells
IgA PCs
Percentrage of maximum
Kyn
FMO
Kyn
Kyn + BCH
Kyn + Leu
Kyn + Lys

C.

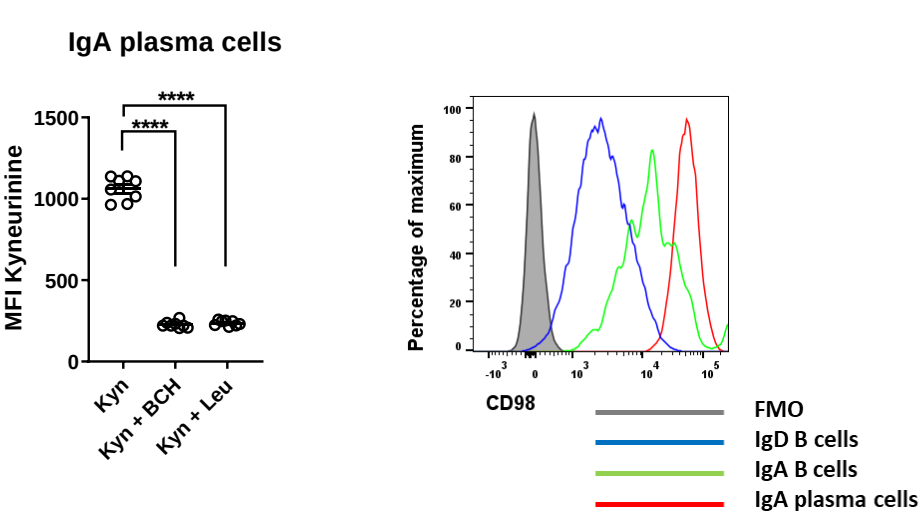
IgA plasma cells
MFI Kyneurinine
1500
1000
500
0
****
****
Kyn
Kyn + BCH
Kyn + Leu
Percentage of maximum
CD98
FMO
IgD B cells
IgA B cells
IgA plasma cells

Figure 4.12. IgA+ PCs uptake large amounts of amino acids via the LAT1 transporter.

(A) Surface CD98 expression in small intestinal IgD+ B cells, IgA+ B cells and IgA+ PCs. (Left) Enumerated CD98 mean fluorescence intensity (MFI) normalised to cell size determined by forward scatter (FSC) MFI; (right) example histogram plot of MFI. FMO gated on IgA+ PCs. (B) Analysis of *in vitro* uptake of the amino acid derivative kynurenine. Small intestinal single cell suspensions were treated with kynurenine (kyn) at 37 °C for 4 minutes and then analysed by flow cytometry. (Left) Enumerated kynurenine MFI normalised to cell size determined by FSC MFI; (right) example histogram plot of fluorescence intensity. FMO gated on IgA+ PCs. (C) Kynurenine uptake assay in small intestinal IgA+ PCs. Small intestinal single cell suspensions were treated with kynurenine in the presence or absence of BCH (10 mM), Leucine (Leu; 5 mM) or Lysine (Lys; 5 mM) at 37 °C for 4 min. (Left) Enumerated MFI for each group; (right) example histogram plot of fluorescence intensity. (A) Data representative of three independent experiments (n=6 mice per experiment; C57BL/6 female mice aged 8-10 weeks). (B&C) Data representative of two independent experiments (n=8 mice per experiment; C57BL/6 female mice aged 8-10 weeks). Statistical analysis was conducted by one-way ANOVA and post-hoc Tukey's Test. Bars indicate mean+/-SEM. ***= p<0.001; ****= p<0.0001.

Fatty acids are critical for organelle function and membrane formation within the cell [111, 200]. To evaluate the uptake of fatty acids by cells, we analysed fluorescent fatty acid (Bodipy FL C_{16}) uptake into cells *in vivo*. After normalising for cell size, IgA+ PCs had greater uptake of Bodipy than IgD+ B cells, but not IgA+ B cells, suggesting that the capacity to take up fatty acid was similar between PCs and IgA+ B cells, although overall the fluorescence intensity was low across all groups (Figure 4.13A). We next assessed the accumulation of lipids within PCs and B cell precursors, by incubating single cell suspensions with LipidTOX, which binds to intracellular neutral lipid droplets. IgA+ PCs showed greater staining with LipidTOX than B cell precursors, indicating greater neutral lipid content (Figure 4.13B). Overall, these findings suggest that IgA+ PCs uptake greater amounts of the major metabolic substrates than class-switched IgA+ B cells and naïve IgD+ B cells.

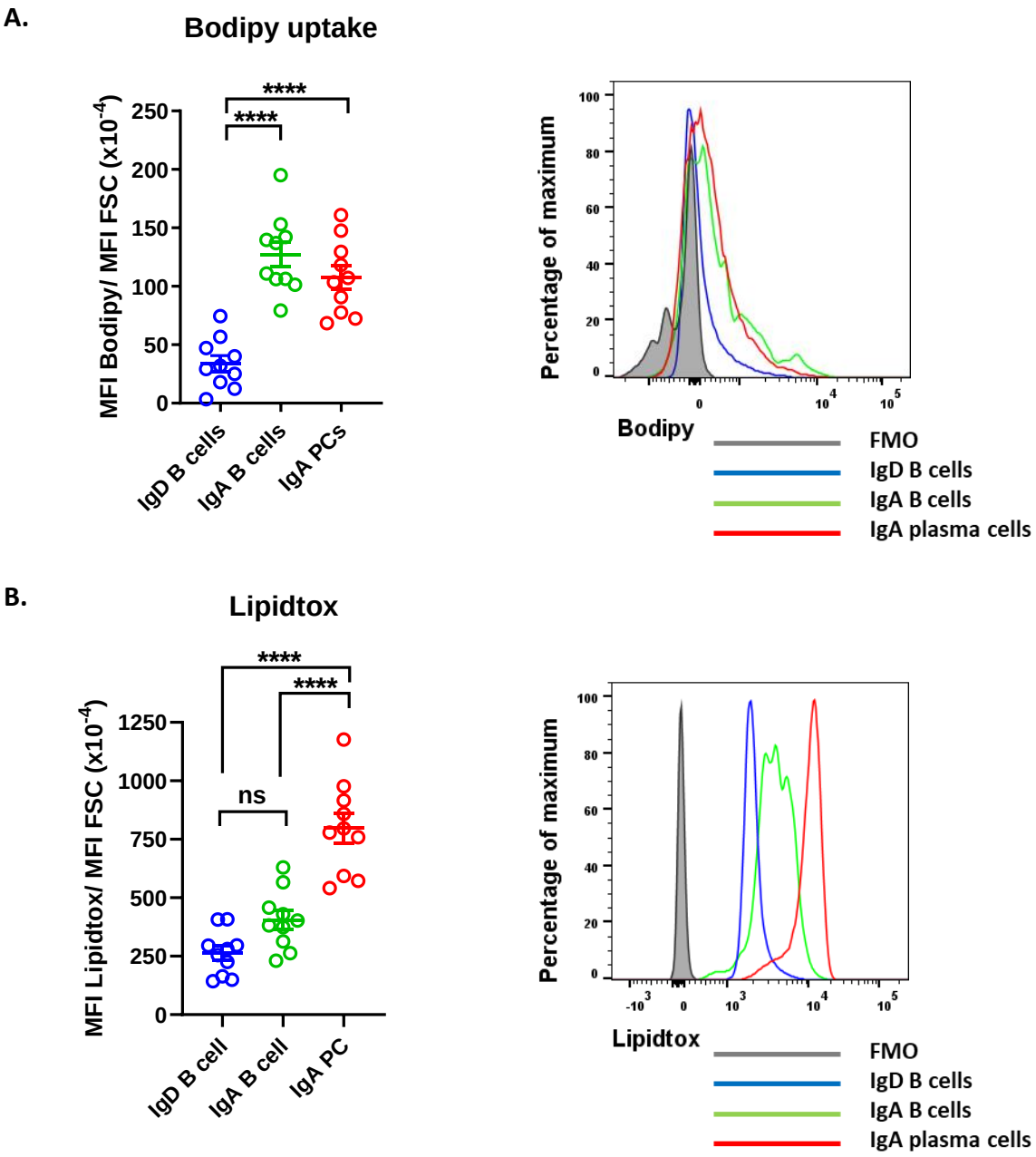

Figure 4.13. IgA+ PCs contain more lipids than B cell precursors.

(A) Analysis of *in vivo* uptake of the lipid analogue Bodipy. Mice were injected intra-peritoneally with Bodipy and euthanised 60 min later; small intestinal single cell suspensions were the analysed by flow cytometry. (Left) Enumerated Bodipy mean fluorescence intensity (MFI) normalised to cell size determined by forward scatter (FSC) MFI; (right) example histogram plot of MFI. FMO gated on IgA+ B cells. (B) Analysis of intracellular lipid content *in vitro*. (Left) Enumerated Lipidtox MFI normalised to cell size determined by FSC MFI; (right) example histogram plot of MFI. FMO gated on IgA+ PCs. IgD+ B cells were pre-gated as CD45+B220+CD3-IgA-CD138-; IgA+ B cells were pre-gated as CD45+B220+CD3-IgD-CD138-; IgA+CD138+ PCs were pre-gated as CD45+MHCII+CD3B220-IgD-. Data representative of (A) one, (B) and two experiments (n=8-10 mice per experiment; C57BL/6 female mice aged 8-10 weeks). Statistical analysis was conducted by one-way ANOVA and post-hoc Tukey's Test. Bars indicate mean+/-SEM. *= p<0.05; ****= p<0.0001.

4.2.6 No difference in the uptake of nutrients or metabolic capacity of IgA+ PCs over the course of the day

Based on our earlier observations, we hypothesised that intrinsic differences in the capacity of IgA+ PCs to uptake and process nutrients over the course of the day might drive rhythmic IgA responses. Therefore, we next employed the same flow cytometry and Seahorse approaches (Chapter 4.2.5) to determine whether differences existed in the capacity of small intestinal IgA+ PCs to uptake these nutrients at different times of the day. We reasoned that potential differences might be apparent during a time of relative nutrient excess (i.e. during feeding), compared with relative nutrient deprivation (i.e. during fasting). Therefore, we housed mice in cabinets with opposing 12 hour light:dark lighting schedules and sampled mice at a single timepoint that corresponded with ZT6 and ZT18, which reflected mid-fasting and mid-feeding, respectively. Using this approach, we found no differences in the capacity of small intestinal IgA+ PCs to take up nutrients, metabolise glucose via glycolysis, or in the lipid content of cells at different times of the day (Figure 4.14A-F).

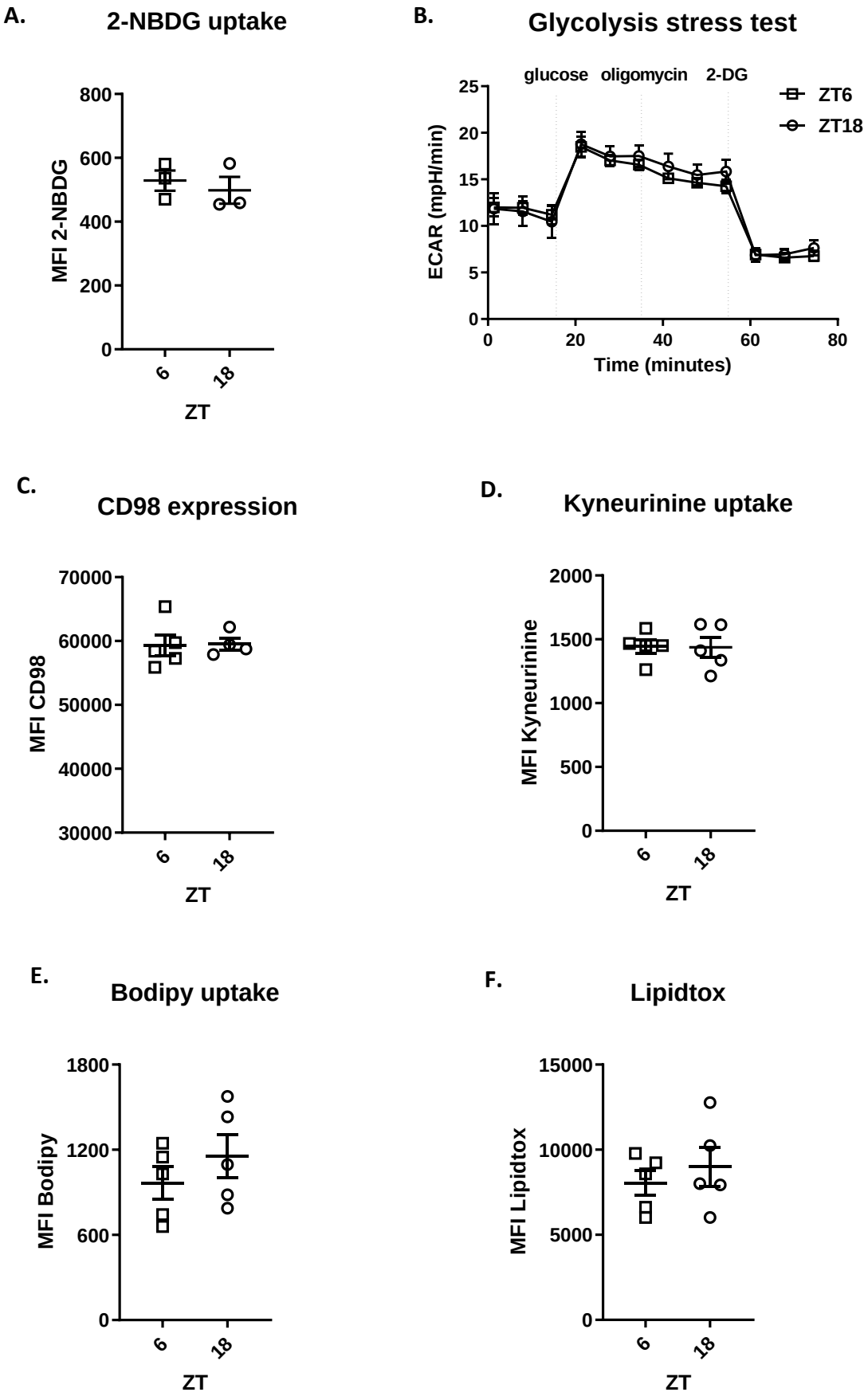
A.
2-NBDG uptake
MFI 2-NBDG
800
600
400
200
0
6
18
ZT
B.
Glycolysis stress test
glucose
oligomycin
2-DG
ZT6
ZT18
ECAR (mpH/min)
25
20
15
10
5
0
0
20
40
60
80
Time (minutes)
C.
CD98 expression
MFI CD98
70000
60000
50000
40000
30000
6
18
ZT
D.
Kyneurinine uptake
MFI Kyneurinine
2000
1500
1000
500
0
6
18
ZT
E.
Bodipy uptake
MFI Bodipy
1800
1200
600
0
6
18
ZT
F.
Lipidtox
MFI Lipidtox
15000
10000
5000
0
6
18
ZT

Figure 4.14. No time of day differences in the capacity of IgA+ PCs to take up nutrients, metabolise glucose via glycolysis, or in the lipid content of cells

Mice were housed in opposing 12hour light:dark cabinets and fed ad libitum for 2 weeks. Subsequently, mice were euthanised at a single timepoint, representative of ZT6 and ZT18 in each cabinet. Small intestinal single cell suspensions were prepared and analysed by flow cytometry. Enumerated mean fluorescence intensity (MFI) plots depicting of (A) *in vivo* uptake of 2NBDG, (B) Seahorse Glycolysis Stress Test in FACS-sorted small intestinal IgA+ PCs, (C) cell surface CD98 expression, (D) *in vitro* uptake of kyneurinine, (E) *in vivo* uptake of bodipy and (F) lipidtox staining, at ZT6 and ZT18 timepoints. (B) Data represents mean extracellular acidification rate (ECAR). 150k sorted cells were plated per replicate; n=3 replicates per group. (A-F) IgA+CD138+ PCs were pre-gated as CD45+MHCII+IgD-B220- cells. B&E data representative of one experiment (B, n=8 mice/ timepoint pooled into 3 replicates per group; E, n=5 mice/ timepoint; C57BL/6 female mice aged 8-10 weeks). A,C-F data representative of two independent experiments (n=3-5 mice/ timepoint; female mice aged 8-10 weeks). Statistical analysis was conducted by Unpaired T test (A,C-F). Bars indicate mean+/-SEM. ZT = Zeitgeber time.

While mice are known to eat predominantly during the night-time [274], *ad libitum* feeding during the daytime may have reduced our ability to detect time of day differences in nutrient uptake. Therefore, to confirm that nutrient uptake into IgA+ PCs is not altered during feeding or fasting, we placed mice on the previously described restricted feeding regime (Figure 4.7A). Mice from each group were then euthanised at a time which represented the mid-point of feeding or fasting, following which we evaluated *ex vivo* uptake of 2-NBDG and kynurenine in small intestinal IgA+ PCs. Analysis of the data showed no difference in the uptake of neither 2-NBDG nor kynurenine into IgA+ PCs from mice under fed or fasting conditions (Figure 4.15A&B). Together, this data suggests that the capacity of small intestinal IgA+ PCs to take up nutrients does not change at different times of the day, nor under different states of nutrient availability. These findings raise the possibility that temporal changes in the availability of nutrients *in vivo* due to feeding and fasting may regulate IgA production rather than the capacity of the cell to utilize those substrates at any given time.

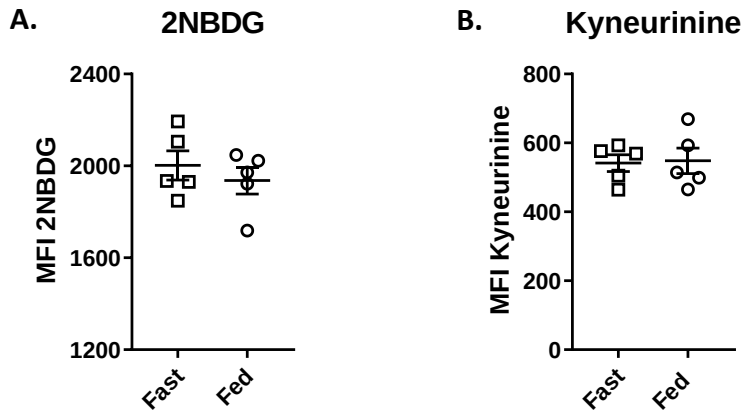

Figure 4.15. No difference in the capacity of small intestinal IgA+ PCs to take up nutrients during feeding or fasting.

Mice were housed under the same 12-hour light:dark lighting conditions and had access to food during a restricted 12-hour window confined to either the light-phase or dark-phase. After 2 weeks, mice were euthanised at the mid-point of the dark phase (representative of ZT18), such that 'fed' mice were 6 hours into their feeding period and 'fasted' mice were 6 hours post their feeding period. Small intestinal single cell suspensions were treated with 2-NBDG or kynurenine at 37 °C for 4 minutes and then analysed by flow cytometry. Mean fluorescence intensity (MFI) plots representative of *in vitro* uptake of (A) 2-NBDG and (B) kynurenine, in small intestinal IgA+ PCs. IgA+CD138+ PCs were pre-gated as CD45+MHCII+IgD-B220- cells. Data representative of one experiment (n=5 mice/ group; C57BL/6 female mice aged 8-10 weeks). Analysis by Unpaired T test.

4.2.7 Modulation of metabolic substrate availability alters the magnitude of IgA secretion

To investigate whether differences in the availability of nutrients might drive rhythmic IgA secretion, we next cultured FACS-sorted small intestinal IgA+ PCs in media containing different concentrations of amino acids and glucose overnight and determined the concentration of IgA in culture supernatants. The data showed that PC IgA production was significantly reduced when the concentration of leucine or glucose was limited (Figure 4.16B&C). To further investigate the role of nutrient sensing and cellular metabolism downstream of metabolic substrate availability, we then cultured IgA+ PCs in media containing inhibitors of mTOR signalling (PP242), the System L transporter (BCH) and glycolysis 2-DG. Inhibiting each of these pathways reduced the amount of IgA produced, in comparison with PCs cultured in the absence of inhibitors (Figure 4.16D). These data show that PC IgA production is significantly reduced when the availability and usage of metabolic substrates, particularly glucose or leucine, are limited.

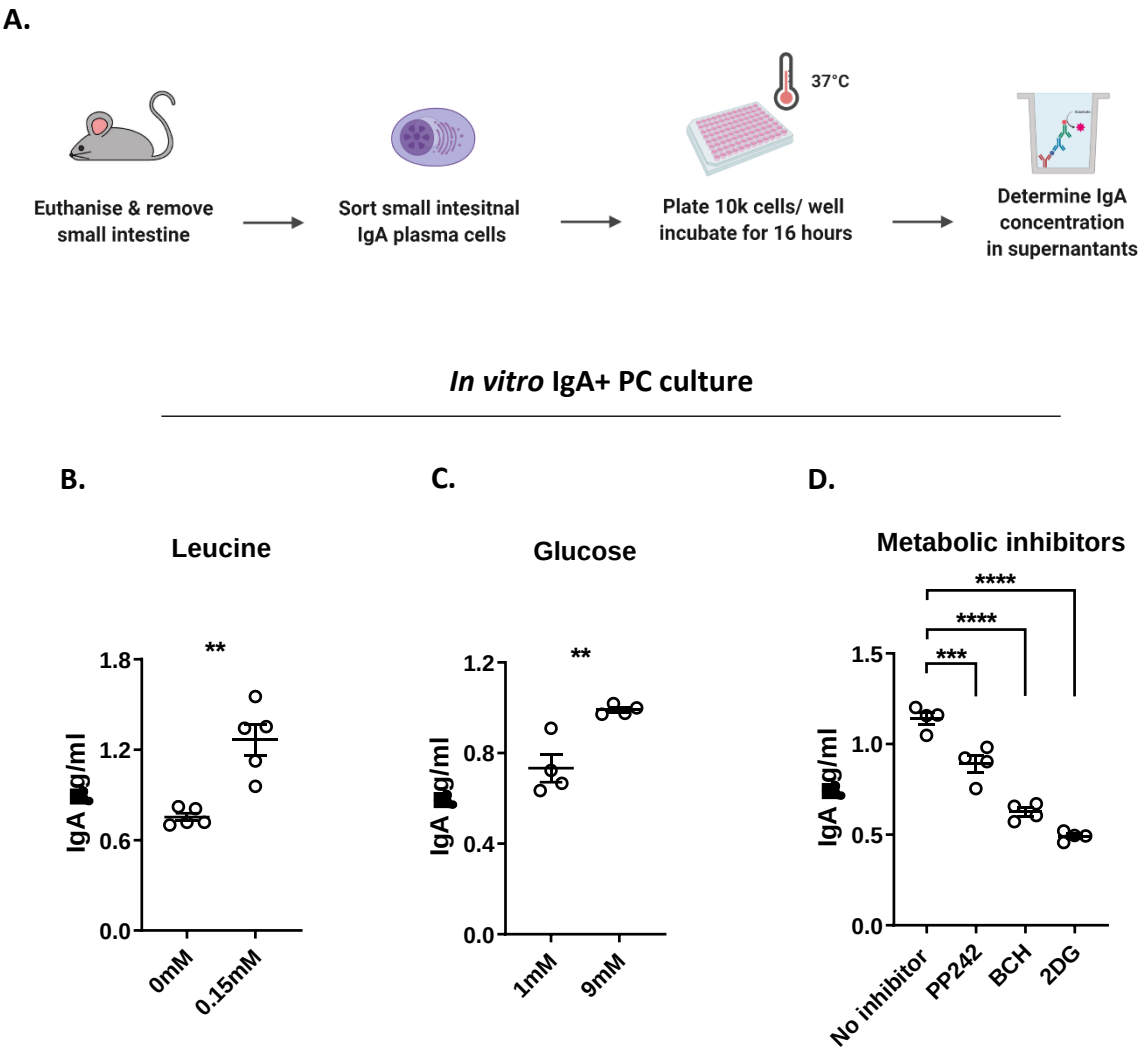

Figure 4.16. Modulation of metabolic substrate availability alters the magnitude of IgA secretion *in vitro*.

(A) Schematic of the experiment. Mice were euthanised and the small intestinal lamina propria was removed. CD138+IgA+ PCs were FACS-sorted from small intestinal lamina propria single cell suspensions. 10,000 cells were plated per well in media with either (B) leucine (0mM & 0.15mM), (C) glucose (1mM & 9mM), or (D) metabolic inhibitors including pp242 (500nM), BCH (10mM), 2-Deoxy-D-glucose (2DG) (1mM). Cells were incubated for 16 hours at 37◦C, following which the culture supernatants were removed and IgA concentrations determined by ELISA. Data representative of two independent experiment (n=4-5 mice/ experiment; C57BL/6 female mice aged 8-10 weeks); bars indicate mean±SEM. Statistical analysis was conducted by Unpaired T test **= p<0.01, ***= p<0.001, ****= p<0.0001.

Thus, our data shows that feeding cues entrain IgA rhythmicity in vivo and that availability of metabolic substrates *ex vivo* acts as a critical regulator of IgA secretory capacity, in part by fuelling downstream metabolic function. We next sought to determine whether perturbations in nutrient levels also modulate IgA secretory capacity and rhythmicity *in vivo*, by evaluating sIgA responses in the setting of excess metabolic substrates. To do this, age and sex matched mice were placed either on a HFD (60% fat) or normal mouse chow diet (~10% fat) for 6 weeks. Fresh faecal pellets were sampled at four, six-hourly timepoints over a single day before the diet was started (baseline) and at weeks 2 and 6 on HFD. As expected, mice fed a HFD demonstrated gained weight by 6 weeks (Figure 4.17A). Blood glucose sampling identified that by 6 weeks, mice had elevated circulating glucose concentrations at rest (Figure 4.17B) but demonstrated no impairment of glucose regulation under fasting conditions (Figure 4.17C), indicating normal glucose/ insulin tolerance. By contrast, mice demonstrated glucose intolerance after prolonged (12 weeks) HFD feeding as expected [387].

A.

Normal mouse chow vs high fat diet

Formula	% by weight	
	Normal	High fat
Protein	~10	20
Carbohydrate	~60	20
Fat	~10	60

B.

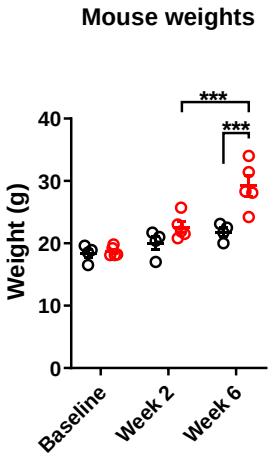

Normal mouse chow High fat diet

C.

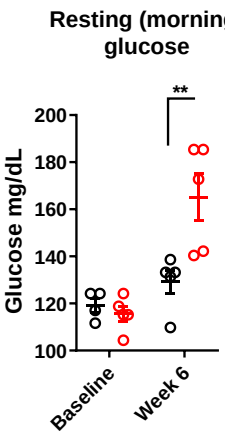

D.

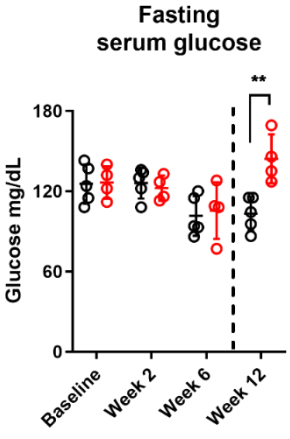

Figure 4.17. Metabolic parameters of mice on a high fat diet.

(A) Age and sex matched mice were fed either a high fat diet (60% fat) or normal mouse chow (~10% fat) for 6 weeks. (B) Mouse weights were recorded before (baseline) and at 2 and 6 weeks after starting the dietary period. (C) Resting serum glucose was measured at a time representative of ZT1 in both groups of mice at indicated timepoints. (D) Fasting serum glucose was measured in both groups of mice at indicated timepoints. For the fasting period, mice were placed into new cages without food from ZT3 to ZT11, after which serum glucose was measured. Data representative of one experiment (n=4-5 mice/ experiment; C57BL/6 female mice aged 8-10 weeks); bars indicate mean±SEM. Statistical analysis was conducted by two-way ANOVA and post-hoc Tukey test. **= p<0.01, ***= p<0.001.

Analysis of faeces showed elevated total levels of sIgA by week 2 and marked differences by week 6 of HFD feeding, in comparison with normal chow-fed mice (Figure 4.18A). Furthermore, HFD-fed mice demonstrated disruption of diurnal rhythmicity in sIgA by week 2 of the dietary period, and complete loss by six weeks, in comparison to mice maintained on a normal chow diet and serially sampled (Figure 4.18B).

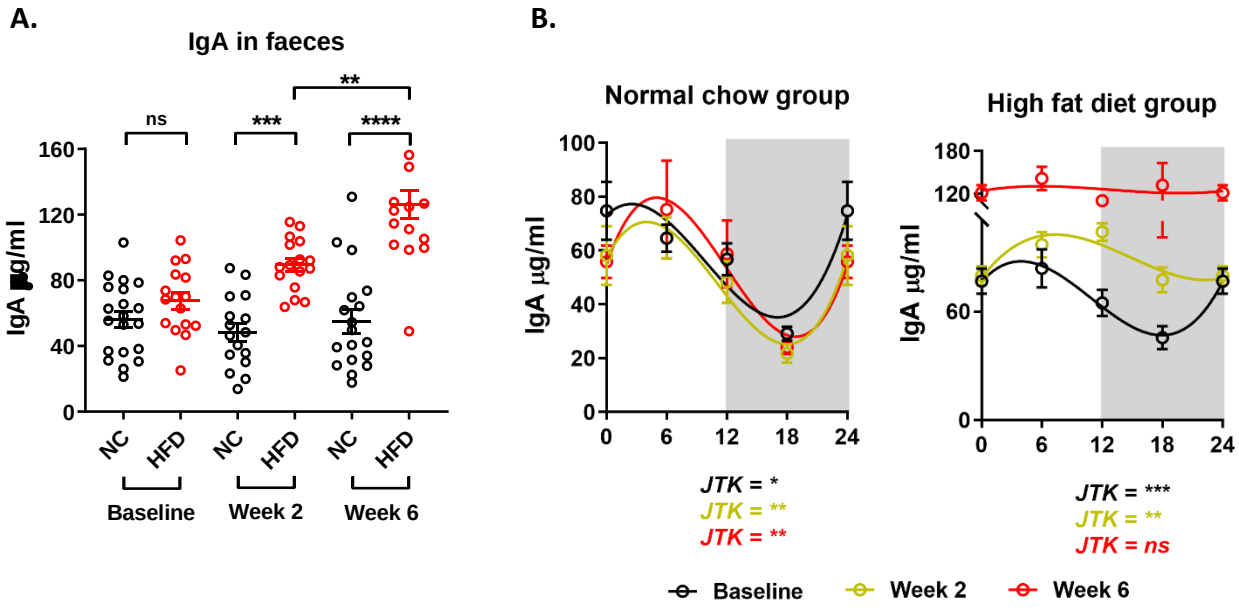

Figure 4.18. A high fat diet is associated with elevated intestinal sIgA and loss of diurnal oscillations in intestinal sIgA

Age and sex matched mice were fed either a HFD (60% fat) or normal mouse chow (~10% fat) for 6 weeks. Faecal pellets were collected at circadian timepoints before (baseline), at 2 and 6 weeks after starting the dietary period. The concentration of faecal secretory (s)IgA normalised by weight was determined by ELISA. (A) The combined daily concentration of faecal sIgA in normal chow and HFD mice at indicated timepoints. (B) The concentration of faecal sIgA over the course of the day in (left) normal chow and (right) HFD fed mice at each ZT timepoints. A third order polynomial line was fitted through the datapoints. Data representative of one experiment (n=4-5 mice/ experiment; C57BL/6 female mice aged 8-10 weeks). Analysis conducted by (A) Two-Way ANOVA and post-hoc Tukey test, and (C&D) JTK analysis and ANOVA. *=p<0.05; **= p<0.01, ***= p<0.001. ZT0 was re-plotted as ZT24 to aide visualisation of the data. NC = normal chow; HFD = high fat diet.

Surprisingly, despite the elevated levels of faecal IgA, flow cytometry analysis revealed a reduction in the frequency and number of IgA+ PCs in both the small and large intestines in HFD mice in comparison with normal chow-fed animals (Figure 4.19A&B), in line with recent findings [122]. Together, this data indicates that dietary modulation of glucose and lipid availability augments the intestinal IgA response.

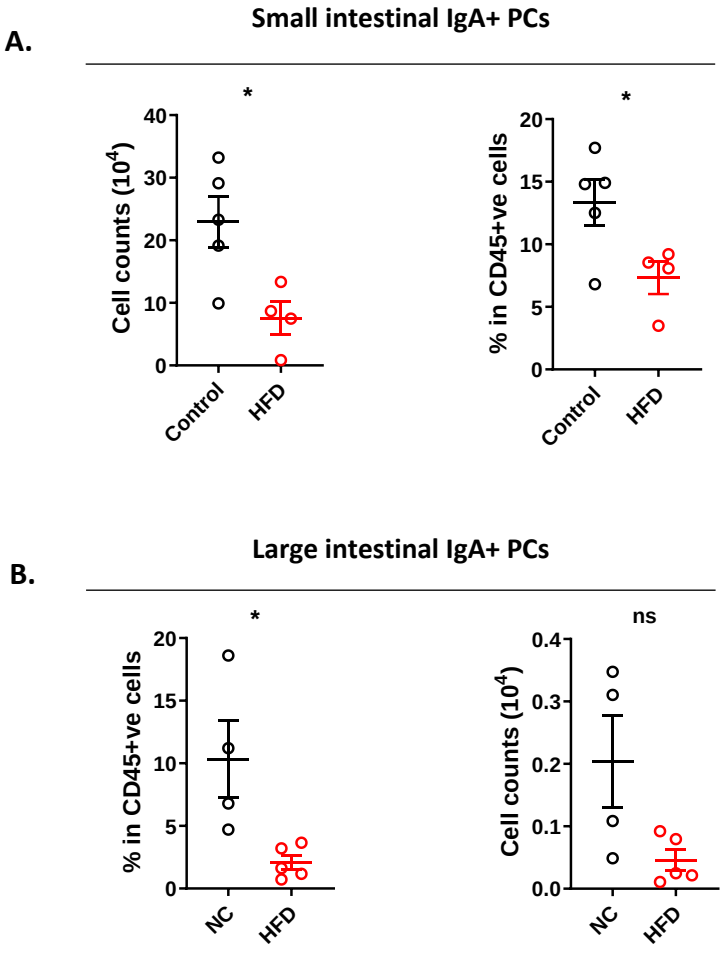

Figure 4.19. A high fat diet is associated with a reduced frequency and number of IgA+ PCs in the small and large intestines.

Age and sex matched mice were fed either a high fat diet (60% fat) or normal mouse chow (~10% fat) for 6 weeks. (A) Frequency (left) and counts (right) of small intestinal lamina propria IgA+ PCs assessed by flow cytometry. IgA+ CD138+ PCs were pre-gated as CD45+ MHCII+ IgD- B220-. (B) Frequency (left) and counts (right) of large intestinal lamina propria IgA+ PCs assessed by flow cytometry. IgA+ B220- PCs were pre-gated as CD45+ MHCII+ IgD- B220. Individual data points from one experiment plotted (n=4-5 mice/ timepoint; C57BL/6 female mice aged 8-10 weeks); bars indicate mean ± SEM. NC= normal chow; HFD = high fat diet.

Having found that the availability of large neutral amino acids, such as leucine, altered the magnitude of IgA secretion, we then evaluated whether altering the protein component of the diet might drive differences in sIgA responses. To do this, mice were fed either a high protein or low protein diet for 3 weeks (Figure 4.20A), after which mice were culled and sIgA was determined in both the terminal ileum and faeces collected either prior to necropsy at a single timepoint (ZT0), or at consecutive timepoints over 24-hour period, respectively. Mice fed a high protein diet gained weight over the 3week dietary period (Figure 4.20B). There was a trend towards increased sIgA responses in the terminal ileum and a blunting of oscillatory sIgA in the faeces of mice fed a high protein diet (Figure 4.20C&D). Taken together, these data indicate that dietary modulation alters intestinal IgA responses, which suggests that temporal changes in nutrient availability may entrain rhythmic PC IgA production.

A.

The high/ low protein diet

Formula	% by weight	
	Low	High
Protein	5.0	21.5
Carbohydrate	75.4	58
Fat	8.1	8.1

B.

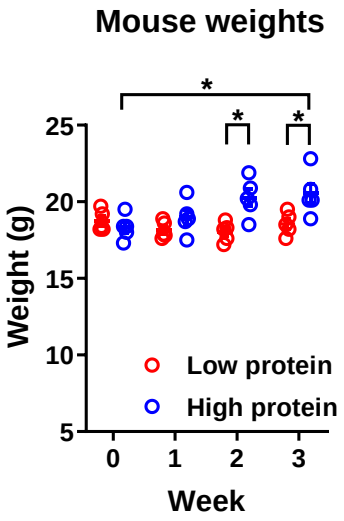

C.

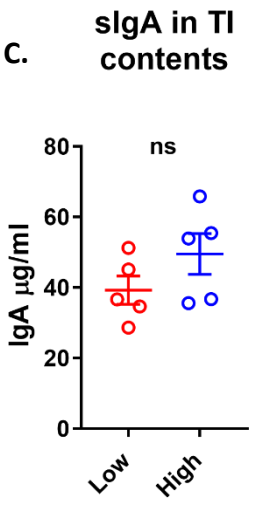

D.

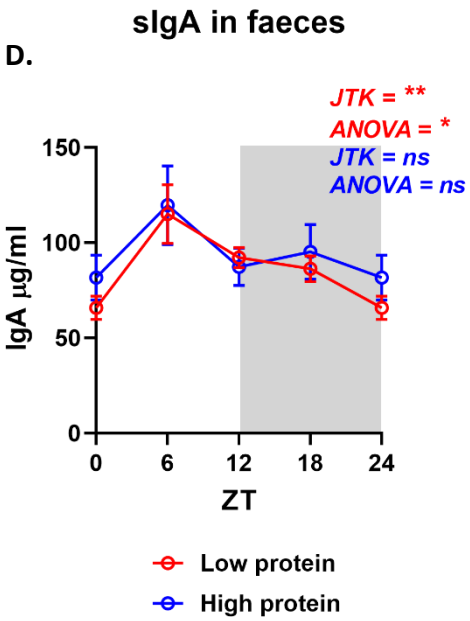

Figure 4.20. Altered sIgA rhythmicity in mice fed a high protein diet.

Age and sex matched mice were fed either a high protein diet or low protein diet for 3 weeks. (A) Table listing the constituents (% by weight) of the high and low protein diets. (B) Weekly weight measurements of mice fed the high or low protein diet. Comparisons between groups conducted by Two-Way ANOVA with post-hoc Tukey; *= $p<0.05$. (C) The terminal ileum was isolated and flushed with 5mls PBS. SIgA concentration of terminal ileal washes was determined by ELISA. (D) Mean faecal sIgA concentration at each timepoint over the circadian day determined by ELISA. ZT0 is replotted as ZT24 to aide visualisation of the data. Differences between each ZT assessed by Krushkal Wallis (KW). Oscillatory nature of data assessed by JTK analysis. *= $p<0.05$; **= $p<0.01$. Data from one experiment plotted (n=4-5 mice/ group; C57BL/6 female mice aged 8-10 weeks); bars indicate mean ± SEM. Ns = non-significant.

4.3 Discussion

Collectively, this data suggests that temporal variation in nutrient availability across the day – due to diurnal feeding patterns – entrains rhythmicity in intestinal IgA production. Under steady state feeding conditions the PC-intrinsic circadian clock appears to be partly dispensable for IgA rhythmicity. However, feeding cues may help to entrain the PC clock and Bmal1 appears to regulate temporal gene expression of nutrient sensing, metabolic and protein synthesis pathways, suggesting a dialogue exists between feeding cues, the biological clock and antibody production within PCs.

We found evidence of oscillations in core clock genes (*Arntl, Per2, Nr1d1*) in fully differentiated IgA+ PCs, but only *Nr1d1* appeared to oscillate in naïve IgD+ B cells. Only one other study has assessed oscillatory clock gene expression in B cells to date. This work identified statistically significant rhythms in the core clock genes in splenic B cells [291]. More recent works have only reported on oscillatory *Nr1d1* expression in B cells [273, 302]. In these previous studies, splenic B cells were purified using a MACS-based approach targeting surface expressed CD19 [273, 291, 302], which provides little information regarding the activation and/ or differentiation state of these cells. Interestingly, recent data suggests that clock function may be altered depending on the activation state of the immune cell [258]. Our data suggests a similar paradigm may exist in B cells – that oscillations in core clock genes are imprinted during the differentiation of B cells towards PCs. Alternatively, studies have shown that Rev-erbα (encoded by *Nr1d1*) is a core transcription factor in ILC3s independent of circadian regulation [311]. Thus, oscillatory *Nr1d1* may regulate gene expression in B cells, independent of the biological clock. Future work could encompass a comparison of oscillatory clock gene expression and function across different stages of B cell activation and maturation to interrogate this further.

We have shown that the availability of metabolic substrates *in vivo* and *ex vivo* modulates the magnitude and rhythmicity of IgA secretion. In accordance with our findings, historical work in IgM-producing mouse hybridoma cell lines has demonstrated that the rate of production of monoclonal antibody increased with increasing concentrations of glucose in the culture medium [388] and more recently, the concentrations of glucose and amino acids were shown to be limiting factors for IgG antibody secretion by PCs [110, 111]. The circulating availability of metabolites including glucose, amino acids and lipids demonstrate clear diurnal rhythmicity

[389]. Notably, in mice fed a normal chow diet *ad libitum*, metabolites reached peak concentrations in the early to mid-light phase both in the serum and across different tissues including the liver [389], which aligns with our findings of peak concentrations of intestinal sIgA in the early to mid-light phase. Together with our data, this suggests that environmental availability, rather than an intrinsic capacity of PCs to augment their nutrient uptake or metabolic capacity in a diurnal manner, mechanistically connects entrainment of IgA oscillations by feeding cues. Intriguingly, recent work has identified that IgA modulates the systemic uptake of nutrients [125], suggesting that a dynamic crosstalk between nutrient availability, IgA responses and nutrient uptake may exist.

Prior work has also demonstrated increased faecal sIgA responses in HFD-fed mice [338]. Others have also shown that feeding mice a HFD leads to a reduction in frequency of intestinal IgA+ PCs [122], suggesting that the difference in sIgA is due to changes in the secretory capacity of IgA+ PCs, as opposed to *de novo* generation PCs in HFD-fed mice. Moreover, feeding mice a HFD (for 10 weeks) leads to major changes in the rhythmic abundance of circulating metabolites, such that circadian oscillations of serum lipids are lost, and serum glucose measurements are constitutively elevated across multiple timepoints, compared with normal chow-fed mice [389]. These findings align with our data of elevated and arrhythmic sIgA in HFD-fed mice and provides further evidence linking nutritional cues with entrainment of IgA rhythmicity, as well as progresses our understanding of how dietary factors can imprint on immune cell function.

Collectively, the evidence suggests that nutrient availability entrains oscillations in sIgA. However, it remains to be determined exactly how the PC-intrinsic clock contributes to rhythmic PC IgA production. While we demonstrated oscillatory sIgA in mice with a B-cell specific deletion of Bmal1, our RNA sequencing data suggests that Bmal1 modulates temporal gene expression of nutrient sensing and protein synthesis pathways in PCs such as mTOR. This is particularly notable, as mTOR is critical in regulating antibody production in mature PCs [352]. Moreover, reversal of feeding inverted Bmal1 gene expression, suggesting a crosstalk exists between nutritional cues, the biological clock and protein synthesis within PCs. Thus, it could be postulated that the clock entrains IgA rhythmicity by mediating cell-intrinsic responses to nutritional cues. This provokes the question of what happens if the feeding pattern is perturbed in mice lacking a functional cell-intrinsic clock? To begin to investigate

this further, future work aims to determine whether IgA rhythms generated under *ad libitum* feeding fail to re-align to reversed feeding of clock-disrupted *Mb1*$^{Cre+/-}$ *x Arntl*$^{flox/flox}$ mice.

Interestingly, diet induced obesity in IgA deficient mice leads to more severe glucose intolerance than in wild type controls [122]. While the mechanisms underlying this are not clear, it was demonstrated that antibiotic administration to obese IgA-deficient mice improved glucose homeostasis, which suggests a role for the gut microbiota in promoting glucose intolerance in the absence of sIgA [122]. Other studies have demonstrated reduced dietary lipid absorption in the intestines [124] and altered systemic availability of fatty acids [125] in mouse models of antibody deficiency. Therefore, by targeting commensal microbes, sIgA may in part regulate the temporal availability of the same nutrients and metabolic substrates that are required for PC IgA production and for host metabolic health. Whether rhythmic sIgA has a functional consequence on regulating the commensal microbiota is evaluated in the following chapter.

5.0 DETERMENING THE CONSEQUENCES OF RHYTHMIC INTESTINAL IGA SECRETION ON HOST-MICROBIAL INTERACTIONS

5.1 Introduction

The composition and function of intestinal commensals undergoes circadian oscillations in both mice and humans [313, 314, 323]. Critically, this results in oscillations in bacterial metabolic, motility and growth pathways, as well as rhythmic systemic availability of microbial nutrient metabolites over a 24-hour period [313, 314, 323]. Microbial rhythmicity in this manner leads to local and systemic effects within the host, including the regulation of immune tolerogenic responses [323], the modulation of transcriptional oscillations in IECs [313, 314] – including the regulation of nutrient uptake [322] and intestinal permeability [323] – and regulation of oscillatory hepatic gene expression and detoxification function within the liver [314]. Loss of microbial rhythmicity (e.g. through changes in diet or light cues, or due to jet lag) is associated with enhanced intestinal inflammation [323] and adverse metabolic outcomes [313, 317, 318, 331]. To this end, microbial oscillations are important determinants of intestinal homeostasis and host metabolic health.

Under homeostatic conditions, intestinal immune cell responses are dedicated to maintaining intestinal health and microbial mutualism [25]. It is increasingly understood that several of these immune responses are imprinted with circadian rhythmicity [251], including our current findings of rhythmic intestinal IgA production. However, importantly, the link between circadian immune function and microbial rhythms is unclear and the precise mechanism(s) driving microbial oscillations is poorly understood. Previous studies have identified that the host clock and the type and timing of feeding can modulate microbial rhythmicity [313, 316, 317]. More recently, it was shown that mice with disrupted ILC3 clock function displayed altered diurnal patterns of commensal microbes [293, 301, 311], suggesting that oscillatory immune function may regulate microbial rhythmicity. Intestinal IgA targets commensal microbes and modulates the composition and function of the gut microbiota in homeostasis [145]. Intriguingly, loss of microbial oscillations leads to increased susceptibility to metabolic derangements including hyperglycaemia and weight gain [313], which aligns with the phenotype in part associated with impaired gut IgA responses [122, 316, 317].

Together, these findings provoke the question of whether oscillatory IgA modulates compositional and/ or functional circadian oscillations of the gut microbiota. In this chapter, we interrogate this hypothesis by determining the consequences of rhythmic intestinal IgA on commensal microbial composition and function over the circadian day.

5.2 Results

5.2.1 Characterisation of a mouse model devoid of secretory antibodies

In order to characterise the role of oscillatory IgA responses on regulating the composition of the intestinal commensal microbiota, we first sought to acquire a mouse strain that was devoid of secretory antibodies. For this purpose, we used the previously generated IgMi mouse strain [390]. In this strain, the constant regions of the IgH chain are deleted, except for the portion of the heavy chain of IgM (Cμ) that is responsible for the maturation of the membrane-form of the IgM heavy chain ($IgH^{\mu 1y}$; Figure 5.1A) [390]. The result is a model in which only B cells expressing IgM as a B-cell receptor on their surface develop and B cells are not able to go through CSR or differentiation to PCs [390], nor secrete any soluble antibodies (Figure 5.1B) [391]. This is unlike other mouse models used within the field such as pIgR-deficient mice (in which sIgA titres are only partially disrupted) [81], IgA-deficient mice [145] (which demonstrate compensatory sIgM which binds many of the same commensals as sIgA [66]) and mice which lack all B cells [392] (which results in significantly impaired mucosal and systemic immunity [392, 393]).

Previous work has validated the phenotype of this mouse strain locally [391]. We confirmed this, by identifying the presence of IgM+ B cells, and lack of class-switched B cells and CD138+ PCs, in IgMi mice compared to WT littermate controls (Figure 5.1C). Further to this, we used an established flow cytometric assay [66] to detect the presence of IgA-bound (IgA+) bacteria in murine faeces. As expected, we detected IgA+ bacteria in WT littermate controls, but not in IgMi mice (Figure 5.1D). Collectively, these data confirm the phenotype of this mouse strain, enabling its use to interrogate the role of rhythmic intestinal IgA in regulating the commensal microbiota.

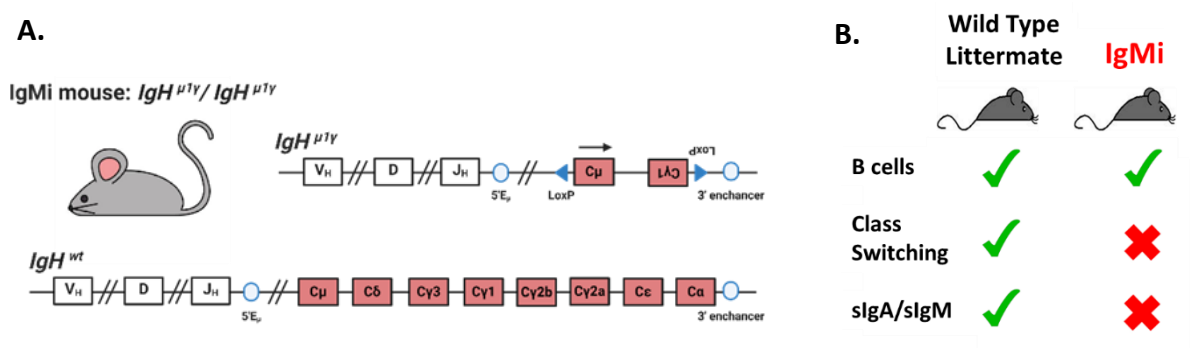
A.
IgMi mouse: IgH μTγ/ IgH μTγ
IgH μTγ
VH
D
JH
Cμ
LoxP
3' enchancer
IgH wt
Cμ
Cδ
Cγ3
Cγ1
Cγ2b
Cγ2a
Cε
Cα
B.
Wild Type Littermate
IgMi
B cells
Class Switching
sIgA/sIgM

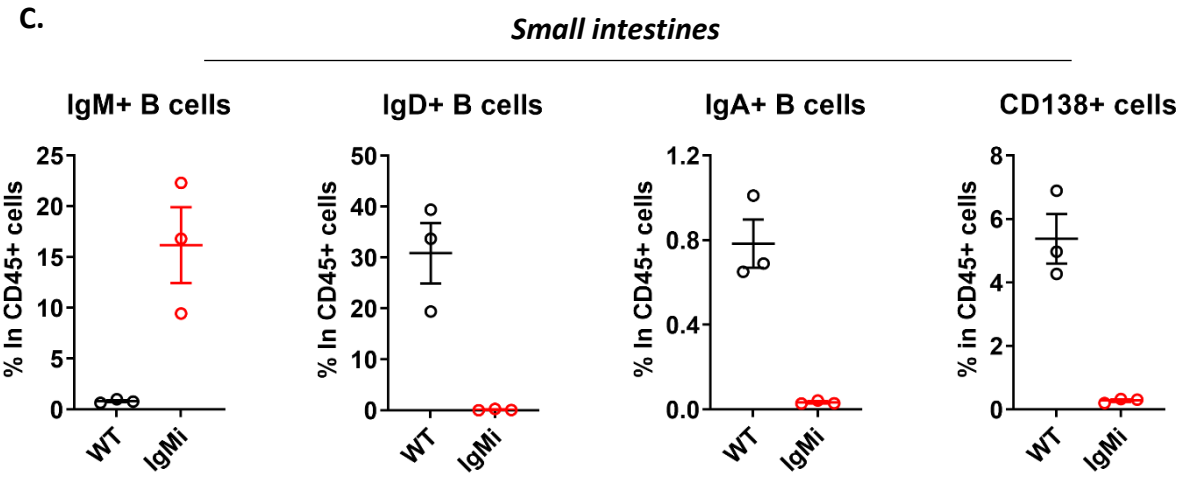
C.
Small intestines
IgM+ B cells
IgD+ B cells
IgA+ B cells
CD138+ cells
% In CD45+ cells
% in CD45+ cells
WT
IgMi

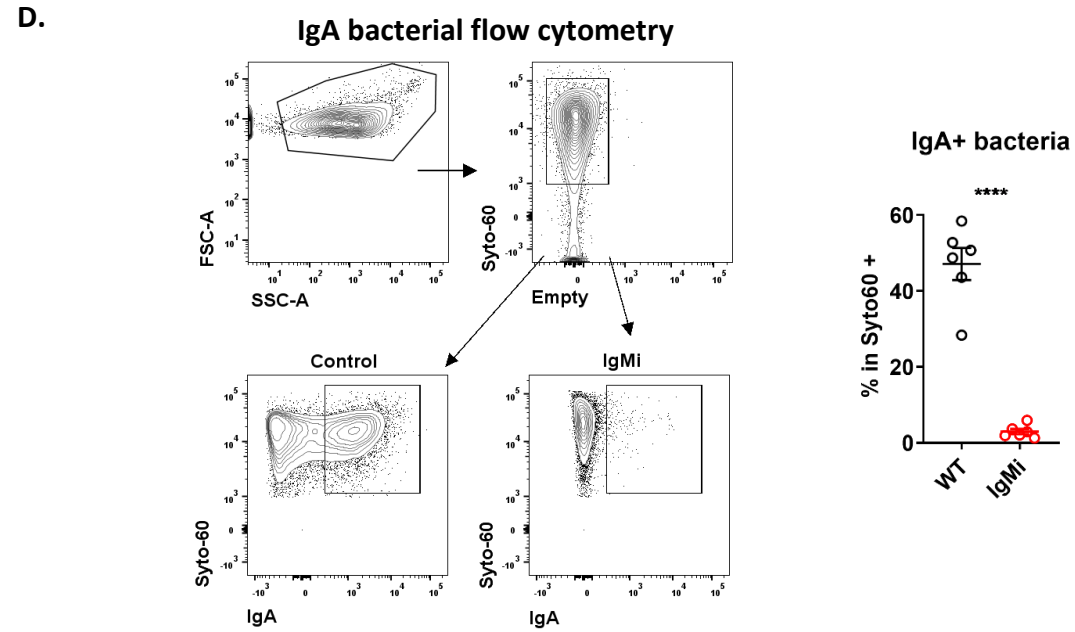
D.
IgA bacterial flow cytometry
FSC-A
SSC-A
Syto-60
Empty
Control
IgMi
IgA
IgA+ bacteria
****
% in Syto60 +
WT
IgMi

Figure 5.1. Characterisation of the IgMi mouse

(A) Schematic representation of the IgH locus of the IgMi ($IgH^{\mu 1y}$) and wild type (IgH^{wt}) mouse. The IgMi mouse is homozygous for the $IgH^{\mu 1y}$ locus, while the wild type (WT) mouse is homozygous for the IgH^{wt} locus. (B) Schematic representing the B cell compartment of the IgMi mouse in comparison with their littermate controls. (C) Frequency of IgM+, IgD+ and IgA+ B cells and CD138+ (plasma) cells (left to right) in small intestinal single cell suspensions of IgMi and WT littermate control mice as determined by flow cytometry. IgM+ IgD- B cells were pre-gated as live CD45+MHCII+B220+ cells; IgD+ IgA- B cells were pre-gated as live CD45+MHCII+B220+ cells; IgA + IgD- B cells were pre-gated as CD45+MHCII+B220+ cells; CD138+ PCs were pre-gated as live CD45+MHCII+B220-IgD- cells. Data representative of one experiment (n=3 mice per group). (D) (Left) Gating strategy (right) enumerated frequencies of IgA bound bacteria (IgA+ bacteria; gated as Syto-60+IgA+ events) in faeces of IgMi and age and sex-matched WT littermate control mice. Unpaired T-Test used to compare differences between groups. Data pooled from two independent experiments (n=3 mice per group; male and female mice aged 10-12 weeks). Bars indicate mean±SEM across all graphs.

5.2.2 The global composition of intestinal commensal bacteria is similar in IgMi and littermate control mice

Having confirmed the specificity of the flow cytometric assay for detecting IgA+ bacteria in the faeces of mice, we next sought to use this assay to determine whether the frequency of IgA+ bacteria varies over the course of the day. To do this, we collected fresh faecal pellets from the same mice at consecutive timepoints over the circadian day. Analysis of IgA staining of bacteria by flow cytometry did not demonstrate any differences across the experimental timepoints (Figure 5.2), suggesting that the total amount of faecal bacteria bound by IgA does not fluctuate over the course of the day.

However, this does not rule out the possibility that individual differences exist in IgA-binding specific microbial communities and/ or the composition of microbes in the presence of sIgA. To investigate this further, we performed 16S rRNA sequencing analysis of faecal microbiota from IgMi and WT littermate control mice every 6 hours over the course of a single 24-hour period. Additionally, to achieve a more extensive analysis of the composition of intestinal commensals in the absence of secreted antibodies in IgMi mice, we also performed 16S rRNA sequencing analysis of bacteria harvested from colonic scrapings at a single timepoint (ZT5) from both groups.

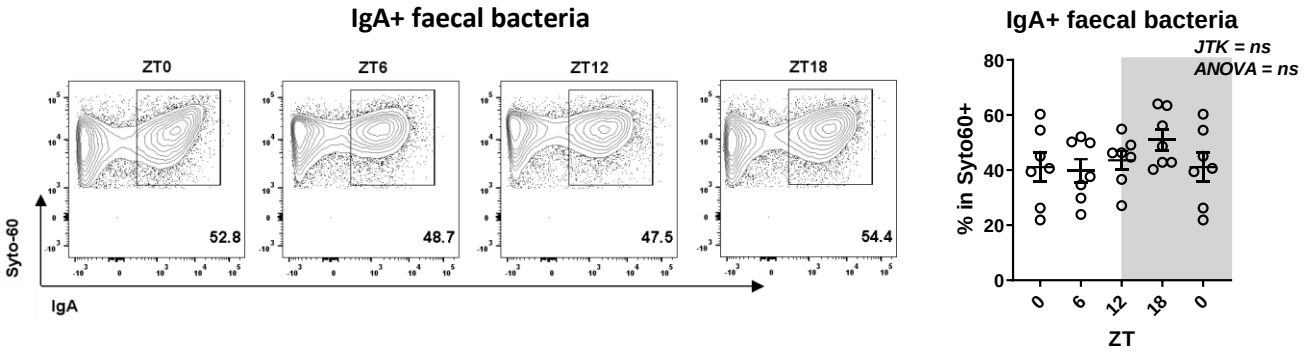

Figure 5.2. No difference in the amount of faecal bacteria bound by IgA over the course of the day.

Frequency of IgA+ bacteria in the faeces of mice sampled over the course of the day, assessed by flow cytometry. (Left) Representative flow plots of IgA+ bacteria; (right) graphed data of each replicate across all sampling timepoints. IgA+ Syto60+ bacteria are pre-gated as FSC and SSC double positive, using SSC as the threshold. ZT0 is double plotted to facilitate viewing the data. Data pooled from two independent experiments (n=3-4 mice/ timepoint; C57BL/6 female mice aged 8-10 weeks). Data representative of n=5 independent experiments. Variance in the data assessed by ANOVA. Oscillatory nature of data assessed by JTK analysis. Horizontal bars represent mean±SEM. Shaded area on graphs represents the dark phase. Bars indicate mean ± SEM.

Initial analyses revealed that the global alpha and beta diversity of intestinal microbes within the faeces and colon were similar between IgMi and age- and sex-matched WT littermate controls (Figure 5.3A&B). We next evaluated the global composition of commensal bacteria with a relative abundance of >2% in the colonic mucosa and/ or faeces in both groups. In general, the global composition of intestinal commensals of IgMi mice and controls were similar, in line with previous reports that IgMi and littermate control mice have largely comparable microbiota compositions [391]. However, we did note a reduction in the presence of bacteria belonging to the phyla *Verrucomicrobia* in the faeces, and a non-significant reduction in the colonic mucosa, of IgMi mice (Figure 5.4 A&B). Furthermore, the composition of intestinal commensals was broadly comparable between groups at the genus level (Figure 5.4C). Indeed, in the faeces, only bacteria belonging to the *Akkermanisa* genus of the *Verrucomicrobia* phyla, and an unclassified genus of the *Desulfovibrionaceae* family of the phyla *Proteobacteria*, displayed significant differences in global relative abundance between groups over all sampled timepoints (Figure 5.4D). In addition, the *Helicobacter* genus of the phyla *Proteobacteria* demonstrated a greater than 2-fold difference in mean

abundance in the faeces between groups, but this did not reach statistical significance (Figure 5.4D). In the colonic mucosa, only the abundance of bacteria belonging to the *Desulfovibrionaceae* (unclass.g) family was identified as being significantly different between groups (Figure 5.4C). Together, this data suggests that the overall composition of intestinal commensal bacteria is largely similar in the presence or absence of IgA.

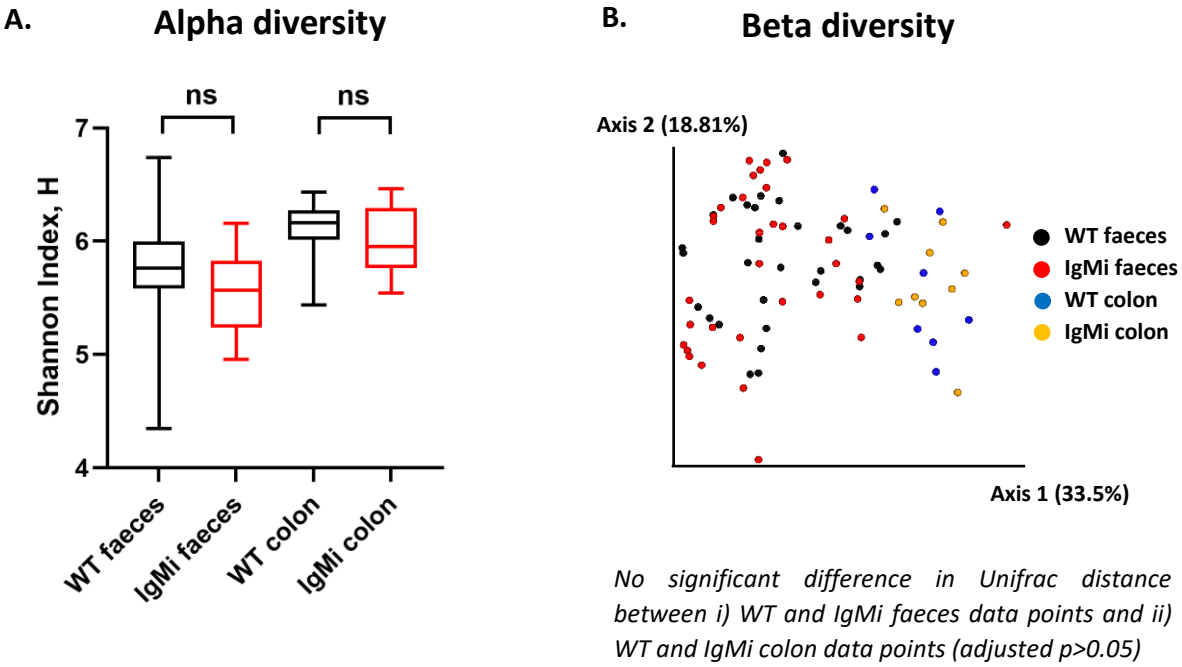

Figure 5.3. Similarities in alpha and beta diversity of faecal and colonic bacteria in IgMi and WT littermate control mice.

(A) Shannon diversity index of faecal and colonic bacteria from IgMi and age and WT littermate control mice. Differences between groups analysed by Kruskal-Wallis and post Hoc Dunn test. Bars indicate median ± interquartile range. (B) Weighted unifrac analysis of faecal and colonic bacteria from IgMi and WT littermate control mice. Differences in UniFrac distances between faeces and colon data in each group compared by Permanova and Pseudo-F test. WT littermates were age- and sex-matched to IgMi mice. Data combined from two independent experiments (for colonic samples, littermates n=8 and IgMi n=9; for faecal samples, littermates n= 31 and n=33 IgMi mice; male and female mice aged 8-14 weeks). Ns = non-significant.

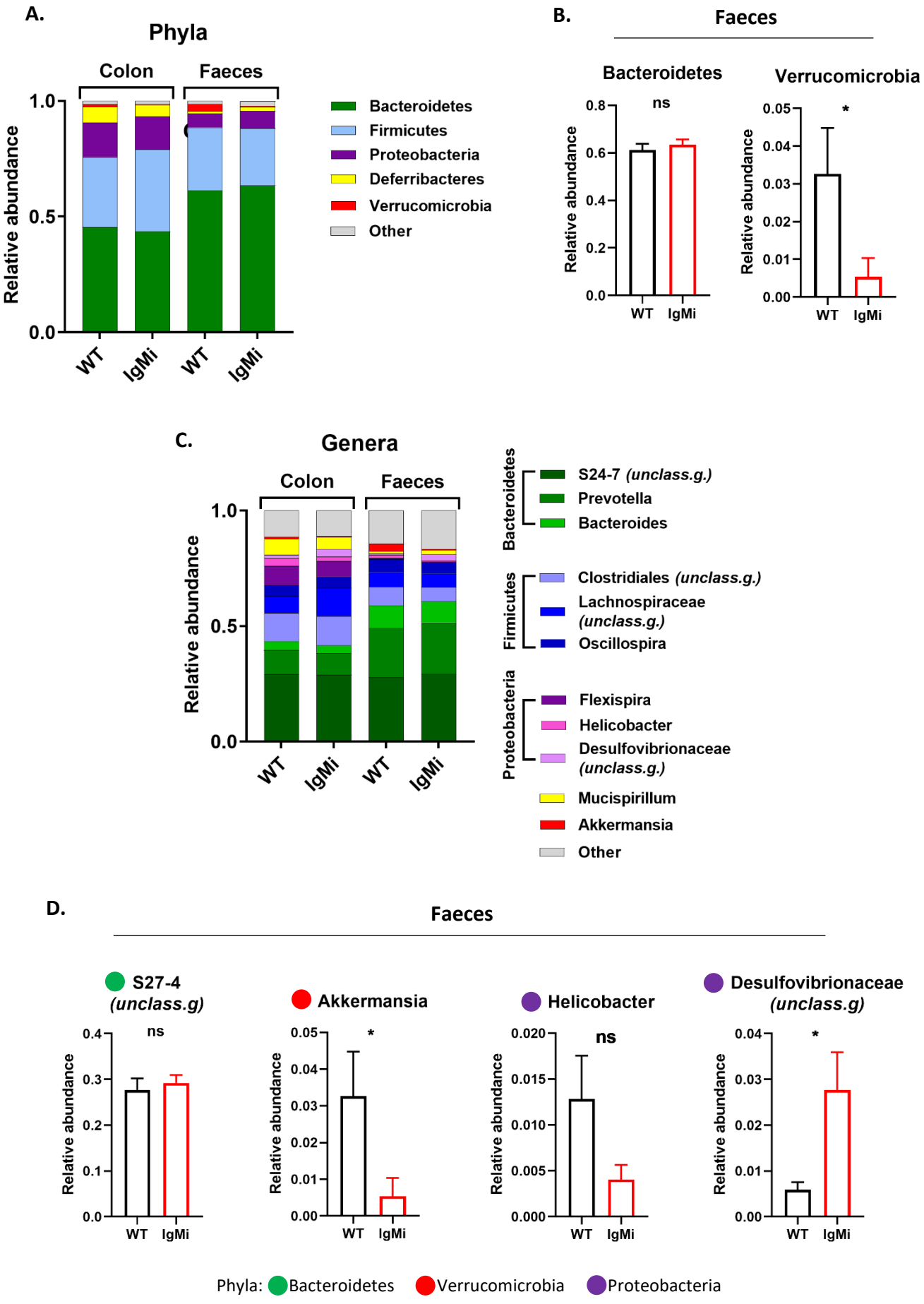
A.
Phyla
Colon
Faeces
Relative abundance
1.0
0.5
0.0
WT
IgMi
WT
IgMi
Bacteroidetes
Firmicutes
Proteobacteria
Deferribacteres
Verrucomicrobia
Other
B.
Faeces
Bacteroidetes
ns
Relative abundance
0.8
0.6
0.4
0.2
0.0
WT
IgMi
Verrucomicrobia
*
0.05
0.04
0.03
0.02
0.01
0.00
C.
Genera
Colon
Faeces
Bacteroidetes
S24-7 (unclass.g.)
Prevotella
Bacteroides
Firmicutes
Clostridiales (unclass.g.)
Lachnospiraceae (unclass.g.)
Oscillospira
Proteobacteria
Flexispira
Helicobacter
Desulfovibrionaceae (unclass.g.)
Mucispirillum
Akkermansia
Other
D.
Faeces
S27-4 (unclass.g)
Akkermansia
Helicobacter
Desulfovibrionaceae (unclass.g)
0.4
0.3
0.2
0.1
0.0
0.05
0.04
0.03
0.02
0.01
0.00
0.020
0.015
0.010
0.005
0.000
Phyla: Bacteroidetes Verrucomicrobia Proteobacteria

Figure 5.4. The composition of commensal bacteria is similar in the colon and faeces of IgMi and WT littermate control mice.

(A) Quantification of the bacterial phylla with a relative abundance >2% in the colonic mucosa and faeces. (B) Representative plots of the relative abundance of Bacteroidetes (left) and Verrucomicrobia (right) from the faecal samples. (C) Quantification of the bacterial genera with a relative abundance >2% in the colonic mucosa or faeces. (D) Representative plots of the relative abundance of (left-right) S27-4 (unclassified genus), Akkermanisa, Helicobacter and Desulfovibrionaceae (unclass.g) in the faeces of IgMi mice and WT littermate controls. Data represent mean values of pooled data from two independent experiments (for colonic samples, WT littermates n=3-5 and IgMi n=3-6; for faecal samples, WT littermates n=8 and IgMi n=9; male and female mice aged 8-14 weeks). *=p<0.05.

5.2.3 Altered diurnal rhythmicity in the composition and function of intestinal commensal bacteria in IgMi mice

To determine whether compositional diurnal changes to the microbiota are altered in the absence of sIgA, we performed JTK analysis on the entire faecal 16S rRNA sequencing analysis dataset. In line with previous work, we considered an OTU to be rhythmic if the adjusted *p* value was <0.05 and FDR <0.1 [313, 314]. In doing so, we detected significant diurnal fluctuations in the relative abundance of 16.3% of all bacterial OTUs in WT mice (Figure 5.5A), which aligns with previous estimates of the proportion of oscillatory intestinal commensal bacteria in the steady state [313, 316]. By contrast, only 10.2% of all bacterial OTUs were oscillatory in IgMi mice (Figure 5.5A), suggesting that differences exist in the number of oscillating bacteria in WT and IgMi mice.

Further to this, we detected differences in the relative abundance of oscillatory OTUs that comprise the main bacterial phyla represented within the faeces in both groups (Figure 5.5B). Interestingly, this included total loss of oscillatory bacteria from the phyla *Firmicutes* and *Cyanobacteria* in IgMi mice. Moreover, IgMi mice had nearly three-times as many oscillatory bacteria within the phyla *Bacteroidetes* and bacteria belonging to an ‘unassigned’ phylum demonstrated oscillatory capacity in IgMi mice, compared with WT mice, suggesting a potential gain in rhythmicity of certain microbes in the absence of sIgA (Figure 5.5B). These differences were largely consistent when analysing absolute bacterial abundance (data not shown), implying that these findings were not the result of a few dominant species driving proportional changes across other phyla, as has been demonstrated previously [315].

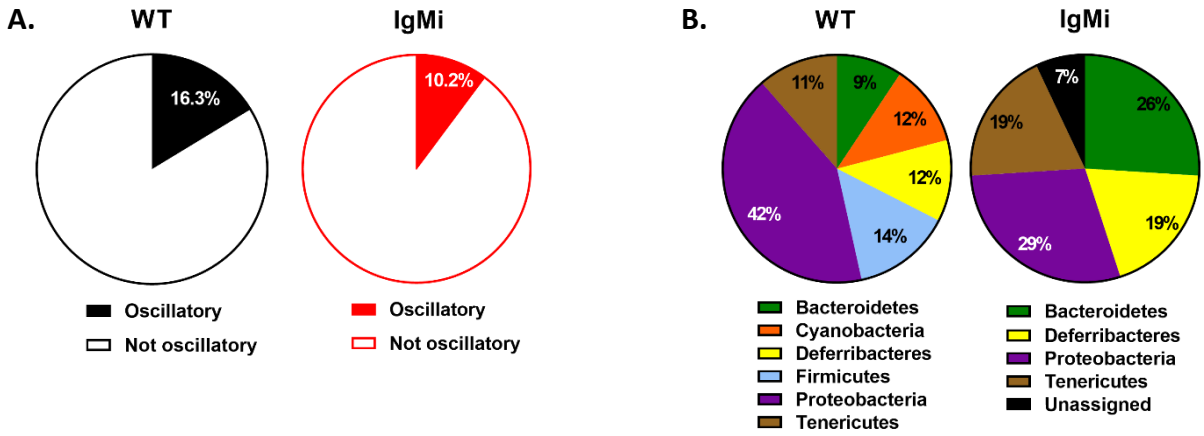

Figure 5.5. Altered diurnal oscillations of intestinal commensal bacteria in IgMi mice.

Fresh faecal pellets were collected from IgMi and age and sex-matched WT littermate control mice at four timepoints, six hours apart over a single day. Bacterial DNA was extracted from the faecal pellets and was subjected to 16S rRNA sequencing. (A) The percentage of all faecal bacterial operational taxonomic units (OTUs) identified as oscillatory, or not oscillatory, in IgMi and WT control mice. (B) The percentage of oscillatory OTUs grouped into respective bacterial phyla. Bacterial OTUs were considered oscillatory if JTK analysis demonstrated an adjusted $p<0.05$ and false discovery rate <0.1. Data pooled from two independent experiments (n=3-5 mice/ timepoint; male and female mice aged 8-14 weeks).

To investigate these differences further, we then evaluated compositional rhythmicity on a genus level. To do this, we grouped all bacteria identified as significantly oscillatory by JTK analysis in both WT and IgMi mice, WT mice only, and IgMi mice only. In doing so, we identified groups of bacteria that either retained, lost or gained rhythmicity in IgMi mice, compared with WT littermate controls (Figures 5.6A-C). In line with our earlier observations, bacteria that demonstrated loss of oscillations in IgMi mice included an unclassified genus of the *YS2* family of the phyla *Cyanobacteria* and genera of the phyla *Firmicutes* including *Gemella*, *Anaerotruncus*, *Streptococcus* and an unclassified genus of the *Lachnospiraceae* family (Figure 5.6B). Several bacteria from the phyla *Proteobacteria* also demonstrated loss of rhythmicity in IgMi mice including *Bilophila*, *Desulfovibrio* and an unclassified genus of the orders *RF32* and *Rickettsiales* (Figure 5.6B).

Interestingly, we found that most of the bacteria that were identified as significantly oscillatory in both groups had apparent phase or amplitude shifts in IgMi mice (Figure 5.6A).

This was particularly apparent when relative abundance scores were plotted against ZT timepoints (Figure 5.7). This included bacteria which have previously been shown to be highly bound by sIgA, such as the genus *Flexispira* of the *Helicobacteraceae* family of *Proteobacteria* and the genus *Mucispirillium* of the phyla *Deferribacteres* [66, 117]. *Mucispirillium* is typically enriched within the intestinal mucus layer [394], along with *Helicobacter*, the other major genus within the *Helicobacteraceae* family of *Proteobacteria,* and *Akkermanisa* [395]. Analysis of these microbes demonstrated non-significant trends towards rhythmic fluctuations over the experimental timepoints in WT but not IgMi mice (Figure 5.8 A&B). Moreover, other bacteria that have been demonstrated as highly bound by sIgA, such as the *S24-7* family of the phyla *Bacteroidetes* [66, 117], gained rhythmicity in the absence of sIgA (Figures 5.6 C). By contrast, *Lactobacillus* of the phyla *Firmicutes*, which is also considered as heavily bound by sIgA within the GI tract [117, 120], demonstrated non-significant differences across the experimental timepoints (Figure 5.8C). Thus, there is evidence of differences in the compositional rhythmicity of intestinal commensal microbes in the absence of sIgA, but the mechanism through which sIgA may modulate commensal rhythmicity is unclear.

Importantly, while we found clear time of day differences in the abundance of several microbes, we also identified bacteria whose abundance consistently did not display temporal variability across the experimental timepoints in both groups (Figure 5.9). This suggests that the differences we observed were specific to those genera, and not a function of global time of day differences across all bacteria. Together, this data provides evidence of altered microbial rhythmicity in IgMi mice and suggests that oscillatory sIgA may, in part, regulate diurnal rhythmicity in the composition of intestinal commensals.

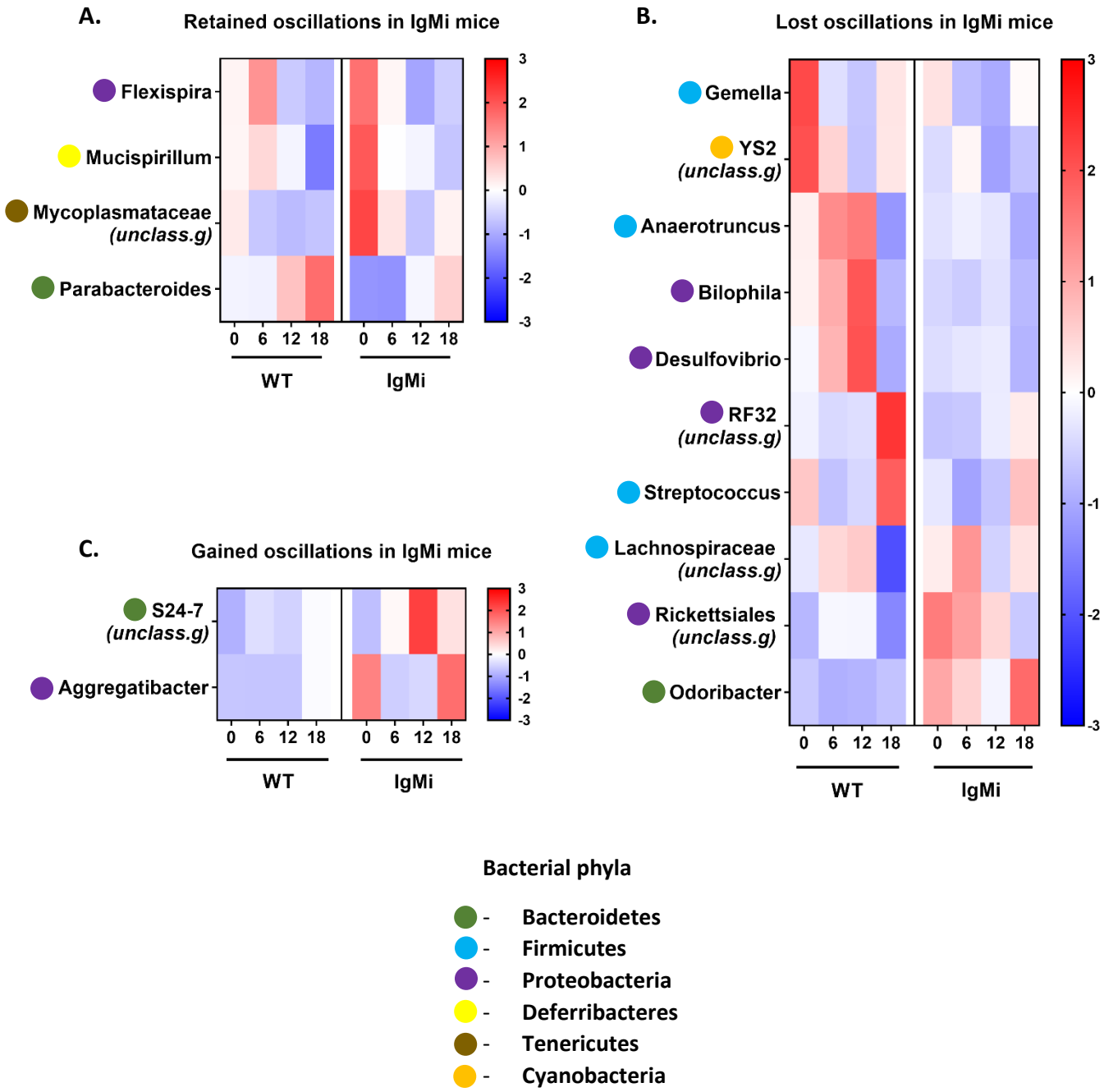

Figure 5.6. Alterations in compositional diurnal oscillations of intestinal bacteria in IgMi mice

Heatmaps of bacterial genera grouped according to whether they were identified as significantly oscillatory (identified by JTK analysis: $p < 0.05$; false discovery rate <0.1) in (A) both WT and IgMi mice (i.e. retained oscillations in IgMi mice); (B) WT mice only (i.e. lost oscillations in IgMi mice); or, (C) IgMi mice only (i.e. gained oscillations in IgMi mice). Colour code represents the phyla each bacterial genus belongs to. Normalised relative abundance is expressed as z-scores (red, high; blue, low). Data pooled from two independent experiments (n=3-5 mice/ timepoint male and female mice aged 8-14 weeks).

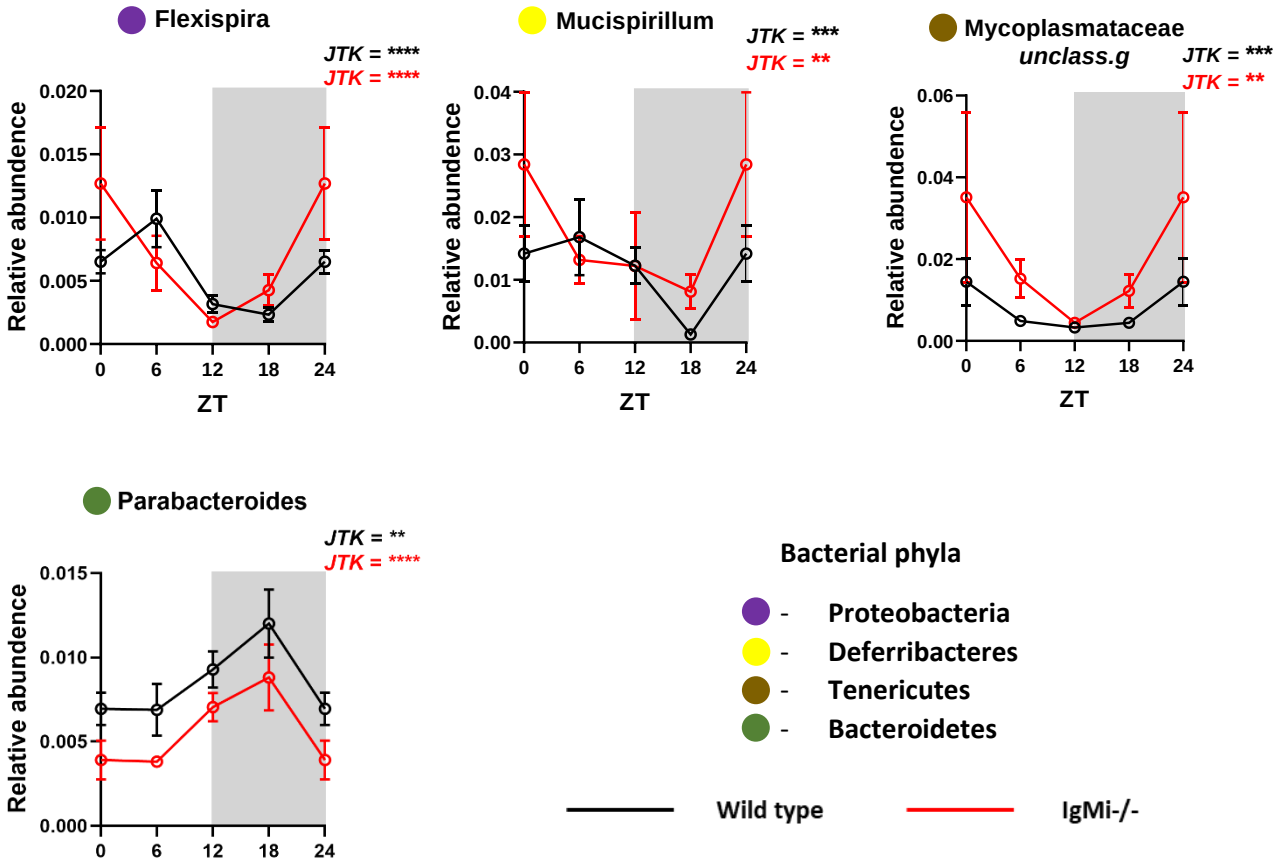

Figure 5.7. Representative plots of retained oscillations of intestinal bacteria in IgMi mice

Representative plots of bacterial genera identified as significantly oscillatory by JTK analysis ($p<0.05$; false discovery rate <0.1) in both IgMi and WT control mice. Data represents relative faecal bacterial abundance across each timepoint. Colour code represents the phyla each bacterial genus belongs to. n=3-5 mice/ timepoint; male and female mice aged 8-14 weeks; **= $p<0.01$, ***= $p<0.001$, ****= $p<0.0001$. ZT0 was re-plotted as ZT24 to aide visualisation of the data. Horizontal bars represent mean±SEM. Shaded area represents dark phase.

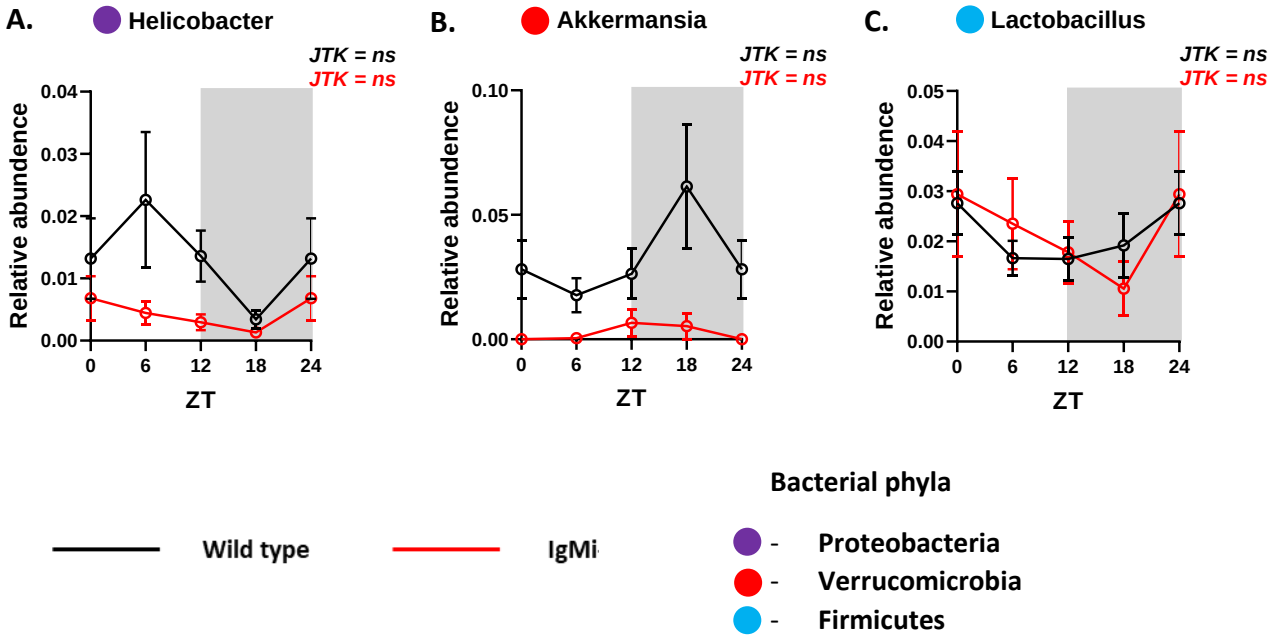

Figure 5.8. Relative abundance of Helicobacter, Akkermansia and Lactobacillus over the experimental timepoints in WT and IgMi mice

Representative plots of bacterial abundance of (A) *Helicobacter*, (B) *Akkermansia*, and (C) *Lactobacillus*, across each timepoint in the faeces of IgMi mice and WT controls. Colour code represents the phyla each bacterial genus belongs to. Data representative of two independent experiments (n=3-5 mice/ group; male and female mice aged 8-14 weeks). Oscillatory nature of data assessed by JTK analysis. ZT0 was re-plotted as ZT24 to aide visualisation of the data. Horizontal bars represent mean±SEM. Shaded area represents dark phase.

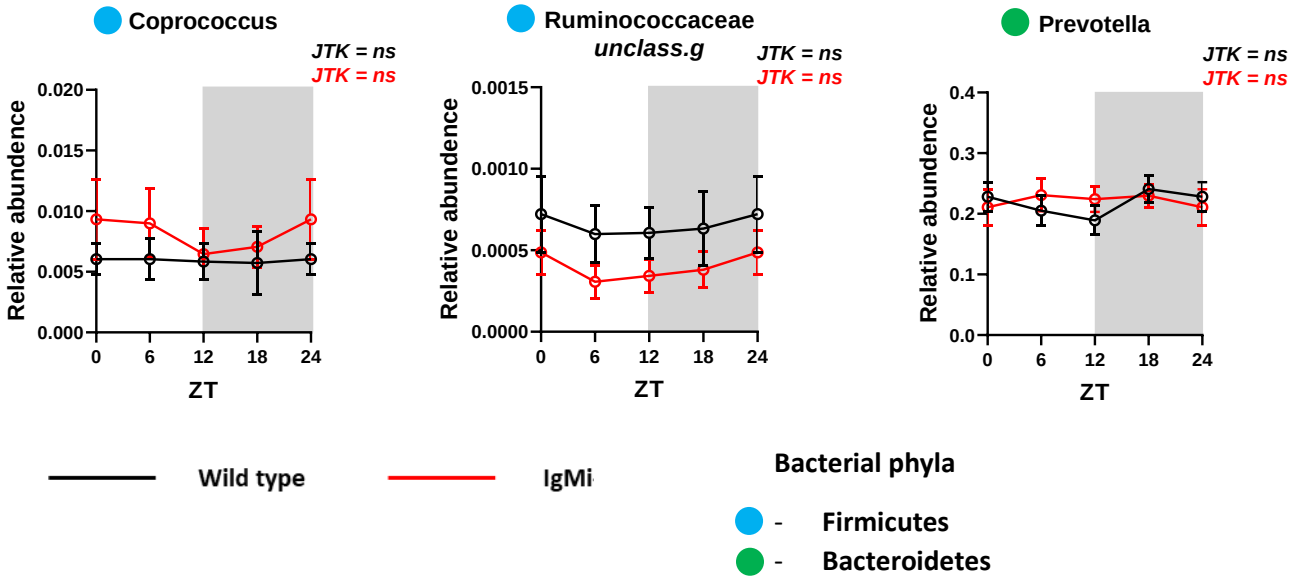

Figure 5.9. Similarities in the composition of intestinal bacteria in IgMi and WT mice over the experimental timepoints.

(Left to right) Selected plots of bacteria identified as non-rhythmic in both IgMi and WT littermate control mice. Colour code represents the phyla each bacterial genus belongs to. Data representative of two independent experiments (n=3-5 mice/ group; male and female mice aged 8-14 weeks. Oscillatory nature of data assessed by JTK analysis. ZT0 was re-plotted as ZT24 to aide visualisation of the data. Horizontal bars represent mean±SEM. Shaded area represents dark phase.

We next analysed whether these differential oscillations in microbiota composition in the absence of sIgA, had consequences for the functional capacities of the intestinal microbes over the course of the day. To do this, we performed shotgun metagenomic sequencing of faecal samples collected every 6 hours over a 24-hour period from IgMi mice and age and sex matched WT littermate controls. The metagenomic reads were mapped to a gut microbial gene catalog [313] and underwent GeneOntology (GO) enrichment analysis to identify associated functional biological processes. We then performed JTK analysis on the pathway data to detect oscillations that occur with a 24-hour rhythm, which were considered rhythmic if the adjusted p value was <0.05 and FDR <0.05 [314, 316]. In accordance with previous work [313], we found that 17% of all functional processes with a coverage of ≥20% in WT mice were rhythmic, whilst, strikingly, only 2% were rhythmic in IgMi mice (Figure 5.10A&B).

We then performed unbiased analysis of the top 20 significantly rhythmic process with the greatest amplitude across both groups. This demonstrated that pathways linked to protein synthesis, DNA replication and glucose metabolism were highly oscillatory in WT mice, but arrhythmic in IgMi mice (Figure 5.10C). By contrast, other processes relating to DNA replication were identified as highly oscillatory in IgMi mice, but not in WT mice (Figure 5.10D). Further analysis of the rhythmic functional pathways in WT mice demonstrated that 25% of significantly oscillatory processes were directly related to the central metabolism of carbohydrates and lipids. Notably, several steps in the *Glycolysis* and *Gluconeogenesis* pathways [396] were oscillatory in WT animals but were arrhythmic in IgMi mice (Figure 5.11A-D). Moreover, the activity of enzymes involved in the generation of intermediates of the TCA cycle were also identified as rhythmic in WT mice, but not IgMi mice (Figure 5.12), suggesting loss of rhythmic metabolic function in bacteria in the absence of sIgA. Intriguingly, peak oscillations of protein synthesis and central metabolic processes consistently timed around the mid-light phase, suggesting a potential timestamp of bacterial cell-intrinsic metabolic activity that occurs during the resting period. By contrast, we observed a small number of predicted GO-term functional pathways that gained oscillatory activity in the absence of IgA (Figure 5.10D), which included *Flagellum Assembly* and *Extrachromosomal Circular DNA* (Figure 5.13).

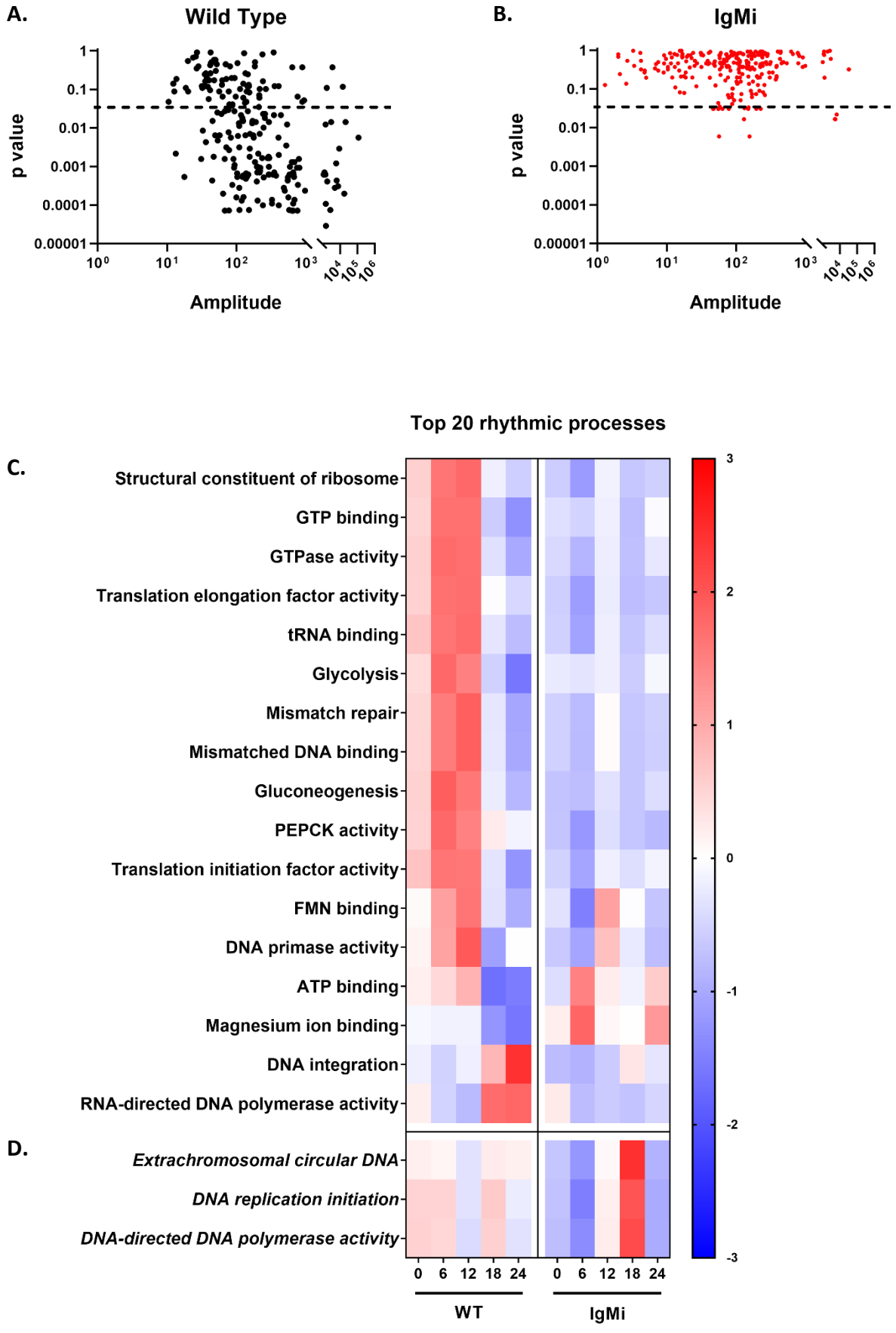
A.
Wild Type
p value
1
0.1
0.01
0.001
0.0001
0.00001
10^0 10^1 10^2 10^3 10^4 10^5 10^6
Amplitude
B.
IgMi
p value
1
0.1
0.01
0.001
0.0001
0.00001
10^0 10^1 10^2 10^3 10^4 10^5 10^6
Amplitude
C.
Top 20 rhythmic processes
Structural constituent of ribosome
GTP binding
GTPase activity
Translation elongation factor activity
tRNA binding
Glycolysis
Mismatch repair
Mismatched DNA binding
Gluconeogenesis
PEPCK activity
Translation initiation factor activity
FMN binding
DNA primase activity
ATP binding
Magnesium ion binding
DNA integration
RNA-directed DNA polymerase activity
D.
Extrachromosomal circular DNA
DNA replication initiation
DNA-directed DNA polymerase activity
3
2
1
0
-1
-2
-3
0 6 12 18 24
0 6 12 18 24
WT
IgMi

Figure 5.10. Loss of functional diurnal oscillations of intestinal bacteria in IgMi mice

GO pathways demonstrating diurnal oscillations in (A) age and sex-matched WT and (B) IgMi mice. Adjusted *p* value and amplitude derived from JTK analysis. Dashed line indicates an adjusted *p* value of 0.05. (C&D) Heatmap of top 20 significantly rhythmic GO pathways based on amplitude in both WT and IgMi mice. GO processes plotted in (C) were only significantly oscillatory in WT mice only and those in (D) significantly oscillatory in IgMi mice only. Normalised relative abundance is expressed as z-scores (red, high; blue, low). ZT24 represents a separate experimental timepoint from ZT0. Data from one experiment (n=5 mice/ timepoint; male and female mice aged 10-14 weeks). PEPCK activity = Phosphoenolpyruvate carboxykinase activity.

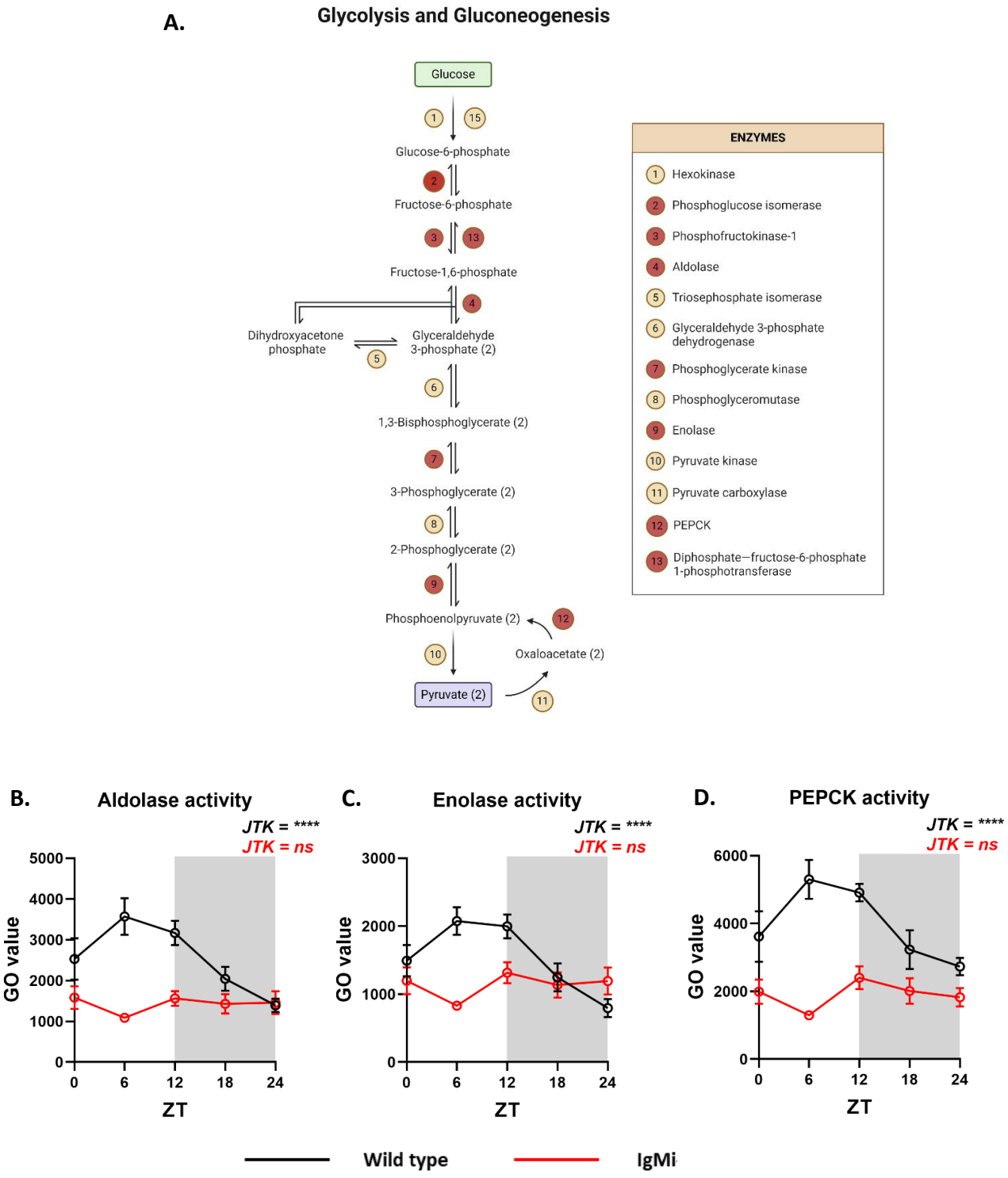

Figure 5.11. Loss of rhythmicity of microbial glycolysis and gluconeogenesis in IgMi mice

(A) Schematic of glycolysis (top to bottom) and gluconeogenesis (bottom to top) pathways (adapted from [396]). Key enzymes involved in each step are listed in the table; enzyme activity of those highlighted in red were significantly oscillatory (JTK analysis $p<0.05$; FDR <0.05) in WT mice, but not in IgMi mice. (B-D) Selected plots of GO values over experimental timepoints for enzymes identified from (A). Data from one experiment; n=5 mice/ timepoint; male and female mice aged 10-14 weeks; ZT24 represents a separate experimental timepoint from ZT0. ****=$p<0.0001$.

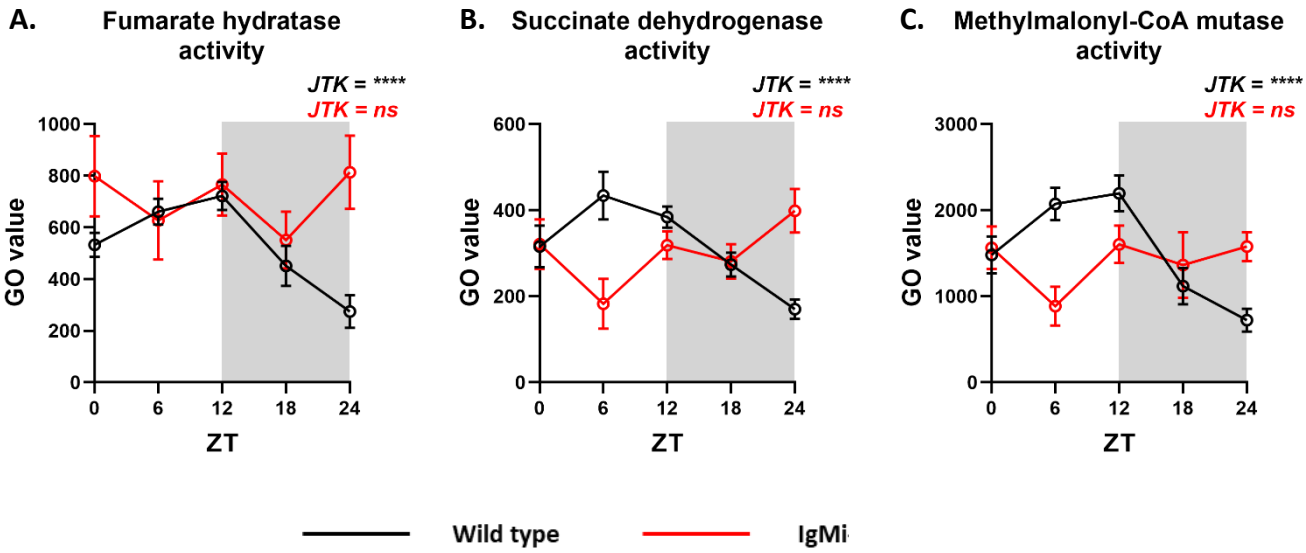

Figure 5.12. Loss of rhythmicity of microbial metabolic enzyme activity in IgMi mice

(Left to right) Selected plots of enzymes identified as significantly oscillatory in WT mice, but not in IgMi littermate mice (JTK analysis adjusted p<0.05; FDR<0.05). Data from one experiment; n=5 mice/ timepoint; male and female mice aged 10-14 weeks. ZT24 represents a separate experimental timepoint from ZT0. ****=p<0.0001.

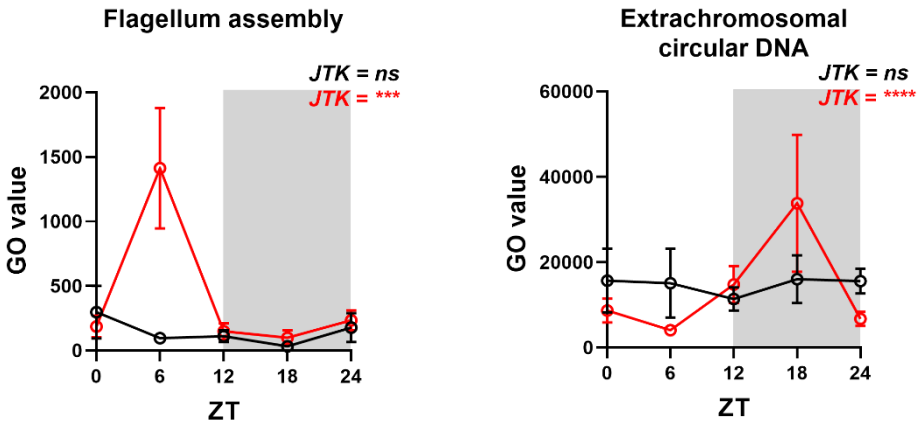

Figure 5.13. Gain of rhythmicity of pathways relating to extrachromosomal circular DNA and flagellum assembly in IgMi mice

(Left and right) Selected plots of functional GO pathways identified as significantly oscillatory in IgMi mice, but not in WT littermate controls (JTK analysis adjusted p<0.05; FDR <0.05). Data from one experiment; n=5 mice/ timepoint; male and female mice aged 10-14 weeks. ZT24 represents a separate experimental timepoint from ZT0. ****=p<0.0001.

We next sought to determine whether alterations in the composition and function of the gut commensal microbiota led to changes in the nutrient availability within the intestines. To do this, we performed metabolomics on serially collected faecal samples from IgMi and WT littermate control mice. In doing so, we observed clear rhythmicity in the relative abundance of several short chain fatty acids in WT control mice, which were blunted in IgMi mice (Figure 5.14A-C). We also observed non-significant differences in the relative abundance of glucose across experimental timepoints in both groups (Figure 4.14D). By contrast, Succinate demonstrated comparable relative abundance over the course of the day in the presence or absence of IgA (Figure 5.14E).

Finally, to evaluate the potential impact of rhythmic IgA on systemic nutrient availability, we next serially sampled blood glucose from IgMi and littermate control mice over the circadian day. This demonstrated expected oscillations in blood glucose in littermate controls, which were blunted in the absence of IgA (Figure 5.15).

Taken together, this data suggests that rhythmic IgA may, in part, regulate compositional and functional oscillations in the intestinal microbiota. In doing so, oscillatory IgA modulates the rhythmic availability of nutrients both locally within the intestines and systemically within the host over the course of the day.

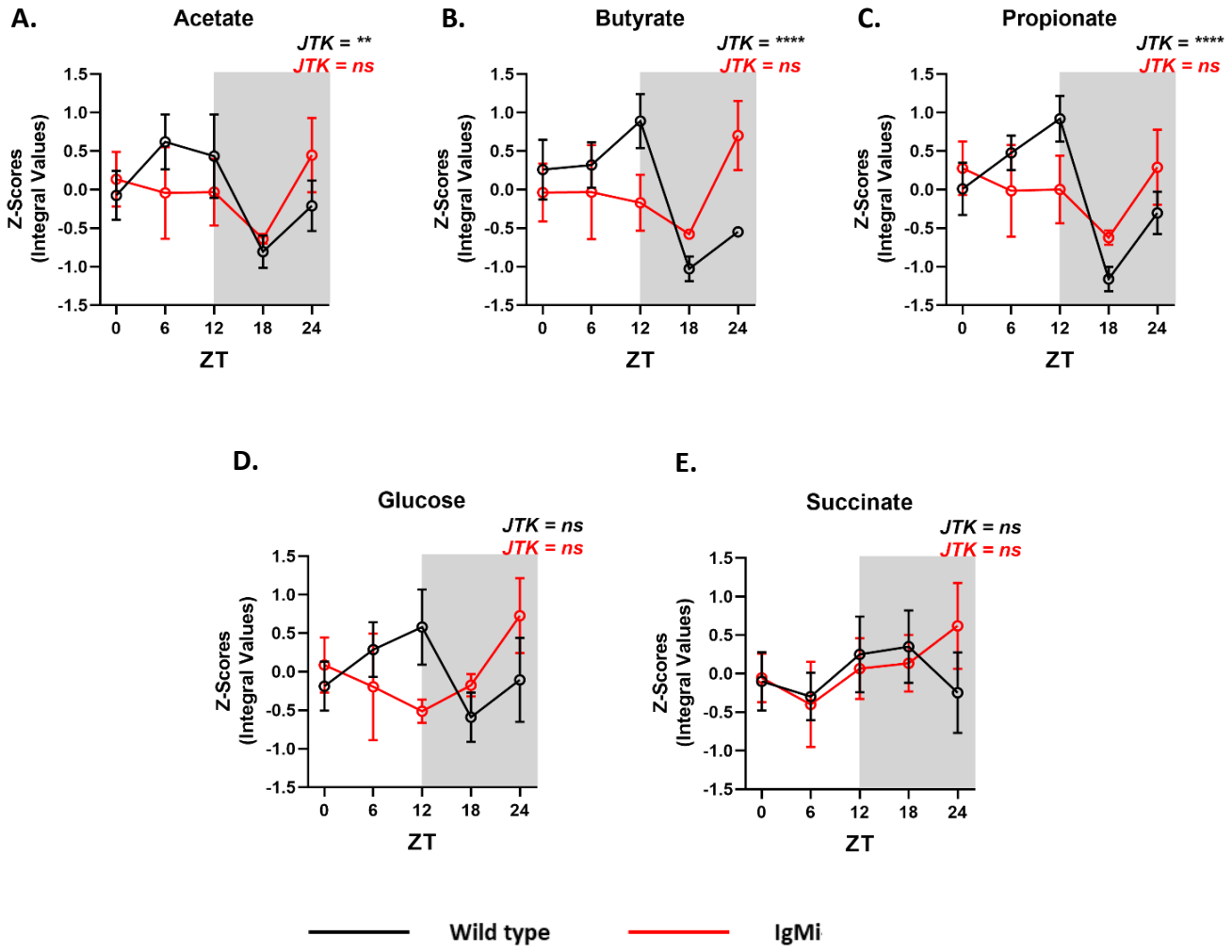

Figure 5.14. Dysregulation of circadian metabolites in the absence of mucosal antibody

Fresh faecal pellets were collected from IgMi and age and sex-matched WT littermate control mice at five timepoints, six hours apart over a single day. (A-E) Selected plots of faecal-assocaited metabolites in WT and IgMi mice. Data from one experiment; n=5 mice/ timepoint; male and female mice aged 10-14 weeks. ZT24 represents a separate experimental timepoint from ZT0. ** =p<0.01; ****=p<0.0001.

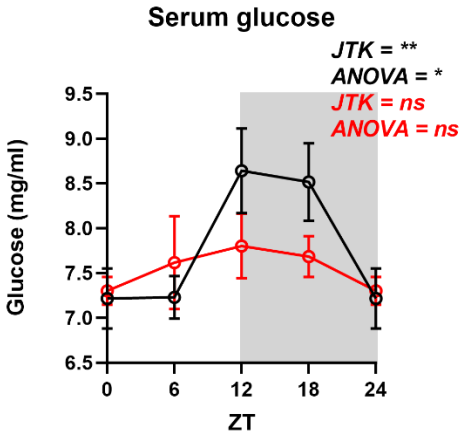

Figure 5.15. Loss of oscillatory serum glucose in the absence of IgA

Blood glucose levels were serially sampled from WT and IgMi mice at five 6 hour intervals over a circadian day (performed by Dr Rita Domingues). *N*=8-12 mice/ group per timepoint; C57BL/6 male and female mice aged 8-10 weeks. Representative of data pooled from two independent experiments. All data shown as +/- SEM. *=p< 0.05, ** p< 0.01.

5.3 Discussion

Previous studies have demonstrated that diurnal oscillations in the composition and function of the gut microbiota are entrained by circadian and/ or feeding cues [313-317]. However, the immune mechanism(s) which drive these changes remained poorly understood. Our data suggests that sIgA may, in part, regulate rhythmicity of the microbiota. To this end, these findings suggest that sIgA modulates the composition and function of intestinal commensals in a more nuanced manner than previously appreciated.

In accordance with our findings, others have identified oscillations in microbes belonging to the *Firmicutes* and *Bacteroidetes* phyla, including *Gemella* [397], *Odoribacter* [313], *Streptococcus* [313] and *Lachnospiraceae* [313, 317, 318]. Prior studies have demonstrated rhythmicity in other common intestinal commensals such as *Lactobacillus* [313] and *Bacteroides* [318], which were non-rhythmic in our data, and previous work [313]. Furthermore, the oscillatory phase of different microbes does not appear to follow a consistent pattern across different studies [313, 314, 316-318]. This may be due to differences in the sampling site of the microbiota in these studies, which range from the caecum [316], colonic mucus layer [314] and faeces [313, 317]. Moreover, prior studies have been conducted across different geographical locations, in animals of different ages and gender, and raised on different dietary chow – factors which are well known to generate variability in the composition of the intestinal microbiota [315, 398, 399] – suggesting that the configuration of oscillating commensals may also be affected by these biological and environmental factors.

By contrast, and as we found presently, the percentage of oscillating microbes under homeostatic conditions appears to be largely conserved across different studies [313, 316]. Consistency is also apparent in the proportion of oscillating functional bacterial processes in the steady state between different studies [313]. Therefore, the relative proportion of oscillating vs non-oscillating elements within the microbiota may be a more accurate reflection of how microbial rhythmicity changes under different conditions. With this in mind, we detected a reduced frequency of compositional and functional microbial oscillations in IgMi mice, suggesting that sIgA modulates rhythmicity within the intestinal microbial community.

Specifically, we identified altered rhythmicity of *Mucispirilium* in IgMi mice. *Mucispirilium* is typically found within the mucus layer in close proximity to the epithelial surface, along with other microbes such as *Helicobacter* and *Akkermansia* [394, 400, 401]. Previous studies have identified circadian oscillations in the relative abundance of *Akkermansia* in the caecum and colonic mucus layer of mice [313, 316]. By contrast, we only sampled faeces over serial timepoints presently, which may explain why we detected non-significant fluctuations in *Akkermansia* and *Helicobacter* over the course of the day, and analysis of the colonic mucus layer may provide a more accurate evaluation of the oscillatory nature of these bacteria. Interestingly, we did observe significantly reduced overall abundance of these microbes in IgMi mice. Studies have shown that *Mucispirilium* and *Akkermansia* drive TD humoral responses in the gut under homeostatic conditions [66, 402] and that these bacteria are heavily labelled by sIgA [66, 98, 119]. It is increasingly appreciated that gut commensals can exploit IgA-binding to promote their establishment within the gut [65, 67], which may explain our findings of reduced, or altered temporal, abundance of these mucus-residing bacteria in the absence of IgA in IgMi mice.

We also observed that microbes of the *Cyanobacteria* phylum lost rhythmicity in IgMi mice. Other species within this phylum, such as *Synechococcus elongatus* of the order *Synechococcales*, which typically colonise marine environments, have their own cell-intrinsic circadian oscillators which drive cell-intrinsic circadian rhythms in bacterial gene expression [403]. More recently, cell-autonomous oscillatory gene expression, akin to circadian-clock controlled rhythmicity, was demonstrated in the gut commensal *Bacillus subtilis* [404]. Thus, evidence suggests that microbes themselves may regulate their own transcriptome in a circadian manner. Whether cell-intrinsic oscillations in the bacterial transcriptome may interact with oscillatory IgA is unclear but suggests a further layer of regulation of microbial oscillatory activity may exist in certain commensals.

It could be considered that oscillations in the abundance of microbes may reflect their temporal outgrowth within, or clearance from, the GI tract and that enhanced clearance at specific times of the day may be important to balance appropriate nutrient metabolism within the gut [405]. In this manner, metabolism of nitrogenous material derived from the diet by commensal microbes results in the production of hydrogen sulphide, which has important physiological functions locally [406], but in excess is associated with inflammatory conditions

such as IBD [407] and colorectal cancer [408]. *Desulfovibrio* and *Bilophila* are key hydrogen sulphide-producing bacteria [405, 406] and studies have found their abundance increased in individuals with IBD [409, 410]. Our data indicates overall increased abundance of the family *Desulfovibrionaceae*, as well as loss of rhythmic abundance of *Desulfovibrio* and *Bilophila*, in the absence of IgA. Therefore, oscillatory IgA may regulate the temporal clearance of these bacteria from the gut to balance maximising beneficial microbial processes alongside limiting detrimental responses associated with their outgrowth.

Mechanistically, it is well recognised that bacteria proliferate in response to feeding [313, 411]. SIgA has been shown to mediate the cross-linking, or enchained-growth, of proliferating bacteria, which consequently enhances microbial clearance from the gut [114]. Therefore, enhanced host IgA responses may be aligned with feeding-induced bacterial proliferation to facilitate enchained-growth and clearance of proliferating microbes from the intestines. Intriguingly, we observed that the presence of IgA led to dampened oscillatory activity in pathways relating to the expression of genes for survival under stress (e.g. *Extrachromosomal Circular DNA*) [412] and motility (e.g *Flagellum Assembly*), suggesting a possible mechanism through which IgA may regulate colonised bacteria within the gut and alter the composition of the intestinal niche.

Moreover, rhythmic attachment of microbes such as SFB and mucus-dwelling commensals to the colonic epithelium is thought to entrain transcriptional oscillations within IECs, including regulating appropriate rhythmicity of pathways relating to carbohydrate, amino acid and lipid metabolism [314]. Microbial oscillatory activity also leads to the rhythmic production of metabolites by bacteria, which is important for maintaining systemic rhythmicity and organ health [314, 318]. Several lines of evidence have demonstrated that an arrhythmic, dysbiotic microbiota can result in the development of glucose intolerance, obesity and type 2 diabetes [313, 318, 331], suggesting that impaired rhythmicity of the intestinal microbiota links to alterations in host metabolic health. We demonstrated alterations in the rhythmicity of mucus-dwelling commensals in the absence of mucosal antibodies and observed blunting of oscillations of key metabolites both locally in the gut and systemically in the circulation in the absence of IgA. These findings provoke the question of whether sIgA-mediated regulation of microbial rhythmicity has physiological consequences for host metabolism? – this is addressed in the final chapter.

Intriguingly, how microbial oscillations induce transcriptional rhythmicity within IECs remains to be determined [320, 323]. Interestingly, microbes in close proximity to the IEC surface are heavily bound by sIgA [66, 117, 119]. sIgA itself can bind cell-surface expressed receptors, including Fc receptor for IgA, CD71 and M-cell receptors [413-415], leading to the activation of signal transduction pathways within the cell. Therefore, it could be postulated that IgA-bound microbes interact with IgA receptors on IECs, to induce the activation of signalling pathways within the cell. In a similar manner, prior work has demonstrated sIgA can crosslink dietary proteins, such as gluten (gliadin peptides), following which sIgA-gluten complexes interact with CD71 on the luminal side of the IEC, to mediate signalling and transport inside the IEC [416]. SIgA is capable of crosslinking bacteria and intriguingly, these crosslinks begin to degrade after a matter of hours [114]. Thus, sIgA crosslinking with gut commensals may enable an intrinsically transient interaction with receptors on the IEC surface, which would result in temporal signal transduction and gene transcription within the cell over the circadian day.

Finally, it should also be considered whether the changes that we observed are the result of more widespread alterations that result in the setting of conditional impairment of soluble antibody production in this mouse model. For instance, previous work has identified that IgMi mice display reduced frequencies of CD103+ DCs and increased B-cell derived IL-10 production in the mLN compared with WT controls [391]. While our data confirms that of others [391], that these changes largely do not alter the global composition of the intestinal microbiota in these mice, the consequences of these perturbations in intestinal immune tolerogenic and regulatory responses are unclear. Therefore, to further define the role of sIgA in modulating rhythmicity in the microbiota, we could perform these sequencing experiments in a recently developed mouse model of inducible PC-specific deficiency [417].

Taken together, our findings identify a previously unappreciated role of sIgA in regulating the temporal variation in the composition and function of the intestinal microbiota. The mechanisms behind this are unclear but may involve sIgA directly or indirectly regulating temporal selection pressures on colonised bacteria, by modulating their response to nutrients and/ or access to specific niches within the tissue. Furthering our understanding of this may provide critical information regarding how dysbiosis leads to altered host health and metabolic outcomes.

6.0 FINAL DISCUSSION

Under homeostatic conditions, intestinal immune cell responses are dedicated to maintaining intestinal health and microbial mutualism [25]. It is increasingly understood that several of these immune cells and/ or their responses are imprinted with circadian rhythmicity [251]. This may confer an advantage to the host, as co-ordinating cell responses around temporal changes in environmental cues, or partitioning their maximal response around the time of greatest need, may optimise energy-efficient responses and thereby promote survival [321].

Intestinal dwelling PCs constitutively produce IgA in the steady state, which targets gut commensals and shapes the composition and function of the intestinal commensal niche to promote mutualism and homeostasis [418]. However, it was not previously known whether intestinal IgA responses were imprinted with circadian rhythmicity. This was intriguing for several reasons: firstly, oscillatory production of IgA in homeostasis might be bioenergetically favourable to the host; secondly, the microbiota undergoes circadian oscillations in composition and function, however the precise mechanism(s) driving microbial oscillations are poorly understood; finally, loss of microbial rhythmicity has adverse outcomes for host metabolism, which aligns in part with the health consequences associated with impaired mucosal antibody responses [122-125].

Therefore, we hypothesised that IgA-mediated regulation of the microbiota is subject to temporal entrainment by circadian cues. We further postulated that dysregulation of rhythmicity in mucosal antibody secretion could have important consequences for host metabolism and health.

To address these hypotheses, we took a mechanistic experimental approach to characterise intestinal IgA responses over the circadian day (*Chapter 3*), define the mechanisms that entrain rhythmic PC IgA production (*Chapter 4*), and determine the consequences of rhythmic intestinal IgA on daily commensal microbial composition and function (*Chapter 5*). In doing so, our findings suggest that the intrinsic production of IgA by PCs varies over the course of the day (*Chapter 3*), in response to nutrient availability (*Chapter 4*), and that rhythmic IgA in part modulates compositional and functional oscillations in the intestinal microbiota (*Chapter 5*) (Figure 6.1). Together, these results provide novel insights about how IgA+ PC responses adapt to changing environmental cues over the course of the day, and further understanding about sIgA-mediated regulation of the commensal intestinal microbiota.

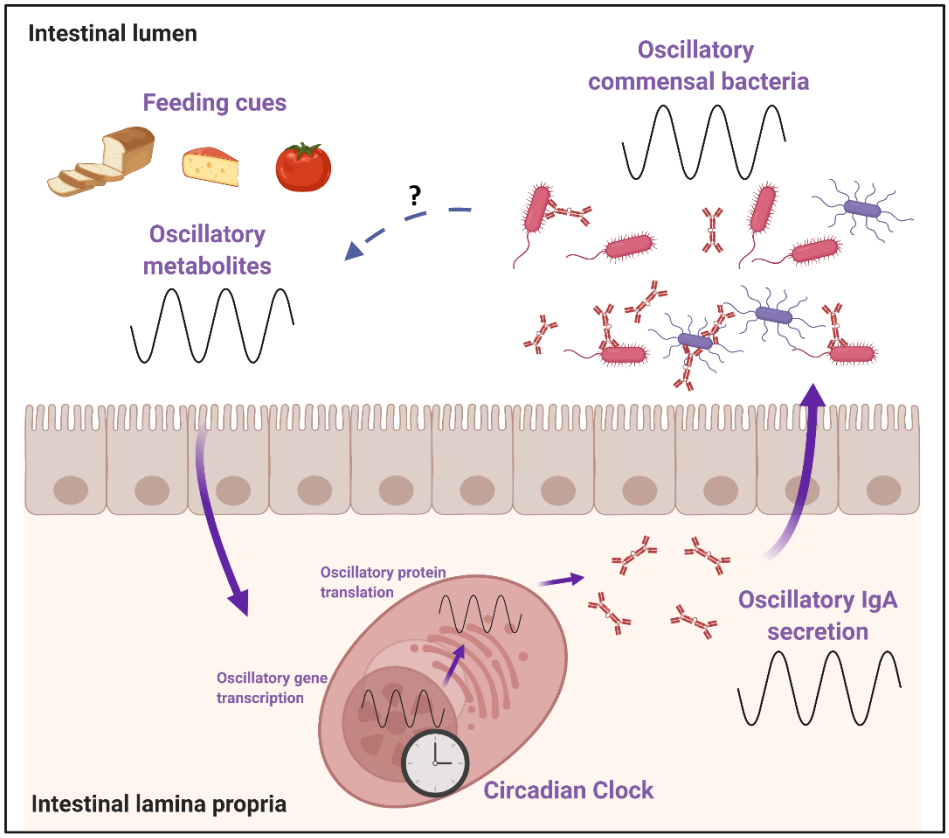

Figure 6.1. Schematic overview of our findings. Our data suggests that oscillations in dietary-derived metabolites entrain rhythmic gene transcription within small intestinal IgA+ PCs, which drive oscillations in IgA secretion into the intestinal lumen. Oscillatory sIgA consequently drives, in part, compositional and functional oscillations in the commensal microbiota. The role of the PC-intrinsic circadian clock in this process remains unclear. In addition, whether compositional and functional oscillations in the commensal microbiota help drive oscillations in feeding-derived metabolites, remains to be determined (illustrated by dashed line).

Notably, these data provoke several further questions, including:

i) Does rhythmic sIgA-mediated regulation of the commensal microbiota have physiological consequences for host metabolism?

ii) Do rhythmic IgA responses promote host protective immunity?

iii) Is the PC-intrinsic circadian clock functionally redundant?

6.1 Does rhythmic sIgA-mediated regulation of the commensal microbiota have physiological consequences for host metabolism?

The small intestine is the major site of dietary nutrient absorption [12], of which dietary-derived microbial metabolites constitute a significant proportion of absorbed nutrients [125, 419]. Gut-derived microbial metabolites stimulate the release of gut hormones, promote the development and maturation of immune cells, and are utilised by the host in cellular metabolic pathways both locally within the intestines and systemically throughout the body [426, 427]. In this manner, microbial metabolites are important regulators of metabolic health in the steady state, and altered microbial composition and/ or function has been implicated in dysregulated metabolism and conditions such as obesity and type 2 diabetes mellitus [243-248].

The small intestines also harbours the largest population of IgA+ PCs within the body and intestinal sIgA has recently been implicated in the regulation of microbial metabolite nutrient uptake within the intestines [124,125]. Indeed, antibody deficiency has been shown to lead to altered dietary lipid absorption in the gut [124], and IgA-deficient mice fed a HFD diet have more severe glucose intolerance than wild type controls fed the same diet [122], the effect of which can be reduced following antibiotic administration [122], suggesting a mechanistic link between IgA, the gut microbiota and host metabolism. In support of this, recent isotope tracing studies have demonstrated that intestinal IgA can modulate host microbial-metabolite uptake and its systemic dissemination, by regulating the intestinal transit time of gut commensals [125]. In this manner, antibody-deficient mice had an increased dwell time of bacteria in the small intestines and had altered circulating availability of microbial-metabolites, including elevated levels of circulating fatty acids and lipids, compared with wild type mice [125]. Thus, intestinal IgA responses may modulate the appropriate local and systemic availability of nutrient metabolites.

It is increasingly apparent that the microbiota undergoes circadian oscillations in its composition and function, and that this diurnal rhythmicity is an important determinant for host metabolic health [320]. This can be inferred from human and murine studies which have characterised that both microbial dysbiosis and circadian disruption (i.e. due to shift work, jet lag, or altering feeding cues) are associated with obesity, the metabolic syndrome and/ or type 2 diabetes [317, 318, 330, 331, 420-422]. More recently, it was shown that type 2

diabetes is associated with loss of diurnal rhythmicity of intestinal commensals in humans, confirming the importance of oscillatory bacterial activity across species [331]. Mechanistically, animal studies have shown that jet-lagged mice develop dysbiosis with loss of microbial oscillations and develop obesity and glucose intolerance [313]. These metabolic outcomes can be ameliorated in antibiotic-treated mice and recapitulated via faecal microbial transfer from jet-lagged mice or humans into germ-free animals housed under steady state conditions [313], providing empirical data that impaired rhythmic oscillations lead to adverse host metabolism. Further studies have shown that loss of rhythmic microbial activity, with consequent perturbations in the production of rhythmic bacterial metabolites, leads to re-programming of transcriptomic oscillations in the liver, including glucose signalling, fatty acid metabolism and lipid homeostasis [313,314]. The liver is the major organ involved in orchestrating metabolic homeostasis within the body. Therefore, these findings suggest a mechanism through which intestinal microbial rhythmicity may regulate systemic metabolic health.

In this study, we have demonstrated that intestinal IgA is imprinted with circadian rhythmicity, and observed impaired gut microbial rhythmicity – both in terms of composition and metabolic function – in the setting of antibody-deficiency. Therefore, in the context of the findings from these earlier studies, our data suggests that intestinal IgA may have a previously unrecognised role in modulating the rhythmic microbial regulation of host metabolic health. In support of this, our preliminary metabolomic data suggested that antibody-deficient mice have altered local and systemic metabolite availability over the course of the day in comparison with wild type controls. Furthermore, based on our findings that nutrient metabolites drive oscillatory IgA production by PCs, it is tempting to speculate whether microbial rhythmicity generates diurnal variations in local metabolite availability, which in turn helps entrain oscillatory IgA production (Figure 6.1). However, further studies are warranted to validate these early observations and dissect more comprehensively the mechanisms through which IgA may modulate intestinal commensal rhythmicity and host metabolism.

In this manner, we plan to evaluate systemic metabolic responses – such as glucose tolerance, amount of visceral adipose tissue and oxygen consumption/ carbon dioxide release – in IgMi and wild type control mice, using serial blood testing, magnetic resonance scanning and

mouse cages which enable metabolic parameters to be monitored, respectively. More specifically, we also plan to use transcriptomics and functional assays to determine whether metabolic pathways within the liver and hepatic function are dysregulated in the absence of rhythmic IgA. Moreover, we plan to dissect the effect of the microbiota on oscillatory IgA responses, using either antibiotics to deplete the intestinal commensal community, or germ-free mouse lines. These data will provide further information on whether oscillatory intestinal IgA responses have a physiological role in modulating host metabolic health. It is hoped that in doing so, these studies will provide new understanding of, and possible novel therapeutic avenues for, human metabolic diseases such as the metabolic syndrome and type 2 diabetes.

6.2 Do rhythmic IgA responses promote host protective immunity?

As previously discussed, several aspects of the host immune response to infection are now known to be entrained by circadian cues and oscillate in a diurnal manner [250,251,253]. In this manner, studies have shown that immune cell trafficking around the body, activation of the innate and adaptive immune responses and host-pathogen interactions demonstrate diurnal responses [250-254]. These studies have suggested that the circadian control of immune cell responses is timed around the anticipated increased risk of exposure to pathogens during certain times of the day, which may result in timely anti-pathogen responses and thereby maximise host survival [251].

When considering the timing of these diurnal immune responses, the host is considered at greatest risk of exposure to pathogens during the active phase, as this times with social activities which may put animals at greater risk of exposure to airborne pathogens [287]. Previous work has demonstrated that mice exposed to respiratory pathogens such as *Streptococcus pneumoniae* towards the beginning of the resting phase (ZT0) have a more aggressive infection than those exposed towards the beginning of the active phase (ZT12) [428]. It has been further shown that rhythmic immune responses towards Influenza virus and Sendai virus are impaired in mice with disrupted circadian clock function [429,430], and that these mice have greater disease burden than wild type controls, suggesting that the circadian entrained immune responses towards pathogens may confer an advantage to the host.

The active phase of animals not only increases their risk of exposure to airborne pathogens, but behaviour during wakefulness may also expose animals to other microorganisms, such as food-derived microbes [287]. Previous studies have shown that mice infected with the enteric pathogen *Listeria monocytogenes* at the beginning of the rest phase (ZT0), have higher bacterial burden than those infected towards the mid- to end of the resting phase (ZT8) [431]. Similarly, mice infected with *Salmonella typhimurium* during the resting phase (ZT4) had greater bacterial burden within the colon, PPs and spleen, compared with mice infected during the active phase (ZT16), at 72 hours post-infection [432]. Therefore, oscillatory immune responses may have evolved to anticipate temporal changes in host exposure risk to enteric pathogens [287]. Interestingly, it is well established that intestinal IgA responses are directed towards foreign microbes such as *S.typhimurium*, which helps protect against pathogen colonisation and invasion of the intestinal epithelium [223, 224]. However, sIgA has not been previously evaluated in the context of time-of-day differences in GI infections. Therefore, it is tempting to speculate that the temporal differences in disease burden and infectivity observed in these earlier studies may in part be explained by oscillatory sIgA.

With this in mind, on the one hand, our findings of peak luminal sIgA levels during the early to mid-resting phase, and nadir during the mid-active phase, may argue against an involvement of sIgA in diurnal host immune responses towards enteric pathogens. However, several factors need to be considered before evaluating the timing of anti-pathogen responses. Indeed, previously, mice were exposed to *L.monocytogenes* via an intraperitoneal route, which does not reflect 'natural' GI exposure to this bacteria [431]. By contrast, mice were exposed to *S.typhimurium* via oral gavage [432]; however, the transit of food through the GI tract can take several hours, meaning it is difficult to accurately determine the timing of when peak responses might be most advantageous for the host. Moreover, we measured sIgA levels in faeces, which may reflect luminal sIgA levels several hours prior to sampling.

Therefore, it is currently not clear how our findings of rhythmic IgA production, or the respective phase of IgA oscillations, aligns with these previous findings of temporal variation in the disease burden and infectivity of GI pathogens. To investigate this further, we plan to measure bacterial burden and infectivity of an enteric pathogen such as *S.typhimurium*, alongside intestinal sIgA levels, at shorter time intervals (i.e. 3-hourly) throughout the circadian day. This would help determine the timing of any possible correlation between

infectivity and intestinal IgA. Furthermore, by modifying our IgA:bacterial flow cytometry assay, we could determine whether there was a difference in IgA:*S.typhimurium*-binding at different times of the day. Moreover, we plan to evaluate whether there is a loss of difference in disease burden/ infectivity in mice both lacking sIgA, and mice in which sIgA is arrhythmic (i.e. HFD-fed mice), as well as interrogate bacterial burden and infectivity in reverse-fed mice. Together, it is hoped that these studies will provide further insights about how intestinal sIgA promotes host protective immunity to enteric pathogens. This has potential clinical implications, as it may provide further understanding of the course and prognosis of mammalian GI infections.

6.3 Is the PC-intrinsic clock functionally redundant?

The findings from this study have also provided novel evidence to suggest that intestinal IgA+ PCs have a cell-intrinsic biological clock. While our data suggests that oscillatory IgA was not dependent on an intact clock within PCs, these findings do not discount altogether a functional role for the PC-intrinsic clock. Indeed, we found that *Bmal1* may modulate temporal gene expression of nutrient sensing and protein synthesis pathways within PCs, including genes relating to the mTOR pathway. This is particularly notable, as the mTOR pathway has previously been shown to be critical in regulating antibody production within mature PCs [352]. Furthermore, we found that reversal of feeding inverted *Bmal1* expression within PCs, and also demonstrated that light-time feeding inverted the phase of oscillatory sIgA. Together, these data suggest that a crosstalk may exist between nutritional cues, the biological clock and protein synthesis within PCs.

Previous work has identified that the mTOR pathway exerts control over the timing and magnitude of gene oscillations of the biological clock [357,433], and conversely the biological clock can regulate mTOR pathway activities [434], as well as the rhythmic expression of several cellular pathways relating to protein translation within cells [355,435]. It has been speculated that this may be advantageous to the host, as it may enable the alignment of cellular processes relating to protein synthesis around a time when nutrient availability is at its greatest [435]. Therefore, it is tempting to postulate that the PC-intrinsic clock helps facilitate alignment of cellular processes for antibody production, at a time of peak energy and nutrient availability. To evaluate this further, we plan to determine whether IgA rhythms generated under *ad libitum* feeding, fail to re-align to reversed feeding of clock-disrupted

Mb1$^{Cre+/-}$ *x Arntl*$^{flox/flox}$ mice. Moreover, we aim to repeat the in vitro IgA secretion assays in varying concentrations of metabolic nutrients and inhibitors, with PCs sorted from *Mb1*$^{Cre+/-}$ *x Arntl*$^{flox/flox}$ and littermate control mice. This will provide further information about whether the biological clock has a functional role in regulating nutrient sensing and protein synthesis pathways within PCs.

Notably, when considering the potential functional role of the PC-intrinsic clock, it is important to highlight that we only evaluated *Bmal1* deficiency in the PC clock. It has previously been demonstrated that some biological clock genes can regulate gene expression independent of the biological clock [311,436]. Therefore, we also plan to evaluate whether rhythmic IgA responses and/ or PC function is altered in mice with impaired clock function resulting from disruption of other core clock genes, such as *Per2* and/ or *Nr1d1*.

Another important consideration of these data relates to the finding that core clock genes did not appear to oscillate in IgD+ B cells, but did oscillate in fully differentiated PCs. In this setting, IgD+ B cells are antigen-inexperienced naïve B cells which, upon antigen encounter and in the presence of appropriate co-signals, undergo CSR and differentiation into antibody-secreting PCs [71]. The metabolic requirements of B cells across these different stages of activation are very different, such that antigen-inexperienced naïve IgD+ B cells have very few metabolic demands, whereas the metabolic requirements of antigen-activated B cells undergoing CSR and proliferation are much higher [200]. By contrast, fully differentiated PCs have the greatest metabolic requirements, which are largely focused on supporting antibody production [200]. Therefore, the finding that the biological clock within B cells does not oscillate at a cellular differentiation stage which has relatively few energy requirements, but does oscillate when the cell has very high energy requirements, supports the concept that the biological clock has a non-redundant role in orchestrating cellular processes within PCs. The stage of B cell differentiation at which the biological clock beings to oscillate could be further determined. To address this, B cell subsets at different stages of maturation and differentiation will be isolated by FACS-sorting tissue preparations sampled over the course of the day and subsequently, clock gene expression interrogated. Further to this, it might be interesting to investigate the molecular switch(es) which lead to activation of the biological clock within B cells/ PCs.

Finally, it is noteworthy that we focused solely on intestinal IgA-class switched PCs in the present study. As discussed previously, IgM+ and IgG+ PCs can be found within the intestinal LP in the steady state, albeit at a lower frequency than their IgA+ PC counterparts [108]. While it is well known that the presence of specific co-stimulatory signals and factors within the microenvironment direct CSR towards specific isotypes [71,107,108], it is plausible that the same environmental and/ or local endogenous factors might support antibody production from all fully differentiated PCs residing within the same tissue niche. This would suggest that both IgM+ and IgG+ PCs located within the small intestines might generate oscillatory antibody responses in a similar manner to IgA+ PCs. We plan to evaluate this by measuring IgM and IgG titres in faecal samples collected at serial timepoints over the circadian day.

Furthermore, class-switched PCs are located within peripheral lymph nodes and the bone marrow, where they secrete antibodies into the circulation [107,108]. Whether PCs at these distinct sites outside of the GI tract demonstrate oscillatory antibody responses is unknown. Feeding/ fasting cycles generate rhythms in the availability of nutrients throughout the body [437], which argues in favour of oscillatory antibody responses being present at distinct sites outside of the GI tract. However, immune cells are exposed to different environmental and endogenous signals within different tissue niches [12,111], suggesting regional differences in immune cell regulation. Indeed, previous data has suggested that B cell and PC responses within distinct tissue niches may be regulated by different cell-extrinsic cues [110,212,383]. To investigate this further, we plan to measure IgG and IgM antibody levels in serum sampled over the course of the circadian day. If temporal changes in antibody titres were detected, we plan to isolate PCs from these peripheral tissue sites and repeat key transcriptomic and functional assays, including RNA sequencing and PC secretion assays, as performed within the present study. It is envisaged that together, these data will provide further insights into the potential functional role of the PC-intrinsic clock.

6.4 Concluding remarks

In conclusion, these data suggest a previously unappreciated circadian dialogue exists between dietary cues, intestinal IgA and the commensal microbiota. As the GI tract is the largest interface between the host and microorganisms, rhythmic intestinal antibody responses may have evolved to facilitate the promotion of host:microbial mutualism. These findings have clinical implications for furthering our understanding of the development and

treatment of metabolic diseases, such as obesity and diabetes, which are increasingly recognised to associate with circadian misalignment.

7.0 REFERENCES

1. France, M.M. and J.R. Turner, *The mucosal barrier at a glance.* Journal of Cell Science, 2017. **130**: p. 307-314.
2. Turner, J.R., *Intestinal mucosal barrier function in health and disease.* Nature Reviews Immunology, 2009. **9**(11): p. 799-809.
3. Trivedi, B., *Microbiome: The surface brigade.* Nature, 2012. **492**(7429): p. S60-S61.
4. Huang, Y.J. and H.A. Boushey, *The microbiome in asthma.* Journal of Allergy and Clinical Immunology, 2015. **135**(1): p. 25-30.
5. Manichanh, C., et al., *The gut microbiota in IBD.* Nat Rev Gastroenterol Hepatol, 2012. **9**(10): p. 599-608.
6. Plottel, Claudia S. and Martin J. Blaser, *Microbiome and Malignancy.* Cell Host & Microbe, 2011. **10**(4): p. 324-335.
7. Maeda, Y. and K. Takeda, *Host–microbiota interactions in rheumatoid arthritis.* Experimental & molecular medicine, 2019. **51**(12): p. 1-6.
8. Needham, B.D., R. Kaddurah-Daouk, and S.K. Mazmanian, *Gut microbial molecules in behavioural and neurodegenerative conditions.* Nature Reviews Neuroscience, 2020. **21**(12): p. 717-731.
9. Thomas, R.M. and C. Jobin, *Microbiota in pancreatic health and disease: the next frontier in microbiome research.* Nature Reviews Gastroenterology & Hepatology, 2020. **17**(1): p. 53-64.
10. Tilg, H., P.D. Cani, and E.A. Mayer, *Gut microbiome and liver diseases.* Gut, 2016. **65**(12): p. 2035.
11. Jie, Z., et al., *The gut microbiome in atherosclerotic cardiovascular disease.* Nature Communications, 2017. **8**(1): p. 845.
12. Mowat, A.M. and W.W. Agace, *Regional specialization within the intestinal immune system.* Nat Rev Immunol, 2014. **14**(10): p. 667-85.
13. E, M., *The Wilde Medal and Lecture of the Manchester Literary and Philosophical Society* BMJ, 1901. **1**: p. 1027-1028.
14. Tropini, C., et al., *The Gut Microbiome: Connecting Spatial Organization to Function.* Cell Host Microbe, 2017. **21**(4): p. 433-442.
15. Savage, D.C., *MICROBIAL ECOLOGY OF THE GASTROINTESTINAL TRACT.* Annual Review of Microbiology, 1977. **31**(1): p. 107-133.
16. Luckey, T.D., *Introduction to intestinal microecology.* Am J Clin Nutr, 1972. **25**(12): p. 1292-4.
17. Bouskra, D., et al., *Lymphoid tissue genesis induced by commensals through NOD1 regulates intestinal homeostasis.* Nature, 2008. **456**(7221): p. 507-510.
18. Moreau, M., et al., *Increase in the population of duodenal immunoglobulin A plasmocytes in axenic mice associated with different living or dead bacterial strains of intestinal origin.* Infection and immunity, 1978. **21**(2): p. 532-539.
19. Ivanov, I.I., et al., *Induction of intestinal Th17 cells by segmented filamentous bacteria.* Cell, 2009. **139**(3): p. 485-498.
20. Kelly, C.J., et al., *Crosstalk between microbiota-derived short-chain fatty acids and intestinal epithelial HIF augments tissue barrier function.* Cell host & microbe, 2015. **17**(5): p. 662-671.
21. Maynard, C.L., et al., *Reciprocal interactions of the intestinal microbiota and immune system.* Nature, 2012. **489**(7415): p. 231-241.
22. Belkaid, Y. and O.J. Harrison, *Homeostatic immunity and the microbiota.* Immunity, 2017. **46**(4): p. 562-576.
23. Johansson, M.E.V., et al., *The inner of the two Muc2 mucin-dependent mucus layers in colon is devoid of bacteria.* Proceedings of the National Academy of Sciences, 2008. **105**: p. 15064-15069.

24. Lueschow, S.R. and S.J. McElroy, *The Paneth Cell: The Curator and Defender of the Immature Small Intestine.* Frontiers in Immunology, 2020. **11**(587).
25. Bäckhed, F., et al., *Host-bacterial mutualism in the human intestine.* Science, 2005. **307**(5717): p. 1915-20.
26. Belkaid, Y. and T.W. Hand, *Role of the microbiota in immunity and inflammation.* Cell, 2014. **157**(1): p. 121-141.
27. Xavier, R.J. and D.K. Podolsky, *Unravelling the pathogenesis of inflammatory bowel disease.* Nature, 2007. **448**(7152): p. 427-434.
28. Lasry, A., A. Zinger, and Y. Ben-Neriah, *Inflammatory networks underlying colorectal cancer.* Nat Immunol, 2016. **17**(3): p. 230-40.
29. Horta-Baas, G., et al., *Intestinal dysbiosis and rheumatoid arthritis: a link between gut microbiota and the pathogenesis of rheumatoid arthritis.* Journal of immunology research, 2017. **2017**.
30. Main, B.S. and M.R. Minter, *Microbial immuno-communication in neurodegenerative diseases.* Frontiers in neuroscience, 2017. **11**: p. 151.
31. Boursier, J., et al., *The severity of nonalcoholic fatty liver disease is associated with gut dysbiosis and shift in the metabolic function of the gut microbiota.* Hepatology, 2016. **63**(3): p. 764-75.
32. Sabino, J., et al., *Primary sclerosing cholangitis is characterised by intestinal dysbiosis independent from IBD.* Gut, 2016. **65**(10): p. 1681-1689.
33. Ley, R.E., et al., *Human gut microbes associated with obesity.* nature, 2006. **444**(7122): p. 1022-1023.
34. Bäckhed, F., et al., *The gut microbiota as an environmental factor that regulates fat storage.* Proc Natl Acad Sci U S A, 2004. **101**(44): p. 15718-23.
35. Meresse, B., et al., *Celiac disease: from oral tolerance to intestinal inflammation, autoimmunity and lymphomagenesis.* Mucosal Immunology, 2009. **2**(1): p. 8-23.
36. Steele, L., L. Mayer, and M.C. Berin, *Mucosal immunology of tolerance and allergy in the gastrointestinal tract.* Immunologic research, 2012. **54**(1-3): p. 75-82.
37. Rawla, P., T. Sunkara, and A. Barsouk, *Epidemiology of colorectal cancer: incidence, mortality, survival, and risk factors.* Przeglad gastroenterologiczny, 2019. **14**(2): p. 89-103.
38. Kassam, Z., et al., *Inflammatory bowel disease cause-specific mortality: a primer for clinicians.* Inflamm Bowel Dis, 2014. **20**(12): p. 2483-92.
39. Janani, K., et al., *Health-related quality of life in liver cirrhosis patients using SF-36 and CLDQ questionnaires.* Clin Exp Hepatol, 2018. **4**(4): p. 232-239.
40. Katz, D.A., C.A. McHorney, and R.L. Atkinson, *Impact of obesity on health-related quality of life in patients with chronic illness.* J Gen Intern Med, 2000. **15**(11): p. 789-96.
41. C, D., et al., *Quality of life in celiac disease and the effect of gluten-free diet.* JGH Open, 2018. **2**(4): p. 124-128.
42. Gohar, A., et al., *Health-related quality of life and outcome in atherosclerosis - Does sex matter?* Int J Cardiol, 2016. **212**: p. 303-6.
43. Sichien, D., et al., *Development of conventional dendritic cells: from common bone marrow progenitors to multiple subsets in peripheral tissues.* Mucosal Immunology, 2017. **10**(4): p. 831-844.
44. Guermonprez, P., et al., *Antigen presentation and T cell stimulation by dendritic cells.* Annu Rev Immunol, 2002. **20**: p. 621-67.
45. Persson, E.K., et al., *Dendritic cell subsets in the intestinal lamina propria: ontogeny and function.* European journal of immunology, 2013. **43**(12): p. 3098-3107.
46. McDole, J.R., et al., *Goblet cells deliver luminal antigen to CD103+ dendritic cells in the small intestine.* Nature, 2012. **483**(7389): p. 345-349.
47. Jang, M.H., et al., *Intestinal villous M cells: an antigen entry site in the mucosal epithelium.* Proceedings of the National Academy of Sciences, 2004. **101**(16): p. 6110-6115.

48. Mazzini, E., et al., *Oral tolerance can be established via gap junction transfer of fed antigens from CX3CR1⁺ macrophages to CD103⁺ dendritic cells.* Immunity, 2014. **40**(2): p. 248-61.
49. Knoop, K.A., M.J. Miller, and R.D. Newberry, *Trans-epithelial antigen delivery in the small intestine: different paths, different outcomes.* Current opinion in gastroenterology, 2013. **29**(2): p. 112.
50. Jang, M.H., et al., *CCR7 is critically important for migration of dendritic cells in intestinal lamina propria to mesenteric lymph nodes.* The Journal of Immunology, 2006. **176**(2): p. 803-810.
51. Iwata, M., et al., *Retinoic acid imprints gut-homing specificity on T cells.* Immunity, 2004. **21**(4): p. 527-538.
52. Wendland, M., et al., *CCR9 is a homing receptor for plasmacytoid dendritic cells to the small intestine.* Proceedings of the National Academy of Sciences, 2007. **104**: p. 6347-6352.
53. Pabst, O., et al., *Chemokine receptor CCR9 contributes to the localization of plasma cells to the small intestine.* J Exp Med, 2004. **199**(3): p. 411-6.
54. Bird, L., *The T cell collective.* Nature Reviews Immunology, 2020. **20**(4): p. 206-207.
55. Szabo, S.J., et al., *Molecular Mechanisms RegulatinG Th1 Immune Responses.* Annual Review of Immunology, 2003. **21**(1): p. 713-758.
56. Walker, J.A. and A.N.J. McKenzie, *TH2 cell development and function.* Nature Reviews Immunology, 2018. **18**(2): p. 121-133.
57. Harrison, O.J. and F.M. Powrie, *Regulatory T cells and immune tolerance in the intestine.* Cold Spring Harb Perspect Biol, 2013. **5**(7).
58. Park, J.H., et al., *Immune dysregulation, polyendocrinopathy, enteropathy, X-linked (IPEX) syndrome: A systematic review.* Autoimmun Rev, 2020. **19**(6): p. 102526.
59. Rubtsov, Y.P., et al., *Regulatory T cell-derived interleukin-10 limits inflammation at environmental interfaces.* Immunity, 2008. **28**(4): p. 546-558.
60. Li, M.O., Y.Y. Wan, and R.A. Flavell, *T cell-produced transforming growth factor-β1 controls T cell tolerance and regulates Th1-and Th17-cell differentiation.* Immunity, 2007. **26**(5): p. 579-591.
61. Wing, K., et al., *CTLA-4 control over Foxp3+ regulatory T cell function.* Science, 2008. **322**(5899): p. 271-275.
62. Collison, L.W., et al., *The inhibitory cytokine IL-35 contributes to regulatory T-cell function.* Nature, 2007. **450**(7169): p. 566-569.
63. Maloy, K.J. and F. Powrie, *Regulatory T cells in the control of immune pathology.* Nature immunology, 2001. **2**(9): p. 816-822.
64. Cong, Y., et al., *A dominant, coordinated T regulatory cell-IgA response to the intestinal microbiota.* Proceedings of the National Academy of Sciences, 2009. **106**(46): p. 19256-19261.
65. Nakajima, A., et al., *IgA regulates the composition and metabolic function of gut microbiota by promoting symbiosis between bacteria.* J Exp Med, 2018. **215**(8): p. 2019-2034.
66. Bunker, J.J., et al., *Innate and Adaptive Humoral Responses Coat Distinct Commensal Bacteria with Immunoglobulin A.* Immunity, 2015. **43**(3): p. 541-53.
67. Donaldson, G.P., et al., *Gut microbiota utilize immunoglobulin A for mucosal colonization.* Science, 2018. **360**: p. 795-800.
68. Mantis, N.J., N. Rol, and B. Corthésy, *Secretory IgA's complex roles in immunity and mucosal homeostasis in the gut.* Mucosal immunology, 2011. **4**(6): p. 603-611.
69. Kawamoto, S., et al., *Foxp3+ T Cells Regulate Immunoglobulin A Selection and Facilitate Diversification of Bacterial Species Responsible for Immune Homeostasis.* Immunity, 2014. **41**(1): p. 152-165.
70. Vinuesa, C.G., et al., *Follicular Helper T Cells.* Annual Review of Immunology, 2016. **34**(1): p. 335-368.
71. Cerutti, A., *The regulation of IgA class switching.* Nature Reviews Immunology, 2008. **8**(6): p. 421-434.

72. Nurieva, R.I., et al., *Generation of T follicular helper cells is mediated by interleukin-21 but independent of T helper 1, 2, or 17 cell lineages.* Immunity, 2008. **29**(1): p. 138-149.
73. Webb, L.M.C. and M.A. Linterman, *Signals that drive T follicular helper cell formation.* Immunology, 2017. **152**(2): p. 185-194.
74. Hirota, K., et al., *Plasticity of TH 17 cells in Peyer's patches is responsible for the induction of T cell–dependent IgA responses.* Nature immunology, 2013. **14**(4): p. 372-379.
75. Bettelli, E., et al., *Reciprocal developmental pathways for the generation of pathogenic effector TH 17 and regulatory T cells.* Nature, 2006. **441**(7090): p. 235-238.
76. Gaboriau-Routhiau, V., et al., *The key role of segmented filamentous bacteria in the coordinated maturation of gut helper T cell responses.* Immunity, 2009. **31**(4): p. 677-689.
77. Chung, H., et al., *Gut Immune Maturation Depends on Colonization with a Host-Specific Microbiota.* Cell, 2012. **149**(7): p. 1578-1593.
78. Lécuyer, E., et al., *Segmented Filamentous Bacterium Uses Secondary and Tertiary Lymphoid Tissues to Induce Gut IgA and Specific T Helper 17 Cell Responses.* Immunity, 2014. **40**(4): p. 608-620.
79. Kumar, P., et al., *Intestinal Interleukin-17 Receptor Signaling Mediates Reciprocal Control of the Gut Microbiota and Autoimmune Inflammation.* Immunity, 2016. **44**(3): p. 659-671.
80. Cao, A.T., et al., *Th17 cells upregulate polymeric Ig receptor and intestinal IgA and contribute to intestinal homeostasis.* J Immunol, 2012. **189**(9): p. 4666-73.
81. Johansen, F.-E., et al., *Absence of epithelial immunoglobulin a transport, with increased mucosal leakiness, in polymeric immunoglobulin receptor/secretory component–deficient mice.* The Journal of experimental medicine, 1999. **190**(7): p. 915-922.
82. Elson, C.O., et al., *Monoclonal anti-interleukin 23 reverses active colitis in a T cell-mediated model in mice.* Gastroenterology, 2007. **132**(7): p. 2359-2370.
83. Fujino, S., et al., *Increased expression of interleukin 17 in inflammatory bowel disease.* Gut, 2003. **52**(1): p. 65-70.
84. O'Connor, W., Jr., et al., *A protective function for interleukin 17A in T cell-mediated intestinal inflammation.* Nat Immunol, 2009. **10**(6): p. 603-9.
85. Hanash, A.M., et al., *Interleukin-22 protects intestinal stem cells from immune-mediated tissue damage and regulates sensitivity to graft versus host disease.* Immunity, 2012. **37**(2): p. 339-50.
86. Aparicio-Domingo, P., et al., *Type 3 innate lymphoid cells maintain intestinal epithelial stem cells after tissue damage.* J Exp Med, 2015. **212**(11): p. 1783-91.
87. Lindemans, C.A., et al., *Interleukin-22 promotes intestinal-stem-cell-mediated epithelial regeneration.* Nature, 2015. **528**(7583): p. 560-564.
88. Hepworth, M.R., et al., *Innate lymphoid cells regulate CD4+ T-cell responses to intestinal commensal bacteria.* Nature, 2013. **498**(7452): p. 113-7.
89. Goto, Y., et al., *Innate lymphoid cells regulate intestinal epithelial cell glycosylation.* Science, 2014. **345**(6202): p. 1254009.
90. Colonna, M., *Innate Lymphoid Cells: Diversity, Plasticity, and Unique Functions in Immunity.* Immunity, 2018. **48**(6): p. 1104-1117.
91. Melo-Gonzalez, F. and M.R. Hepworth, *Functional and phenotypic heterogeneity of group 3 innate lymphoid cells.* Immunology, 2017. **150**(3): p. 265-275.
92. Penny, H.A., S.H. Hodge, and M.R. Hepworth, *Orchestration of intestinal homeostasis and tolerance by group 3 innate lymphoid cells.* Semin Immunopathol, 2018. **40**(4): p. 357-370.
93. Sonnenberg, G.F. and D. Artis, *Innate lymphoid cells in the initiation, regulation and resolution of inflammation.* Nat Med, 2015. **21**(7): p. 698-708.
94. Mortha, A., et al., *Microbiota-dependent crosstalk between macrophages and ILC3 promotes intestinal homeostasis.* Science, 2014. **343**(6178): p. 1249288.

95. Pabst, O., et al., *Cryptopatches and isolated lymphoid follicles: dynamic lymphoid tissues dispensable for the generation of intraepithelial lymphocytes.* European Journal of Immunology, 2005. **35**(1): p. 98-107.
96. Hamada, H., et al., *Identification of Multiple Isolated Lymphoid Follicles on the Antimesenteric Wall of the Mouse Small Intestine.* The Journal of Immunology, 2002. **168**: p. 57-64.
97. Tsuji, M., et al., *Requirement for Lymphoid Tissue-Inducer Cells in Isolated Follicle Formation and T Cell-Independent Immunoglobulin A Generation in the Gut.* Immunity, 2008. **29**(2): p. 261-271.
98. Melo-Gonzalez, F., et al., *Antigen-presenting ILC3 regulate T cell–dependent IgA responses to colonic mucosal bacteria.* Journal of Experimental Medicine, 2019. **216**(4): p. 728-742.
99. Tarlinton, D., *B cells still front and centre in immunology.* Nature Reviews Immunology, 2019. **19**(2): p. 85-86.
100. Spencer, J. and L.M. Sollid, *The human intestinal B-cell response.* Mucosal Immunology, 2016. **9**(5): p. 1113-1124.
101. Treanor, B., *B-cell receptor: from resting state to activate.* Immunology, 2012. **136**(1): p. 21-7.
102. Maity, P.C., et al., *B cell antigen receptors of the IgM and IgD classes are clustered in different protein islands that are altered during B cell activation.* Science Signaling, 2015. **8**(394): p. ra93-ra93.
103. Xu, Z., et al., *Immunoglobulin class-switch DNA recombination: induction, targeting and beyond.* Nature Reviews Immunology, 2012. **12**(7): p. 517-531.
104. Moore, K.W., et al., *Expression of IgD may use both DNA rearrangement and RNA splicing mechanisms.* Proc Natl Acad Sci U S A, 1981. **78**(3): p. 1800-4.
105. Maki, R., et al., *The role of DNA rearrangement and alternative RNA processing in the expression of immunoglobulin delta genes.* Cell, 1981. **24**(2): p. 353-365.
106. Honjo, T., K. Kinoshita, and M. Muramatsu, *Molecular Mechanism of Class Switch Recombination: Linkage with Somatic Hypermutation.* Annual Review of Immunology, 2002. **20**(1): p. 165-196.
107. Brandtzaeg, P., et al., *The B-cell system of human mucosae and exocrine glands.* Immunological reviews, 1999. **171**(1): p. 45-87.
108. Brandtzaeg, P. and F.-E. Johansen, *Mucosal B cells: phenotypic characteristics, transcriptional regulation, and homing properties.* Immunological Reviews, 2005. **206**(1): p. 32-63.
109. Jonard, P.P., et al., *Secretion of immunoglobulins and plasma proteins from the jejunal mucosa. Transport rate and origin of polymeric immunoglobulin A.* J Clin Invest, 1984. **74**(2): p. 525-35.
110. Lam, W.Y., et al., *Metabolic and Transcriptional Modules Independently Diversify Plasma Cell Lifespan and Function.* Cell Rep, 2018. **24**(9): p. 2479-2492.e6.
111. Lam, W.Y., et al., *Mitochondrial Pyruvate Import Promotes Long-Term Survival of Antibody-Secreting Plasma Cells.* Immunity, 2016. **45**(1): p. 60-73.
112. Lycke, N., et al., *Lack of J chain inhibits the transport of gut IgA and abrogates the development of intestinal antitoxic protection.* The journal of immunology, 1999. **163**(2): p. 913-919.
113. Boullier, S., et al., *Secretory IgA-Mediated Neutralization of Shigella flexneri Prevents Intestinal Tissue Destruction by Down-Regulating Inflammatory Circuits.* The Journal of Immunology, 2009. **183**: p. 5879-5885.
114. Moor, K., et al., *High-avidity IgA protects the intestine by enchaining growing bacteria.* Nature, 2017. **544**(7651): p. 498-502.
115. Van der Waaij, L., et al., *In vivo IgA coating of anaerobic bacteria in human faeces.* Gut, 1996. **38**(3): p. 348-354.
116. Tsuruta, T., et al., *The amount of secreted IgA may not determine the secretory IgA coating ratio of gastrointestinal bacteria.* FEMS Immunology & Medical Microbiology, 2009. **56**(2): p. 185-189.

117. Palm, N.W., et al., *Immunoglobulin A coating identifies colitogenic bacteria in inflammatory bowel disease.* Cell, 2014. **158**(5): p. 1000-1010.
118. Gopalakrishna, K.P., et al., *Maternal IgA protects against the development of necrotizing enterocolitis in preterm infants.* Nature Medicine, 2019. **25**(7): p. 1110-1115.
119. Catanzaro, J.R., et al., *IgA-deficient humans exhibit gut microbiota dysbiosis despite secretion of compensatory IgM.* Sci Rep, 2019. **9**(1): p. 13574.
120. Huus, K.E., et al., *Commensal Bacteria Modulate Immunoglobulin A Binding in Response to Host Nutrition.* Cell Host & Microbe, 2020. **27**(6): p. 909-921.e5.
121. Peterson, D.A., et al., *IgA Response to Symbiotic Bacteria as a Mediator of Gut Homeostasis.* Cell Host & Microbe, 2007. **2**(5): p. 328-339.
122. Luck, H., et al., *Gut-associated IgA+ immune cells regulate obesity-related insulin resistance.* Nature Communications, 2019. **10**(1): p. 3650.
123. Tran, H.Q., et al., *Flagellin-elicited adaptive immunity suppresses flagellated microbiota and vaccinates against chronic inflammatory diseases.* Nature Communications, 2019. **10**(1): p. 5650.
124. Shulzhenko, N., et al., *Crosstalk between B lymphocytes, microbiota and the intestinal epithelium governs immunity versus metabolism in the gut.* Nat Med, 2011. **17**(12): p. 1585-93.
125. Uchimura, Y., et al., *Antibodies Set Boundaries Limiting Microbial Metabolite Penetration and the Resultant Mammalian Host Response.* Immunity, 2018. **49**(3): p. 545-559.e5.
126. Lu, R., et al., *Tracking single hematopoietic stem cells in vivo using high-throughput sequencing in conjunction with viral genetic barcoding.* Nature biotechnology, 2011. **29**(10): p. 928-933.
127. Deenick, E.K., et al., *Follicular helper T cell differentiation requires continuous antigen presentation that is independent of unique B cell signaling.* Immunity, 2010. **33**(2): p. 241-253.
128. Grusby, M.J., et al., *Depletion of CD4+ T cells in major histocompatibility complex class II-deficient mice.* Science, 1991. **253**(5026): p. 1417-1420.
129. Linterman, M.A., et al., *IL-21 acts directly on B cells to regulate Bcl-6 expression and germinal center responses.* Journal of Experimental Medicine, 2010. **207**(2): p. 353-363.
130. Kawabe, T., et al., *The immune responses in CD40-deficient mice: impaired immunoglobulin class switching and germinal center formation.* Immunity, 1994. **1**(3): p. 167-178.
131. Allen, C.D., et al., *Imaging of germinal center selection events during affinity maturation.* Science, 2007. **315**(5811): p. 528-531.
132. Kocks, C. and K. Rajewsky, *Stepwise intraclonal maturation of antibody affinity through somatic hypermutation.* Proceedings of the National Academy of Sciences, 1988. **85**(21): p. 8206-8210.
133. Gitlin, A.D., Z. Shulman, and M.C. Nussenzweig, *Clonal selection in the germinal centre by regulated proliferation and hypermutation.* Nature, 2014. **509**(7502): p. 637-640.
134. Berek, C., A. Berger, and M. Apel, *Maturation of the immune response in germinal centers.* Cell, 1991. **67**(6): p. 1121-1129.
135. Mesin, L., J. Ersching, and G.D. Victora, *Germinal Center B Cell Dynamics.* Immunity, 2016. **45**(3): p. 471-482.
136. Macpherson, A.J., et al., *A primitive T cell-independent mechanism of intestinal mucosal IgA responses to commensal bacteria.* Science, 2000. **288**(5474): p. 2222-2226.
137. Kroese, F.G., et al., *Many of the IgA producing plasma cells in murine gut are derived from self-replenishing precursors in the peritoneal cavity.* International immunology, 1989. **1**(1): p. 75-84.
138. Hesslein, D.G., S.Y. Yang, and D.G. Schatz, *Origins of peripheral B cells in IL-7 receptor-deficient mice.* Molecular immunology, 2006. **43**(4): p. 326-334.
139. von Freeden-Jeffry, U., et al., *Lymphopenia in interleukin (IL)-7 gene-deleted mice identifies IL-7 as a nonredundant cytokine.* Journal of Experimental Medicine, 1995. **181**(4): p. 1519-1526.

140. Vos, Q., et al., *B-cell activation by T-cell-independent type 2 antigens as an integral part of the humoral immune response to pathogenic microorganisms.* Immunol Rev, 2000. **176**: p. 154-70.
141. Magri, G., et al., *Innate lymphoid cells integrate stromal and immunological signals to enhance antibody production by splenic marginal zone B cells.* Nature Immunology, 2014. **15**(4): p. 354-364.
142. Kruglov, A.A., et al., *Nonredundant Function of Soluble LTα₃ Produced by Innate Lymphoid Cells in Intestinal Homeostasis.* Science, 2013. **342**: p. 1243-1246.
143. Reboldi, A., et al., *IgA production requires B cell interaction with subepithelial dendritic cells in Peyer's patches.* Science, 2016. **352**.
144. Fagarasan, S., et al., *Adaptive Immune Regulation in the Gut: T Cell–Dependent and T Cell–Independent IgA Synthesis.* Annual Review of Immunology, 2010. **28**(1): p. 243-273.
145. Bunker, J.J. and A. Bendelac, *IgA Responses to Microbiota.* Immunity, 2018. **49**(2): p. 211-224.
146. Golby, S.J. and J. Spencer, *Where do IgA plasma cells in the gut come from?* Gut, 2002. **51**(2): p. 150-1.
147. Breedveld, A. and M. van Egmond, *IgA and FcαRI: Pathological Roles and Therapeutic Opportunities.* Front Immunol, 2019. **10**: p. 553.
148. Williams, A.F. and A.N. Barclay, *The immunoglobulin superfamily—domains for cell surface recognition.* Annual review of immunology, 1988. **6**(1): p. 381-405.
149. Schroeder, H.W., Jr. and L. Cavacini, *Structure and function of immunoglobulins.* J Allergy Clin Immunol, 2010. **125**(2 Suppl 2): p. S41-52.
150. Stavnezer, J., J.E. Guikema, and C.E. Schrader, *Mechanism and regulation of class switch recombination.* Annu Rev Immunol, 2008. **26**: p. 261-92.
151. Muramatsu, M., et al., *Class switch recombination and hypermutation require activation-induced cytidine deaminase (AID), a potential RNA editing enzyme.* Cell, 2000. **102**(5): p. 553-563.
152. Revy, P., et al., *Activation-Induced Cytidine Deaminase (AID) Deficiency Causes the Autosomal Recessive Form of the Hyper-IgM Syndrome (HIGM2).* Cell, 2000. **102**(5): p. 565-575.
153. Rush, J.S., et al., *Expression of activation-induced cytidine deaminase is regulated by cell division, providing a mechanistic basis for division-linked class switch recombination.* Proceedings of the National Academy of Sciences, 2005. **102**(37): p. 13242-13247.
154. Bergqvist, P., et al., *Gut IgA Class Switch Recombination in the Absence of CD40 Does Not Occur in the Lamina Propria and Is Independent of Germinal Centers.* The Journal of Immunology, 2006. **177**: p. 7772-7783.
155. Dedeoglu, F., et al., *Induction of activation-induced cytidine deaminase gene expression by IL-4 and CD40 ligation is dependent on STAT6 and NFκB.* International immunology, 2004. **16**(3): p. 395-404.
156. Hasbold, J., et al., *Cell division number regulates IgG1 and IgE switching of B cells following stimulation by CD40 ligand and IL-4.* European journal of immunology, 1998. **28**(3): p. 1040-1051.
157. Tangye, S.G., et al., *The good, the bad and the ugly — TFH cells in human health and disease.* Nature Reviews Immunology, 2013. **13**(6): p. 412-426.
158. Litinskiy, M.B., et al., *DCs induce CD40-independent immunoglobulin class switching through BLyS and APRIL.* Nature immunology, 2002. **3**(9): p. 822-829.
159. Tezuka, H., et al., *Regulation of IgA production by naturally occurring TNF/iNOS-producing dendritic cells.* Nature, 2007. **448**(7156): p. 929-33.
160. He, B., et al., *Intestinal bacteria trigger T cell-independent immunoglobulin A2 class switching by inducing epithelial-cell secretion of the cytokine APRIL.* Immunity, 2007. **26**(6): p. 812-826.
161. Xu, W., et al., *Epithelial cells trigger frontline immunoglobulin class switching through a pathway regulated by the inhibitor SLPI.* Nature immunology, 2007. **8**(3): p. 294-303.

162. Chaudhuri, J., et al., *Transcription-targeted DNA deamination by the AID antibody diversification enzyme.* Nature, 2003. **422**(6933): p. 726-730.
163. Manis, J.P., M. Tian, and F.W. Alt, *Mechanism and control of class-switch recombination.* Trends in immunology, 2002. **23**(1): p. 31-39.
164. Cyster, J.G. and C.D.C. Allen, *B Cell Responses: Cell Interaction Dynamics and Decisions.* Cell, 2019. **177**(3): p. 524-540.
165. Cazac, B.B. and J. Roes, *TGF-β Receptor Controls B Cell Responsiveness and Induction of IgA In Vivo.* Immunity, 2000. **13**(4): p. 443-451.
166. Defrance, T., et al., *Interleukin 10 and transforming growth factor beta cooperate to induce anti-CD40-activated naive human B cells to secrete immunoglobulin A.* The Journal of experimental medicine, 1992. **175**(3): p. 671-682.
167. McIntyre, T.M., M.R. Kehry, and C.M. Snapper, *Novel in vitro model for high-rate IgA class switching.* The Journal of Immunology, 1995. **154**(7): p. 3156-3161.
168. Mora, J.R., et al., *Generation of gut-homing IgA-secreting B cells by intestinal dendritic cells.* Science, 2006. **314**(5802): p. 1157-1160.
169. Cao, A.T., et al., *Interleukin (IL)-21 promotes intestinal IgA response to microbiota.* Mucosal Immunology, 2015. **8**(5): p. 1072-1082.
170. Park, M.-H., et al., *Retinoic acid induces expression of Ig germ line α transcript, an IgA isotype switching indicative, through retinoic acid receptor.* Genes & Genomics, 2011. **33**(1): p. 83-88.
171. Castigli, E., et al., *Impaired IgA class switching in APRIL-deficient mice.* Proceedings of the National Academy of Sciences of the United States of America, 2004. **101**: p. 3903-3908.
172. Papavasiliou, F.N. and D.G. Schatz, *Somatic Hypermutation of Immunoglobulin Genes: Merging Mechanisms for Genetic Diversity.* Cell, 2002. **109**(2): p. S35-S44.
173. Bemark, M., et al., *Limited clonal relatedness between gut IgA plasma cells and memory B cells after oral immunization.* Nature communications, 2016. **7**(1): p. 1-15.
174. Lycke, N.Y. and M. Bemark, *The regulation of gut mucosal IgA B-cell responses: recent developments.* Mucosal Immunology, 2017. **10**(6): p. 1361-1374.
175. Victora, G.D., et al., *Germinal center dynamics revealed by multiphoton microscopy with a photoactivatable fluorescent reporter.* Cell, 2010. **143**(4): p. 592-605.
176. Tas, J.M., et al., *Visualizing antibody affinity maturation in germinal centers.* Science, 2016. **351**(6277): p. 1048-1054.
177. Suzuki, K., et al., *The Sensing of Environmental Stimuli by Follicular Dendritic Cells Promotes Immunoglobulin A Generation in the Gut.* Immunity, 2010. **33**(1): p. 71-83.
178. Victora, G.D. and M.C. Nussenzweig, *Germinal centers.* Annual review of immunology, 2012. **30**: p. 429-457.
179. Sage, P.T. and A.H. Sharpe, *T follicular regulatory cells in the regulation of B cell responses.* Trends in Immunology, 2015. **36**(7): p. 410-418.
180. Sage, P.T., et al., *Suppression by TFR cells leads to durable and selective inhibition of B cell effector function.* Nature Immunology, 2016. **17**(12): p. 1436-1446.
181. Bergqvist, P., et al., *Re-utilization of germinal centers in multiple Peyer's patches results in highly synchronized, oligoclonal, and affinity-matured gut IgA responses.* Mucosal immunology, 2013. **6**(1): p. 122-135.
182. Barone, F., et al., *IgA-Producing Plasma Cells Originate From Germinal Centers That Are Induced by B-Cell Receptor Engagement in Humans.* Gastroenterology, 2011. **140**(3): p. 947-956.
183. Bunker, J.J., et al., *Natural polyreactive IgA antibodies coat the intestinal microbiota.* Science, 2017. **358**(6361).
184. Casola, S., et al., *B cell receptor signal strength determines B cell fate.* Nature immunology, 2004. **5**(3): p. 317-327.
185. de Vinuesa, C.G., et al., *Germinal Centers without T Cells.* Journal of Experimental Medicine, 2000. **191**(3): p. 485-494.

186. Pabst, O. and E. Slack, *IgA and the intestinal microbiota: the importance of being specific.* Mucosal Immunology, 2020. **13**(1): p. 12-21.
187. Kabashima, K., et al., *Plasma cell S1P1 expression determines secondary lymphoid organ retention versus bone marrow tropism.* The Journal of experimental medicine, 2006. **203**(12): p. 2683-2690.
188. Husband, A.J. and J.L. Gowans, *The origin and antigen-dependent distribution of IgA-containing cells in the intestine.* The Journal of experimental medicine, 1978. **148**(5): p. 1146-1160.
189. Kunkel, E.J., et al., *CCR10 expression is a common feature of circulating and mucosal epithelial tissue IgA Ab-secreting cells.* J Clin Invest, 2003. **111**(7): p. 1001-10.
190. Cobaleda, C., et al., *Pax5: the guardian of B cell identity and function.* Nature immunology, 2007. **8**(5): p. 463-470.
191. Minnich, M., et al., *Multifunctional role of the transcription factor Blimp-1 in coordinating plasma cell differentiation.* Nature immunology, 2016. **17**(3): p. 331-343.
192. Shi, W., et al., *Transcriptional profiling of mouse B cell terminal differentiation defines a signature for antibody-secreting plasma cells.* Nature immunology, 2015. **16**(6): p. 663-673.
193. Klein, U., et al., *Transcription factor IRF4 controls plasma cell differentiation and class-switch recombination.* Nature immunology, 2006. **7**(7): p. 773-782.
194. Sciammas, R., et al., *Graded expression of interferon regulatory factor-4 coordinates isotype switching with plasma cell differentiation.* Immunity, 2006. **25**(2): p. 225-236.
195. Shapiro-Shelef, M., et al., *Blimp-1 is required for the formation of immunoglobulin secreting plasma cells and pre-plasma memory B cells.* Immunity, 2003. **19**(4): p. 607-620.
196. Tellier, J., et al., *Blimp-1 controls plasma cell function through the regulation of immunoglobulin secretion and the unfolded protein response.* Nature immunology, 2016. **17**(3): p. 323-330.
197. Tellier, J. and S.L. Nutt, *Plasma cells: The programming of an antibody-secreting machine.* European Journal of Immunology, 2019. **49**(1): p. 30-37.
198. Taubenheim, N., et al., *High rate of antibody secretion is not integral to plasma cell differentiation as revealed by XBP-1 deficiency.* The Journal of Immunology, 2012. **189**(7): p. 3328-3338.
199. Kallies, A., et al., *Plasma cell ontogeny defined by quantitative changes in blimp-1 expression.* The Journal of experimental medicine, 2004. **200**(8): p. 967-977.
200. Lam, W.Y. and D. Bhattacharya, *Metabolic Links between Plasma Cell Survival, Secretion, and Stress.* Trends in Immunology, 2018. **39**(1): p. 19-27.
201. Peperzak, V., et al., *Mcl-1 is essential for the survival of plasma cells.* Nature Immunology, 2013. **14**(3): p. 290-297.
202. Cassese, G., et al., *Plasma Cell Survival Is Mediated by Synergistic Effects of Cytokines and Adhesion-Dependent Signals.* The Journal of Immunology, 2003. **171**: p. 1684-1690.
203. Gomez, M.R., et al., *Basophils Support the Survival of Plasma Cells in Mice.* The Journal of Immunology, 2010. **185**: p. 7180-7185.
204. Rozanski, C.H., et al., *Sustained antibody responses depend on CD28 function in bone marrow–resident plasma cells.* Journal of Experimental Medicine, 2011. **208**(7): p. 1435-1446.
205. Chevrier, S., et al., *CD93 is required for maintenance of antibody secretion and persistence of plasma cells in the bone marrow niche.* Proceedings of the National Academy of Sciences, 2009. **106**: p. 3895-3900.
206. McCarron, M.J., P.W. Park, and D.R. Fooksman, *CD138 mediates selection of mature plasma cells by regulating their survival.* Blood, 2017. **129**(20): p. 2749-2759.
207. Mattioli, C.A. and T.B. Tomasi, Jr., *The life span of IgA plasma cells from the mouse intestine.* J Exp Med, 1973. **138**(2): p. 452-60.

208. Lemke, A., et al., *Long-lived plasma cells are generated in mucosal immune responses and contribute to the bone marrow plasma cell pool in mice.* Mucosal immunology, 2016. **9**(1): p. 83-97.
209. Hapfelmeier, S., et al., *Reversible microbial colonization of germ-free mice reveals the dynamics of IgA immune responses.* Science, 2010. **328**(5986): p. 1705-9.
210. Landsverk, O.J., et al., *Antibody-secreting plasma cells persist for decades in human intestine.* Journal of Experimental Medicine, 2017. **214**(2): p. 309-317.
211. Kim, M., et al., *Gut Microbial Metabolites Fuel Host Antibody Responses.* Cell Host Microbe, 2016. **20**(2): p. 202-14.
212. Kunisawa, J., et al., *Mode of Bioenergetic Metabolism during B Cell Differentiation in the Intestine Determines the Distinct Requirement for Vitamin B1.* Cell Reports, 2015. **13**(1): p. 122-131.
213. Brandtzaeg, P.E.R., *Presence of J chain in human immunocytes containing various immunoglobulin classes.* Nature, 1974. **252**(5482): p. 418-420.
214. Halpern, M.S. and M.E. Koshland, *Novel subunit in secretory IgA.* Nature, 1970. **228**(5278): p. 1276-1278.
215. Kaetzel, C.S., et al., *The polymeric immunoglobulin receptor (secretory component) mediates transport of immune complexes across epithelial cells: a local defense function for IgA.* Proceedings of the National Academy of Sciences, 1991. **88**(19): p. 8796-8800.
216. Brandtzaeg, P. and H. Prydz, *Direct evidence for an integrated function of J chain and secretory component in epithelial transport of immunoglobulins.* Nature, 1984. **311**(5981): p. 71-73.
217. Mathias, A. and B. Corthésy, *N-Glycans on secretory component.* Gut Microbes, 2011. **2**(5): p. 287-293.
218. van Egmond, M., et al., *IgA and the IgA Fc receptor.* Trends in Immunology, 2001. **22**(4): p. 205-211.
219. Kilian, M., et al., *Biological significance of IgA1 proteases in bacterial colonization and pathogenesis: critical evaluation of experimental evidence.* Apmis, 1996. **104**(1-6): p. 321-338.
220. Steffen, U., et al., *IgA subclasses have different effector functions associated with distinct glycosylation profiles.* Nature Communications, 2020. **11**(1): p. 120.
221. Kett, K., et al., *Different subclass distribution of IgA-producing cells in human lymphoid organs and various secretory tissues.* The Journal of Immunology, 1986. **136**(10): p. 3631-3635.
222. Tarkowski, A., et al., *Immunization of humans with polysaccharide vaccines induces systemic, predominantly polymeric IgA2-subclass antibody responses.* The Journal of Immunology, 1990. **144**: p. 3770-3778.
223. Williams, R.C. and R.J. Gibbons, *Inhibition of Bacterial Adherence by Secretory Immunoglobulin A: A Mechanism of Antigen Disposal.* Science, 1972. **177**: p. 697-699.
224. Stokes, C.R., J.F. Soothill, and M.W. Turner, *Immune exclusion is a function of IgA.* Nature, 1975. **255**(5511): p. 745-746.
225. Wijburg , O.L.C., et al., *Innate secretory antibodies protect against natural Salmonella typhimurium infection.* Journal of Experimental Medicine, 2006. **203**(1): p. 21-26.
226. Apter, F., et al., *Monoclonal immunoglobulin A antibodies directed against cholera toxin prevent the toxin-induced chloride secretory response and block toxin binding to intestinal epithelial cells in vitro.* Infection and immunity, 1993. **61**(12): p. 5271-5278.
227. Hendrickx, A.P.A., et al., *Antibiotic-Driven Dysbiosis Mediates Intraluminal Agglutination and Alternative Segregation of Enterococcus faecium from the Intestinal Epithelium.* mBio, 2015. **6**.
228. Fernandez, M.I., et al., *Anti-Inflammatory Role for Intracellular Dimeric Immunoglobulin A by Neutralization of Lipopolysaccharide in Epithelial Cells.* Immunity, 2003. **18**(6): p. 739-749.
229. Corthésy, B., et al., *Rotavirus anti-VP6 secretory immunoglobulin A contributes to protection via intracellular neutralization but not via immune exclusion.* J Virol, 2006. **80**(21): p. 10692-9.

230. Johansen, K. and L. Svensson, *Neutralization of rotavirus and recognition of immunologically important epitopes on VP4 and VP7 by human IgA.* Archives of Virology, 1997. **142**(7): p. 1491-1498.
231. Silvey, K.J., et al., *Role of Immunoglobulin A in Protection against Reovirus Entry into Murine Peyer's Patches.* Journal of Virology, 2001. **75**: p. 10870-10879.
232. Burns, J.W., et al., *Protective Effect of Rotavirus VP6-Specific IgA Monoclonal Antibodies That Lack Neutralizing Activity.* Science, 1996. **272**: p. 104-107.
233. Suzuki, K., et al., *Aberrant expansion of segmented filamentous bacteria in IgA-deficient gut.* Proceedings of the National Academy of Sciences, 2004. **101**: p. 1981-1986.
234. Mathias, A., et al., *Potentiation of polarized intestinal Caco-2 cell responsiveness to probiotics complexed with secretory IgA.* Journal of Biological Chemistry, 2010. **285**(44): p. 33906-33913.
235. Macpherson, A.J. and S.C. Ganal-Vonarburg, *IgA-about the unexpected.* J Exp Med, 2018. **215**(8): p. 1965-1966.
236. Cullender, Tyler C., et al., *Innate and Adaptive Immunity Interact to Quench Microbiome Flagellar Motility in the Gut.* Cell Host & Microbe, 2013. **14**(5): p. 571-581.
237. Hoces, D., et al., *Growing, evolving and sticking in a flowing environment: understanding IgA interactions with bacteria in the gut.* Immunology, 2020. **159**(1): p. 52-62.
238. Cho, I., et al., *Antibiotics in early life alter the murine colonic microbiome and adiposity.* Nature, 2012. **488**(7413): p. 621-6.
239. Cox, L.M., et al., *Altering the intestinal microbiota during a critical developmental window has lasting metabolic consequences.* Cell, 2014. **158**(4): p. 705-721.
240. Arrieta, M.C., et al., *Early infancy microbial and metabolic alterations affect risk of childhood asthma.* Sci Transl Med, 2015. **7**(307): p. 307ra152.
241. Örtqvist, A.K., et al., *Fetal and early life antibiotics exposure and very early onset inflammatory bowel disease: a population-based study.* Gut, 2019. **68**(2): p. 218-225.
242. Kau, A.L., et al., *Functional characterization of IgA-targeted bacterial taxa from undernourished Malawian children that produce diet-dependent enteropathy.* Sci Transl Med, 2015. **7**(276): p. 276ra24.
243. Ridaura, V.K., et al., *Gut Microbiota from Twins Discordant for Obesity Modulate Metabolism in Mice.* Science, 2013. **341**.
244. Tilg, H., et al., *The intestinal microbiota fuelling metabolic inflammation.* Nature Reviews Immunology, 2020. **20**(1): p. 40-54.
245. He, Y., et al., *Regional variation limits applications of healthy gut microbiome reference ranges and disease models.* Nature medicine, 2018. **24**(10): p. 1532-1535.
246. Gao, R., et al., *Dysbiosis signatures of gut microbiota along the sequence from healthy, young patients to those with overweight and obesity.* Obesity, 2018. **26**(2): p. 351-361.
247. Sedighi, M., et al., *Comparison of gut microbiota in adult patients with type 2 diabetes and healthy individuals.* Microbial pathogenesis, 2017. **111**: p. 362-369.
248. Wu, X., et al., *Molecular characterisation of the faecal microbiota in patients with type II diabetes.* Current microbiology, 2010. **61**(1): p. 69-78.
249. Eckel-Mahan, K. and P. Sassone-Corsi, *Metabolism and the circadian clock converge.* Physiol Rev, 2013. **93**(1): p. 107-35.
250. Butler, T.D. and J.E. Gibbs, *Circadian Host-Microbiome Interactions in Immunity.* Frontiers in Immunology, 2020. **11**(1783).
251. Scheiermann, C., et al., *Clocking in to immunity.* Nature Reviews Immunology, 2018. **18**(7): p. 423-437.
252. Mazzoccoli, G., et al., *The Circadian Clock, the Immune System, and Viral Infections: The Intricate Relationship Between Biological Time and Host-Virus Interaction.* Pathogens, 2020. **9**(2): p. 83.

253. Gibbs, J.E., et al., *The nuclear receptor REV-ERBα mediates circadian regulation of innate immunity through selective regulation of inflammatory cytokines.* Proceedings of the National Academy of Sciences, 2012. **109**: p. 582-587.
254. Patke, A., M.W. Young, and S. Axelrod, *Molecular mechanisms and physiological importance of circadian rhythms.* Nature Reviews Molecular Cell Biology, 2020. **21**(2): p. 67-84.
255. Challet, E., *The circadian regulation of food intake.* Nature Reviews Endocrinology, 2019. **15**(7): p. 393-405.
256. Takahashi, J.S., *Molecular Architecture of the Circadian Clock in Mammals*, in *A Time for Metabolism and Hormones*, P. Sassone-Corsi and Y. Christen, Editors. 2016, Springer

Copyright 2016, The Author(s). Cham (CH). p. 13-24.
257. Takahashi, J.S., *Transcriptional architecture of the mammalian circadian clock.* Nature Reviews Genetics, 2017. **18**(3): p. 164-179.
258. Hand, L.E., et al., *Regulatory T cells confer a circadian signature on inflammatory arthritis.* Nature Communications, 2020. **11**(1): p. 1658.
259. Hemmers, S. and A.Y. Rudensky, *The Cell-Intrinsic Circadian Clock Is Dispensable for Lymphocyte Differentiation and Function.* Cell Rep, 2015. **11**(9): p. 1339-49.
260. Buxton, O.M., et al., *Adverse metabolic consequences in humans of prolonged sleep restriction combined with circadian disruption.* Science translational medicine, 2012. **4**(129): p. 129ra43-129ra43.
261. Pan, A., et al., *Rotating night shift work and risk of type 2 diabetes: two prospective cohort studies in women.* PLoS Med, 2011. **8**(12): p. e1001141.
262. Arble, D.M., et al., *Circadian timing of food intake contributes to weight gain.* Obesity, 2009. **17**(11): p. 2100-2102.
263. Turek, F.W., et al., *Obesity and Metabolic Syndrome in Circadian Clock Mutant Mice.* Science, 2005. **308**: p. 1043-1045.
264. Weintraub, Y., et al., *Clock Gene Disruption Is an Initial Manifestation of Inflammatory Bowel Diseases.* Clin Gastroenterol Hepatol, 2020. **18**(1): p. 115-122.e1.
265. Xiong, H., et al., *Loss of the clock gene PER2 is associated with cancer development and altered expression of important tumor-related genes in oral cancer.* International journal of oncology, 2018. **52**(1): p. 279-287.
266. Momma, T., et al., *Expression of circadian clock genes in human colorectal adenoma and carcinoma.* Oncology letters, 2017. **14**(5): p. 5319-5325.
267. Balsalobre, A., F. Damiola, and U. Schibler, *A Serum Shock Induces Circadian Gene Expression in Mammalian Tissue Culture Cells.* Cell, 1998. **93**(6): p. 929-937.
268. Aton, S.J., et al., *Vasoactive intestinal polypeptide mediates circadian rhythmicity and synchrony in mammalian clock neurons.* Nat Neurosci, 2005. **8**(4): p. 476-83.
269. Bass, J. and M.A. Lazar, *Circadian time signatures of fitness and disease.* Science, 2016. **354**(6315): p. 994-999.
270. Herzog, E.D., J.S. Takahashi, and G.D. Block, *Clock controls circadian period in isolated suprachiasmatic nucleus neurons.* Nat Neurosci, 1998. **1**(8): p. 708-13.
271. Yamaguchi, S., et al., *Synchronization of cellular clocks in the suprachiasmatic nucleus.* Science, 2003. **302**(5649): p. 1408-12.
272. Domingues, R.G. and M.R. Hepworth, *Immunoregulatory Sensory Circuits in Group 3 Innate Lymphoid Cell (ILC3) Function and Tissue Homeostasis.* Frontiers in Immunology, 2020. **11**(116).
273. Druzd, D., et al., *Lymphocyte Circadian Clocks Control Lymph Node Trafficking and Adaptive Immune Responses.* Immunity, 2017. **46**(1): p. 120-32.
274. Greenwell, B.J., et al., *Rhythmic Food Intake Drives Rhythmic Gene Expression More Potently than the Hepatic Circadian Clock in Mice.* Cell Rep, 2019. **27**(3): p. 649-657.e5.
275. Hopwood, T.W., et al., *The circadian regulator BMAL1 programmes responses to parasitic worm infection via a dendritic cell clock.* Sci Rep, 2018. **8**(1): p. 3782.

276. Damiola, F., et al., *Restricted feeding uncouples circadian oscillators in peripheral tissues from the central pacemaker in the suprachiasmatic nucleus.* Genes & development, 2000. **14**(23): p. 2950-2961.
277. Stokkan, K.-A., et al., *Entrainment of the circadian clock in the liver by feeding.* Science, 2001. **291**(5503): p. 490-493.
278. Hogenesch, J.B., et al., *The basic-helix-loop-helix-PAS orphan MOP3 forms transcriptionally active complexes with circadian and hypoxia factors.* Proc Natl Acad Sci U S A, 1998. **95**(10): p. 5474-9.
279. Gekakis, N., et al., *Role of the CLOCK protein in the mammalian circadian mechanism.* Science, 1998. **280**(5369): p. 1564-9.
280. Zheng, B., et al., *Nonredundant roles of the mPer1 and mPer2 genes in the mammalian circadian clock.* Cell, 2001. **105**(5): p. 683-94.
281. van der Horst, G.T., et al., *Mammalian Cry1 and Cry2 are essential for maintenance of circadian rhythms.* Nature, 1999. **398**(6728): p. 627-30.
282. Preitner, N., et al., *The orphan nuclear receptor REV-ERBalpha controls circadian transcription within the positive limb of the mammalian circadian oscillator.* Cell, 2002. **110**(2): p. 251-60.
283. Sato, T.K., et al., *A functional genomics strategy reveals Rora as a component of the mammalian circadian clock.* Neuron, 2004. **43**(4): p. 527-37.
284. Ko, C.H. and J.S. Takahashi, *Molecular components of the mammalian circadian clock.* Hum Mol Genet, 2006. **15 Spec No 2**: p. R271-7.
285. Durrington, H.J., et al., *The circadian clock and asthma.* Thorax, 2014. **69**(1): p. 90.
286. Gibbs, J.E. and D.W. Ray, *The role of the circadian clock in rheumatoid arthritis.* Arthritis Research & Therapy, 2013. **15**(1): p. 205.
287. Tognini, P., et al., *Circadian Coordination of Antimicrobial Responses.* Cell Host Microbe, 2017. **22**(2): p. 185-192.
288. Logan, R.W., et al., *Altered Circadian Expression of Cytokines and Cytolytic Factors in Splenic Natural Killer Cells of Per1−/− Mutant Mice.* Journal of Interferon & Cytokine Research, 2013. **33**(3): p. 108-114.
289. Arjona, A. and D.K. Sarkar, *Circadian oscillations of clock genes, cytolytic factors, and cytokines in rat NK cells.* The Journal of Immunology, 2005. **174**(12): p. 7618-7624.
290. Keller, M., et al., *A circadian clock in macrophages controls inflammatory immune responses.* Proceedings of the National Academy of Sciences, 2009. **106**(50): p. 21407-21412.
291. Silver, A.C., et al., *Circadian expression of clock genes in mouse macrophages, dendritic cells, and B cells.* Brain, behavior, and immunity, 2012. **26**(3): p. 407-413.
292. Seillet, C., et al., *The neuropeptide VIP confers anticipatory mucosal immunity by regulating ILC3 activity.* Nature Immunology, 2019: p. 1-10.
293. Godinho-Silva, C., et al., *Light-entrained and brain-tuned circadian circuits regulate ILC3s and gut homeostasis.* Nature, 2019. **574**(7777): p. 254-258.
294. Bollinger, T., et al., *Circadian clocks in mouse and human CD4+ T cells.* PloS one, 2011. **6**(12): p. e29801.
295. Yang, X.O., et al., *T helper 17 lineage differentiation is programmed by orphan nuclear receptors ROR alpha and ROR gamma.* Immunity, 2008. **28**(1): p. 29-39.
296. Ivanov, I.I., et al., *The Orphan Nuclear Receptor RORγt Directs the Differentiation Program of Proinflammatory IL-17⁺ T Helper Cells.* Cell, 2006. **126**(6): p. 1121-1133.
297. Geiger, T.L., et al., *Nfil3 is crucial for development of innate lymphoid cells and host protection against intestinal pathogens.* Journal of Experimental Medicine, 2014. **211**(9): p. 1723-1731.
298. Xu, W., et al., *NFIL3 orchestrates the emergence of common helper innate lymphoid cell precursors.* Cell reports, 2015. **10**(12): p. 2043-2054.
299. Yu, X., et al., *TH17 cell differentiation is regulated by the circadian clock.* Science, 2013. **342**(6159): p. 727-30.

300. Talbot, J., et al., *Feeding-dependent VIP neuron-ILC3 circuit regulates the intestinal barrier.* Nature, 2020. **579**(7800): p. 575-580.
301. Teng, F., et al., *A circadian clock is essential for homeostasis of group 3 innate lymphoid cells in the gut.* Science Immunology, 2019. **4**(40): p. eaax1215.
302. He, W., et al., *Circadian Expression of Migratory Factors Establishes Lineage-Specific Signatures that Guide the Homing of Leukocyte Subsets to Tissues.* Immunity, 2018. **49**(6): p. 1175-1190.e7.
303. Shimba, A., et al., *Glucocorticoids Drive Diurnal Oscillations in T Cell Distribution and Responses by Inducing Interleukin-7 Receptor and CXCR4.* Immunity, 2018. **48**(2): p. 286-298.e6.
304. Baptista, A.P., et al., *Colonic patch and colonic SILT development are independent and differentially regulated events.* Mucosal Immunology, 2013. **6**(3): p. 511-521.
305. Suzuki, K., et al., *Adrenergic control of the adaptive immune response by diurnal lymphocyte recirculation through lymph nodes.* J Exp Med, 2016. **213**(12): p. 2567-2574.
306. Vivier, E., et al., *Functions of natural killer cells.* Nature immunology, 2008. **9**(5): p. 503-510.
307. Gatti, G., et al., *Circadian changes in human natural killer-cell activity.* Prog Clin Biol Res, 1987. **227a**: p. 399-409.
308. Zhou, J., et al., *Glucocorticoid Regulation of Natural Cytotoxicity: Effects of Cortisol on the Phenotype and Function of a Cloned Human Natural Killer Cell Line.* Cellular Immunology, 1997. **178**(2): p. 108-116.
309. Kronfol, Z., et al., *Circadian immune measures in healthy volunteers: relationship to hypothalamic-pituitary-adrenal axis hormones and sympathetic neurotransmitters.* Psychosom Med, 1997. **59**(1): p. 42-50.
310. Logan, R.W., et al., *Chronic shift-lag alters the circadian clock of NK cells and promotes lung cancer growth in rats.* The Journal of Immunology, 2012. **188**(6): p. 2583-2591.
311. Wang, Q., et al., *Circadian rhythm-dependent and circadian rhythm-independent impacts of the molecular clock on type 3 innate lymphoid cells.* Sci Immunol, 2019. **4**(40).
312. Castanon-Cervantes, O., et al., *Dysregulation of inflammatory responses by chronic circadian disruption.* The Journal of Immunology, 2010. **185**(10): p. 5796-5805.
313. Thaiss, C.A., et al., *Transkingdom control of microbiota diurnal oscillations promotes metabolic homeostasis.* Cell, 2014. **159**(3): p. 514-529.
314. Thaiss, C.A., et al., *Microbiota diurnal rhythmicity programs host transcriptome oscillations.* Cell, 2016. **167**(6): p. 1495-1510. e12.
315. Liang, X., F.D. Bushman, and G.A. FitzGerald, *Rhythmicity of the intestinal microbiota is regulated by gender and the host circadian clock.* Proceedings of the National Academy of Sciences, 2015. **112**(33): p. 10479-10484.
316. Zarrinpar, A., et al., *Diet and Feeding Pattern Affect the Diurnal Dynamics of the Gut Microbiome.* Cell Metabolism, 2014. **20**(6): p. 1006-1017.
317. Leone, V., et al., *Effects of diurnal variation of gut microbes and high-fat feeding on host circadian clock function and metabolism.* Cell host & microbe, 2015. **17**(5): p. 681-689.
318. Beli, E., et al., *Loss of Diurnal Oscillatory Rhythms in Gut Microbiota Correlates with Changes in Circulating Metabolites in Type 2 Diabetic db/db Mice.* Nutrients, 2019. **11**(10): p. 2310.
319. Hatori, M., et al., *Time-restricted feeding without reducing caloric intake prevents metabolic diseases in mice fed a high-fat diet.* Cell metabolism, 2012. **15**(6): p. 848-860.
320. Nobs, S.P., T. Tuganbaev, and E. Elinav, *Microbiome diurnal rhythmicity and its impact on host physiology and disease risk.* EMBO reports, 2019. **20**(4): p. e47129.
321. Bass, J., *Circadian topology of metabolism.* Nature, 2012. **491**(7424): p. 348-356.
322. Kuang, Z., et al., *The intestinal microbiota programs diurnal rhythms in host metabolism through histone deacetylase 3.* Science, 2019. **365**(6460): p. 1428-1434.
323. Tuganbaev, T., et al., *Diet Diurnally Regulates Small Intestinal Microbiome-Epithelial-Immune Homeostasis and Enteritis.* Cell, 2020. **182**(6): p. 1441-1459.e21.

324. Montagner, A., et al., *Hepatic circadian clock oscillators and nuclear receptors integrate microbiome-derived signals.* Sci Rep, 2016. **6**: p. 20127.
325. Tahara, Y., et al., *Gut Microbiota-Derived Short Chain Fatty Acids Induce Circadian Clock Entrainment in Mouse Peripheral Tissue.* Sci Rep, 2018. **8**(1): p. 1395.
326. Voigt, R.M., et al., *Circadian Disorganization Alters Intestinal Microbiota.* PLOS ONE, 2014. **9**(5): p. e97500.
327. Voigt, R.M., et al., *The circadian clock mutation promotes intestinal dysbiosis.* Alcoholism: Clinical and Experimental Research, 2016. **40**(2): p. 335-347.
328. Shi, S.-q., et al., *Circadian Disruption Leads to Insulin Resistance and Obesity.* Current Biology, 2013. **23**(5): p. 372-381.
329. Scheer, F.A., et al., *Adverse metabolic and cardiovascular consequences of circadian misalignment.* Proceedings of the National Academy of Sciences, 2009. **106**(11): p. 4453-4458.
330. Mukherji, A., et al., *Shifting eating to the circadian rest phase misaligns the peripheral clocks with the master SCN clock and leads to a metabolic syndrome.* Proc Natl Acad Sci U S A, 2015. **112**(48): p. E6691-8.
331. Reitmeier, S., et al., *Arrhythmic gut microbiome signatures for risk profiling of Type-2 Diabetes.* 2019.
332. Sinclair, L.V., et al., *Single cell analysis of kynurenine and System L amino acid transport in T cells.* Nature Communications, 2018. **9**(1): p. 1981.
333. Beckonert, O., et al., *Metabolic profiling, metabolomic and metabonomic procedures for NMR spectroscopy of urine, plasma, serum and tissue extracts.* Nat Protoc, 2007. **2**(11): p. 2692-703.
334. Hughes, M.E., J.B. Hogenesch, and K. Kornacker, *JTK_CYCLE: an efficient nonparametric algorithm for detecting rhythmic components in genome-scale data sets.* J Biol Rhythms, 2010. **25**(5): p. 372-80.
335. Oliva-Ramírez, J., et al., *Crosstalk between circadian rhythmicity, mitochondrial dynamics and macrophage bactericidal activity.* Immunology, 2014. **143**(3): p. 490-497.
336. Cao, Q., et al., *Circadian clock cryptochrome proteins regulate autoimmunity.* Proceedings of the National Academy of Sciences, 2017. **114**(47): p. 12548-12553.
337. Burns, P., et al., *Variability in gut mucosal secretory IgA in mice along a working day.* BMC Res Notes, 2018. **11**(1): p. 98.
338. Kobayashi, R., et al., *Circadian Rhythm Affects the Dynamics of S-IgA Mucosal Secretion .* International Journal of Oral-Medical Sciences, 2015. **14**(1): p. 1-7.
339. Royo, F., et al., *Impact of chronic catheterization and automated blood sampling (Accusampler) on serum corticosterone and fecal immunoreactive corticosterone metabolites and immunoglobulin A in male rats.* J Endocrinol, 2004. **180**(1): p. 145-53.
340. Eriksson, E., et al., *Effect of metabolic cage housing on immunoglobulin A and corticosterone excretion in faeces and urine of young male rats.* Exp Physiol, 2004. **89**(4): p. 427-33.
341. Vincent, F.B., et al., *The BAFF/APRIL system in SLE pathogenesis.* Nature Reviews Rheumatology, 2014. **10**(6): p. 365-373.
342. Liu, G.Y. and D.M. Sabatini, *mTOR at the nexus of nutrition, growth, ageing and disease.* Nature Reviews Molecular Cell Biology, 2020. **21**(4): p. 183-203.
343. Jeon, T.I. and T.F. Osborne, *SREBPs: metabolic integrators in physiology and metabolism.* Trends Endocrinol Metab, 2012. **23**(2): p. 65-72.
344. DeBose-Boyd, R.A. and J. Ye, *SREBPs in Lipid Metabolism, Insulin Signaling, and Beyond.* Trends Biochem Sci, 2018. **43**(5): p. 358-368.
345. Gruenbacher, G. and M. Thurnher, *Mevalonate Metabolism in Immuno-Oncology.* Frontiers in Immunology, 2017. **8**(1714).
346. Su, T., et al., *Reduced Immunoglobulin A Transcytosis Associated with Immunoglobulin A Nephropathy and Nasopharyngeal Carcinoma *.* Journal of Biological Chemistry, 2011. **286**(52): p. 44921-44925.

347. Natvig, I.B., et al., *Mechanism for enhanced external transfer of dimeric IgA over pentameric IgM: studies of diffusion, binding to the human polymeric Ig receptor, and epithelial transcytosis.* J Immunol, 1997. **159**(9): p. 4330-40.
348. Schwarz, R., et al., *Gastrointestinal transit times in mice and humans measured with 27Al and 19F nuclear magnetic resonance.* Magn Reson Med, 2002. **48**(2): p. 255-61.
349. Mesin, L., et al., *Long-lived plasma cells from human small intestine biopsies secrete immunoglobulins for many weeks in vitro.* The Journal of Immunology, 2011. **187**(6): p. 2867-2874.
350. Nguyen, K.D., et al., *Circadian gene Bmal1 regulates diurnal oscillations of Ly6Chi inflammatory monocytes.* Science, 2013. **341**(6153): p. 1483-1488.
351. Sintes, J., et al., *mTOR intersects antibody-inducing signals from TACI in marginal zone B cells.* Nature Communications, 2017. **8**(1): p. 1462.
352. Jones, D.D., et al., *mTOR has distinct functions in generating versus sustaining humoral immunity.* J Clin Invest, 2016. **126**(11): p. 4250-4261.
353. Benhamron, S., et al., *mTOR Activation Promotes Plasma Cell Differentiation and Bypasses XBP-1 for Immunoglobulin Secretion.* Molecular and Cellular Biology, 2015. **35**: p. 153-166.
354. Zhang, S., et al., *B Cell–Specific Deficiencies in mTOR Limit Humoral Immune Responses.* The Journal of Immunology, 2013. **191**: p. 1692-1703.
355. Lipton, Jonathan O., et al., *The Circadian Protein BMAL1 Regulates Translation in Response to S6K1-Mediated Phosphorylation.* Cell, 2015. **161**(5): p. 1138-1151.
356. Cao, R., et al., *Circadian regulation of mammalian target of rapamycin signaling in the mouse suprachiasmatic nucleus.* Neuroscience, 2011. **181**: p. 79-88.
357. Crosby, P., et al., *Insulin/IGF-1 Drives PERIOD Synthesis to Entrain Circadian Rhythms with Feeding Time.* Cell, 2019. **177**(4): p. 896-909.e20.
358. Bibby, J.A., et al., *Cholesterol metabolism drives regulatory B cell IL-10 through provision of geranylgeranyl pyrophosphate.* Nature Communications, 2020. **11**(1): p. 3412.
359. Trindade, B.C., et al., *Intracellular sterol sensing controls intestinal B cell differentiation.* bioRxiv, 2020: p. 2020.11.03.367177.
360. Dufort, F.J., et al., *Glucose-dependent de novo lipogenesis in B lymphocytes: a requirement for atp-citrate lyase in lipopolysaccharide-induced differentiation.* J Biol Chem, 2014. **289**(10): p. 7011-24.
361. ter Haar, N.M., et al., *The Phenotype and Genotype of Mevalonate Kinase Deficiency: A Series of 114 Cases From the Eurofever Registry.* Arthritis & Rheumatology, 2016. **68**(11): p. 2795-2805.
362. Matsumoto, E., et al., *Time of Day and Nutrients in Feeding Govern Daily Expression Rhythms of the Gene for Sterol Regulatory Element-binding Protein (SREBP)-1 in the Mouse Liver*.* Journal of Biological Chemistry, 2010. **285**(43): p. 33028-33036.
363. Gilardi, F., et al., *Genome-Wide Analysis of SREBP1 Activity around the Clock Reveals Its Combined Dependency on Nutrient and Circadian Signals.* PLOS Genetics, 2014. **10**(3): p. e1004155.
364. Benson, M.J., et al., *Cutting Edge: The Dependence of Plasma Cells and Independence of Memory B Cells on BAFF and APRIL.* The Journal of Immunology, 2008. **180**: p. 3655-3659.
365. O'Connor , B.P., et al., *BCMA Is Essential for the Survival of Long-lived Bone Marrow Plasma Cells.* Journal of Experimental Medicine, 2004. **199**(1): p. 91-98.
366. Cornelis, R., et al., *Stromal Cell-Contact Dependent PI3K and APRIL Induced NF-κB Signaling Prevent Mitochondrial- and ER Stress Induced Death of Memory Plasma Cells.* Cell Reports, 2020. **32**(5).
367. Sanderson, R.D., P. Lalor, and M. Bernfield, *B lymphocytes express and lose syndecan at specific stages of differentiation.* Cell regulation, 1989. **1**(1): p. 27-35.

368. Moreaux, J., et al., *APRIL and TACI interact with syndecan-1 on the surface of multiple myeloma cells to form an essential survival loop.* European Journal of Haematology, 2009. **83**(2): p. 119-129.
369. Tai, Y.-T., et al., *APRIL and BCMA promote human multiple myeloma growth and immunosuppression in the bone marrow microenvironment.* Blood, 2016. **127**(25): p. 3225-3236.
370. Novak, A.J., et al., *Expression of BCMA, TACI, and BAFF-R in multiple myeloma: a mechanism for growth and survival.* Blood, 2004. **103**(2): p. 689-94.
371. Sulli, G., M.T.Y. Lam, and S. Panda, *Interplay between Circadian Clock and Cancer: New Frontiers for Cancer Treatment.* Trends Cancer, 2019. **5**(8): p. 475-494.
372. Aiello, I., et al., *Circadian disruption promotes tumor-immune microenvironment remodeling favoring tumor cell proliferation.* Science Advances, 2020. **6**(42): p. eaaz4530.
373. Pickard, A., et al., *Preservation of circadian rhythms by the protein folding chaperone, BiP.* Faseb j, 2019. **33**(6): p. 7479-7489.
374. Chang, J., et al., *Circadian control of the secretory pathway maintains collagen homeostasis.* Nature Cell Biology, 2020. **22**(1): p. 74-86.
375. Wu, R., et al., *The circadian protein Period2 suppresses mTORC1 activity via recruiting Tsc1 to mTORC1 complex.* Cell metabolism, 2019. **29**(3): p. 653-667. e6.
376. Cretenet, G., M. Le Clech, and F. Gachon, *Circadian clock-coordinated 12 hr period rhythmic activation of the IRE1α pathway controls lipid metabolism in mouse liver.* Cell metabolism, 2010. **11**(1): p. 47-57.
377. Cissé, Y.M., et al., *Time-Restricted Feeding Alters the Innate Immune Response to Bacterial Endotoxin.* The Journal of Immunology, 2018. **200**(2): p. 681-687.
378. Nussbaum, J.C., et al., *Type 2 innate lymphoid cells control eosinophil homeostasis.* Nature, 2013. **502**(7470): p. 245-248.
379. Wada, M., et al., *Circadian clock-dependent increase in salivary IgA secretion modulated by sympathetic receptor activation in mice.* Sci Rep, 2017. **7**(1): p. 8802.
380. Park, S.-J. and H. Tokura, *Bright light exposure during the daytime affects circadian rhythms of urinary melatonin and salivary immunoglobulin A.* Chronobiology international, 1999. **16**(3): p. 359-371.
381. Dimitriou, L., N. Sharp, and M. Doherty, *Circadian effects on the acute responses of salivary cortisol and IgA in well trained swimmers.* British journal of sports medicine, 2002. **36**(4): p. 260-264.
382. Plangsangmas, T., et al., *Circadian Rhythm of Salivary Immunoglobulin A and Associations with Cortisol as A Stress Biomarker in Captive Asian Elephants (Elephas maximus).* Animals (Basel), 2020. **10**(1).
383. Gommerman, J.L., O.L. Rojas, and J.H. Fritz, *Re-thinking the functions of IgA(+) plasma cells.* Gut Microbes, 2014. **5**(5): p. 652-62.
384. Vollmers, C., et al., *Time of feeding and the intrinsic circadian clock drive rhythms in hepatic gene expression.* Proc Natl Acad Sci U S A, 2009. **106**(50): p. 21453-8.
385. Scheving, L.A., *Biological clocks and the digestive system.* Gastroenterology, 2000. **119**(2): p. 536-549.
386. Nagai, M., et al., *Fasting-Refeeding Impacts Immune Cell Dynamics and Mucosal Immune Responses.* Cell, 2019. **178**(5): p. 1072-1087.e14.
387. Della Vedova, M.C., et al., *A Mouse Model of Diet-Induced Obesity Resembling Most Features of Human Metabolic Syndrome.* Nutr Metab Insights, 2016. **9**: p. 93-102.
388. Lee, Y.-K., A.-P. Teoh, and P.-K. Yap, *Regulation of glucose and glutamine uptake and the production of monoclonal antibody in hybridoma cultures.* Enzyme and Microbial Technology, 1997. **21**(6): p. 429-435.
389. Dyar, K.A., et al., *Atlas of Circadian Metabolism Reveals System-wide Coordination and Communication between Clocks.* Cell, 2018. **174**(6): p. 1571-1585.e11.

390. Waisman, A., et al., *IgG1 B cell receptor signaling is inhibited by CD22 and promotes the development of B cells whose survival is less dependent on Igα/β.* The Journal of experimental medicine, 2007. **204**(4): p. 747-758.
391. Sahputra, R., et al., *Evaluating the IgMi mouse as a novel tool to study B-cell biology.* European Journal of Immunology, 2018. **48**(12): p. 2068-2071.
392. Chen, J., et al., *Immunoglobulin gene rearrangement in B cell deficient mice generated by targeted deletion of the JH locus.* International Immunology, 1993. **5**(6): p. 647-656.
393. Golovkina, T.V., et al., *Organogenic role of B lymphocytes in mucosal immunity.* Science, 1999. **286**(5446): p. 1965-8.
394. Robertson, B.R., et al., *Mucispirillum schaedleri gen. nov., sp. nov., a spiral-shaped bacterium colonizing the mucus layer of the gastrointestinal tract of laboratory rodents.* International journal of systematic and evolutionary microbiology, 2005. **55**(3): p. 1199-1204.
395. Derrien, M., et al., *Akkermansia muciniphila gen. nov., sp. nov., a human intestinal mucin-degrading bacterium.* International Journal of Systematic and Evolutionary Microbiology, 2004. **54**(5): p. 1469-1476.
396. Lunt, S.Y. and M.G.V. Heiden, *Aerobic Glycolysis: Meeting the Metabolic Requirements of Cell Proliferation.* Annual Review of Cell and Developmental Biology, 2011. **27**(1): p. 441-464.
397. Takayasu, L., et al., *Circadian oscillations of microbial and functional composition in the human salivary microbiome.* DNA Research: An International Journal for Rapid Publication of Reports on Genes and Genomes, 2017. **24**: p. 261 - 270.
398. Goertz, S., et al., *Geographical location influences the composition of the gut microbiota in wild house mice (Mus musculus domesticus) at a fine spatial scale.* PLOS ONE, 2019. **14**(9): p. e0222501.
399. Yatsunenko, T., et al., *Human gut microbiome viewed across age and geography.* Nature, 2012. **486**(7402): p. 222-227.
400. Chai, J.N., et al., *Helicobacter species are potent drivers of colonic T cell responses in homeostasis and inflammation.* Science immunology, 2017. **2**(13): p. eaal5068.
401. Derrien, M., et al., *The Mucin degrader Akkermansia muciniphila is an abundant resident of the human intestinal tract.* Applied and environmental microbiology, 2008. **74**(5): p. 1646-1648.
402. Ansaldo, E., et al., *Akkermansia muciniphila induces intestinal adaptive immune responses during homeostasis.* Science, 2019. **364**(6446): p. 1179-1184.
403. Vijayan, V., R. Zuzow, and E.K. O'Shea, *Oscillations in supercoiling drive circadian gene expression in cyanobacteria.* Proc Natl Acad Sci U S A, 2009. **106**(52): p. 22564-8.
404. Eelderink-Chen, Z., et al., *A circadian clock in a nonphotosynthetic prokaryote.* Science Advances, 2021. **7**(2): p. eabe2086.
405. Rath, S., et al., *Pathogenic functions of host microbiota.* Microbiome, 2018. **6**(1): p. 174.
406. Blachier, F., et al., *Luminal sulfide and large intestine mucosa: friend or foe?* Amino Acids, 2010. **39**(2): p. 335-47.
407. Ohge, H., et al., *Association between fecal hydrogen sulfide production and pouchitis.* Diseases of the colon & rectum, 2005. **48**(3): p. 469-475.
408. Yazici, C., et al., *Race-dependent association of sulfidogenic bacteria with colorectal cancer.* Gut, 2017. **66**(11): p. 1983-1994.
409. Rowan, F., et al., *Desulfovibrio bacterial species are increased in ulcerative colitis.* Diseases of the Colon & Rectum, 2010. **53**(11): p. 1530-1536.
410. Devkota, S., et al., *Dietary-fat-induced taurocholic acid promotes pathobiont expansion and colitis in Il10−/− mice.* Nature, 2012. **487**(7405): p. 104-108.
411. Singh, R.K., et al., *Influence of diet on the gut microbiome and implications for human health.* J Transl Med, 2017. **15**(1): p. 73.

412. Koo, D.-H., et al., *Extrachromosomal circular DNA-based amplification and transmission of herbicide resistance in crop weed Amaranthus palmeri.* Proceedings of the National Academy of Sciences, 2018. **115**(13): p. 3332-3337.
413. Pasquier, B., et al., *Identification of FcαRI as an inhibitory receptor that controls inflammation: dual role of FcRγ ITAM.* Immunity, 2005. **22**(1): p. 31-42.
414. Mantis, N.J., et al., *Selective adherence of IgA to murine Peyer's patch M cells: evidence for a novel IgA receptor.* J Immunol, 2002. **169**(4): p. 1844-51.
415. Moura, I.C., et al., *Identification of the transferrin receptor as a novel immunoglobulin (Ig)A1 receptor and its enhanced expression on mesangial cells in IgA nephropathy.* J Exp Med, 2001. **194**(4): p. 417-25.
416. Matysiak-Budnik, T., et al., *Secretory IgA mediates retrotranscytosis of intact gliadin peptides via the transferrin receptor in celiac disease.* J Exp Med, 2008. **205**(1): p. 143-54.
417. Xu, A., R. Barbosa, and D. Calado, *Jchain-driven cre enables specific genetic manipulation and timestamping of plasma cell in their niche.* bioRxiv, 2020.
418. Huus, K.E., C. Petersen, and B.B. Finlay, *Diversity and dynamism of IgA-microbiota interactions.* Nat Rev Immunol, 2021.
419. Agus, A., K. Clément, and H. Sokol, *Gut microbiota-derived metabolites as central regulators in metabolic disorders.* Gut, 2021. **70**(6): p. 1174.
420. Ando, H., et al., *Impairment of peripheral circadian clocks precedes metabolic abnormalities in ob/ob mice.* Endocrinology, 2011. **152**(4): p. 1347-54.
421. Larsen, N., et al., *Gut Microbiota in Human Adults with Type 2 Diabetes Differs from Non-Diabetic Adults.* PLOS ONE, 2010. **5**(2): p. e9085.
422. Axelsson, J. and S. Puttonen, *Night shift work increases the risk for type 2 diabetes.* Evidence Based Medicine, 2012. **17**(6): p. 193.
423. Petersen, M.C., D.F. Vatner, and G.I. Shulman, *Regulation of hepatic glucose metabolism in health and disease.* Nature Reviews Endocrinology, 2017. **13**(10): p. 572-587.
424. McCusker, C., J. Upton, and R. Warrington, *Primary immunodeficiency.* Allergy, Asthma & Clinical Immunology, 2018. **14**(2): p. 61.
425. Berthet, F., et al., *Clinical Consequences and Treatment of Primary Immunodeficiency Syndromes Characterized by Functional T and B Lymphocyte Anomalies (Combined Immune Deficiency).* Pediatrics, 1994. **93**(2): p. 265-270.
426. Martin AM, Sun EW, Rogers GB, Keating DJ. The Influence of the Gut Microbiome on Host Metabolism Through the Regulation of Gut Hormone Release. Front Physiol. 2019;16;10:428.
427. Rooks MG, Garrett WS. Gut microbiota, metabolites and host immunity. Nat Rev Immunol. 2016;16(6):341-352.
428. Gibbs, J., et al. An epithelial circadian clock controls pulmonary inflammation and glucocorticoid action. Nature medicine 2014;20(8):919-926.
429. Edgar RS, et al. Cell autonomous regulation of herpes and influenza virus infection by the circadian clock. Proc Natl Acad Sci U S A. 2016 Sep 6;113(36):10085-90.
430. Ehlers A, et al. BMAL1 links the circadian clock to viral airway pathology and asthma phenotypes. Mucosal Immunol. 2018 Jan;11(1):97-111.
431. Nguyen KD, et al. Circadian gene Bmal1 regulates diurnal oscillations of Ly6C(hi) inflammatory monocytes. Science. 2013 Sep 27;341(6153):1483-8.
432. Bellet MM, et al. Circadian clock regulates the host response to Salmonella. Proc Natl Acad Sci U S A. 2013 Jun 11;110(24):9897-902.
433. Ramanathan, C., et al. mTOR signaling regulates central and peripheral circadian clock function. PLoS Genet. 2018;14:e1007369.
434. Panda S, et al. coordinated transcription of key pathways in the mouse by the circadian clock. Cell 2002;109: 307–320.
435. Jouffe C, et al. The Circadian Clock Coordinates Ribosome Biogenesis. PLOS Biology 2013;11(1):e1001455.

436. Wang, J, et al. Circadian clock-dependent and -independent posttranscriptional regulation underlies temporal mRNA accumulation in mouse liver. PNAS 2018;115:E1916-E1925.
437. Dyar KA, et al. Circadian Metabolomics in Time and Space. Front Neurosci. 2017;11:369.